CRANFIELD UNIVERSITY

Farhan A. Mirza

Nanofunctionalised Orthopaedic Implants

School of Engineering

PhD
Academic Year: 2012-2018

Supervisor: Dr Yi Ge
January 2018

CRANFIELD UNIVERSITY

School of Engineering
Faculty of Medicine and Biosciences

PhD

Academic Year 2012-2018

Farhan A. Mirza

Nanofunctionalised Orthopaedic Implants

Supervisor: Dr Yi Ge
January 2018

This thesis is submitted in partial fulfilment of the requirements for the degree of PhD

ABSTRACT

Due to an aging population and younger patients presenting with musculoskeletal disorders, there is a need for orthopaedic implants with improved healing rates and longer implant life. Numerous research has developed implant surfaces with micro-topography and biomolecules to imitate the native extra cellular matrix (also known as biomimetic surfaces). This research has utilised such a biomimetic approach by immobilising the cell adhesive peptide, RGD (Arginine-Glycine-Aspartic Acid), to a titanium alloy Ti6Al4V surface. This research polymerised Hyperbranched Polyglycerol (HBPG) from the titanium surface using Ring Opening Multi-Branching Polymerisation (ROMBP). HBPG is a biologically compatible and non-toxic synthetic biopolymer, able to reduce non-specific protein adsorption, increase the titanium surface wetting (hydrophilicity), thereby limiting foreign body reactions. Extensive hydroxyl groups at the periphery of HBPG provides conjugation sites for biomolecule attachment. In this work the RGD peptide was conjugated to the polymer via a siloxane layer.

This research developed a novel passivation solution for the preparation of the titanium alloy surface, using a mixture of hydrogen peroxide and nitric acid (a passivation mixture not used in the literature). This novel mixture was shown to etch the titanium surface, producing micro and nano surface features, both of which have been shown to improve cellular function in the literature. The hydrogen peroxide/nitric acid solution showed extensive oxidising ability on titanium, leading to the formation of reactable hydroxyl groups. Contact-angle measurements showed that the novel passivating solution produces a hydrophilic surface similar to that of peroxidation for 12-hours, but achieved in only 2-hours. In conjunction with the etching and oxidising abilities of hydrogen peroxide, the nitric acid reacts with the titanium surface, leading to the formation of a protective titanium oxide layer, enhancing corrosion resistance and improving biocompatibility.

Biological investigations with the pre-osteoblast cell line MC3T3-E1 showed greater osteoblast cell attachment and adhesion strength, as well as improved bone matrix mineralisation on the passivated titanium surface functionalised with HBPG and the RGD peptide, compared to the raw and passivated titanium surfaces. Antibacterial testing of HBPG revealed substantially reduced bacterial cell colonies on the passivated/polymerised titanium surface, possibly arising from electrostatic and hydrophobic repulsion.

This research has successfully developed a new titanium passivation solution (hydrogen peroxide/nitric acid) that can yield a contact-angle of around 35° in just 2-hours, rivalling the

Piranha solution. The successful immobilisation of a cyclic RGD (cyclic-RGDfc) to a titanium surface functionalised with HBPG, has been shown in this research to drastically improve mineralised bone matrix production from the MC3T3-E1 cell line. This indicates earlier osseointegration of the implant may be possible, thereby improving patient healing times.

Keywords:

Adhesion

Antibacterial

Attachment

Biomimetic

Biomolecule

Detachment

Glycidol

Hydrophilic

Hydroxyapatite

Hyperbranched

Implant

Integrin

Mineralisation

Nano

Orthopaedic

Osseointegration

Osteoblasts

Osteoconduction

Osteoid

Osteoinduction

Passivation

Polyglycerol

Polymerisation

Proliferation

RGD

Roughness

Titanium

ACKNOWLEDGEMENTS

First and foremost, I would like to thank God, without whom nothing is possible. I would like to thank Alessio Giuliani of SinteaPlustek for giving me the opportunity to carry out clinically impacting research of high importance. A special thanks to my supervisor's Dr Yi Ge and Dr Iva Chianella for all their help and support throughout the whole research process, and their wisdom and guidance. I would like to thank all Cranfield Health staff and colleagues for their research training. Lastly a very special thank you to my parents and family for their encouragement, belief and endless support in my work.

Table of Contents

List of Figures

List of Tables

List of Schemes

LIST OF ABBREVIATIONS

AFM Atomic Force Microscopy

ALP	Alkaline Phosphatase enzyme
ANOVA	Analysis of Variance
APTES	(3-Aminopropyl)Triethoxysilane
BCA	Bicinchoninic Acid
BIC	Bone Implant Contact
BMP	Bone Morphogenetic Protein
CHO	Chinese Hamster Ovary cells
CLSM	Confocal Laser Scanning Microscope
DCC	Dicycloheylcarbodiimide
DCM	Dichloromethane
DGEA	Cell Adhesion Peptide Aspartic Acid-Glycine-Glutamic Acid-Alanine
DMF	Dimethylformamide
DMSO	Dimethyl Sulfoxide
DPBS	Dulbecco's Phosphate-Buffered Saline
DNA	Deoxyribonucleic Acid
ECM	Extra Cellular Matrix
E. coli	Escherichia Coli
EDC	1-Ethyl-3-(3-dimethylaminopropyl)carbodiimide
EDS	Energy Dispersive X-ray Spectroscopy
EDTA	Ethylenediaminetetraacetic Acid
EDXF	Energy Dispersive X-Ray Fluorescence
ESEM	Environmental Scanning Electron Microscope
FAK	Focal Adhesion Kinase
FF-RGD	Fully Functionalised RGD Sample (Passivated-Polymerised-RGD immobilised Titanium Sample)
FITC	Fluoresceine Isothiocyanate
FITC-RGD	Fluoresceine Isothiocyanate Tagged RGD Peptide
GFOGER	Cell Adhesion Peptide Glycine-Phenylalanine-Hydroxyproline-Glycine-Glutamic Acid-Arginine
HA	Hydroxyapatite
HB	Hyperbranched
HBPG	Hyperbranched Polyglycerol
HEMA	Hydroxyethyl Methacrylate
HNO3	Nitric Acid

HNO3/H2O2	Nitric Acid/Hydrogen Peroxide Mixture
H2O2	Hydrogen Peroxide
HOBt	Hydroxybenzotriazole
IKVAV	Cell Adhesion Peptide Isoleucine-Lysine-Valine-Alanine-Valine
IPA	Isopropanol
JNK	c-Jun NH-terminal Protein Kinase
LRE	Cell Adhesion Peptide Leucine-Arginine-Glutamic Acid
LRGDN	Cell Adhesion Peptide Leucine-Arginine-Glycine-Aspartic Acid-Asparagine
MAPK	Mitogen-Activated Protein Kinase
MC3T3	Mouse Calvaria Preosteoblast Cell Line
MEM	Minimum Essential Medium
MRSA	Methicillin Resistant Staphylococcus Aureus
MSCRAMM	Microbial Surface Components Recognising Adhesive Matrix Molecules
MUP	Methylumbelliferyl Phosphate
NHS	N-Hydroxysuccinimide
NO3	Nitrate
NOX	Nitrous Oxides
OH	Hydroxyl
PEG	Poly(Ethylene Glycol)
PG	Polyglycerol
PGA	Poly(Glycolic Acid)
PHSRN	Cell Adhesion Peptide Proline-Histidine-Serine-Arginine-Asparagine
PJI	Prosthetic Joint Infections
PKC	Protein Kinase C enzyme
PLA	Poly(Lactic Acid)
PLGA	Poly(Lactic-Co-Glycolic Acid)
PMMA	Poly(Methyl Methacrylate)
P-value	Probability Value
PZC	Point of Zero Charge
Ra	Roughness Average
REDV	Cell Adhesion Peptide Arginine-Glutamic Acid-Aspartic Acid-Valine
RFU	Relative Fluorescence Units
RGD	Arginine-Glycine-Aspartic Acid Peptide

RGDfc	Integrin Binding Peptide Arginine-Glycine-Aspartic Acid-D-Phenylalanine-Cysteine
RGDfK	Integrin Binding Peptide Arginine-Glycine-Aspartic Acid-D-Phenylalanine-Lysine
RGDS	Integrin Binding Peptide Arginine-Glycine-Aspartic Acid-Serine
Rmax	Maximum Roughness Depth
ROMBP	Ring Opening Multi-Branching Polymerisation
ROP	Ring Opening Polymerisation
SAPK	Stress-Activated Protein Kinase
S. aureus	Staphylococcus Aureus
SBF	Simulated Body Fluid
SE	Standard Error
SMA	Slow Monomer Addition
SPM	Scanning Probe Microscope
TGF	Transforming Growth Factor
THF	Tetrahydrofuran
Ti6Al4V	Titanium alloy with 6% Aluminium and 4% Vanadium
Ti-O	Titanium Oxide
TiO2	Titanium Dioxide
Ti-OH	Titanium Hydroxide
UV	Ultra Violet
VAPG	Cell Adhesion Peptide Valine-Alanine-Proline-Glycine

1 Introduction

Over the last decade or so, interest in artificial materials and their importance in medicine have been growing. The field of tissue engineering was developed in order to serve the research need for artificial biocompatible materials as substitutes for damaged organs and tissues. Shortcomings of current traditional implants such as compatibility, early implant failure, and prolonged healing times, have yielded a general consensus which outlines the need for novel biomaterials as orthopaedic implants. Biomaterials are crucial for scientific research of artificial templates of the Extra Cellular Matrix (ECM), thus facilitating the study of ECM signals in controlling cell adhesion, proliferation, and differentiation (VANDEVONDELE *et al.*, 2003, WANG *et al.*, 2002).

Three main groups of biomaterials are generally considered for use as implants; inorganics (e.g. titanium, steel, and hydroxyapatite (HA)), organics (natural and synthetic polymeric structures), and inorganic-organic hybrids that combine the advantages of both. Great strides have been made in the way of HA coatings, mainly due to their inherent osteoinductive and osteoconductive properties, although exhibiting poor strength and brittleness; such coatings have a tendency to crack thereby causing implant loosening and failure. Polymer constructed organic biomaterials on the other hand, provide a cell supportive scaffold which degrades in vivo as host cells adhere and infiltrate. In time the organic coating diminishes, leaving behind only the implant material which is now colonised with host cells. This allows the implant surface to maintain an intimate connection with the host bone as it develops, forming a much stronger Bone-Implant Contact (BIC). However organic coatings have been shown to possess less than average osteoconductive properties, as well as little to no osteoinductive properties.

Two main strategies for the modulation of cell-material interactions exist when constructing biocompatible implants. One is the creation of a biologically inert surface that does not allow ECM proteins to adsorb readily and hence disallow cell adhesion. This prevents activation of the

immune system, and inflammatory and wound healing interactions between the material and surrounding cellular environment, and is used in the creation of heads and cups for joint prostheses (COOK *et al.*, 1997) for example. Another strategy is the modulation of a biomaterial to promote cell adhesion, proliferation, differentiation, and long-term cell functioning, an example of which is an orthopaedic implant that induces the formation of mineralised bone tissue at the bone-implant interface.

As our knowledge regarding the environment that is favourable to cellular tissue development expands, it becomes clearer how dynamic and biologically reactive an environment must be to support new tissue growth. Synthetically developed tissue engineering scaffolds present an obstacle in their role as the ECM. Such materials are unable to recreate the correct environment during tissue engineering to promote accurate tissue development. Thus, a synthetic biomaterial must possess properties to accommodate multiple cell types, respond to changes commanded by the cells (i.e. tissue remodelling), and introduce signals to these cells for tissue growth and maintenance. Inclusion of these properties has led to the development of polymers with reactive sites, open to modification for attachment of biomolecules, or sites engineered into the polymer backbone to aid enzymatic degradation (Dang and Leong, 2006). The development of next-generation engineered tissues aims to produce biological scaffolds, which can relay information to the ECM and cells to stimulate cell attachment, proliferation and growth. The use of biomolecules, such as growth factors and proteins, have been sought (usually animal derived) to manipulate the host healing response to facilitate tissue repair and tissue growth, thus developing bio-functionalised engineered tissues. The strategy is then one of biomimicry, imitating the ECM and endowing information or signalling for cell function to impart requirements of dynamic reciprocity for tissue engineering (Malafaya *et al.*, 2007).

2 Background Literature

2.1 Bone Repair around Osseous Implants

Bone repair around an orthopaedic implant is governed by three processes; osteoinduction, osteoconduction and osseointegration. Osteoinduction is accelerated new bone formation. It is a process in which undifferentiated and pluripotent cells (stem cells) are recruited and stimulated to develop into the bone-forming cell lineage, preosteoblasts and subsequently into osteoblasts (Figure 1). It can also be said that this is the process by which osteogenesis is induced (sometimes known as ossification, the process of laying down new bone material by osteoblasts). Osteoinduction can also be sub-defined as active (biological growth factor activity) or passive (nano/microstructure of biomaterial surface induces osteogenic cell differentiation, or osteostimulation) (DACULSIA *et al.*, 2013).

Osteoconduction is the process of bone growth on a surface, be it on existing bone or an orthopaedic implant. Osseointegration, described as the direct anchorage of an implant, is the direct contact of the host bone tissue with an implant surface, without the growth of fibrous tissue at the bone-implant interface. However, a more precise definition, with clinical application and from a biomechanical sense, is the process where the rigid fixation of an implant is successful and maintained in bone during functional loading, and that is cli'nically asymptomatic (Albrektsson and Johansson, 2001).

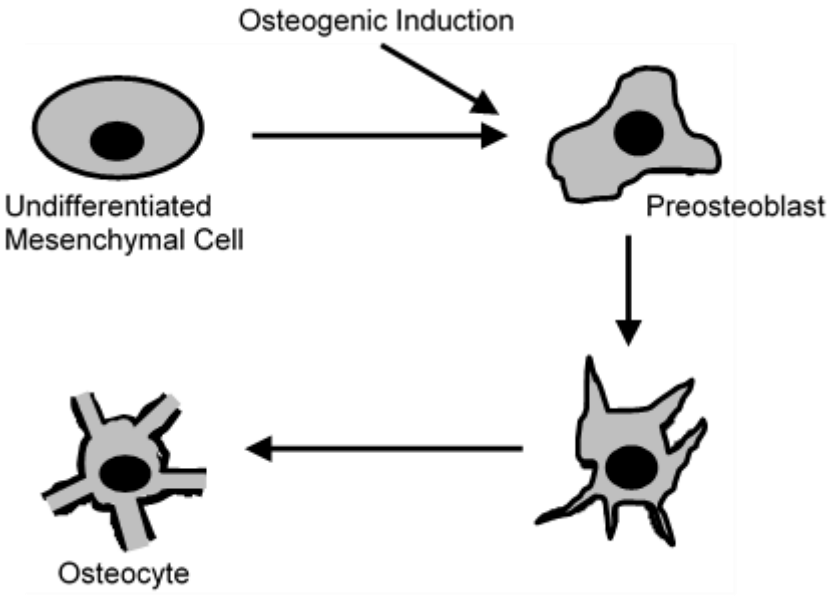

Figure 1 - At the time of bone damage/injury, pluripotent cells differentiate through the osteoinductive process into the bone-forming cell lineage (preosteoblasts) (Albrektsson and Johansson, 2001).

Bone healing differs from other musculoskeletal tissue in that it has an extraordinary ability to heal without scar tissue formation. The processes involved are determined by biomechanical stability and the biological environment. Bone healing depends on the supply of blood to the bone and the extent of bone damage and surrounding tissue: the greater the damage the slower the rate of bone healing. The bone healing pattern is often modified by external factors such as the mechanical environment (excessive movement of the implant may hinder osseointegration) which can in turn be influenced by surgical interventions. The mechanical environment, and hence stability of bone at the region of damage, is to ensure maximum biology of healing and reduce the time to bone union and function restoration (Westerman and Scammell, 2012, Wraighte and Scammell, 2006).

Principally bone healing can proceed via two mechanisms, both of which are dependent upon the mechanical and biological environment: primary (direct) and secondary (indirect). Primary

healing occurs when there is absolute stability (no motion between bone injury surfaces under load) i.e. with anatomical reduction and internal fixation procedures, and is commonly associated with intramembranous ossification. Secondary healing occurs when there is relative stability (some controlled micromotions between bone injury surfaces under load) i.e. with plaster cast treatment or external fixation (Wraighte and Scammell, 2006).

Bone healing following orthopaedic implantation occurs via the processes outlined in Figure 2 below. Initially, bleeding occurs which lasts for a few hours, after which vasodilation induces the supply of plasma and leucocytes, with macrophages that recycle the cellular and tissue fragments. Inflammation occurs and a subsequent clot involving platelets is formed, as cells synthesise growth factors that regulate cell proliferation, differentiation and migration. These growth factors are essential in the process as they play a crucial role in fabricating the ECM. The biological cascade proceeds with angiogenesis (growth of new blood vessels) at the site of healing, permitting cell metabolism to become viable. Mesenchymal stem cells differentiate into osteoblasts which head-up the formation of bone, and vascularisation allows the delivery of calcium ions, phosphorus ions and growth factors to be made and concomitant synthesis of a bony mineral matrix occurs (Ambard and Swider, 2006).

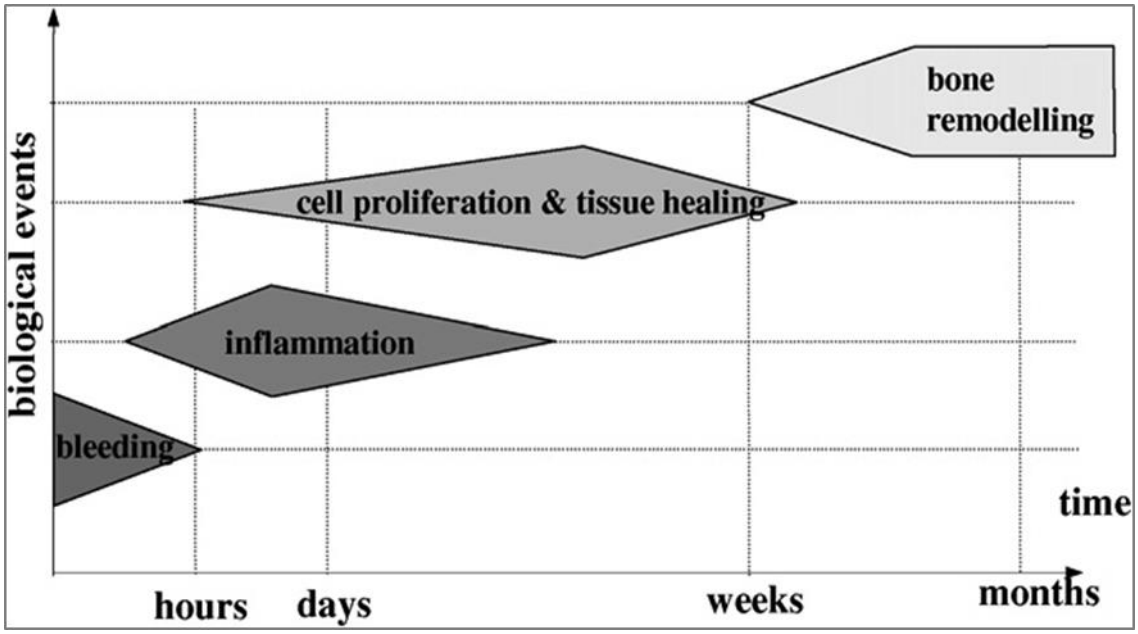

Figure 2 - Biological events of bone healing following orthopaedic implantation (Ambard and Swider, 2006).

Periprosthetic tissue healing is thus a process conducted by intramembranous ossification (mesenchymal stem cells differentiate into osteoblasts which secrete osteoid matrix that is later mineralised into woven bone), and the osteoid matrix conversion into bone precedes the formation of conjunctive fibrous tissue without an intermediary cartilage phase (a process seen in endochondral ossification) (Ambard and Swider, 2006). Therefore, successful clinical outcomes for orthopaedic implantation requires complete rigid fixation of the implant to promote bone healing via the primary healing pathway. This ensures maximum osseointegration of the implant; excessive mobility of the implant through micromotions greater than 150µm may induce the formation of a fibrous membrane around the implant, causing displacement of the bone-implant interface hindering osseointegration (Marco *et al.*, 2005, Kuzyk and Schemitsch, 2011).

2.2 Cellular Adhesion on Implant Surfaces

The surface features of titanium implants influence certain biochemical processes immediately following placement of the implant, and these dictate the success of the implant. Upon implant placement, water from the extracellular fluid surrounds and coats the implant surface, forming a hydration layer (SHARD and TOMLINS, 2006). The hydration layer facilitates the adsorption of proteins from the surrounding biological environment onto the implant surface, forming a surface protein layer; the conformation, composition, and orientation of which are possibly affected by the implant surface properties and topography (WILSON *et al.*, 2005, RAUT *et al.*, 2005, WEI and LATOUR, 2008).

Cells in the immediate vicinity of the implant adhere to the implant surface via the adsorbed protein layer, mainly through cell surface bound receptor mediated communication, creating a cell-protein surface bound interface (taking minutes to days to form following implant placement). Cell adhesion to the implant via the adsorbed protein layer is mostly initiated by cell surface bound receptors of the integrin family. Recognition by these receptors leads to the activation of signal transduction and biochemical secretions that trigger signalling for cell adhesion, proliferation, differentiation, and ECM deposition (CHANG and WANG, 2011). The orchestration of these complex biochemical interactions essentially leads to wound healing, tissue regeneration, and implant integration (Singhatanadgit, 2009). This wound healing phase is regulated by biological factors that include cell surface bound proteins, cytoskeletal proteins and extracellular proteins, environmental aspects of the ECM, cell behaviour, and may also be influenced to some extent by the implant surface chemistry and topography (RATNER and BRYANT, 2004, CHANG and WANG, 2011). The final response of the body to the inserted orthopaedic implant is the continuous development of the prior mentioned stages, resulting in

mineralised bone and subsequent remodelling of such active and functional bone (Singhatanadgit, 2009).

When anchorage-dependent cells attach to a surface that supports cellular growth, the cells go through a developmental process whereby their shape changes from almost spherical to discoid. During this stage, the formation of focal adhesions and plaques mediate adhesion to the surface (focal adhesions and plaques are constructed from an assemblage of transmembrane bound integrin receptors which secure the cytoskeleton to the ECM secreted by surface bound cells) (LIU *et al.*, 2007b).

Vogler expressed an adjunct theory to cell adhesion based on a study in which it was shown that cell contact through attachment, normally observed in cell culture medium, could also be replicated in the absence of proteins (VOGLER, 1988, VOGLER, 1989, VOGLER, 1993). In this study, a detergent solution was used to match the interfacial tension of serum-containing medium (Fetal Bovine Serum – FBS). This suggests that the early stages of cell attachment are also dictated by physical forces, and not significantly ECM production. Thus, implant surface chemistry could influence cell attachment to a greater degree than previously thought (LIU *et al.*, 2007b).

Liu and co-workers emphasize that cell attachment time is an important variable when correlating cell morphology to substratum properties, such as chemical topology. Their experience suggests that cell flattening on a surface is independent of the substratum compatibility with the cell. On surfaces with poor cell compatibility, cells remained round for a longer period of time when compared with compatible surfaces. Also on the poorly compatible surfaces, if the cells survived they would eventually flatten out and populate the surface. It was then suggested that the expression of morphological traits could be seen as delayed on poorly

compatible surfaces, where cells are occupied in an extended process of secreting ECM into their microenvironment in order to make the surface compatible (Liu *et al.*, 2007a).

2.2.1 Cell Adhesion and the Integrin Receptor

It has become more apparent that full and successful integration of an implant hinges on its ability to mimic normal physiological responses such as cell attachment, and as such cell adhesion is sometimes regarded as a 'condicio sine qua non' (an essential action without which it cannot be) for the effective applications of modern bioengineering, more so where the application is the implantation of a biomedical scaffold colonised by the patient's own cells (Costa e Silva Filho and Conde Menezes, 2004).

Cell adhesion to an implant surface dictates the development and maintenance of neo osseous tissue. Adhesion reactions of the implant surface with ECM components is essential for osteoblast survival, differentiation, proliferation, bone matrix mineralisation, and is also important for osteoclast functions related to bone remodelling. Cell adhesion pathways related to bone cells and ECM ligands involved in bone tissue repair, are mediated by the integrin superfamily of transmembrane receptors (Garcia and Reyes, 2005).

Native ECM proteins, such as fibronectin, laminin, vitronectin and collagen for example, contain the tripeptide sequence RGD (Arginine-Glycine-Aspartic acid) in their macromolecular structure which represents a recognition site for specific binding to integrin receptors that are present in virtually all cells. The interaction of these proteins with the integrin receptor (receptor-ligand binding) induces cell adhesion, adhesion strengthening and cell spreading on the surface presenting the RGD sequence (Garcia and Reyes, 2005).

Cell adhesion regulated by integrins encompasses four cascade events; cell attachment, cell spreading, actin cytoskeleton organisation, and focal adhesion formation. The first step is described as the initial attachment as the cell contacts a surface and some ligand-receptor binding occurs. Ligand-integrin binding leads to the association of integrins with actin filaments of the cell cytoskeleton, a process whereby the cell begins to flatten after which actin organises into bundles of microfilaments, also known as stress fibres. The final step concludes with the formation of focal adhesion points connecting ECM molecules to the cytoskeleton (Hersel *et al.*, 2003). The actin filaments cluster into focal adhesions that contain signalling and structural cues.

These focal adhesions are macromolecular complexes that link the ECM with the cytoskeleton and are essential for governing stable cell adhesion and migration. Focal adhesions combine with growth factors to activate signalling mechanisms such as: Mitogen-Activated Protein Kinase (MAPK), which regulates cellular functions such as gene expression, mitosis, differentiation, proliferation and cell survival; and the Stress-Activated Protein Kinase (SAPK) member of the MAPK, the c-Jun NH-terminal protein Kinase (JNK). These integrin mediated signalling pathways are crucial for the commitment of mesenchymal cells and osteoblast differentiation (Garcia and Reyes, 2005).

The cell spreading step is crucial and dictates whether a cell will survive. If the cell attachment is poor (i.e. non-immobilised ligand), the cell will not flatten and exhibit a more spherical structure which will lead to cell death via apoptosis (also known as 'anoikis' a Greek word meaning homelessness) (Hersel *et al.*, 2003), as loss of cellular adhesion deactivates the integrin receptor pathways leading to limited cell function (Schneider *et al.*, 2001). This mechanism is illustrated in the following Figure 3.

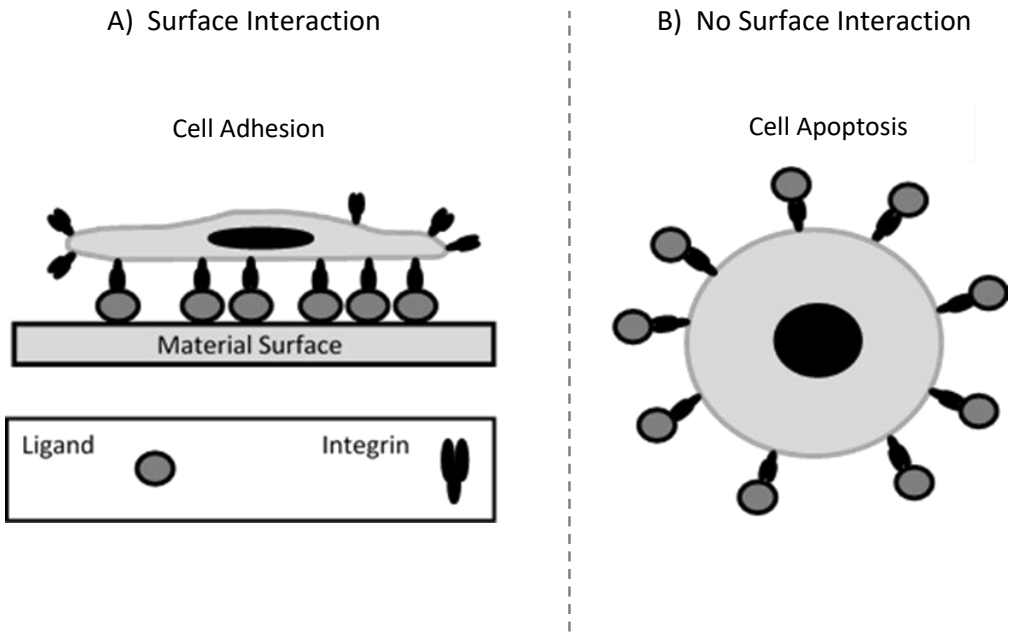

Figure 3 - Integrin-ligand binding effects. Ligands that are immobilised on a surface exhibit agonistic effects of the ECM, inducing cell adhesion and survival, whereas free flowing ligands antagonise and lead to cell detachment and apoptosis (Hersel et al., 2003).

The integrin transmembrane signalling receptors are unique in that they can relay signals in both directions (outside-in and inside-out). Once activated, signal transduction occurs via the aforementioned kinase proteins via phosphorylation and dephosphorylation events, leading to the up and down-regulation of cellular functions. This is the principal pathway that regulates bone cell functions from the initial attachment and adhesion of cells, right through to cell differentiation, proliferation and growth (Figure 5). Generally, ligand-receptor interactions bring about a physiological change in the responding cell, and can include responses such as differentiation, proliferation, migration, production of ECM components, as well as others (Figure 4) (de Boer *et al.*, 2008).

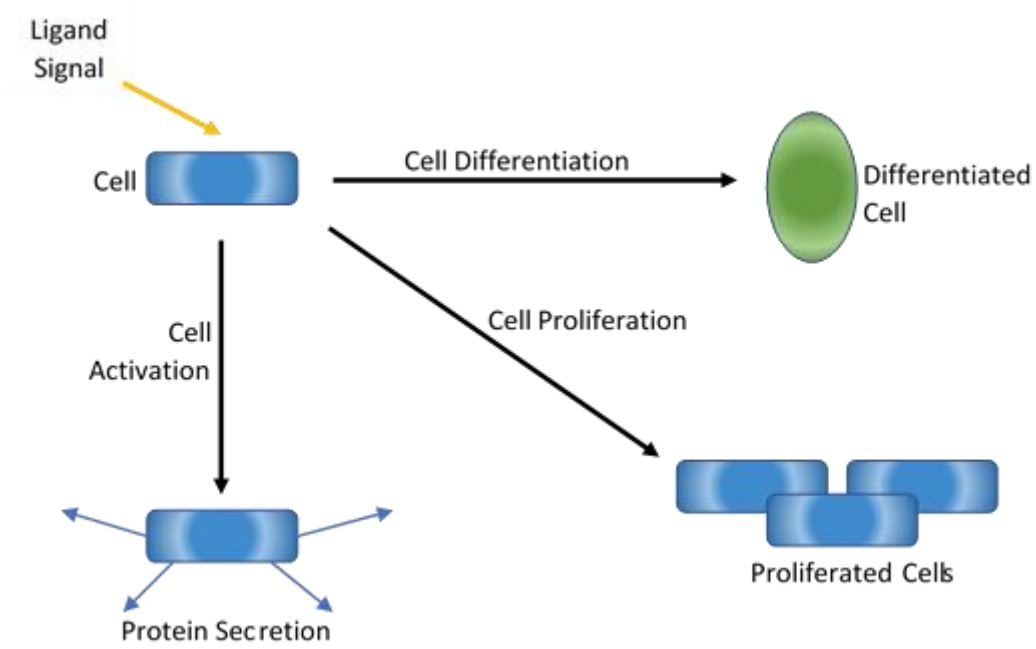

Figure 4 - Diagram illustrating cell signalling leading to 3 potential physiological responses by the responding cell (de Boer et al., 2008).

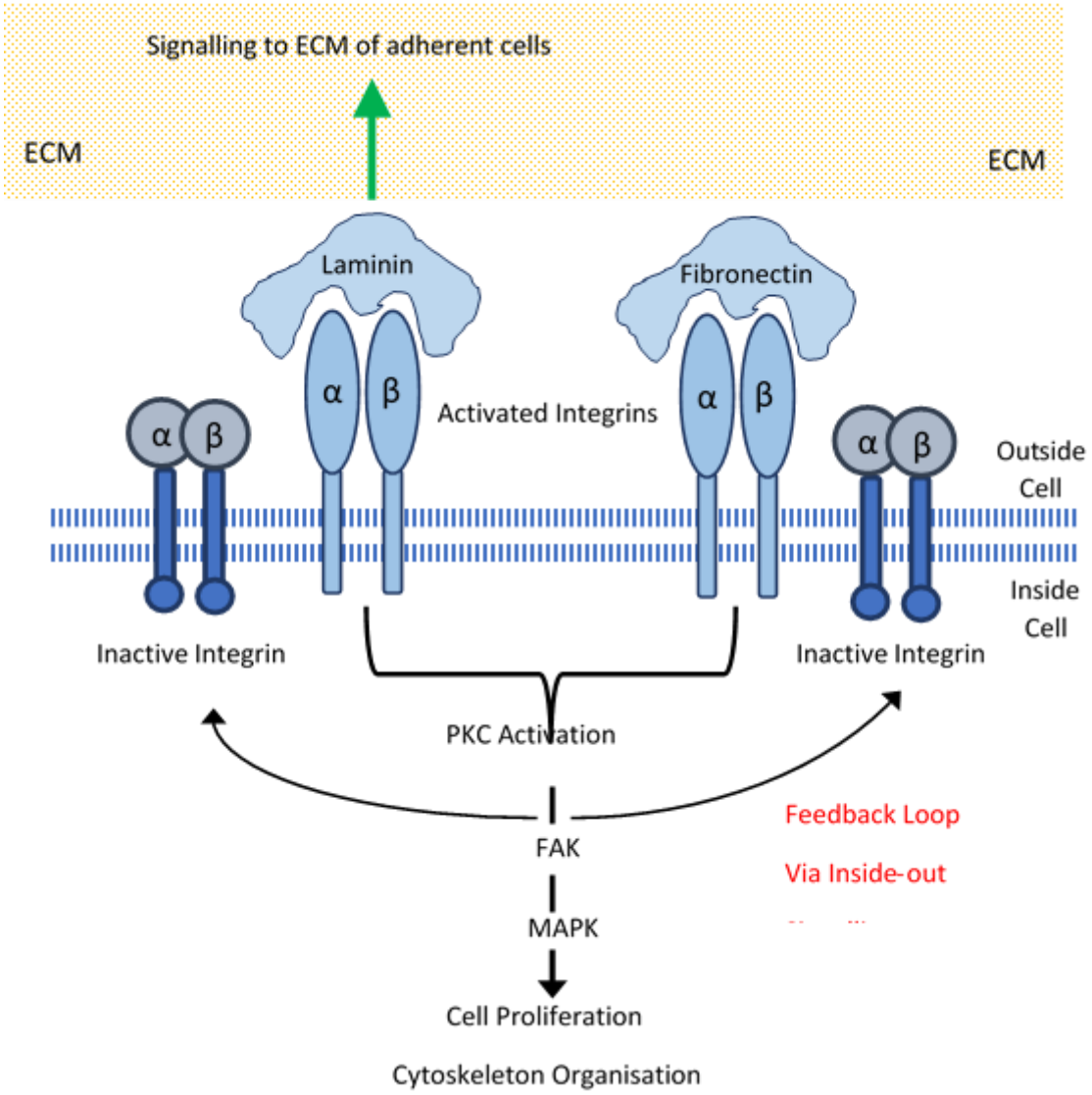

Figure 5 - Diagrammatic overview of the integrin-mediated activation leading to inside-out and outside-in signalling. Ligand-integrin binding activates Protein Kinase C enzyme (PKC) causing auto-phosphorylation of Focal Adhesion Kinase (FAK). This outside-in signal, as well as others, activates the Mitogen Activated Protein Kinase (MAPK) pathway, leading to cell proliferation and spreading. The inside-out signalling occurs when changes inside the cell affects the affinity of the integrin pair for its target ligand (de Boer et al., 2008).

2.2.2 RGD Cell Adhesive Peptide

The ECM contains multifunctional signalling cues in the form of proteins such as fibronectin, laminin and vitronectin that control the development and maintenance of cell functions. The transmembrane receptor, integrin, connects the cell cytoskeleton with the exterior ECM

through signalling pathways. Via this pathway, integrins relay information pertaining to cell adhesion, growth, division, survival, migration, cell differentiation, and apoptosis across the cell membrane.

Integrins are a superfamily of cell membrane receptors that regulate cell-to-cell and cell-to-matrix attachments. Integrins therefore play an important role in cell signalling and control the biological activity of cells, thus coating a titanium implant surface with integrin recognition motifs may enhance peri-implant osteogenesis (Singhatanadgit, 2009). Identifying small integrin binding oligopeptide sequences native to the ECM creates a therapeutic conduit to conjugate a tissue engineering scaffold with these biological cues, allowing biomolecular recognition of the surface by host cells.

A major limitation of tissue engineering scaffolds is their lack of cell specific adhesion, and research has investigated the use of cell adhesion peptides derived from ECM proteins which represent important cell adhesion targets. Cell adhesion peptides are usually derived from ECM proteins such as fibronectin (RGD, REDV and PHSRN peptides), laminin (IKVAV, LRE and LRGDN peptides), collagen (DGEA and GFOGER peptides) and elastin (VAPG peptide), and one of the most commonly researched peptides is RGD, a cell binding domain derived from fibronectin, laminin and collagen (Zhu, 2010).

ECM signalling proteins, such as fibronectin and laminin, contain a short tripeptide sequence known as RGD (Arginine-Glycine-Aspartic Acid) which can bind integrin receptors and induce cell adhesion signals. RGD enhances the osteoconductivity of many polymer scaffolds simply by attachment, and it has been extensively investigated to promote biomolecular recognition, cell attachment and function (van Gaalen *et al.*, 2008). Structurally RGD exists as linear and cyclic forms, although it has been discussed that the cyclic form plays an essential role particularly in terms of affinity and activity.

In vivo, RGD has been reported to increase osteointegration in some studies (ELMENGAARD *et al.*, 2005, Germanier *et al.*, 2006, Schuler *et al.*, 2006a), but not others (Petrie *et al.*, 2008, Barber *et al.*, 2007). The biological activity of RGD is less potent than that of native fibronectin or the fibronectin fragment FNIII7-10 (Garcia and Reyes, 2005, Petrie *et al.*, 2006). This suggests that the linear RGD peptide alone may be insufficient for optimal interaction of the cell with its substrate or extracellular matrix.

Some researchers provide the premise that the RGD sequence in the cell binding domain of fibronectin is exposed at the tip of a loop, generating a spatial constraint that leads to enhanced affinity for cell binding (Zhu, 2010). The cyclic RGD better mimics the native loop structure of the peptide in the source protein, benefiting cell specific adhesion (Zhu, 2010). The use of such short peptide sequences is founded on a principle that suitable sequences found in proteins, can lead to molecular constructs with affinity and activity similar to that of the entire protein, without the need of such a large molecule (Liskamp *et al.*, 2008). Thus, the cyclic peptide RGD tries to mimic the activity of the larger aforementioned proteins in a 'pars pro toto' method (a part taken for the whole). As the cyclic variant of the RGD peptide shows greater specificity and binding affinity to integrin receptors, a cyclic RGD peptide was utilised in this work, specifically cyclo-RGDfc (Figure 6). Due to their greater level of integrin activity, the cyclic RGD peptides are being actively researched (Heller *et al.*, 2018, Hahn *et al.*, 2017), although most of the research surrounding RGD peptides is based on cancer detection and targeting.

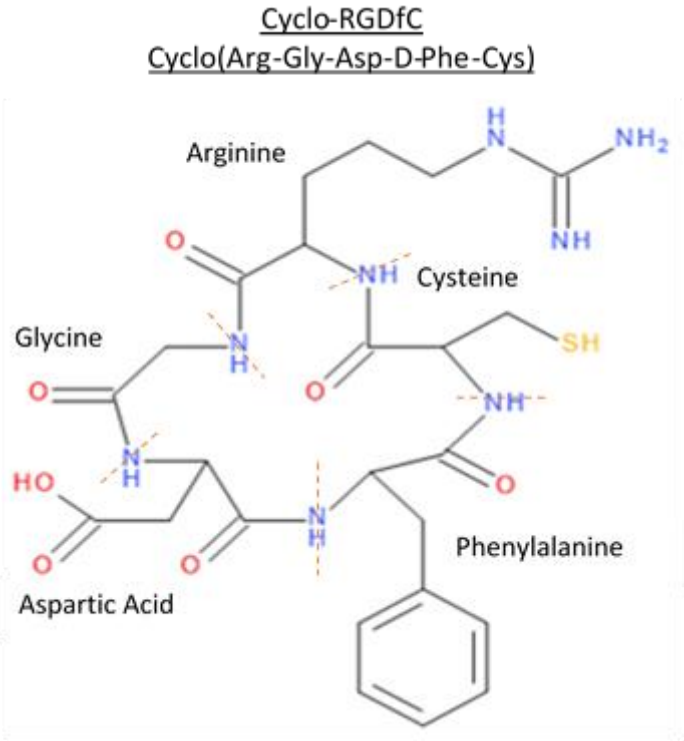

Figure 6 - 2-Dimensional structure of the cyclic RGD peptide cyclo-RGDfc. Structure adapted from peptide sales website (BACHEM) and drawn using Acelrys Draw software.

Integrins are transmembrane proteins consisting of two subunits, α and β that form heterodimers, of which over 20 have been elucidated (Anselme, 2000, GRONTHOS *et al.*, 2001, Hersel *et al.*, 2003). The combinations of the subunits will ultimately determine the ligand specific binding of integrin. RGD was an effort to take a macromolecular ligand and downscale it into a small recognition motif, and was first identified more than 30 years ago as a cell adhesion peptide sequence found in fibronectin. Integrins that have been investigated and known to bind to ECM molecules via the RGD sequence are α2β1, α3β1, α5β1, α8β1, αVβ1, αVβ3, αVβ5, αVβ6, and αVβ8, although the most highly researched integrins which have shown more prominent roles in osteoblastic adhesion and subsequent mineralisation are αVβ3, α2β1, and α5β1 (McCarthy *et al.*, 2004, Schneider *et al.*, 2001).

Most integrins can bind several ligands, such as α3β1 which binds laminin, collagen and fibronectin, and some ligands can activate more than one integrin; collagen and laminin can bind α3β1 and α2β1, whereas other integrins are specific for just one protein; α7β1 binds only laminin and αVβ6 binds only fibronectin (Verrier *et al.*, 2002). RGD is not the only cell adhesion motif and others have been found however, RGD is unique in its broad range of usage in that it can be programmed to bind just one target integrin or many (Hersel *et al.*, 2003). The following figure is a schematic and ribbon diagram of the αVβ3 integrin showing the spatial location of the RGD binding domain (Figure 7).

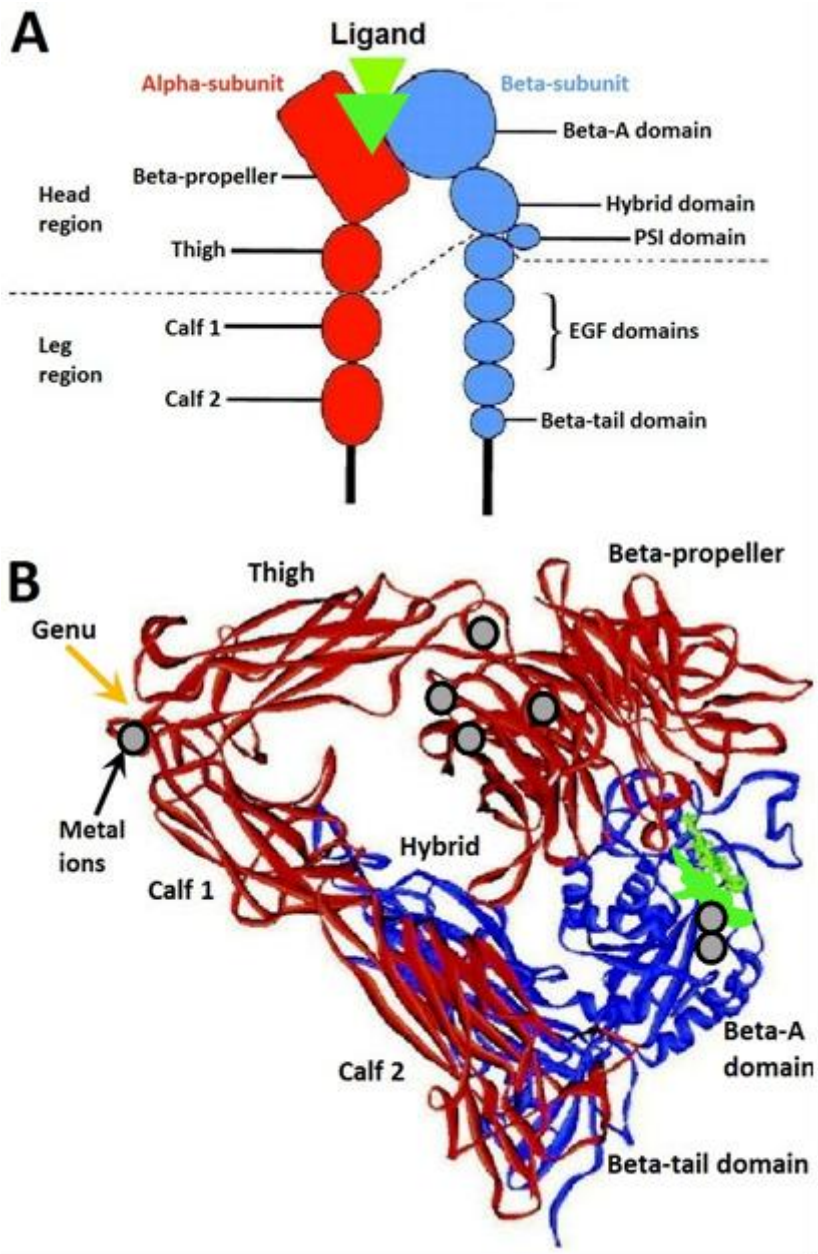

Figure 7 - Integrin structure: A) Structural diagram of integrin receptor, composed of a head region supported on two legs. Ligand binding takes place at the interface between the Beta-Propeller Domain and Beta-A Domain. B) Ribbon diagram of ecto-domain (domains extending into the ECM) of integrin αVβ3 in complexation with cyclic-RGD peptide ligand (in Green). The α-subunit is in red and the β-subunit in blue. Divalent calcium ions (silver spheres) Line the base of the Propeller and the top face of the Beta-A Domain. Protein is shown in closed form, which is bent at the 'Genu' (Indicated by Orange Arrow) (Askari et al., 2009).

The RGD sequence binds to a multitude of integrin species but the synthetic peptide provides many advantages for biomaterials use. The functionality of RGD is maintained even after post-processing techniques such as sterilisation, actions that would normally denature the source protein. Synthetic RGD negates the risk of immune responsiveness or pathogenic transfer which is problematic with xenografts (tissue transplantation from one species into another) or cadaver and animal sourced proteins. Modern chemistry techniques allow RGD to be fully conjugated to many material surfaces, organic and inorganic, at controllable distributions and orientations to maximise the potency of the peptide for binding. Lastly, RGD can be synthesised readily and inexpensively allowing direct translation of the therapy into the clinical setting (Bellis, 2011).

Although the design criteria for synthesising RGD containing peptides is sparse, the only mention being the addition of a few amino acids (found in the source protein) in front and behind the RGD sequence inferring similar abilities compared to the whole protein. Work done by Verrier and co-workers showed that the addition or removal of just one amino acid to the RGD sequence led to a reversal in cell adhesion from adherent to non-adherent, and vice versa. In fact they revealed that the addition of the amino acid serine after the RGD sequence (RGDS) inhibited the adhesion of vitronectin onto osteoprogenitor cells (Verrier *et al.*, 2002). This shows that the conformation and orientation of the amino acid residues is an important aspect in receptor recognition, the correct sequence of amino acids will dictate a conformational structure that will either allow cell adhesion or inhibit it (Lieb *et al.*, 2005).

The use of the cyclic RGD peptide over its linear analogue is preferred due to four main criteria; affinity, activity, degradation, and solubility. Studies by Verrier *et al* (2002) showed major advantages of using cyclic RGD compared with linear. Their results indicated enhanced affinity to vitronectin receptors and increased cell adhesion of cyclic RGD peptides to bone marrow stromal cells, with the highest observed cell adhesion efficiency. Furthermore, their quantitative

results exhibited increased cell adhesion to titanium at 3 hours and even after 24 hours, when the surface was derivatised with cyclic RGD, confirming that it is a good ligand substitute to the source protein (Verrier *et al.*, 2002).

Other authors also confirm the higher binding affinity of RGD containing peptides with integrin receptors (Bogdanowich-Knipp *et al.*, 1999b, Haubner *et al.*, 1996a). Haubner also demonstrated that cyclic RGD exhibits greater affinity to integrin αVβ3 and has a biological activity some 240 times that of the linear analogue (Haubner *et al.*, 1996b). This greater cell binding ability of cyclic RGD is important in promoting strong and rapid cell adhesion due to greater receptor affinity, especially when time is of the essence in situations such as the clinical setting (Hersel *et al.*, 2003).

Many studies have proven that the cyclic variant of RGD bears greater resistance to enzymatic and chemical degradation when compared to the linear constructs (Bogdanowich-Knipp *et al.*, 1999a, Verrier *et al.*, 2002). Bogdanowich-Knipp and co-workers state that this enhanced stability against degradation could be due to the rigid backbone of the RGD peptide resulting from cyclisation. They hypothesised that the chain rigidity prevents the carboxyl group on the aspartic acid residue from appropriately positioning itself for attack on the peptide backbone, increasing the stability of the cyclic peptide 30 fold over the linear variant at neutral pH (Bogdanowich-Knipp *et al.*, 1999a). Further experimental investigation indicated the presence of a salt bridge between side chain groups Arginine and Aspartic Acid residues in the cyclic peptide, most notably at neutral pH. This salt bridge in conjunction with decreased flexibility arising from the ring structure, imparts the cyclic peptide with great rigidity (Bogdanowich-Knipp *et al.*, 1999b). With regards to solubility, many synthesised RGD peptides are soluble in aqueous environments, although solubility can be enhanced by the addition of highly charged amino acid residues into the peptide structure.

Some authors have revealed that non-immobilised ligands for integrins cause apoptosis via 'anoikis' due to non-cell adhesion, as previously mentioned (Hersel *et al.*, 2003, Schneider *et al.*, 2001), and limited studies have shown negative results to RGD peptides in terms of cellular adhesion. However, Yang and co-workers studied RGD by simply coupling the peptide to a polymeric surface via electrostatic interactions on a porous implant surface, and subsequently inserted the samples into the femur and tibiae of adult white rabbits (Yang *et al.*, 2009b). They observed increased BIC and greater removal torque needed for the RGD coated implants compared to controls, indicating more bone tissue growth and enhanced osseointegration. Additionally, they observed no or very little sign of inflammatory reactions, possibly due to the RGD peptides exhibiting antithrombotic properties via restriction of fibrinogen-receptor interactions (Bogdanowich-Knipp *et al.*, 1999b).

2.3 Titanium Alloy Ti6Al4V and Surface Properties

Titanium alloys are generally classified into 5 groups; α, near-α, α+β, metastable β, or stable β depending on the microstructure at room temperature. The α and β refer to the metals used in the titanium alloying. Titanium can be alloyed with a multitude of elements falling into three main categories; 1) α-stabilisers (such as aluminium or carbon); 2) β-stabilisers (such as vanadium or molybdenum); and 3) neutrals (such as zirconium). The α and near-α alloys show considerable corrosion resistance with low temperature strength. Contrastingly, α+β alloys have higher strength as they possess both α and β phases. Finally the β phase provides such titanium alloys with a lower modulus of elasticity and enhanced corrosion resistance (Moore *et al.*, 2014)

Material properties hinge on the relative proportions of, and therefore composition of, the α and β phases (Moore *et al.*, 2014, Petrie *et al.*, 2008). The titanium alloy Ti6Al4V contains aluminium and vanadium (α+β alloy) therefore possesses excellent corrosion resistance, strength, and lower elastic moduli of ~100 GPa, when compared to more conventional stainless steel (~200 GPa) and chromium (~280 GPa) (Moore *et al.*, 2014, Benoit and Anseth, 2005, Rosales-Leal *et al.*, 2010). This titanium alloy has the closest tensile elasticity to that of human bone (~20 GPa), making it the far better choice as hard tissue replacements in artificial bones, joints and dental implants. Its low elastic modulus is a biomechanical advantage which results in lower stress shielding (Wolff's law).

The areas of bone that are subjected to the most resorption and formation are those where tension and compression dominate respectively, also known as Wolff's Law. Bone that is subjected to high compressive forces, or load bearing, will exhibit greater bone formation leading to denser, stronger bone. If load bearing forces are withdrawn from the bone, then tension will result in higher rates of bone resorption ultimately making the bone weaker (Moore, 2011). If an orthopaedic implant has strength and elastic moduli much greater than that of the surrounding bone tissue, load-bearing forces will shift onto the implant and away from the surrounding bone tissue, leading to bone resorption around the implant, and subsequently implant loosening. Therefore, the relatively low elasticity modulus of the titanium alloy Ti6Al4V ensures a more uniform transfer of stress across the implant and surrounding bone, preventing bone resorption.

The favourable properties of titanium and its alloys, such as corrosion resistance, ability for re-passivation, chemical inertness and biocompatibility, are thought to stem from the stability and structure of the native oxide layer on the titanium surface (Moore *et al.*, 2014). Like most metals, titanium can rapidly oxidise (even in normal atmosphere) spontaneously to yield a native

oxide layer just nanometres thick. Work done by Sano and Shiba show that titanium surfaces are uniformly coated with amorphous phase titanium dioxide (TiO_2) (Sano and Shiba, 2003).

The biocompatibility of titanium and its alloys is also thought to be derived from its ability to allow the nucleation of apatite crystals (HA) on its surface. It has been suggested that OH groups in the oxide layer directly induce apatite formation on exposure to biological fluids, and in vitro research has shown this to be the case when titanium, or its alloys, are subjected to Hank's solution or Simulated Body Fluid (SBF) (Pan *et al.*, 1996), both of which contain calcium phosphate ions for apatite nucleation. Even though the oxide film formed on the titanium surface is inert, the surface remains active. It reacts with moisture in air and in solution to rapidly form hydroxyl groups on the surface (Figure 8). The biocompatibility of titanium and its alloys is also linked with the oxide layer. A thicker oxide layer leads to a more wettable surface, and enhanced osteoblast ALP enzyme expression (a major indicator of osteoblast cell differentiation) (LEE *et al.*, 2012).

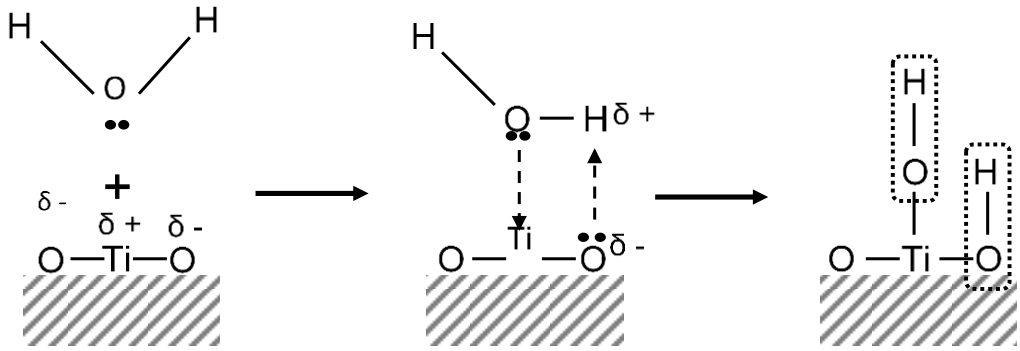

Figure 8 - Formation of hydroxyl groups on titanium oxide surface, from passivation/oxidation of (Hanawa, 2011).

When titanium dental implants are inserted into the jaw bone, calcium, phosphate and sulphur are reconstituted into the surface oxide film (Zhu *et al.*, 2004, ESPOSTITO *et al.*, 1999). Calcium phosphate is also formed on the surface of Ti6Al4V when it is used for fracture fixation. Furthermore, when titanium or its alloys are submerged in Hank's solution, calcium phosphate has been found to be deposited (HANAWA and OTA, 1991, HANAWA and OTA, 1992, HEALY and DUCHEYNE, 1992, SERRO *et al.*, 1997). These findings show that the physiological processes that occur in the body are well reflected by in vitro experiments.

The Point of Zero Charge (PZC) of the titanium oxide layer is roughly pH 5, meaning that at biological pH 7, the oxide layer is negatively charged. In vitro work conducted by Ellingsen showed that on exposure of the titanium oxide layer (TiO_2) to calcium, calcium deposited onto the negatively charged oxide layer, inducing selective protein binding (Ellingsen, 1991). This negative charge may also be an important factor in apatite nucleation, which occurs on OH-groups in the oxide layer. Although further information related to the properties and composition of the oxide layer is beyond the scope of this research, as it has been numerously dealt with in the literature.

Commercially pure titanium and the titanium alloy Ti6Al4V represent the gold standard materials for use as orthopaedic implants, due to their high biocompatibility, osteoconductivity and mechanical strength. Pure titanium naturally oxidises in air to form an oxide layer on the surface which prevents excessive corrosion however, and some research has disputed whether the native oxide layer on titanium is inert. Studies have shown that when implanted, the oxide layer of titanium implants can increase from around 5nm to some 200nm following 5 years of implantation, denoting that the titanium surface is continually oxidised (Mosser, 1992, HOSSAIN and GAO, 2008).

In vitro studies have also shown that mineral ions pass through the adsorbed protein layer on the titanium surface, changing the native oxide layer into complex phosphates of titanium and calcium containing hydroxyl groups and surface bound water (Zhu *et al.*, 2004). The vanadium portion of the Ti6Al4V titanium alloy helps to prevent further corrosion, making this titanium alloy a better choice; as the corrosion rate here is further reduced over pure titanium, there is less chance of titanium ions being released into surrounding tissue and causing foreign body reactions. Although there are still some reports that show continued passivation of the Ti6Al4V alloy in simulated bodily fluids (HANAWA and OTA, 1991).

There has been widespread research into improving the surface of such titanium alloys to promote osteoconductivity, and even osteoinductivity; such as nano-scale surface roughening, HA coatings, and biomolecules that could initiate and/or promote biochemical processes to achieve osseointegration (biomimetic coatings).

Modification of the titanium surface is the fundamental step to achieving complete osseointegration of orthopaedic implants, and has been an importantly researched avenue. Implant surface characteristics play a large role in the formation and maintenance of bone at the alloplastic surface (MASUDA *et al.*, 1998, Kieswetter *et al.*, 1996a). Such surface features include roughness, chemistry, hydrophilicity/hydrophobicity, and attached coatings; and these surface characteristics of the implant dictate the success, or failure, of osteoblastic cells to adhere to the implant surface. The most highly researched processes to modifying titanium surfaces include; sand-blasting, acid-etching, oxidising (otherwise known as passivation), plasma spraying, and calcium phosphate coating (or HA coating).

2.3.1 Wettability

The wettability of surfaces is a crucial physicochemical property of biomaterials that may regulate protein adsorption and hence cellular behaviour. When a biomaterial, such as an implant, is exposed to body fluid or a cell culture medium, the adsorption of ECM proteins on the material surface plays a critical role in the initial cell attachment process (WEI *et al.*, 2009). The hydrophilicity of implant surfaces is known to greatly influence cell response, and studies have shown that hydrophilic surfaces associate with greater cell adhesion (Goddard and Hotchkiss, 2007, XU and SIEDLECKI, 2007), it is therefore generally regarded in the scientific community that osteoblast cell adhesion is better achieved on hydrophilic surfaces (Altankov and Groth, 1994).

Chang reported that as a surface becomes more hydrophobic, the adhesion of osteoblast cells to the surface decreases (CHANG and WANG, 2011), although the hydrophilicity of a surface also affects other cell behaviour such as cell spreading and differentiation (WEI *et al.*, 2009, YILDIRIM *et al.*, 2010). Wei and co-workers demonstrated MC3T3-E1 Murine osteoblasts to exhibit a more fractal cellular morphology when seeded onto hydrophilic surfaces, while the 7F2 Murine osteoblast cell line has been shown to improve metabolic activity and differentiation on hydrophilic surfaces, with contact angles in the range 24-31°, when compared to hydrophobic surfaces with a contact angle of around 72° (YILDIRIM *et al.*, 2010, WEI *et al.*, 2009). Similarly Wei demonstrated that the murine osteoblast cell line MC3T3-E1 presented greater cell attachment within 3-hours on hydrophilic surfaces, and that such hydrophilic surfaces promoted the adsorption of the cell adhesion promoting protein fibronectin (WEI *et al.*, 2009).

Hydrophilicity of the implant surface affects the hydration layer formed, such as the rate of formation and extent of hydration; and the hydration layer is important in dictating the adsorption of the subsequent protein layer. Not only does the hydration layer facilitate the

adsorption of ECM proteins to the implant surface, but it also permits the reorganisation of these proteins. On extremely hydrophobic substrates, the adsorbed cell-adhesion mediating proteins become stiff and resistant to reorganisation. If the adsorbed proteins cannot reorganise, their specific amino acid sequences that constitute the cell adhesion motif, may not be accessible to cell-surface bound integrin receptors, thereby preventing cell adhesion (GARCIA *et al.*, 1999, GROTH *et al.*, 1999).

The adsorption of cell adhesive serum proteins, such as fibronectin and vitronectin, play crucial roles in the adhesion of cells to a biomaterial surface (GRINNELL and FELD, 1982, HORBETT and SCHWAY, 1988, STEELE *et al.*, 1992). When a biomaterial surface is exposed to cell medium containing serum, the protein albumin (which is one of the most abundant serum proteins) is expected to preferentially adsorb onto the surface at the early stages of formation of the adsorbed protein layer. It is then assumed that albumin will be competitively displaced by cell adhesive proteins (Arima and Iwata, 2007). A study by Wei in which surfaces of varying contact angles were exposed to cell medium containing a mixture of fibronectin and albumin, was conducted to test the competitive adsorption of these two proteins to such biomaterial surfaces. They demonstrated that on hydrophilic surfaces, fibronectin was able to displace albumin and hence achieve greater initial cell attachment of murine osteoblast cells. Whereas on hydrophobic surfaces albumin dominated, thus lowering the cell attachment of osteoblast cells within 3 hours of incubation (WEI *et al.*, 2009).

Through the many studies that have been performed in the scientific community, it is now generally regarded that hydrophilic surfaces are better for cell adhesion (Altankov and Groth, 1994), due to the permitted adsorption of cell adhesive proteins, and allowing their composition and reorganisation in order to better recognise cell-bound integrin receptors.

2.3.2 Surface Charge

Polymer surfaces with neutral hydroxyl functional groups have been shown to exhibit better cell adhesion than negatively charged carboxyl groups. It is thought that specific hydrogen bonding between the material surface hydroxyl groups of the polymer and polar groups of the cell surfaces are responsible (LEE *et al.*, 1991, CURTIS *et al.*, 1983). Similarly, Lee *et al* (1994) demonstrated better cell growth on neutral hydroxyl group surfaces than negative carboxyl groups. Positively charged and neutral functional groups surfaces show better cell adhesion and cell growth than negatively charged ones possibly due to the abundant ECM proteins that are negatively charged, such as fibronectin and vitronectin, thus exhibiting strong electrostatic interactions. A greater level of attachment of these specific proteins to a surface directly influences cell adhesion and hence cell growth (LEE *et al.*, 1994).

Principally, there are three ways in which implant surface charge can influence cellular responses; surface charge density, charge polarity, and the type of functional group. Jung et al demonstrated that as the surface charge density of poly(styrene-ran-acrylic acid) was increased, cultured cells exhibited greater adhesion and proliferation (JUNG *et al.*, 2008). Studies have also shown that ionic polarity is also a determining factor for biocompatibility, cell affinity, and differentiation on implant surfaces (Bet *et al.*, 2003), as demonstrated by Schneider *et al* (2004). Their research showed that when the 2-hydroxyethyl methacrylate (HEMA) hydrogel was incorporated with positive charges, seeded osteoblast cells exhibited higher cell attachment and spreading (SCHNEIDER *et al.*, 2004).

Work conducted by Lee et al showed that various functional groups with differing charges can also modify cell behaviour (LEE *et al.*, 1994). They prepared polyethylene surfaces with different functional groups (carboxylic, hydroxyl, and amine). When seeded with Chinese Hamster Ovary (CHO) cells, they found greater cell adhesion on the functional group grafted surfaces than

controls. They hypothesised that the cause could be related to increased wettability of hydrophilic functional groups. It is also theorised that surface charges modulate protein adsorption onto the implant, thus affecting integrin binding and specificity (CHANG and WANG, 2011).

Keselowsky *et al* showed that different functional groups with varying charges could modify the adsorption of fibronectin to surfaces, thereby controlling osteoblast cell adhesion by directing integrin binding (Keselowsky *et al.*, 2003). They concluded that MC3T3 osteoblast cell adherence to fibronectin surfaces was greater on the hydroxyl grafted surface, followed by carboxylic (which is comparable to amine). Keselowsky also demonstrated that amine and hydroxyl grafted surfaces up-regulated osteoblastic gene expression, Alkaline Phosphatase (ALP) enzyme activity, and bone matrix mineralisation (Keselowsky *et al.*, 2005). Finally, Schmidt reported that neutral hydrophilic hydroxyl groups promoted osteoblast differentiation (including positive hydrophilic amine groups), while negative hydrophilic carboxyl groups facilitated osteoblast attachment (SCHMIDT *et al.*, 2000).

2.3.3 Surface Roughness

Varying surface roughness and topographies can be achieved through different surface modification techniques such as plasma-spraying, anodic oxidation, sand-blasting, and acid-etching. Sandblasting typically uses micron-scale particles to produce a micro rough surface, whereas acid-etching produces roughness at the micron and sub-micron level (ZHAO *et al.*, 2007).

Studies have numerously shown that osteoblast cell adhesion, proliferation and cell spreading is enhanced on smoother surfaces. And on the other hand, rougher surfaces stimulate better

cell differentiation. Studies have shown that osteoblast cells cultured on rougher surfaces exhibited elevated levels of ALP enzyme and osteocalcin bone protein. Therefore on rough titanium surfaces, osteoblasts alter their microenvironment to one which is more osteogenic to regulate bone remodelling, which is characterised by the release of local factors to promote cell differentiation (BOYAN *et al.*, 2003). These results are in agreement with animal studies that have demonstrated enhanced BIC on rougher titanium surfaces (BUSER *et al.*, 1991), as well as greater torque removal from bone pull out testing (WENNERBERG *et al.*, 1997, KLOKKEVOLD *et al.*, 1997).

Numerous studies have shown that implant surface changes in topography affect cell adhesion. In vitro research tells us that osteoblast cell attachment, proliferation, and cell spreading are all increased when grown on smooth surfaces (Anselme and Bigerelle, 2005), although rougher surfaces have shown to exhibit better cell differentiation, bone matrix mineralisation, and growth factor production (Ji *et al.*, 2008). Again, SEM studies of bone cells grown on materials of varying roughness, exhibited better cell spreading and continuous cell layer formation on smooth surfaces compared to rougher ones (Anselme, 2000, Kieswetter *et al.*, 1996b).

However, it is not so 'cut and dry', the literature is riddled with conflicting results. Bowers and Stanford showed a higher number of adherent primary cultured osteoblasts on rougher surfaces (BOWERS *et al.*, 1992), while other studies showed a decrease in cell attachment (HULSHOFF *et al.*, 1995, LOHMANN *et al.*, 2000, MUSTAFA *et al.*, 2000). This could be due to certain studies not adequately controlling other surface characteristics between sample groups such as surface charge and wettability.

It is hypothesised that reduced cell proliferation is preceded by expression of the more differentiated phenotype (LIAN and STEIN, 1992, STEIN *et al.*, 1990). Therefore, cells cultured on rougher surfaces may present at a later stage of differentiation than cells grown on smoother

surfaces. It has also been suggested that differences between immature and mature cells indicates that cell maturation is a more crucial factor in cell response than the cell type or species (Kieswetter *et al.*, 1996b).

Many studies have evidenced that implant surface roughness can increase the BIC much more early after implantation, leading to early osseointegration of the implant (Cooper, 2000). Other studies have shown that surface roughness of titanium implants can alter the biosynthetic ability and differentiation of adhered osteoblast cells. Cooper explained that one of the mechanisms causing this phenomenon could be a modification in the expression of bone matrix proteins (Cooper, 2000). ALP activity and osteocalcin were shown to be expressed at a more elevated level on rougher titanium surface (Davies, 1998), and Martin explained that this was especially the case when cells were grown on sand blasted and acid etched surfaces compared to machined titanium surfaces (MARTIN *et al.*, 1995). Similarly, it was demonstrated that micron and sub-micron roughened surfaces yielded advantageous bone tissue formation when using osteogenic cell culture models (ZINGER *et al.*, 2004, WIELAND *et al.*, 2005). In addition, Schwartz and co-workers showed that micro and sub-micron roughened surface topography promoted the early development of mineralised bone matrix, which was not apparent on machined smooth surfaces (SCHWARTZ FO *et al.*, 2007).

Of the many ways in which surface roughness can be achieved on titanium implants, passivation has been highly researched; where the passivation solution is generally a mixture of hydrogen peroxide and an acid. Acid etched surfaces have been shown to promote the formation of bone-like nodules in rat osteogenic subcultures (WIELAND *et al.*, 2005). Bone nodule formation is a key factor of osteoblast differentiation, and are formed by differentiated osteoblasts, thus bone nodule formation can be a marker for the differentiation of osteoblasts. Bone nodules formed by differentiated osteoblasts represent counterparts to differentiated osteoclasts and bone

resorption. The balance between these two processes, also known as bone remodelling, is vital for the formation of healthy bone tissue.

It has been reported that nano surface topography achieved through passivation of titanium surfaces using sulphuric acid and hydrogen peroxide (Piranha solution), yields greater osteoblast proliferation whilst inhibiting fibroblast growth. And Vetrone and colleagues found that nano topography of titanium substrates increased extracellular accumulation of the bone proteins osteopontin and bone sialoprotein, indicating accelerated cell differentiation, and more efficient protein adsorption on such nano roughened surfaces (Vetrone *et al.*, 2009). Many other in vitro studies have also shown significant increases in osteoconductivity by facilitating mesenchymal stem cells and osteogenic cells attachment and proliferation, when performed on nanoscale surface features (but not smooth surfaces) (Depprich *et al.*, 2008, Qin *et al.*, 2016, Moore *et al.*, 2013, Steinhilber *et al.*, 2011, Wei *et al.*, 2014, Mabilleau *et al.*, 2006).

The topic of surface roughness on cell function has been actively debated, and yet it is unclear whether micro surface features perform better than nano, or vice versa. Research conducted by Dalby and co-workers has shown great potential for nanostructured surfaces. Their work has demonstrated strong responses from mesenchymal cells and osteoprogenitors to nanoscale surface features, with increased levels of osteocalcin and osteopontin, two of the most important matrix proteins in bone healing (Drelich *et al.*, 2011). Their work implicates nanostructured surfaces to facilitate implant osteoinductive properties by enhancing osteoblast differentiation of osteoprogenitor cells.

Dalby also hypothesised that progenitor cells are much more responsive to surface topography than mature cell types, in that they are vigorously seeking out surface signals from the microenvironment (Yang *et al.*, 2009a). Although the mechanisms behind this phenomenon are not well known, it could be possible that optimally sized nano surface features, such as pits,

pores and cracks, allow stem cell elongation influencing cytoskeletal stress, and subsequently promoting stem cell differentiation to the osteoblastic cell lineage (Singhatanadgit, 2009).

Although the mechanisms by which biomaterial surfaces affect cellular function are elusive, Davies hypothesised that acid-etched titanium implant surfaces enhanced the wettability of the surface and improved clot retention, resulting in better wound healing and osseointegration, possibly due to the mechanisms that encourage osteoconduction at the implant surface (Davies, 1998). However, research presents contradictory evidence of the influence of surfaces features on osteoblast cell functions.

2.3.4 Biologically Active Molecules

As well as modifying biomaterial surfaces to enhance biological action, certain biomolecules can be attached to implant surfaces in order to initiate cellular responses. The most widely researched biomolecules for such functionalisation methods include those of the Transforming Growth Factor (TGF) superfamily, particularly the Bone Morphogenetic Proteins (BMPs), and the RGD cell adhesive peptide.

The use of peptides and growth factors to functionalise implant surfaces was conceptualised from the hypothesis that imitating the in vivo environment of bone could enhance implant performance, promoting the initial biological response, otherwise known as biomimesis. Biomolecular functionalisation of implant surfaces has attracted a lot of research interest from the scientific community in recent years, as these bio-functionalised surfaces could reduce unspecific protein adsorption that leads to fibrotic capping, improve attachment of osteogenic cells with a view to enhance BIC, and present receptor-mediated signals to invoke the bone healing response (RAMAZANOGLU and OSHIDA, 2011).

The general architecture of the so called biomimetic surface is short oligopeptide or carbohydrate ligands for integrin or proteoglycan receptors, respectively, to promote interactions between the biomaterial surface and surrounding cells, often leading to improved cell adhesion, proliferation, and/or differentiation. An advantage of using such biomolecules negates the need for the entire protein molecule, preventing inflammatory responses, thrombosis, and even device-associated infections (TANG *et al.*, 1998, VANDEVONDELE *et al.*, 2003). Other advantages include cell selective response, allowing one cell type to flourish over others, thus preventing fibrosis for example.

The use of BMPs adsorbed onto orthopaedic implants has led to wide spread research in order to induce and maintain implant osseointegration (Bessho *et al.*, 1999, BOYNE and JONES, 2004, Liu *et al.*, 2005, WIKESJO *et al.*, 2002). Although promising as they are, such factors must be released in a controlled method progressively into the microenvironment surrounding the implant. BMPs have the ability to induce differentiation of stem cells to the osteogenic cell line, and enhance the proliferation of newly formed bone cells. If BMPs are released into systemic circulation, they could cause bone formation in other organs, the kidneys in particular, therefore causing severe damage to health (HARWOOD and GIANNOUDIS, 2005, RIPAMONTI *et al.*, 2001).

A new approach to the use of biomolecules is Platelet-Rich-Plasma (PRP). In PRP therapy a small fraction of the patient's blood is prepared, containing a high concentration of platelets, or thrombocytes (cells that clump together forming a blood clot and stopping bleeding). Its composition is mainly a fibrin matrix (fibrin is a protein found in the blood clotting process) in which platelets are dispersed. In addition to the platelets, PRP also contains various growth factors and cytokines, which can influence cell behaviour directly (Tejero *et al.*, 2014). PRP has been utilised in dental implant surgery to potentially enhance the bioactivity of titanium. Centrifugation of the patient's own blood is all that is required to obtain PRP, it is then deposited

onto the titanium implant as a gel. PRP coating if titanium has shown improved bone regeneration (Tejero *et al.*, 2014). The action of PRP begins at the early stages of titanium implantation, and supports a provisional 3D fibrin matrix with a complex environment over the titanium. PRP then facilitates neovascularisation (new blood capillary formation) and osteoblast cell recruitment, thereby enhancing titanium osseointegration, and contributing to implant success (Inchingolo *et al.*, 2015).

Another heavily researched biomolecule is the RGD peptide. This tripeptide is natively found in the structure of bone matrix proteins such as fibronectin and osteopontin. It interacts with a superfamily of cell bound receptors known as integrins that are crucial for cell to cell attachments, as well as cell to ECM attachments, playing a major role in cellular signalling and thus controlling biological activity. The interaction of cells with an implant surface is mainly mediated by integrin receptors which bind the RGD portion of certain ECM bone proteins, facilitating cell adhesion and signalling through biochemical transduction mechanisms. Research has numerously shown the positive effects of RGD to promote cellular adhesion to implant materials, and increase osteoblast differentiation, thereby enhancing peri-implant osteogenesis (SCHLIEPHAKE *et al.*, 2005), and bone to implant bonding (Yang *et al.*, 2009b), leading to enhanced fixation of mechanical implants, with decreased fibrous tissue capping (ELMENGAARD *et al.*, 2005).

It is thought that RGD presenting biomaterial surfaces improve cellular adhesion to the implant surface earlier after implantation, and promote bioactivity of adhering cells, leading to early cell differentiation attributed by higher ALP enzyme levels (Singhatanadgit, 2009). Similarly, in vivo research utilising animal models has suggested that implants coated with integrin binding sites can improve BIC and peri-implant bone formation (SCHLIEPHAKE *et al.*, 2005), while other

studies have suggested that RGD functionalised implant surfaces may promote bone formation during the early bone regeneration stages (Benoit and Anseth, 2005).

Generally, the RGD peptide is considered a more sustainable solution than BMPs; as the peptide must be immobilised onto the implant surface, there is no concerns with biomolecule release into surrounding tissues, and subsequent ectopic bone formation.

2.4 Natural and Synthetic Biopolymers

Organic biomaterials, such as natural and synthetic polymers, have been utilised in medicine for many decades. Due to their ease of synthesis and subsequent modification to tailor properties such as chemical composition, structure and reactivity. Thus, they have been extensively researched for tissue engineering purposes as most of them can be, or are made to be, biologically compatible and degrade into harmless by-products in vivo. These researches have culminated in the ubiquitous use of polymeric materials to be inserted into the body and successfully used as hard and soft tissue substitutes (Chang, 1981).

The use of natural biopolymers has stemmed from trends in biomimicry where the general idea is that materials from nature should be able to repair said nature. Natural biopolymers demonstrate how properties exhibited by biological systems are established by the physicochemical properties of the constituent monomeric sequence. Thus, a well characterised structure can result in a plethora of complex functions at the mesoscale. This is where structural flexibility, interactions and functional properties are tailored by the chain of monomeric sub-units (Malafaya *et al.*, 2007).

2.4.1 Natural Biopolymers

Fundamentally three types of natural polymers exist; protein based (e.g. collagen), polysaccharide based (e.g. Chitosan) and peptide based; which are also known as biopolymers (polymers existing in organisms, such as protein and DNA). All three types of natural polymers have been suggested, and highly researched, for their use in tissue engineering. The relatively low toxicity, interactions with living cells, and biological compatibility of these polymer types, have led to their numerous research in the literature. Protein based polymers have a distinct advantage as they can mimic certain features of the ECM to direct cell migration, growth and organisation during tissue regeneration and wound healing. Polysaccharide based polymers also show similar properties but have lower costs compared to other biopolymers such as collagen (Malafaya *et al.*, 2007). A major advantage of natural polymer coatings in bone tissue engineering, is that that are able to activate specific biological signalling pathways, induce cell adhesion, and modify bone remodelling (Civantos *et al.*, 2017).

Drawbacks of natural polymers are their batch variation possibility (due to animal sources), narrow and limited range of mechanical properties, and conventional methods used to produce polymers may find it difficult to process naturally derived polymers. Also, natural polymers derived from animal sources can exhibit some level of immunogenicity and could potentially carry infection. Although recombinant technologies can be sought to overcome these problems as well as eliminate polydispersity, and control defined properties. These naturally derived polymers also have the advantages of biocompatibility, cell-controlled degradation, cellular interactions, as well as the predictable placement of cross-linkers, addition of biomolecules at specific sites along the chain or programmable degradation, making them very attractive for tissue engineering purposes (Gomes *et al.*, 2008).

When considering natural polymers from a manufacturing viewpoint, their composition is far more complex than synthetic polymers. Also, synthetic polymers can be synthesised and modified through a wide variety of chemical techniques, with defined and well-known compositions. Contrastingly, natural polymers present complex structures, making it very challenging to synthesise them homogeneously, therefore possibly limiting their use clinically (Civantos *et al.*, 2017).

The polysaccharide-containing ECM component, Glycosaminoglycans (GAGs), have been applied to implants and found that they interact with surrounding cells, increasing implant biocompatibility (Goodman *et al.*, 2013). The GAG, chondroitin sulfate (CS) has been shown to bind ECM molecules and interact with osteoblast cells, accelerating ECM-binding to integrins and facilitating the formation of focal adhesions, improving cell attachment (Goodman *et al.*, 2013).

Type I collagen is a natural biopolymer that makes up a large part of the bone ECM, making up approximately 90% of the osteoid phase. An osteoinductive biomolecular coating, it is one of the most highly studied proteins to improve implant surface bioactivity (Civantos *et al.*, 2017). Sartori and colleagues functionalised titanium surfaces with type I collagen, and when these implants were inserted into the femoral condyle of healthy and osteopenic (low bone mineral density) rats, the total bone-implant contact, as well as bone ingrowth, was increased (Sartori *et al.*, 2015).

A very new therapy which utilises natural biopolymers is Platelet-Rich-Plasma, a small fraction of the patient's blood that contains a high concentration of platelets, or thrombocytes, cells which clump together and clot so as to prevent bleeding. PRP is composed of a fibrin matrix (a blood clotting protein) in which the platelets are dispersed. PRP also contains various growth factors and cytokines, which can influence cell behaviour directly (Inchingolo *et al.*, 2015). PRP

has already been utilised in dental implant surgery to enhance the bioactivity of titanium. From centrifugation of the patient's blood, the resultant PRP is deposited onto the titanium implant, and has been shown to improve bone regeneration (Inchingolo *et al.*, 2015). The action of PRP begins at the early stages of titanium implantation, supporting the 3D fibrin matrix with complex environments around the titanium. PRP also facilitates neovascularisation and osteoblast cell recruitment, speeding up osseointegration times (Tejero *et al.*, 2014).

2.4.2 Synthetic Biopolymers

Synthetic polymers have been commonly used in medicine for decades. Their ease of synthesis, biocompatibility and high modifiability to precisely alter chemical and physical properties, have made them a popular biomaterial for use in tissue engineering. This allows tailoring of biopolymers to provide a range of properties that are more predictable, giving a clear advantage over natural biopolymers. As such synthetic biopolymers are the primary material of choice for the fabrication of scaffolds in tissue engineering applications. Polymers that have been approved for use in biomedical applications, and thus are in use, include poly(lactic acid) (PLA), poly(glycolic acid) (PGA), poly(ethylene glycol) (PEG), and poly(methyl methacrylate) (PMMA) to name but a few. Although the biopolymers PLA, PGA (and their co-polymer poly(lactic-co-glycolic acid) or PLGA), and PEG are the most extensively researched and the most popular for tissue engineering applications (Liu *et al.*, 2007a, Ramakrishna *et al.*, 2001). And the degradable synthetic polymer, polyphosphazenes, is currently under clinical stage investigation.

Due to the ability of modifying synthetic biopolymers, important aspects such as size, shape and degradation can be precisely controlled, giving rise to structures such as solids, fibres, fabrics, films and gels. Through chemical modification, synthetic biopolymers can be altered to degrade

in vivo yielding harmless by-products. This can be via simple hydrolysis or enzymatic cleavage of chemical linkages. Also, by introducing further degradable bonds, or altering existing ones, the degradation rate of the biopolymer can be precisely controlled. This is an important factor as previously mentioned, the degradation rate of the biological scaffold may influence implant success.

A synthetic biopolymer that has garnered much attention in recent years in polyglycerol (PG). Scientists have shown great interest in PG as it is non-toxic and biocompatible, eliciting extremely low levels of foreign body interactions. This research has used polyglycerol (PG) as a tissue engineering scaffold, and an anchor for the conjugation of the bioactive peptide RGD, and more detailed information relating to this polymer will be explained forthwith.

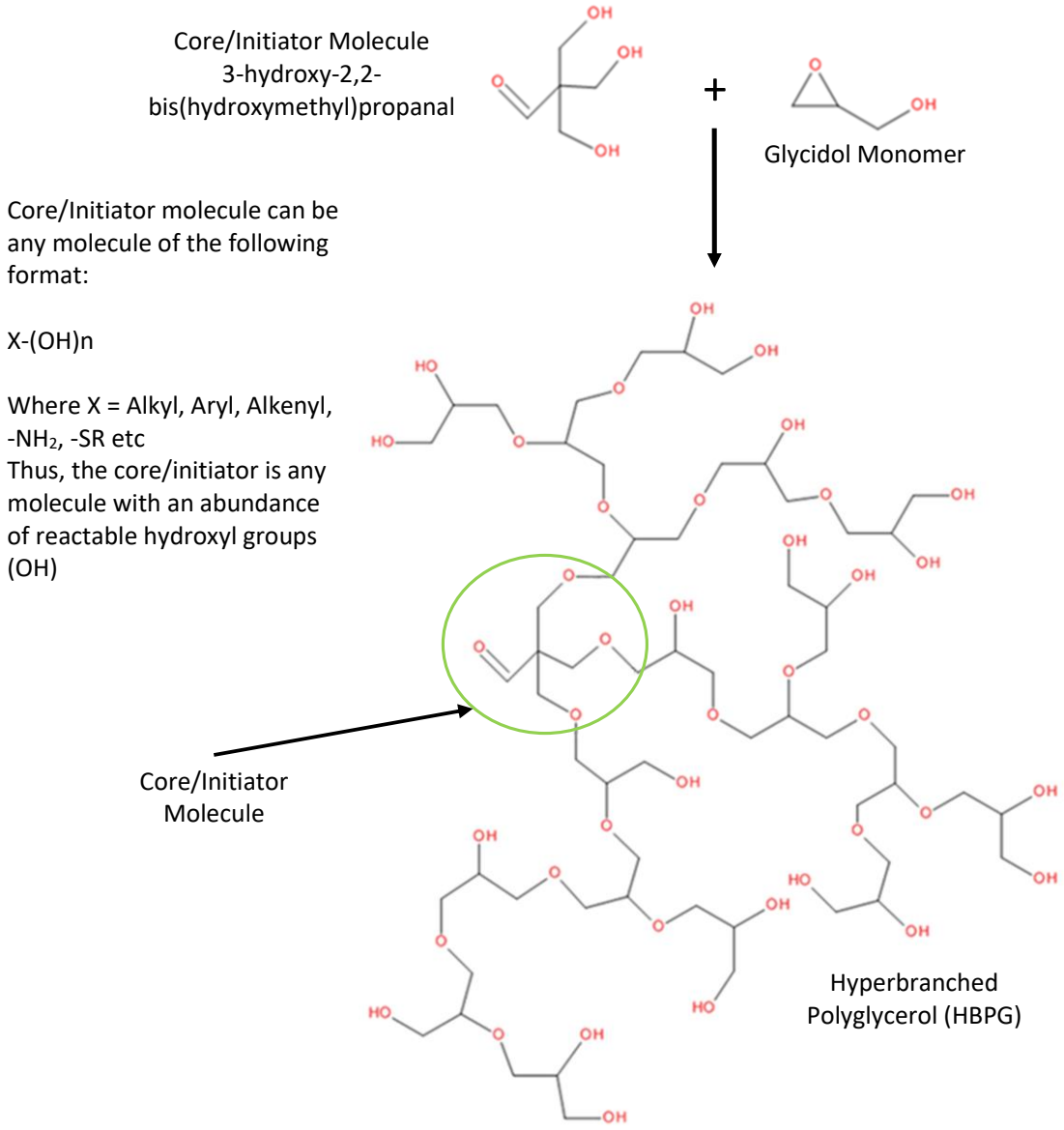

Scheme 1 - Basic chemical synthesis and structure of Hyperbranched Poly(glycerol). Adapted from Sunder et al. (1999) using Acelrys Draw software. The glycidol monomer is reacted with a core/initiator species which contains many hydroxyl groups. The glycidol monomer reacts with and attaches to each hydroxyl group on the core/initiator. The core/initiator becomes incorporated into the polymer structure, as a focal point from where the polymer branches out.

The structure of PG consists of an inert backbone of polyether groups and can be fabricated from the Ring Opening Polymerisation (ROP) of the epoxide derivative of glycerol, glycidol (Scheme 1). Unlike PEG, the structure of PG contains many hydroxyl functional groups which impart it with extreme water solubility. Due to its biocompatibility and extremely low toxicity,

the use of PG in medicine was realized many years ago, although its investigation and use has been constrained to a drug delivery vehicle.

Unlike other biocompatible polymers, PG was one of the first to be synthesised in a highly branched fashion in a relatively easy one-pot synthesis method. This allowed 3D constructs of dendrimer-like Hyperbranched PG (HBPG) to be fabricated, giving rise to a cheap and viable alternative to dendrimers. This has moved research in HBPG from just drug delivery applications to the formation of 3D bio-scaffolds for tissue engineering.

The term “dendrimer” comes from a Greek word which roughly translates into “part of a tree” thus giving an insight into their structure which resembles the branches of a tree. Also known as arborals, these macromolecules were first prepared using organic chemistry over 50 years ago. They are highly branched constructs with nanospherical architecture and differ from linear polymeric structures, in that their structure is highly precise and controlled presenting them with tailorable and predictable molecular weights, biodegradability and biocompatibility (depending on the constituent monomers) (Oliveira *et al.*, 2010). Dendrimers exhibit remarkable advantages including nanoscale spherical architecture, narrow polydispersity and highly modifiable surface functional groups. The intramolecular cavity is relatively empty and allows encapsulation of guest molecules for controlled release, such as medicinal agents (Duncan and Izzo, 2005) (**Error! Reference source not found.**).

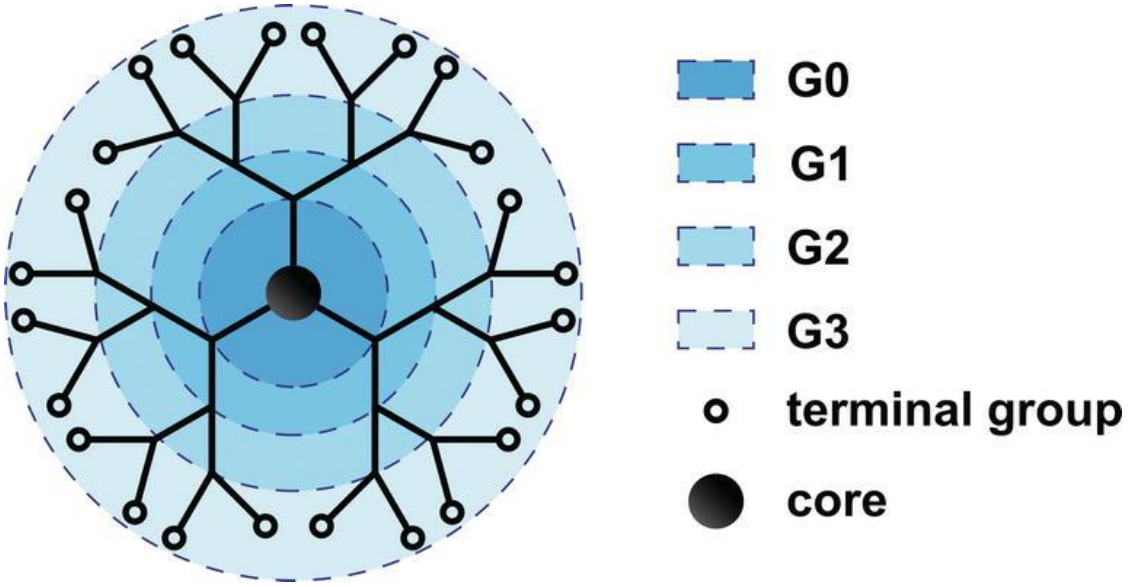

Figure 9 - Representation of a 3rd generation dendrimer, indicating unique structural units; central core, dendritic (within the generations), and terminal groups (Mlynarczyk et al., 2017).

The surface functional groups are extremely versatile and can be modified to alter the physicochemical properties of the dendrimer, and tailor it to a precise application. Using simple organic chemistry properties such as size, shape, topology, surface functionality and reactivity, can all be precisely controlled. As a result of these properties, including narrow molecular weight distributions, allows them to be prepared with reproducible pharmacokinetic profiles and high solubility in a wide range of organic solvents; researchers have investigated dendrimers for potential use in biomedical applications (Oliveira *et al.*, 2010). Dendrimers are classified by their generation number. The generations of a dendrimer are the number of repeated branching cycles performed during synthesis. Each successive generation generally leads to a dendrimer of twice the molecular weight of the previous dendrimer. Dendrimers of higher generation have more exposed surface functional groups, which can be customised for any application. The previous figure (Figure 9) gives a schematic representation of a generation 3 dendrimer.

The high number of hydroxyl groups on PG allows this polymer to be modified by co-polymerisation with other degradable polymers, or to convert the hydroxyl groups into other functional groups, providing a route to the grafting of biomolecules. These modifications also allow tailoring of the polymer properties such as solubility, drug release kinetics, degradation and polymer scaffold rigidity.

PG is one of the first polymers to be synthesised with a hyperbranching structure using a 'one pot' synthesis scheme. The glycidol monomer is often referred to as a latent AB2 monomer (A and B representing reactive functional groups), the epoxide ring of which can be opened using a base catalyst. When opened, the now glycerol molecule contains 2 hydroxyl groups and a 3rd alkoxide ion. The alkoxide ion allows glycerol to react with a deprotonated functional core molecule, starting the chain growth. Simultaneously through intermolecular and intramolecular ion transfer, a rapid cation exchange equilibrium ensues between the hydroxyls and alkoxides, which leads to chain propagation from all of the hydroxyls in the polymer chain, creating a hyperbranching structure (KAINTHAN *et al.*, 2006). Hence all hydroxyl groups on the polymer chain are potential active sites for chain growth, thus producing random branching (Scheme 2).

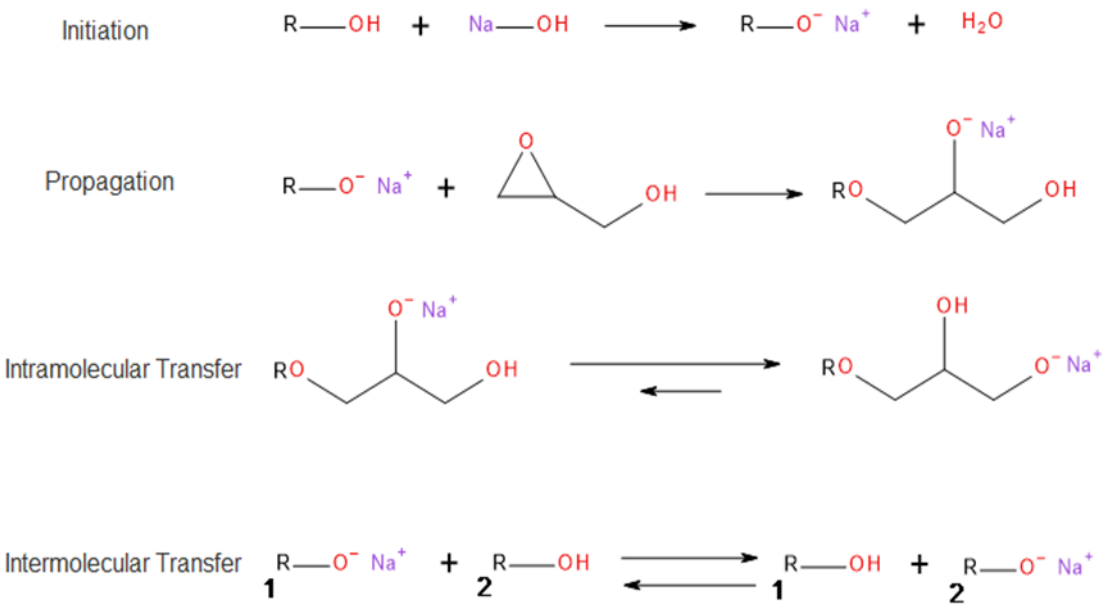

Scheme 2 - Activation of Hydroxyl Groups Using Base Catalyst (Initiation Forms Alkoxide Ion O-Na+), and Subsequent Propagation of Glycidol Monomer Ring Opening from Alkoxide Ion, and Intramolecular/Intermolecular Transfer of the Alkoxide Ion on Glycidol Monomer, Hence Each Hydroxyl Group on Monomer is Potential Polymerisation Active Site. Adapted from Sunder et al (1999) using Acelrys Draw software.

HBPG has been highly researched in recent years for its ability to conjugate biomolecules relatively easily. The abundance of hydroxyl groups at the polymer periphery, and within the core, allow attachment of a high number of biologically active substances. As well as biofunctionalisation, PG can be modified to alter its properties such as glass transition temperature, charge, hydrophilicity, and degradation, thus it has been a research interest of many scientists for use as a drug delivery vehicle or tissue engineering scaffold. Another advantage of PG is its hydrophilic character brought on by the hydroxyl groups in its structure. The polymer therefore improves the hydrophilic character of a biomaterial surface and prevents non-specific protein adsorption, similarly to 'stealth' polymers such as PEG, which may prevent foreign-body reactions.

This research has sought the use of PG; a biologically compatible and non-toxic polymer, as a tissue engineering scaffold mainly for the purpose of anchoring immobilised RGD peptides to an

implant surface. PG was synthesised with hyperbranching architecture similar to that seen in dendrimers. The highly branched nature of the polymer allows compacting of the polymer chains, creating a polymeric structure within the nano-scale domain, as well as having a plethora of functional hydroxyl groups within the polymer core and at the polymer periphery.

2.5 Implant Associated Infections

Infectability remains to be a major problem in the use of biomaterials for medical applications, being the principal cause of implant failures, it presents unresolved issues to the clinician. Although efforts have been made to adhere to strict sterile and aseptic conditions to prevent infection in patients, such as 'deep clean' procedures for hospital wards and surgical theatres, and protocols for peri-operative antibiotic prophylaxis, which have proved effective but fall short in completely controlling the occurrence of this serious condition (Montanaro *et al.*, 2007). Even under aseptic sterile conditions, up to 50,000 skin particles are detached from each physician, that contains microorganisms from the flora or human microbiota; an aggregation of microorganisms residing on the surface and in deep layers of skin, in saliva, oral mucosa, and intestinal tract such as fungi and bacteria. Some form a symbiotic relationship with the host while others do not and are harmless.

Around 90% of clean wounds can be found infected with Staphylococcus Aureus at the time of wound closure (Oakes and Wood, 1986). The main sources of implant infection caused by microorganisms are the skin of the physician performing surgery and the host during implant insertion, then migration of bacterial cells through incisions to the device surfaces, followed by haematogenous spread. The type and location of the implant material used determines the microbiological profile of the implant-related infection. Total joint replacements

(endoprostheses) are typically infected by opportunistic Staphylococci, Enterococci and Candida species, as well as infecting catheters, cardiac valves and pacemakers (Schierholz and Beuth, 2001).

It is generally considered that two points of infection onset befall orthopaedic implants, or any medically implantable device, which classify as Prosthetic Joint Infections (PJI). These are early, delayed or late. Early onset of infection that establishes immediately following surgical intervention is defined as the appearance of symptoms within the first 3 months following surgery, and is associated with peri-implant contamination (infection from a microorganism during surgery) and remains to be the most common route. Delayed onset is the first appearance of symptoms generally between 3 months and 2 years following surgery. Late onset of infection generally manifests after 2 years of surgery, and is usually associated with haematogenous infections (infection elsewhere in the patient that travels to the implant site through the blood) (Esposito and Leone, 2008).

Haematogenous infections have been well documented in medical devices that are exposed to the blood stream, such as artificial valves and stents, though they are much less frequent and mainly associated with bacteria originating from respiratory, skin, dental, or urinary tract infections (Galanakos *et al.*, 2009). Early post-operative implant infections more often exhibit acute symptoms of infection, whereas late prosthetic joint infections, which generally develop after a few months or years following surgery, show misleading symptoms of persistent chronic pain and signs of inflammation.

2.5.1 Aetiopathogenesis

Over the last few decades, the distribution of isolated pathogens has not changed much, with Staphylococcus Aureus, coagulase-negative Staphylococci, Enterococcus species and Escherichia

Coli being the most isolated pathogens from SSIs. Also, a higher proportion of SSIs are associated with antibiotic resistance strains like Methicillin-Resistant Staphylococcus Aureus (MRSA), and an increasing incidence of fungal SSIs from species such as Candida Albicans. It is suggested that these outcomes are linked with severely ill patients who are immunocompromised, and the increasingly high use of broad-spectrum antibiotics (Mangram *et al.*, 1999). Staphylococcus Aureus and Staphylococcus Epidermidis are considered the most common infecting microorganisms, which account for around 65% of all PJIs, and are frequently reported in early and late infections of total hip and knee prostheses (Esposito and Leone, 2008).

The aetiology of implant infection has also been related to the implanted materials due to foreign-body reactions. The implanted material offers a surface for microbial anchorage, growth, protection in internal pores, and often provides nutrients that accelerate microbial growth such as ions released from some metals (stainless steel being a material known to attract and harbour microbes), or even resorbable materials (Montanaro *et al.*, 2007). It has been suggested that stainless steel is associated with greater infection rates than titanium implants due to firm adherence of soft tissue on this metal, and also the generation of a fibrous capsule, a recognised reaction to stainless steel. The fibrous capsule contains a non-vascularised fluidic space that is less accessible to the host defences, allowing microbes to spread and freely multiply (Galanakos *et al.*, 2009).

Medical implants, as is the same for all foreign body reactions, creates an interstitial milieu at the implant-tissue interface that is known to be locus minoris resistentiae, in that it presents an environment that has a low resistance and increased susceptibility to infection, and is characterised by depleted immune defences such as a compromised immune system, although formation of a biofilm is important (Galanakos *et al.*, 2009). Immunosuppression develops at the implant-tissue interface due to a granulocyte (white blood cells) defect, which is induced by

non-phagocytosable foreign bodies (the implant material). Granulocytes normally undergo production of superoxide radicals to kill pathogenic microorganisms however, presence of the implant material leads to partially de-granulated granulocytes and impaired killing of invading pathogens (Zimmerli, 2006).

The circumstances of foreign body reactions to the implant and the low pathogenic resistance at the implant-tissue interface, provides opportunistic pathogens a way to gain access to and colonise the implant surface. Successful establishment of the infection, which is made possible by conditions presented by the implant, is concluded by the virulence potential of the microorganism (Montanaro *et al.*, 2007). Hence a pathogen of strong virulence will have a greater likelihood of causing infection, although low virulent pathogens can also gain entry and colonise an implant under such circumstances imposed by the presence of the implant. Local Immunosuppression, brought on by foreign body reactions to implanted materials, lowers the threshold of bacterial infections (Schierholz and Beuth, 2001) and experiments have shown that foreign body presence decreases the minimal infecting dose of Staphylococcus Aureus by 100,000 fold, leading to a permanent abscess. Animal models revealed that just 100 colony forming units of Staphylococcus were enough to infect 95% of subcutaneous implants (Zimmerli, 2006).

2.5.2 Biofilm Formation

Most implant-related infections are the basis for microbiological contamination during insertion at surgery however; they are not the sole result of microorganisms transmitted in a healthcare setting. Bacteria, and on occasion fungi, colonise an implant surface by adhering to it through the formation of a biofilm. These biofilms display further challenges for infection management,

and shielding bacteria from antimicrobial agents (resistance). Biofilms can resist antibiotic concentrations of up to 1,000 times that required to kill planktonic bacteria (free-floating as opposed to sessile) (Alexander, 2010). They can also protect residing bacterial cells from metal toxicity, acid exposure, dehydration and salinity, and even phagocytosis (Hall-Stoodley *et al.*, 2004)

Microorganisms adhere to implant surfaces due to rapid attachment by specific and non-specific factors. Specific factors include adhesins, cell-surface protein components or appendages that facilitate bacterial adhesion to other cells or inanimate surfaces. Adhesins can take the form of pili (hair-like appendages covering bacterial cells, used primarily for transfer of genetic information between cells, or conjugation) or fimbrae (proteinaceous appendages covering most gram-negative bacteria and some gram-positive bacteria, used solely for cell binding). Non-specific factors such as surface tension, hydrophobicity, and electrostatic forces of attraction, can also govern bacterial cell adhesion (Galanakos *et al.*, 2009).

Microorganisms can generally take two forms: a free-floating planktonic form (in which the microorganisms propagate over the surface of the implant), and a sessile form (where the microorganisms are immobile within a biofilm). Bacteria, especially Staphylococci, have a tendency to phenotypic variation, or phase variation. This term governs a group of genetic mechanisms whereby the expression of a gene varies reversibly from generation to generation (Christensen *et al.*, 1990). A phenotypic change induces the expression of enzymes that catalyse the production of an exopolysaccharide substance known as glycocalyx or 'slime' which, in association with the bacterial cells adhering to each other, generates the biofilm (Galanakos *et al.*, 2009, Schierholz and Beuth, 2001). Biofilms are generally composed of many extracellular polymeric substances of varying structure and size, mostly polysaccharides, as well as proteins and DNA (Hall-Stoodley *et al.*, 2004).

Planktonic bacteria undergo phenotypic variation that leads to adhesion, biofilm formation and subsequent resistance to antibiotics and the host immune system (phagocytes and antibodies). Within an established biofilm both adhesive and non-adhesive subpopulations of cells reside. Planktonic bacteria colonised on the implant surface can cause systemic infection to the host, while sessile bacteria survive during attack from antibiotics and the host immune system, leading to chronic indolent infections (Schierholz and Beuth, 2001). Nutrient depletion and/or the accumulation of waste product in the biofilm lead to the microorganisms entering a stationary state (non-growing). In this state the microorganisms become 1,000 times more resistant to most antibiotic therapy than in their planktonic form (Galanakos *et al.*, 2009). The following figure illustrates the key stages in biofilm formation on a surface (Figure 10).

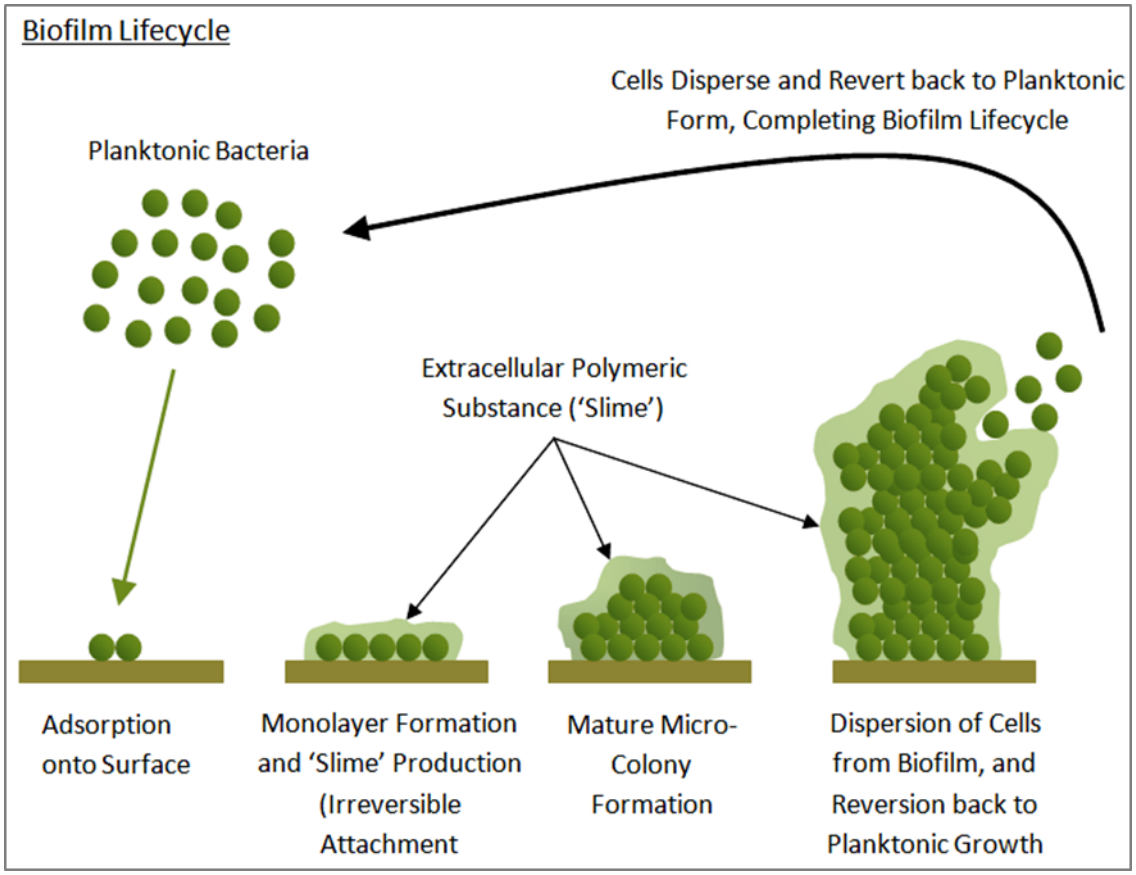

Figure 10 - Biofilm formation life-cycle. Planktonic bacteria adhere to a surface and form a monolayer with the production of 'slime'. Growth and differentiation leads to the formation of a mature micro-colony and subsequently a biofilm. Sessile bacterial cells are dispersed from the biofilm and revert back to their planktonic form, ready to adhere and colonise a surface again, completing the life-cycle. Adapted from Galanakos et al (2009).

2.5.3 Anti-fouling Polymers

Recently much attention has been awarded to antimicrobial polymers as they possess a great deal of qualities that could prove useful in the tissue engineering arm of the medical sector. The use of polymers that exhibit inherent antimicrobial activity in themselves, removes the reliance on conventional antibiotics that are becoming less efficacious due to resistant bacterial strains. Without a need for antimicrobial agents, side effects to the patient are minimised or removed, and antimicrobial polymers provide a longer duration of activity compared with antibiotics. A vast majority of polymers not only exhibit antimicrobial qualities, but they can be modified to

do so, by simply preparing co-polymer blends. Polymer science is at the forefront of tissue engineering, providing biocompatible and biodegradable scaffolds to guide tissue regeneration, but the inclusion of antimicrobial activity offers a sound solution to the ever elusive problem of orthopaedic implant infections (Muñoz-Bonilla and Fernández-García, 2012). Generally speaking, two main types of antimicrobial polymers exist, those that are non-adhesive (inhibit microbial cell colonisation on their surface and subsequently prevent biofilm formation), and those that are bactericidal (kill microbial cells upon contact).

Polymers exhibit a wide range of properties that are essential to the development of surfaces that can be tailored for a variety of biosystems, such as multiple length scales (allowing varying molecular weight polymers to be synthesised into higher organisations by controlling their length), surface chemistries (which are easily modifiable), and mechanical properties. There are many different approaches to achieve antimicrobial polymers: polymers which are biopassive (reduce the adhesion of bacteria to their surface e.g. hydrophilic polymers), bioactive polymers (that kill microbial cells upon contact with their surface), and polymer surfaces that release antimicrobial agents in the vicinity of their surface (Charnley *et al.*, 2011).

Biopassive polymers inhibit the adhesion of extracellular proteins to their surface, consequently preventing bacterial adhesion as well. Bacterial cell adhesion to a surface relies on the adhesion of ECM proteins to the surface, after which certain bacteria contain binding moieties for the adhered proteins. Bacteria contain adhesin proteins that mediate their initial cell attachment to the host tissue. These adhesins are generally given the name Microbial Surface Components Recognising Adhesive Matrix Molecules (MSCRAMM), with one of the most important adhesins being fibronectin binding protein on Staphylococcus Aureus.

Such biopassive polymers are synthesised using hydrophilic well-hydrated monomers, which are either covalently or physically adsorbed onto a surface. As the initial step in the pathogenesis

of implant related infections is the adhesion of bacteria to the implant surface, prevention of bacterial adhesion is an ideal strategy to avoid foreign body infections. Also, biomaterials which are anti-adhesive to ECM proteins and bacterial cells don't lose their antimicrobial properties during use right away; therefore early and late infections can be obviated (KOHNEN and JANSEN, 1995). By inhibiting the adhesion of proteins to a surface, the attachment platform for bacterial cells is removed thereby reducing bacterial colonisation (Charnley *et al.*, 2011).

Concentrations of possible virulent microorganisms in body fluids are mostly below the infection causing limit. However, attachment of microorganisms to a surface leads to local proliferation, biofilm formation, and production of high concentrations of pathogen or systemic infection. Thus, the killing of microorganisms is not always essential, but to prevent their adhesion to surfaces and reducing their virulence. Such non-adhesive polymeric surfaces have none or very few sites for microbial binding and two main principles to effectively repel microbial cells are electrostatic repulsion, and extreme hydrophilicity or hydrophobicity (Figure 11) (Tiller, 2008).

It has been discussed that microbial cells generally carry a negative surface charge. This is largely due to membrane proteins; gram-positive bacteria contain teichoic acids, and gram-negative bacteria contain negatively charged phospholipids (Ortiz *et al.*, 2017). The net negative charge of bacterial cell membranes could potentially be repelled by negatively charged polymers, thereby preventing bacterial cell adhesion with the surface.

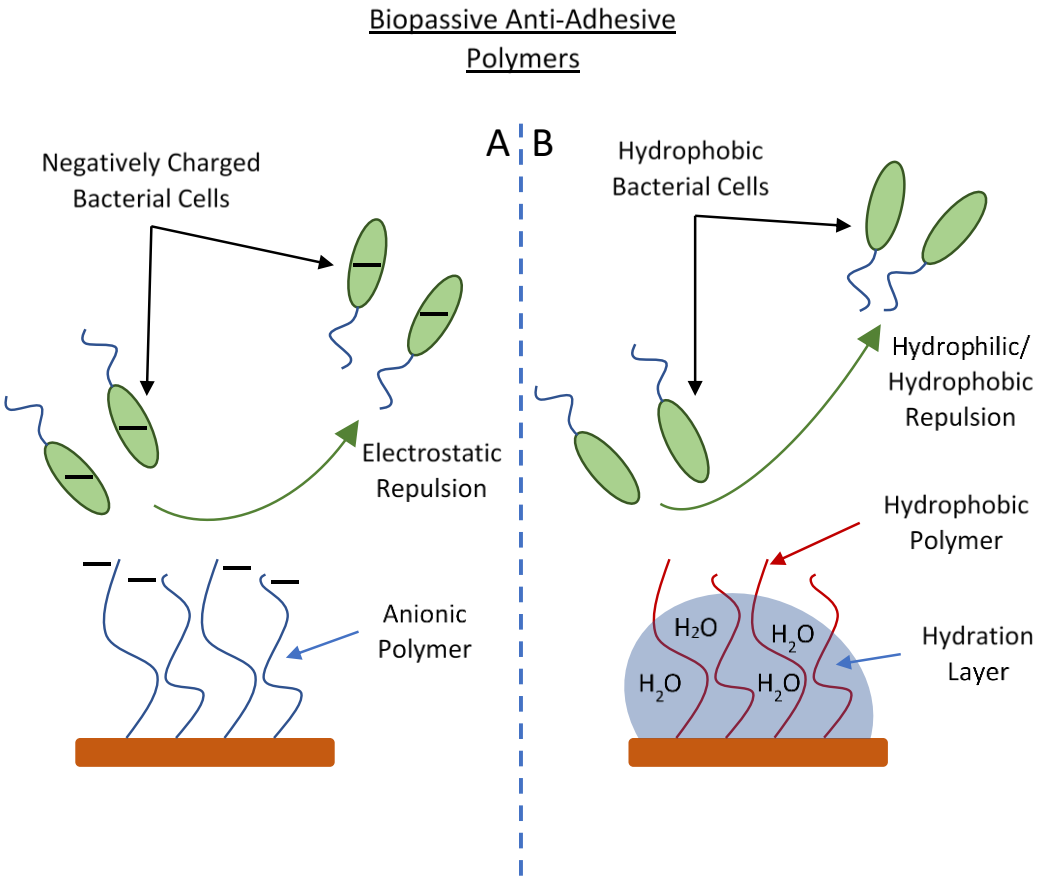

Figure 11 - Diagram Illustrating the two Main Antibacterial Principles of Biopassive Polymers; Electrostatic Repulsion (A) and Hydrophilic/Hydrophobic Repulsion (B). Adapted from Charnley et al (2011) and Siedenbiedel & Tiller (2012).

It has been known for many years that hydrophilic surfaces, such as water soluble polymers, and polymers that swell or hydrogels (polymer networks that form stable gels with water), lower the adhesion of microbial cells (Ackart *et al.*, 1975, Cook *et al.*, 1993). The most widely given explanation of this phenomenon is due to surface free energy. Bacterial cells cannot adhere because an energy minimum is attained by the largest amount of adsorbed water. Furthermore, hydrogels exhibit a lower potential to adhere certain ECM proteins which promote microbial adhesion, such as fibronectin. Another hypothesis is that possible binding sites for microbial

cells are taken up by water, giving them less chance to adhere to the surface (Kuusela *et al.*, 1985, Park *et al.*, 1998).

2.5.3.1 Anti-fouling PEG and PG Polymers

PEG is the most widely studied polymer for inhibiting non-specific protein adsorption to a surface, and hence reducing bacterial adherence. Containing many oxygen atoms in its polymer backbone readily available for hydrogen bonding, PEG is extremely hydrophilic. When PEG polymers are subjected to aqueous fluid, an interfacial layer forms which prevents the PEG surface coating coming into direct contact with proteins and cells (Wang *et al.*, 1997, Yoshimoto *et al.*, 2010).

PEG contains two hydroxyl groups (one at each end of the chain) which can be used to graft to a surface. Research has shown that by grafting PEG to a surface via one of the end hydroxyl groups, it imparts hydrophilicity to that surface and exhibits microbial repelling qualities (Park *et al.*, 1998). PEG can be either grafted into the backbone of a polymer, or introduced into the side chains, forming a densely packed PEG monomolecular layer (Charnley *et al.*, 2011). PEG side chains grafted to a polycationic poly(lysine) backbone, producing a comb-like polymer, has been shown to resist adhesion from Staphylococcus Aureus/epidermidis and Pseudomonas aeruginosa (Harris *et al.*, 2004). Research by Desai et al demonstrated that polyethylene terephthalate films modified with PEG exhibited 70-95% reduction in adherent bacteria compared to unmodified films, indicating the usefulness of PEG modification in reducing the risk of implant associated infections (Desai *et al.*, 1992).

It has been shown that as the density of PEG functions conjugated to collagen increases, there is a decrease in the number of adhered Staphylococcus Aureus cells up to 93% compared to non-

modified collagen (see Figure 12) (Tiller, 2008). Also, by swapping the remaining end hydroxyl group for one with a negative charge can improve the microbial repellence of PEG (negative charge on most bacterial cell surfaces would lead to electrostatic (Tiller, 2008) repulsion), in fact it could lower the adhesion of Staphylococcus epidermidis by fivefold when compared to unmodified PEG grafted surfaces (Han *et al.*, 1998, Tiller, 2008).

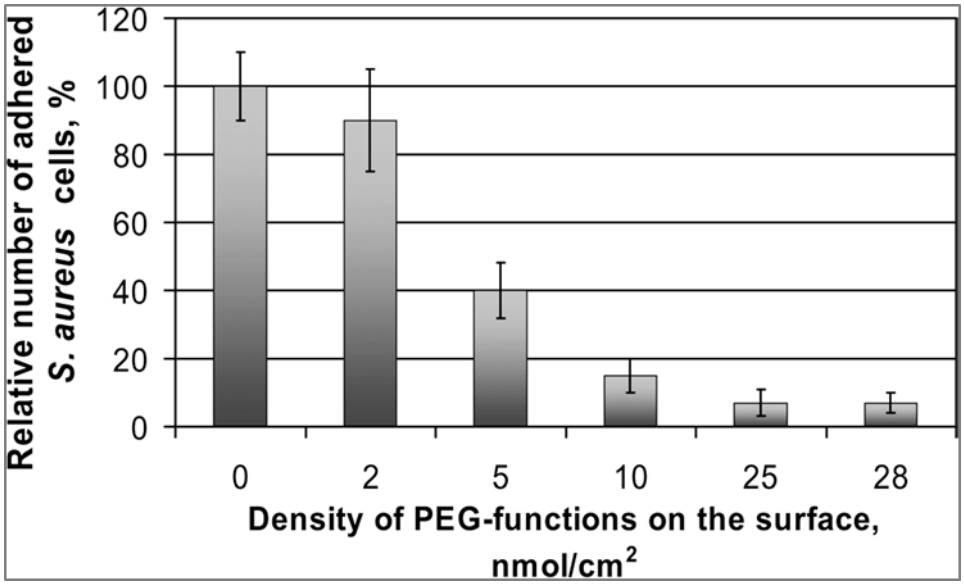

Figure 12 - Number of adhered Staphylococcus Aureus cells on PEG-modified collagen in relation to PEG grafting density (Tiller, 2008).

One fundamental flaw in the utilisation of PEG-based anti-adhesive systems is their lack of long-term stability. PEG is oxidatively degraded in vivo resulting in chain cleavage, leading to loss of surface functionality which means reduced hydrophilicity and less resistance to non-specific adsorption (Charnley *et al.*, 2011).

2.5.4 Anti-Infective RGD Peptide

Research has shown that instead of utilising the protein, a small binding motif can be conjugated to the coating, one which can only be recognised by osteoblasts. The tripeptide amino acid sequence RGD is a small binding domain, found in ECM proteins such as fibronectin and laminin, which is responsible for binding to the integrin receptor. Functionalising antimicrobial surfaces with RGD peptide can enhance osteoblast adhesion and function, whilst not impacting on the antimicrobial activity of the underlying coatings (Charnley *et al.*, 2011, Neoh *et al.*, 2012, Zhao *et al.*, 2009, CHUA *et al.*, 2008). Work by Harris et al and Maddikeri *et al.* showed that PEG grafted poly(L-lysine) with attached RGD motif coated onto titanium substrates was able to resist adhesion of Staphylococcus Aureus/epidermidis, as well as other bacteria, whilst allowing attachment of osteoblasts in a selective bio-interaction pattern, exhibiting the usefulness of this biomaterial in applications of orthopaedic implantology (Harris *et al.*, 2004, Maddikeri *et al.*, 2008). Similar research has shown that RGD peptides exhibit antiadhesive properties against certain bacterial strains (WAGNER *et al.*, 2004).

It has been suggested that the war between pathogenic cells and host cells is a 'race to the surface'. If the pathogenic cells win the surface, they will attach, spread, form a biofilm and proliferate to the point of infection. However, if the pathogenic cells are blocked from attaching to the surface i.e. competitively inhibited by the host cells, then the host cells will win the surface, and the pathogenic cells will not proliferate and may not cause infection. The RGD peptide has been reviewed in this regard, as it allows the preferential attachment of host cells and matrix proteins, forcing advantage towards the host cells, leading to the attachment of fewer pathogenic cells, thus disrupting infection.

2.6 Research Aims and Objectives

There are two aims of this research: the primary aim is to enhance mineralised bone matrix production, and reducing infection is a secondary aim. The former aim will be met by completing three objectives: passivation of the titanium surface (forming hydroxyl groups for conjugation and improving surface wettability, and etching the titanium surface to yield a roughness at the nanoscale), polymerisation of Hyperbranched Polyglycerol (HBPG) directly from the titanium surface, and attachment of the RGD peptide. The secondary aim of reducing infection will be met by completing two objectives: passivation of the titanium surface, and polymerisation of HBPG directly from the titanium surface (Figure 13).

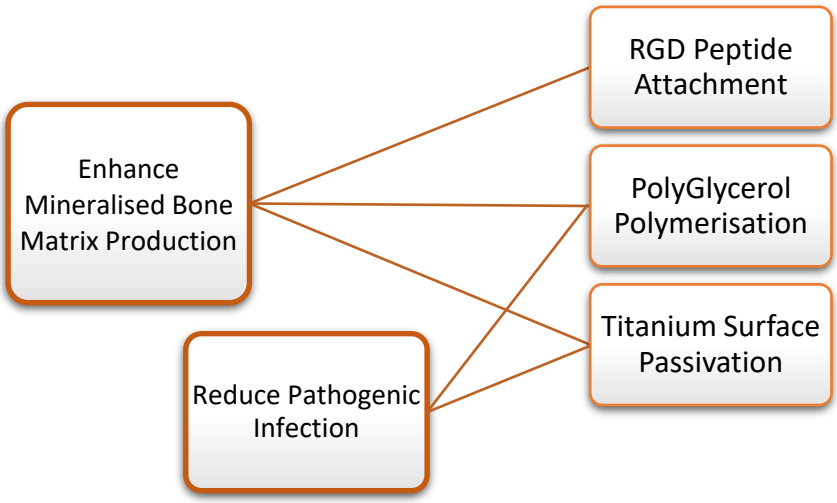

Figure 13 - Flowchart depicting the two aims of this research (Enhanced mineralised bone matrix production and reduced infection), and the four objectives to complete them (RGD peptide attachment, nanoscale surface roughness, Hyperbranched polyglycerol polymerisation, and titanium surface passivation)..

The research tested four experimental hypotheses. The first hypothesis is that passivation of the titanium surface will enhance the wettability and develop nano surface roughness. The

second hypothesis is that polymerisation of PG from the titanium surface will enhance wettability and further develop nano surface features. The third hypothesis is that the same PG layer can reduce infection from pathogenic microorganisms. The fourth and final hypothesis if that the RGD peptide can activate osteoblast cells, thus improving cell attachment and adhesion strength, enhance cell proliferation and differentiation, and increase mineralised bone matrix production.

The null hypotheses are therefore the opposites of the experimental hypotheses. Thus, the null hypotheses state that: passivation will not enhance titanium surface wettability and not develop nano surface roughness, PG polymerisation will not further enhance the titanium surface wettability and not develop surface nano features, PG layer will not reduce infection from pathogenic microorganisms, and the RGD peptide will not improve cell attachment and adhesion strength, not enhance cell proliferation and differentiation, and not increase mineralised bone matrix production.

3 Titanium Surface Preparation

3.1 Passivation

Passivation is an important step when producing a biologically successful titanium implant. The process cleans the surface of all contaminants and develops an oxide layer on the titanium surface, like that of the native oxide layer, thus improving implant biocompatibility (Ratner, 2001, Pan *et al.*, 1996). Some studies have discovered that when titanium is implanted, over the course of some years the native oxide layer continues to grow (Sundgren *et al.*, 1986), and in doing so it can release titanium ions into the surrounding tissue and cause adverse reactions. However, when a titanium surface is passivated, the newly oxidised layer prevents further excessive oxidation of the surface and improves corrosion resistance (Mabilleau *et al.*, 2006), preventing titanium ion release thus minimising toxicity and foreign body reactions.

Passivation could be a safer alternative to other surface modification techniques such as blasting. Alumina blasting is well known and used to create random surface texture (Kantlehner *et al.*, 2000, Weber *et al.*, 2012, Depprich *et al.*, 2008), as well as increased surface area. Although blasting may lead to the development of random bone cell orientations, contributing to the formation of scar tissue (Zarrabi *et al.*, 2014, Kulkarni *et al.*, 2014). The blasting technique may also give rise to increased concentrations of cytotoxic elements released from the implant surface (Weber *et al.*, 2012).

Another technique for oxidising metal surfaces that is widely available is electrochemical treatment. This process may provide the best control for generating consistent oxide layers (Larsson *et al.*, 1994), although they are not completely pure (Lausmaa *et al.*, 1988). However, electrochemical methods are costly and time consuming, making them less commercially attractive (Nanci *et al.*, 1998).

Generally, passivating the titanium surface converts titanium oxide (Ti-O_2) groups in the oxide layer into titanium hydroxide (Ti-OH), or hydroxylation of the titanium surface, like the oxidation of titanium to form the native oxide layer (Figure 8, page 41). The abundant hydroxyl groups on the passivated titanium surface, form hydrogen bonds with water molecules, improving the hydrophilic character of the titanium surface (Figure 14).

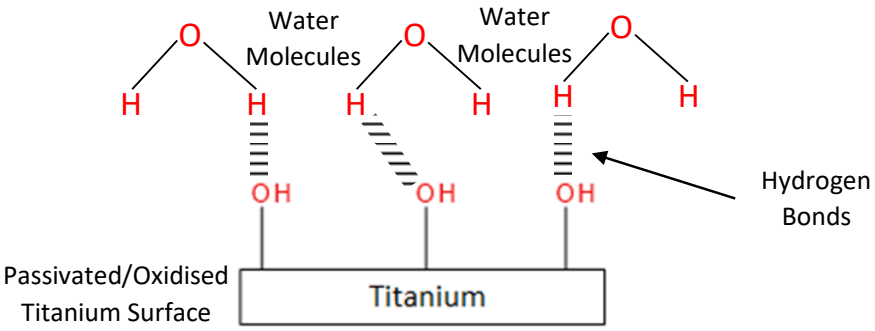

Figure 14 - Diagrammatic representation of hydrogen bond formation between water molecules and -OH groups on passivated/oxidised titanium surface.

This is the case with hydrogen peroxide passivation of titanium however, passivation with nitric acid leads to the formation titanium oxide (Ti-O_2). Formation of the oxide layer is how nitric acid passivation improves corrosion resistance. By broadening the hydroxylate rich region of the oxide layer, many sites the conjugation of biologically active substances are created, as well as providing a positive environment for cell adhesion and function in terms of hydrophilicity and surface charge from the aforementioned hydroxyl groups (Pan *et al.*, 1994).

There are a few well known passivation procedures that utilise certain chemicals; some harsher than others such as Piranha solution. Piranha uses a mixture of concentrated sulphuric acid and hydrogen peroxide (H_2O_2). The acid and H_2O_2 combination cleans the substrate surface, oxidises, and roughens the titanium producing cracks, pits, and pores (also known as etching). While this

mixture is suitable and numerously used in research, Piranha solution is extremely corrosive, explosively unstable, and costly in clean up and waste removal, hence its use is discouraged commercially.

When passivating the titanium surface with hydrogen peroxide, it is well known that the decomposition of hydrogen peroxide to oxygen and water take place at the titanium surface. Titanium oxidation and corrosion then take place concurrently with water uptake and generation of a Ti-H_2O_2 complex, which is responsible for a yellow colouration of the passivation solution also observed in this research. This titanium-hydrogen peroxide complex generates a stable end product, the Ti-OOH adduct (Tengvall *et al.*, 1989). Computational studies of the reaction also shows that other likely stable products are: Ti-OOH + O-H, Ti-OH + Ti-O + O-H, and Ti-OO + O-H + O-H (Huang *et al.*, 2011) (Figure 15).

Reaction Products for Hydrogen Peroxide Passivation of Titanium

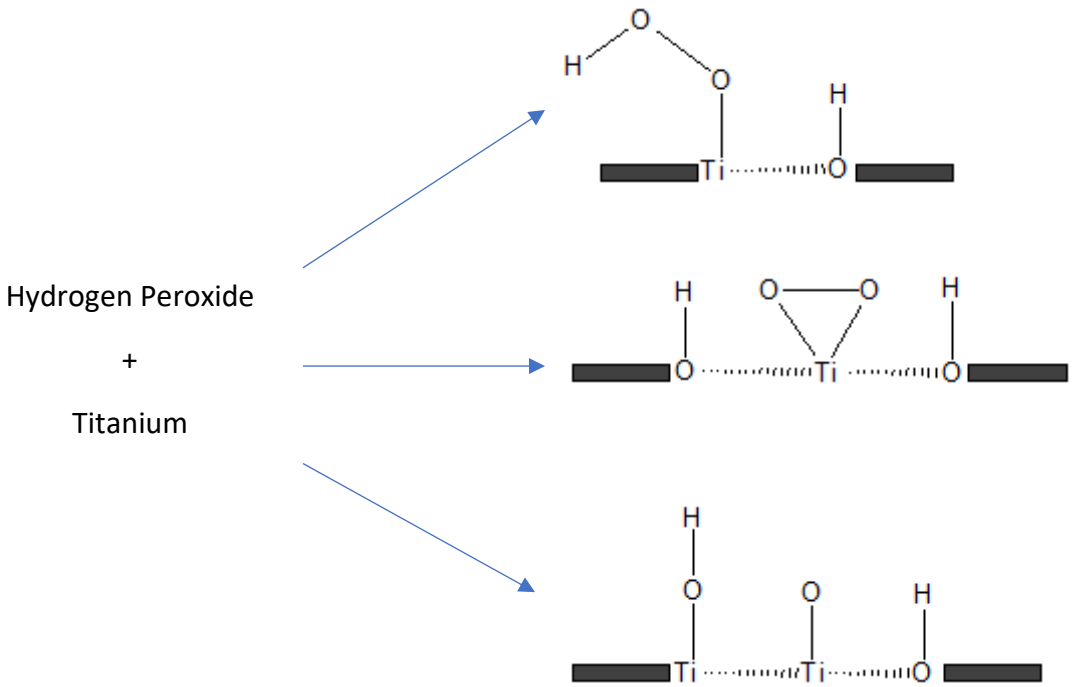

Figure 15 - Hydroxyl group formation on titanium surface when passivating with hydrogen peroxide. These are the three most likely and stable products of the passivation reaction, as analysed by computational studies by Huang et al., (2011).

Another popular passivation solution is nitric acid (HNO_3). This chemical is more widely used and has been considered a 'gold standard' for the passivation of titanium surfaces, as well as other metals, with a view to achieving corrosion resistance. Corrosion can occur on metals when exposed to corrosive biological fluids. In case of titanium and its alloys, cracking of the protective oxide layer can lead to corrosive attack on the underlying surface, with the potential to release metal ions (Pan *et al.*, 1996). Metal ions released from implants are known to cause cytotoxic events in the tissue surrounding the implant site. Most notably, nickel, aluminium, iron, and vanadium have been shown to be toxic, demonstrating poor cell proliferation and viability at concentrations found in patients with musculoskeletal joint replacements (Hamlet *et*

al., 2012). Substantial metal ion release may cause osteolysis and subsequent implant loosening (Alfarsi *et al.*, 2014). Although there is contradictory evidence as to the corrosion resistant effects of HNO_3 passivation, since some studies have found metal ion release from such passivated titanium alloys, as well as continued oxidation of the surface, it remains a popular procedure to impart corrosion resistance to titanium and other metals, thereby minimising potentially toxic metal ion release.

The passivation of titanium surfaces with HNO_3 does not lead to the generation of hydroxyl groups on the substrate surface, but instead cleans the titanium and generates an oxide coating, protecting the surface from corrosion. According to a conference paper delivered at the International Titanium Association (ITA) Conference in 2014, Titanium Europe 2014, the vice president for research and development of SCANACON AB Thorsten Schneiker, a world leader in acid process solutions, and Dr Kerstin Forsberg of KTH – Royal Institute of Technology Sweden, outlined the reaction mechanism for nitric acid passivation of titanium (Schneiker and Forsberg, 2014) (Scheme 3).

$$Ti + 2HNO_3 \longrightarrow TiO_2 + 2HNO_2$$

Scheme 3 - Reaction mechanism for the nitric acid passivation of titanium (Schneiker and Forsberg, 2014).

Although the time to passivate the substrate with HNO_3 is just 30-minutes to a couple of hours, its ability to roughen the titanium surface is limited compared to the use of H_2O_2 and other stronger acids, but the passivation time with H_2O_2 is much lengthier. Some have suggested a passivation time of around 24-hours with H_2O_2 is ideal to oxidise and develop surface features, such as roughness, that is conducive to cell function as well as plasma protein attachment

(Kainthan *et al.*, 2007). It has been suggested in the literature that the use of an acid with H_2O_2 may enhance the oxidising effects, therefore allowing a reduced passivation time. However, for industry scale-up 24-hours is too long a time for preparing the titanium surface.

Mixing H_2O_2 with an acid, such as HNO_3, could enhance the oxidation potential of H_2O_2, and may be the reason why Piranha solution is preferred in the literature. To replicate the acid etching and oxidation ability of Piranha solution, but to minimise dangers of high corrosiveness and instability, H_2O_2 30%wt was mixed with 25% HNO_3 to form the fourth tested passivation solution (H_2O_2/HNO_3).

It was thought that mixing H_2O_2 with HNO_3 could lightly roughen the titanium surface (producing nano rough surface features), whilst increasing oxidation and imparting corrosion resistance simultaneously. Literature reports that H_2O_2 can be mixed with up to 35% HNO_3 strength, yet remain stable enough to mitigate any danger (Morais *et al.*, 2010, Rezania *et al.*, 1999, Nanci *et al.*, 1998). Higher concentrations of HNO_3 with H_2O_2 could yield violent reactions, releasing heat and large volumes of mono-nitrogen oxides (Sah and Miller, 1992).

Schneiker and Forsberg (2014) presented that hydrofluoric acid etching of titanium exposes surface metal atoms which are oxidised through nitric acid passivation, forming adsorbed trivalent titanium cations. These titanium cations are then further oxidised by nitric acid to form the titanium oxide coating (Scheme 4). In this research it is thought that hydrogen peroxide treatment might expose these surface metal atoms in a similar way, thus enhancing the nitric acid led formation of the oxide layer. Therefore, the actions of hydrogen peroxide and nitric acid may help each other to enhance the titanium oxide coating and generate an abundance of hydroxyl groups on the titanium surface.

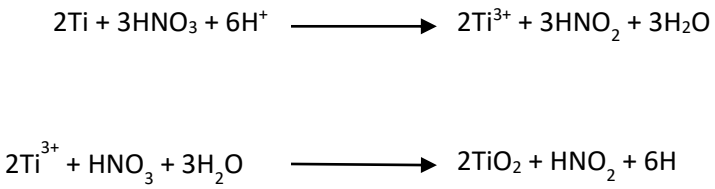

Scheme 4 - Reaction of nitric acid with titanium surface metal atoms and oxidation to yield titanium oxide layer (Schneiker and Forsberg, 2014).

H_2O_2 30%wt was the first solution tested. The literature reports that a passivation time of 24-hours with H_2O_2 alone is best to achieve a hydrophilic surface, along with random surface features such as cracking and pitting, and achieve a micro rough surface (Kainthan *et al.*, 2007). The next solutions tested consisted of two strengths of 70% HNO_3 in deionised water (HNO_3/H_2O): the ratios of HNO_3 to water included 3:7 and 1:1.

The HNO_3/H_2O passivation solutions tested here are derived from a procedure that is in accordance with the protocol specified in 'Standard Practice for Surface Preparation and Marking of Metallic Surgical Implants' in the American Society for Testing and Materials (ASTM) F 86-01 (ASTM, 2013). This protocol is used mainly to clean metal surfaces, making them free from organic contaminants and iron inclusions. As well as cleaning metal surfaces, HNO_3 passivation of titanium leads to the formation of thin (less than 10nm) oxide films, similar to the native oxide layer that covers the titanium alloy surface (Burakowska *et al.*, 2009, Kantlehner *et al.*, 2000, Porte-Durrieu *et al.*, 2004). The detailed effects of passivation on corrosion resistance remains an actively debated topic. It is generally believed that this passivation procedure improves corrosion resistance, via formation of the protective oxide coating, although results found in the literature are conflicting (Burakowska *et al.*, 2009).

3.2 Materials and Methods

Titanium Alloy (Ti6Al4V) circular discs (provided by SinteaPlustek and William Gregor Ltd), with dimensions of 14mm diameter by 1mm thick, machine cut; Acetone ACS Reagent ≥99.5% (Sigma); triple filtered ultra-pure deionised water, Millipore (Cranfield Health); HNO_3 ACS Reagent, 70% (Cranfield Health); H_2O_2 solution, containing inhibitor, 30 wt.% in water, ACS Reagent (216763 Sigma); analogue ultrasonic cleaner (Cranfield Health); contact angle goniometer, with light source, CCD camera and CAM 200 software, conforming to ISO and ASTM standards (Cranfield Health); Environmental Scanning Electron Microscope (ESEM), FEI XL30 (Cranfield School of Applied Science (SAS)); Energy Dispersive X-ray Fluorescence (EDXF), Bruker S2 Ranger (Cranfield SAS); Atomic Force Microscopy (AFM), Digital Instruments (Veeco) Nanoman VS (Cranfield SAS).

Passivation Protocol

Before any titanium discs were immersed in the passivation solutions, they were first ultrasonically cleaned in deionised water and then acetone for 5 minutes in each, followed by drying in a stream of nitrogen gas. The cleaned titanium discs were then immersed in the passivation solutions (5ml solution per titanium disc) chosen for specified periods of time. The passivated titanium discs were then removed and thoroughly rinsed three times in deionised water, followed by drying in nitrogen gas and being stored dry in a desiccator.

In this research four passivation solutions were tested: H_2O_2 30%wt; 70% HNO_3 in water at two ratios (3:7 and 1:1); and a mixture of H_2O_2 30%wt with 70% HNO_3 in water (1:1) (H_2O_2/HNO_3). First H_2O_2 30%wt was tested due to low contact angles with titanium surfaces described in the literature. H_2O_2 was tested at 24-hours passivation, as suggested abundantly in the literature,

followed by a shorter time of 12-hours in efforts to improve processing time. Next HNO_3 was tested at two ratios, the 3:7 ratio solution was tested according to ASTM F 86-01 protocol (30-minutes passivation), followed by a stronger concentration over three passivation times (30-minutes, 1-hour, and 2-hours). Finally, the novel passivation solution H_2O_2/HNO_3 was tested again following 30-minutes, 1-hour and 2-hours of passivation.

Mixing of H_2O_2 and HNO_3 was thought to enhance the oxidation effect of H_2O_2, enable acid etching of the titanium surface, and provide corrosion resistance simultaneously. In fact, sulphuric acid or hydrochloric acid is readily mixed with H_2O_2 for the passivation of titanium and its alloys. The acid etches the titanium surface whilst H_2O_2 oxidises it, increasing the thickness of the oxide layer and generating reactable hydroxyl groups. HNO_3 passivation of metals alone can release harmful NOx gases (nitrous oxides), while mixing HNO_3 with H_2O_2 suppresses the formation of NOx by re-oxidising NOx to $NO3^-$. Here it was thought that mixing HNO_3 with H_2O_2 could accomplish the same; and with the limited acid etching ability of HNO_3, nano surface features might be formed. Although no mention on the use of this mixture to passivate titanium, or its alloys, could be found in the literature, maintaining a degree of novelty for this research.

Surfaces were analysed for contact angle, using the sessile drop technique, imaged and profiled via ESEM and AFM, and a surface elemental analysis carried out using EDX. Before samples were analysed with ESEM, they were gold sputtered, and then imaged using the following parameters: Accelerating Voltage 2kV, Working Distance 57mm, Probe Diameter Spot Magnification. Analysis using AFM was conducted in contact mode with a silicon nitride probe. Three discs per sample group were analysed, and then averaged to give the result.

Table 1 - Passivation Solutions Tested, Passivation Solution Compositions, and Passivation Times (hours).

Passivation Solution	Passivation Time (hours)
H_2O_2 30%wt	12 and 24
70% HNO_3/H_2O (3:7)	0.5
70% HNO_3/H_2O (1:1)	0.5, 1 and 2
30%wt H_2O_2/25% HNO_3 (1:1)	0.5, 1 and 2

3.3 Results of Titanium Surface Passivation and Discussion

3.3.1 Contact-Angle

Contact -Angle-Contact-angle measurements were performed on a goniometer, which consists of a high-resolution camera for the observation and measurement of the angle subtended by a small droplet of liquid on a material surface. The goniometer is best used for planar surfaces such as plaques and films. After the droplet of liquid has been resolved by the camera, computer software calculates the contact-angle in a matter of seconds, making it a popular method of choice when investigating the wettability of a surface. The following images show three instances of contact-angle measurements taken during this work (Figure 17, Figure 18 and Figure 18).

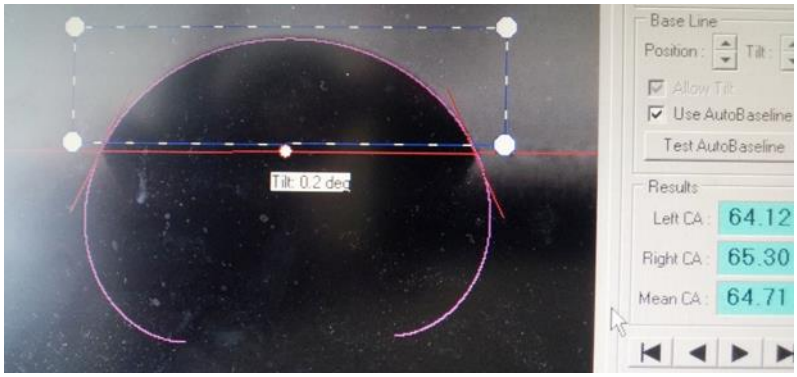

Figure 16 - Photograph of Contact-Angle Measurement of Raw Titanium Disc.

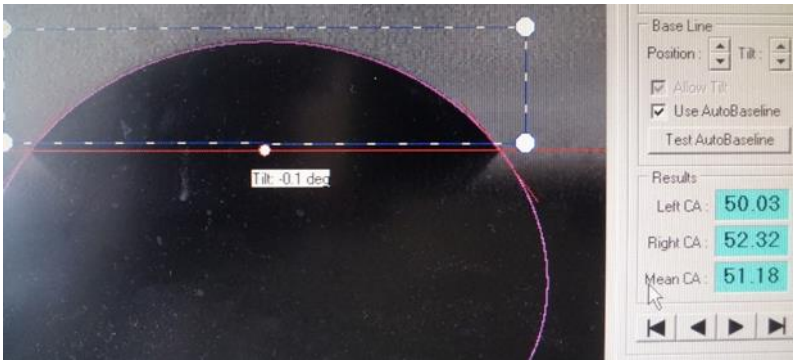

Figure 17 - Photograph of Contact-Angle Measurement of H_2O_2/HNO_3 (1:1) 30-minutes Passivated Titanium Disc.

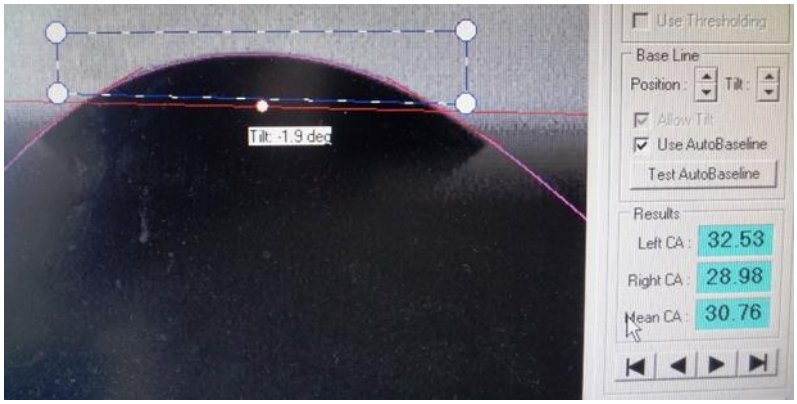

Figure 18 - Photograph of Contact-Angle Measurement of H_2O_2/HNO_3 (1:1) 2-hours Passivated Titanium Disc.

Table 2 - Contact Angles of Raw Titanium Disc (Control) and Titanium Discs Passivated with H_2O_2 30%wt (12 hours), H_2O_2 30%wt (24 hours), and HNO_3/H_2O (3:7) (30 minutes). Contact Angles are Means of 3 Discs per Sample Group. Confidence Intervals are Calculated at 95% significance (P=0.05).

	Passivation Solutions and their Contact Angles (Degrees °)			
	Raw Disc	H_2O_2 30%wt, 12-hours	H_2O_2 30%wt, 24-hours	HNO_3/H_2O (3:7), 30-minutes
Titanium Disc 1	80.72	31.20	19.26	79.64
Titanium Disc 2	82.56	31.15	16.25	74.02
Titanium Disc 3	64.71	40.52	21.09	59.78
Mean	**76.00**	**34.29**	**18.87**	**71.14**
95% Confidence Interval	**11.11**	**6.11**	**2.77**	**11.58**
Standard Deviation	9.82	5.40	2.44	10.24

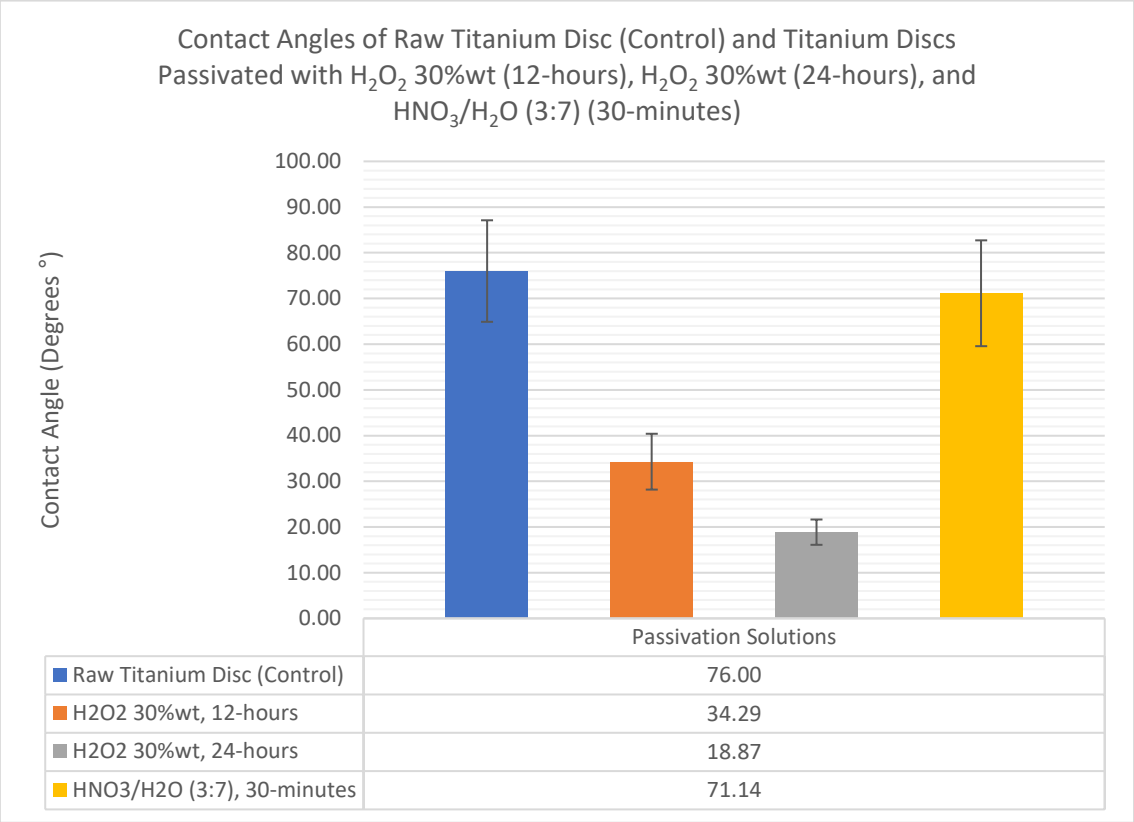

Figure 19 - Passivation results graph showing mean contact angles on Raw, H_2O_2 30%wt (12 and 24-hours), and HNO_3/H_2O (3:7, 30-minutes) Samples. Error bars represent 95% Confidence Intervals (P=0.05).

Contact angle measuring of a material surface has become increasingly popularised over the past two decades, especially since a wide acceptance in the scientific community that hydrophilicity/hydrophobicity can be controlled through simple topography changes and roughness. It is generally regarded that contact angles of 90° and above constitute a hydrophobic surface, while angles less than this can be regarded as hydrophilic (Drelich *et al.*, 2011). Titanium alloy, as well as many other metals, is considered hydrophilic due to the native oxide layer covering its surface. Therefore, it is no surprise that the Raw titanium alloy sample is hydrophilic, though its contact angle is close to the 90° cut-off for hydrophilic surfaces, similar

to values reported in the literature (Yang *et al.*, 2009a, Kutsevlyak *et al.*, 2008) and is the least wettable surface. This result is expected, as the raw titanium surface is hydrophilic but not strongly so, perhaps indicating a very thin oxide layer and/or possible hydrophobic surface contaminants.

Tukey-Kramer comparison analysis reveals that the Raw sample has a contact angle that is significantly greater than both hydrogen peroxide passivations (12-hour and 24-hour), but the same as HNO_3/H_2O (3:7) 30-minute passivation. Also, both hydrogen peroxide passivations (12-hour and 24-hour) are the same but both produce a significantly lower contact angle than the HNO_3/H_2O (3:7) 30-minute passivation solution. In this test group, the hydrogen peroxide passivation (12-hours and 24-hours) yields a significantly lower contact angle, and therefore a more hydrophilic surface (see Appendix sub-chapter 8.3.1 page 199-200).

Passivating with H_2O_2 30%wt resulted in the lowest contact angle after 24-hours of passivation (18.87° ± 2.77°), followed closely by passivating for 12-hours (34.29° ± 6.11°) (Table 2). These values are very close to those reported in the literature (Kainthan *et al.*, 2007), where it is mentioned that passivation with hydrogen peroxide (or peroxidation) can yield one of the most hydrophilic surfaces on titanium and its alloys. Increasing the time of passivation from 12-hours to 24-hours with hydrogen peroxide yielded a significantly reduced contact angle (Figure 19), similar to previously reported trends. Reports in the literature have suggested that the native oxide coating on titanium is composed of 2 layers; a barrier inner layer and a porous outer layer, and it is this outer oxide layer that houses the reactable hydroxyl groups. Furthermore, these reports have also suggested that hydrogen peroxide passivation increases dissolution and oxidation rates of the oxide layer and titanium atoms at the substrate surface, yielding enhanced oxide layer growth (Pan *et al.*, 1996, Liu *et al.*, 2004, Sobieszczyk, 2010). Therefore, increasing

passivation time with hydrogen peroxide could produce a much thicker oxide coating (thicker outer oxide layer), further improving the hydrophilic character of the surface with more hydroxyl groups, agreeing with the results here.

Hydrogen peroxide passivation of the titanium alloy surface is a preferred passivation technique in biomaterial applications research, with numerous research articles utilising hydrogen peroxide mixed with sulphuric acid, or piranha solution. One of the reasons for this is that a titania gel layer can be formed on titanium, and its alloys, through hydrogen peroxide passivation. The titania gel coating can enhance the bioactivity of titanium-based implants by inducing the formation of apatite crystals (theorised by enhanced adsorption of calcium and phosphate ions), thereby improving bone matrix mineralisation (Liu *et al.*, 2004, Mendonca *et al.*, 2008).

Passivating with HNO_3/H_2O (3:7) for 30-minutes yielded contact angles like that of the Raw titanium surface, with a mean contact angle of 71.14° ± 11.58° (Table 2). This high contact angle could indicate that HNO_3 passivation yields a very thin oxide layer, much like the native oxide formed on raw titanium. This coincides with literature reports that indicate the hydrophilic oxide layer formed from nitric acid passivation is very thin at around 10 nm (SMITH *et al.*, 1991). Also, passivating metals with nitric acid is usually conducted to clean surfaces of organic contaminants, such as metallic surgical equipment pre-treatment, and not necessarily to improve surface wetting.

Table 3 - Contact Angles of Titanium Discs Passivated with HNO_3/H_2O (1:1) and H_2O_2/HNO_3 (1:1). Contact Angles were Measured over 30-minutes, 1-hour, and 2-hours Passivation Times. Contact Angles are Means of 3 Discs per Sample Group. Confidence Intervals are Calculated at 95% Significance Level (P=0.05).

		Passivation Solutions and Their Contact Angles (Degrees °)	
		HNO_3/H_2O (1:1)	H_2O_2/HNO_3 (1:1)
30-minutes Passivation Time	Titanium Disc 1	75.09	47.31
	Titanium Disc 2	75.14	51.18
	Titanium Disc 3	75.00	45.34
	Mean	**75.07**	**47.94**
	95% Confidence Interval	**0.07**	**3.36**
	Standard Deviation	0.08	2.97
1-hour Passivation Time	Titanium Disc 1	60.77	48.60
	Titanium Disc 2	72.06	33.74
	Titanium Disc 3	76.50	47.26
	Mean	**69.78**	**43.20**
	95% Confidence Interval	**9.18**	**9.30**
	Standard Deviation	8.11	8.22
2-hours Passivation Time	Titanium Disc 1	71.79	30.76
	Titanium Disc 2	77.76	38.43
	Titanium Disc 3	69.39	36.87
	Mean	**72.98**	**35.35**
	95% Confidence Interval	**4.88**	**4.95**
	Standard Deviation	4.31	4.05

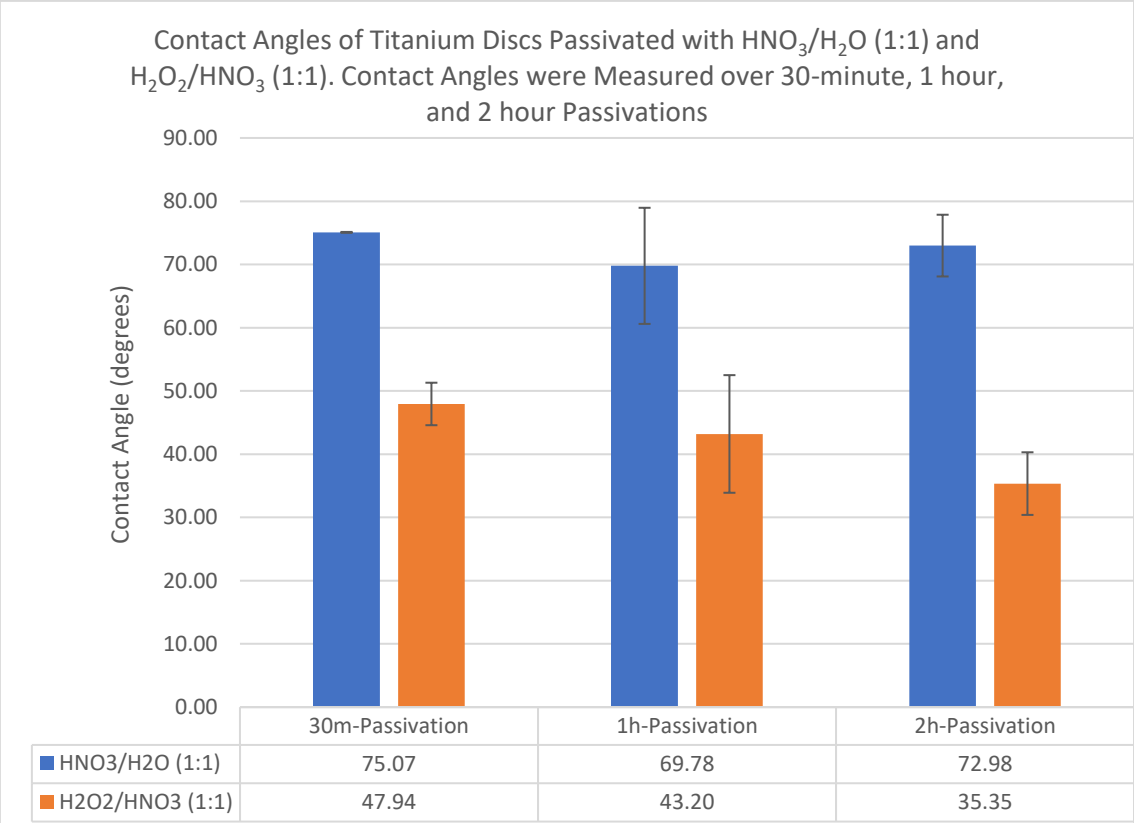

Figure 20 - Passivation results graph comparing mean contact angles of titanium discs passivated with HNO_3/H_2O (1:1) (blue bars) and H_2O_2/HNO_3 (1:1) (orange bars) following passivation times of 30-minutes, 1-hour and 2-hours. Error bars indicate confidence intervals calculated at 95% significance level (P=0.05).

Increasing the strength of the nitric acid passivation solution led to the testing of HNO_3/H_2O in a 1:1 ratio. Again, the results yielded poor contact angles of 75.07° ± 0.07°, 69.78° ± 9.18° and 72.98° ± 4.88° following passivation times of 30-minutes, 1-hour and 2-hours, respectively (Table 3). Tukey-Kramer statistical comparison revealed no significant difference between the three passivation times (see Appendix sub chapter 8.3.1, page 201-202).

Contact angles for passivation with the novel solution H_2O_2/HNO_3 (1:1) were very promising, achieving mean contact angles of 47.94° ± 3.36°, 43.20° ± 9.30° and 35.35° ± 4.95° degrees following passivation times of 30-minutes, 1-hour and 2-hours, respectively (Table 3). The wettability of the titanium alloy surface prepared by this solution is very similar to that of

hydrogen peroxide passivation, and achieved with a much faster passivation time. ANOVA and Tukey-Kramer analysis revealed a statistically significant difference between the 30-minutes and 2-hours passivation times only ($P=2.12^{-06}$), indicating that the 2-hours passivation with this solution yields the best surface in terms of hydrophilicity (excluding hydrogen peroxide passivation alone). Furthermore, a Tukey-Kramer comparison revealed that the 2-hours passivation yielded a contact angle comparable to that of hydrogen peroxide alone at 12-hours passivation (see Appendix sub chapter 8.3.1, page 203). Compared to the Raw titanium surface, H_2O_2/HNO_3 passivation (2-hours) reduced the contact angle of the titanium alloy surface by approximately 53.49%. The contact angle result achieved here with the hydrogen peroxide/nitric acid mixture confirms literature reports; that mixing hydrogen peroxide with an acid enhances its oxidation effect. This enabling a much shorter passivation time to significantly improve hydrophilicity of the titanium surface.

Generally, surfaces with increased wettability are sought to obtain surface characteristics that are conducive to stronger bone-implant bonding, and hydrophobic surfaces have been shown to reduce cellular metabolic activity *in vitro* (Liu *et al.*, 2004).

3.3.2 ESEM Imaging of Titanium Surface

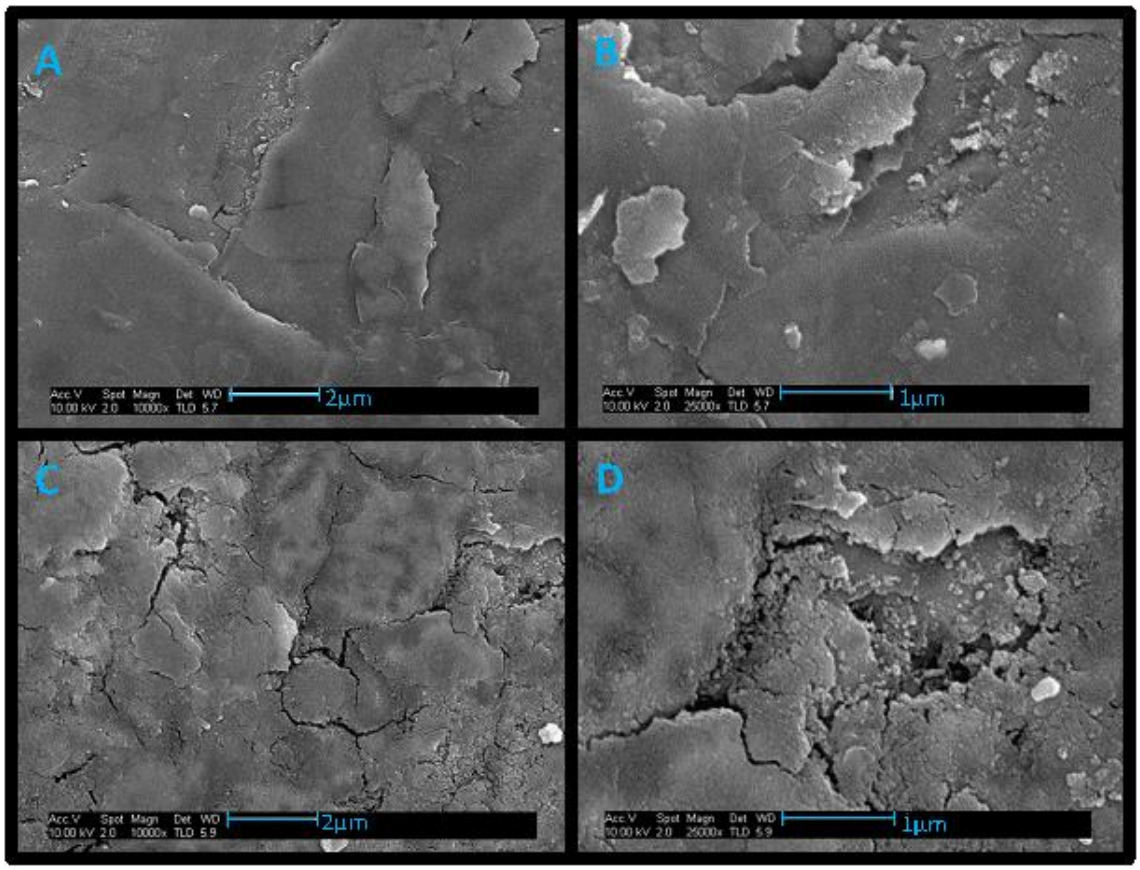

Figure 21 - A) and B) ESEM Images of Raw Titanium Disc at 10k and 25k Magnification, respectively. C) and D) H_2O_2 30%wt, 24 hours Passivation at 10k and 25k Magnification, respectively (10K and 25K Magnification Scale Bars at 2 and 1µm, Respectively).

The SEM images reveal the raw titanium alloy surface to have minimal surface features which is expected as the surface is machined (Figure 21, A and B). The SEM images for H_2O_2 30%wt 24-hours passivation (Figure 21, C and D) show a vastly cracked surface with extensive pitting and crevasses. This agrees with literature reports that passivating titanium with hydrogen peroxide for a prolonged period can etch the surface, leading to sub-micron and nano surfaces features.

The cracks, pits and crevasses produce a level of porosity that could allow infiltration of osteoid matrix and its subsequent mineralisation, thereby enhancing osseointegration.

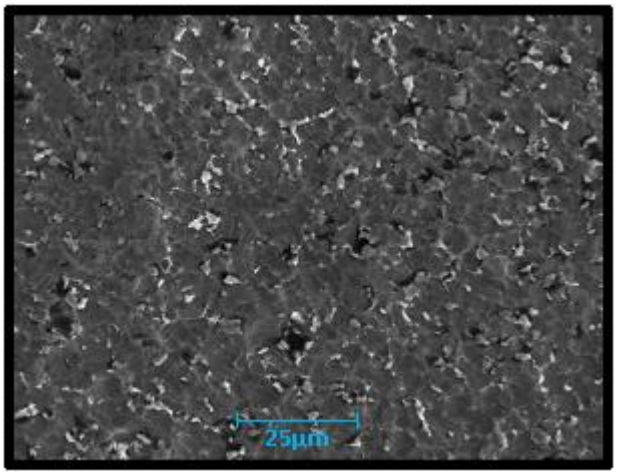

Figure 22 - ESEM Image of Titanium Alloy Disc Passivated with HNO_3/H_2O (3:7) Following 30-minutes Passivation Time (25µm Scale Bar).

The SEM image above (Figure 22) shows that passivating the titanium surface with nitric acid yields more surface features than that of the raw surface, such as cracks and pits. This result is in agreement with literature reports that indicate acid etching with strong acids (such as sulphuric, hydrochloric, or nitric acid) can form micro pits on a titanium implant surface (Manjaiah and Laubscher, 2017), though the extent of surface etching is not superior to that of peroxidation.

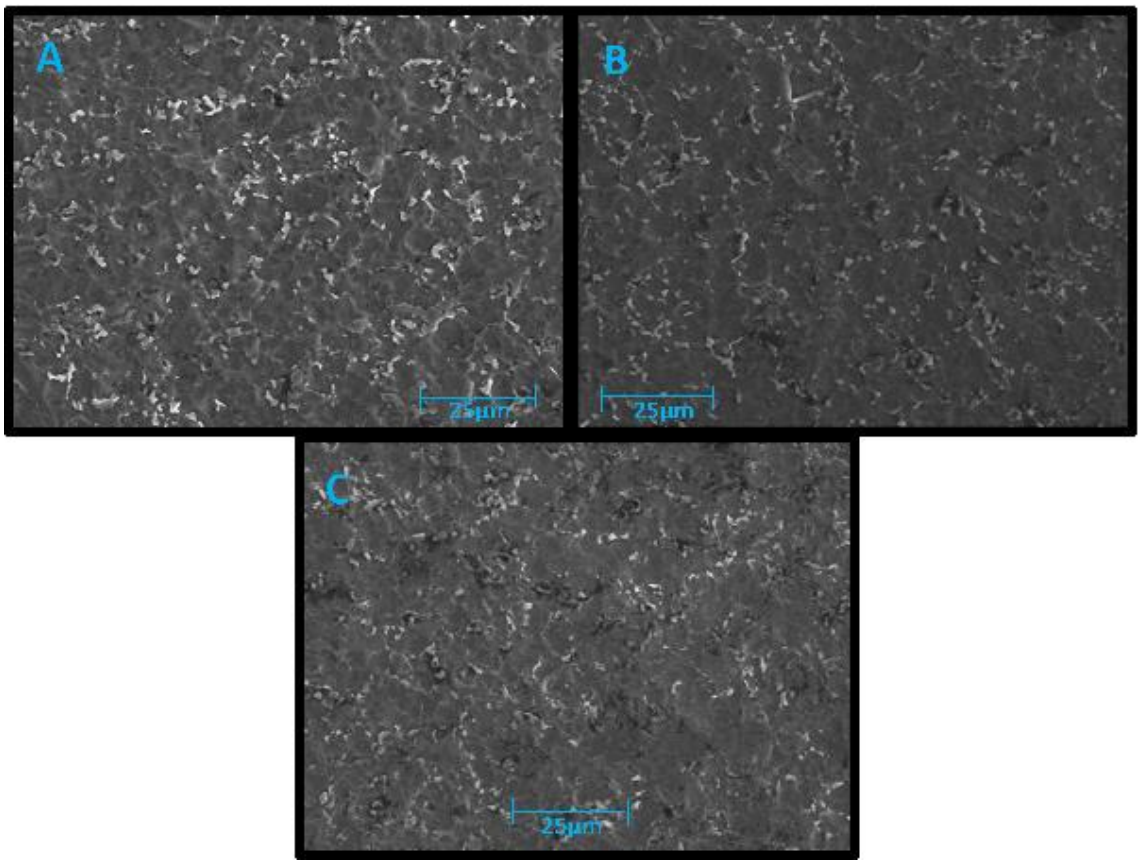

Figure 23 - ESEM Image of Titanium Alloy Discs Passivated with HNO_3/H_2O (1:1) Following A) 30-minutes B) 1-hour and C) 2-hours Passivation Times (25µm Scale Bar).

SEM images (Figure 23 A, B and C) reveal no significant changes to the surface topography when passivated with the stronger nitric acid solution compared to the weaker strength. Passivating the titanium surface with HNO_3 (1:1) shows little difference between the three passivation times (30-minutes, 1-hour, and 2-hours), indicating the inability of nitric acid to further etch the titanium surface after 30-minutes of passivation. This could be a reason why the ASTM F-86 procedure of nitric acid passivation of metals recommends a passivation time of just 30-minutes and no more.

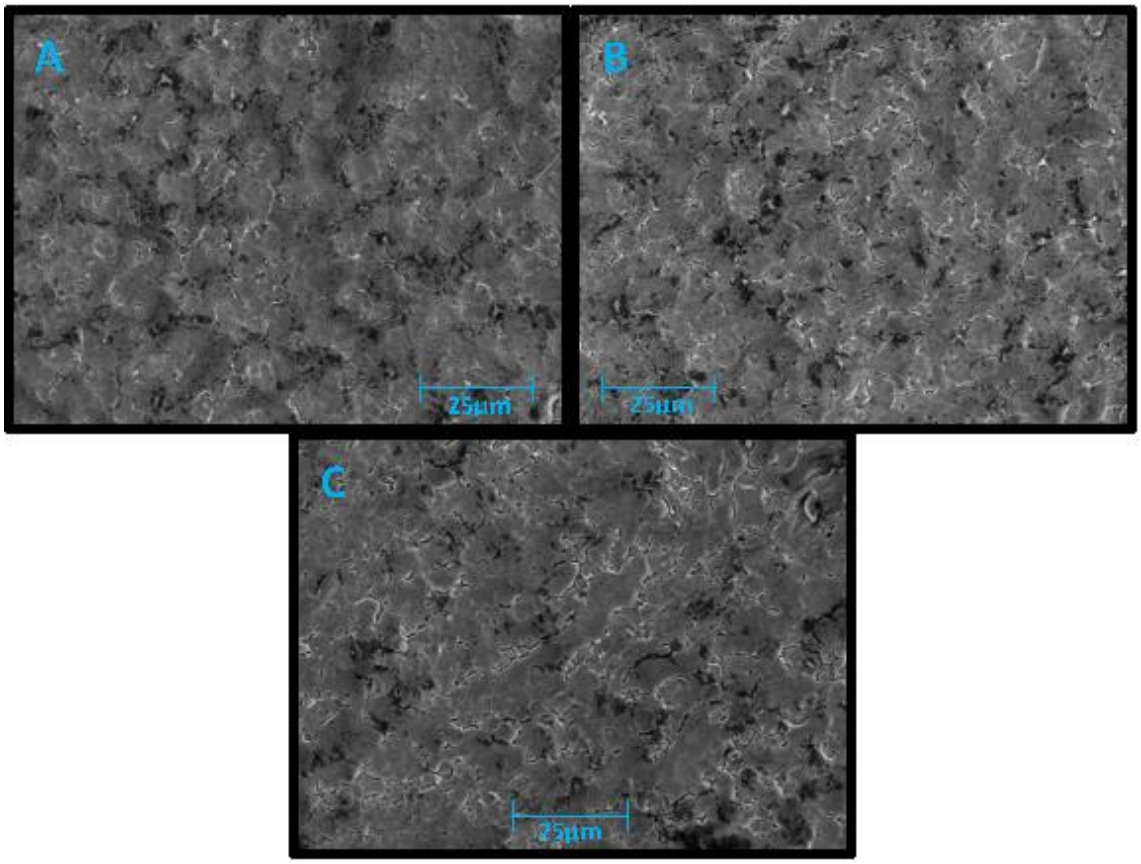

Figure 24 - ESEM Images of Titanium Alloy Discs Passivated with H_2O_2/HNO_3 (1:1) Following A) 30-minutes B) 1-hour and C) 2-hours Passivation Times (25 µm Scale Bars).

SEM images of titanium discs passivated with the novel hydrogen peroxide/nitric acid mixture (Figure 24, A, B and C) show a highly rough surface with extensive cracking. The contrast between light and dark areas on the SEM images indicate the peaks and valleys, respectively. The images here show many different shades from very light regions to much darker lines indicating peaks and valleys (and/or pits), similar to those seen on the SEM images of titanium discs passivated with hydrogen peroxide alone for 24-hours (Figure 21, C and D). The ability of nitric acid to enhance the oxidation effect of hydrogen peroxide is evident in these SEM images. This is expected since piranha solution is popularised with biomaterial surface pre-treatment in the literature, where hydrogen peroxide is mixed with sulphuric acid.

The topography of the titanium surface appears to show what can be described as cracks or valleys in circular formations, creating an anisotropic bumpy-like texture not seen with nitric acid passivation. Clearly this can be attributed to the hydrogen peroxide portion of the passivation mixture, and may be a result of the enhanced dissolution/oxidation effect of the oxide layer and titanium atoms at the surface.

3.3.3 AFM 3D Images of Titanium Surface

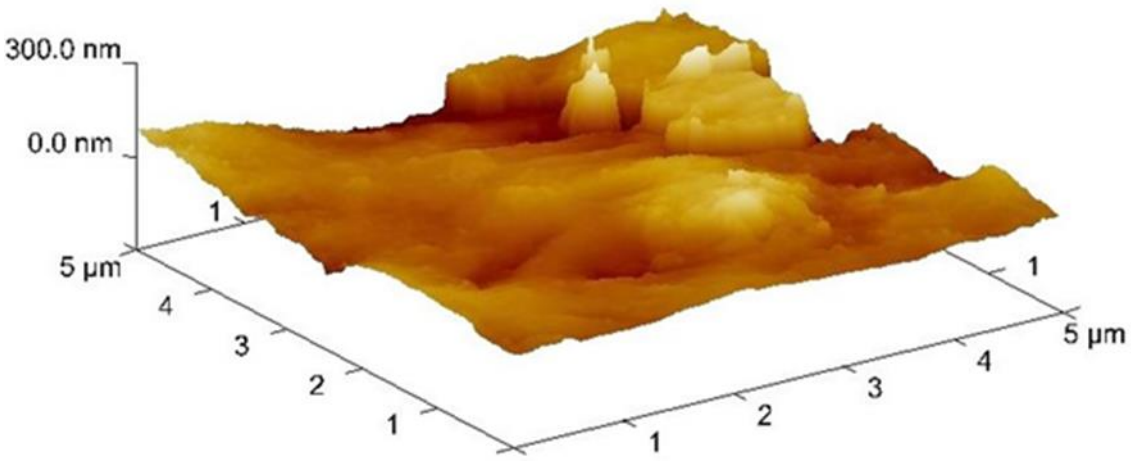

Figure 25 - 3D AFM Image of Raw Titanium Alloy Surface.

The 3D AFM image (Figure 25) clearly shows the raw titanium alloy surface to have minimal topographical features, as previously mentioned. The surface is smooth with some peaks that have sharp steep edges and some straight cracks and scratches (as seen from the SEM image, Figure 21, A and B), indicative of a machined surface.

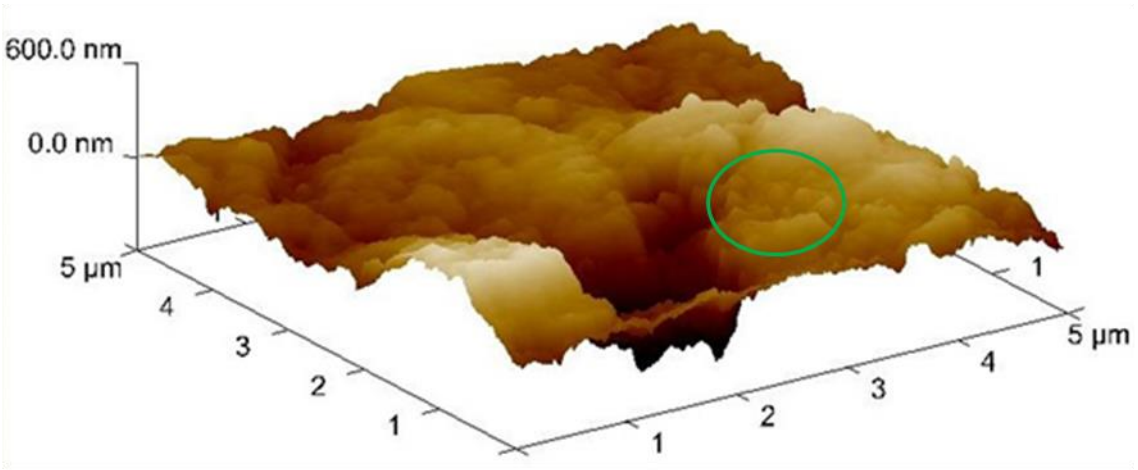

Figure 26 - 3D AFM Image of Titanium Alloy Surface Passivated with H_2O_2 30%wt Following 24-hours Passivation. Area Circles in Green Indicates Circular Bumpy Nanotexture.

The 3D AFM of the H_2O_2 30%wt 24-hours passivated titanium surface shows crevasses and pitting of up to 600nm deep however, on closer examination nano-width valleys can also be seen in circular formations (circled in green on Figure 26), thus creating a bumpy texture that is also seen on the SEM images of titanium discs passivated with the novel hydrogen peroxide/nitric acid mixture (Figure 24), as previously explained. The circular bumpy formations are roughly 250nm in diameter and separated by valleys of about 10nm in width. It is possible this nanoscale bumpy texture lends to the nano rough surface topography of the titanium when passivated with hydrogen peroxide.

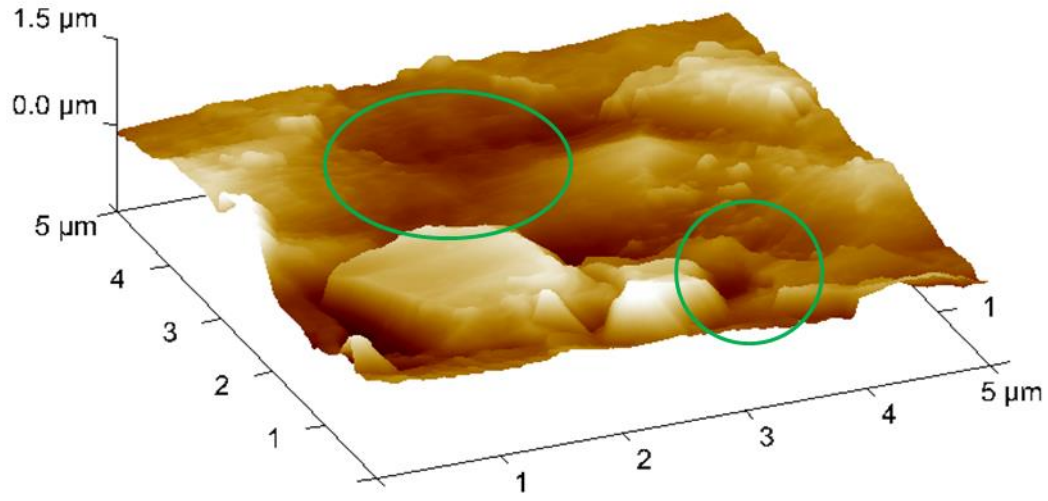

Figure 27 - 3D AFM Image of Titanium Alloy Surface Passivated with HNO_3/H_2O (3:7) Following 30-minutes Passivation Time. Areas Circled in Green Show Pit and Crevasse Formations.

Literature reports indicate that acid etching can infer micro-pits on the titanium surface ranging from 0.5 to 2 µm, and it can be seen in the 3D AFM image pits of approximately 0.3 to 2 µm in diameter (Figure 27, possible pitting is circled in green) when the surface is passivated with HNO_3/H_2O (3:7). Although nitric acid passivation is not natively used for acid etching, clearly the 3D AFM image, as well as the SEM images (Figure 22 and Figure 23), show that nitric acid does have some ability to form random surface features and thus increase the roughness of the titanium surface over that of the raw titanium. Also, the nanoscale bumpy texture seen on the titanium surface passivated with hydrogen peroxide is not seen here, perhaps due to the omission of hydrogen peroxide from the passivation mixture, and therefore no enhanced dissolution/oxidation at the titanium surface.

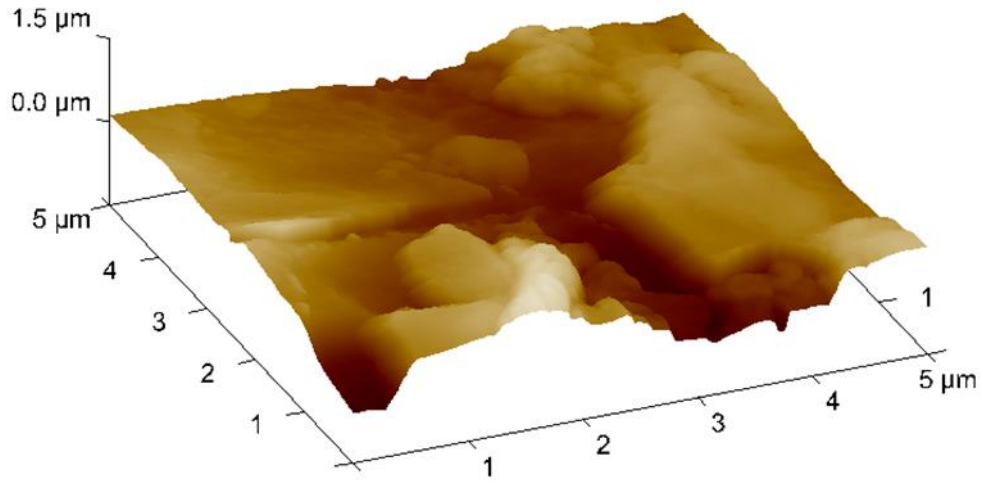

Figure 28 - 3D AFM Image of Titanium Alloy Surface Passivated with HNO_3/H_2O (1:1) Following 30-minutes Passivation Time.

Passivating with the stronger nitric acid solution (HNO_3/H_2O, 1:1) again reveals pitting and/or trenches of roughly 0.5 – 1.5µm deep with a relatively smooth surface after 30-minutes of passivation (Figure 28), similar to that of the weaker strength nitric acid (Figure 27). Although the raised areas appear to have smoother edges as opposed to sharp edges, possibly indicating a further etching of the surface over that of the weaker strength nitric acid passivation. However, the surface of the titanium discs passivated with HNO_3/H_2O (1:1) after 1 and 2-hours of passivation (Figure 54 and Figure 55in the appendix sub chapter 8.1.1, respectively), shows a similar level of surface topography to that of the 30-minutes passivation, showing the inability of nitric acid to further etch the titanium surface beyond this time.

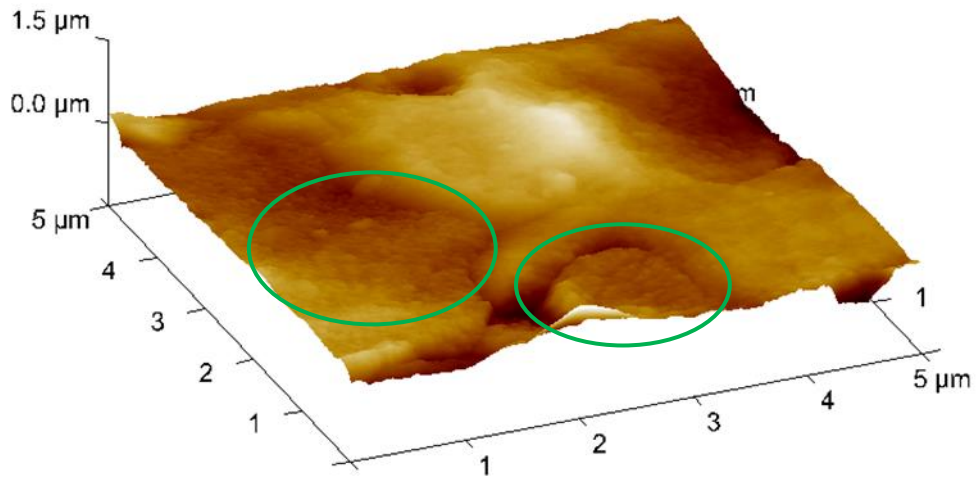

Figure 29 - 3D AFM Image of Titanium Alloy Surface Passivated with H_2O_2/HNO_3 (1:1) Following 2-hours Passivation Time. Areas Circled in Green Indicate Circular Bumpy Nanotexture.

The titanium surface passivated with the novel hydrogen peroxide/nitric acid mixture shows a relatively smoother and flatter surface than nitric acid passivation (Figure 29), with crevasses up to 1-1.5µm deep, but the bumpy texture that was previously seen when passivating with hydrogen peroxide is still visible, although the bumps are much less pronounced and flattened (bumpy texture circled in green on Figure 29). The 3D AFM images for the titanium surfaces passivated with H_2O_2/HNO_3 (1:1) following 30-minutes and 1-hour of passivation time, Figure 56 and Figure 57 in Appendix sub chapter 8.1.1, show a surface topography similar to that passivated at 2-hours. Furthermore, the circular bumpy nanotexture seen on the 2-hour passivation is also is also seen on the 30-minute and 1-hour passivation times however, the circular bumps are larger. Perhaps more time is required to etch the surface and develop the circular bumpy nano surface structures.

3.3.4 AFM Spectral Graphs

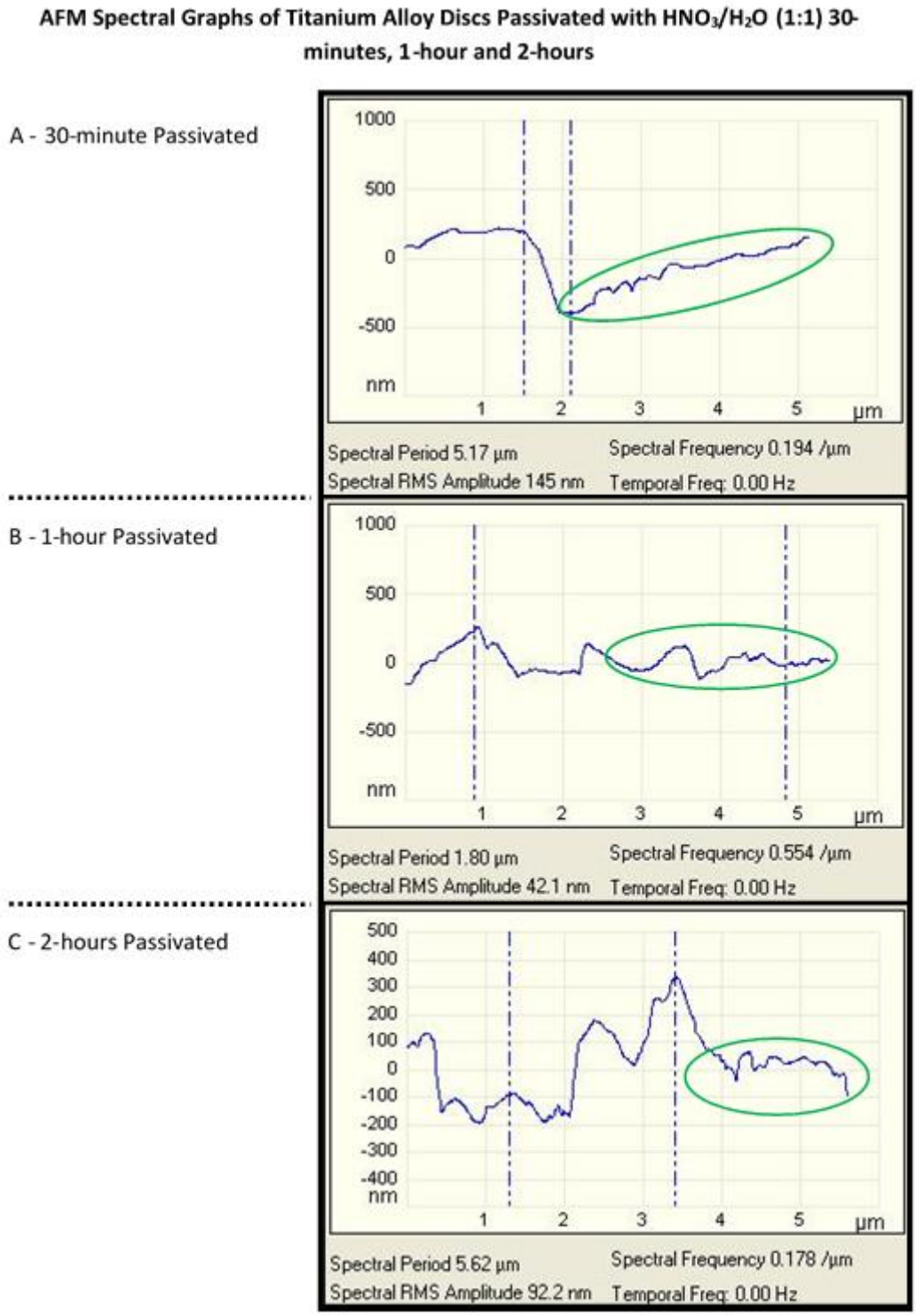

Figure 30 - AFM Spectral Graphs of Titanium Samples Passivated with HNO_3/H_2O (1:1) for A) 30-minutes B)1-hour and C) 2-hours Passivation Times

AFM Spectral Graphs of Titanium Alloy Discs Passivated with HNO_3/H_2O_2 (1:1) 30-minutes, 1-hour and 2-hours

A - 30-minute Passivated

B - 1-hours Passivated

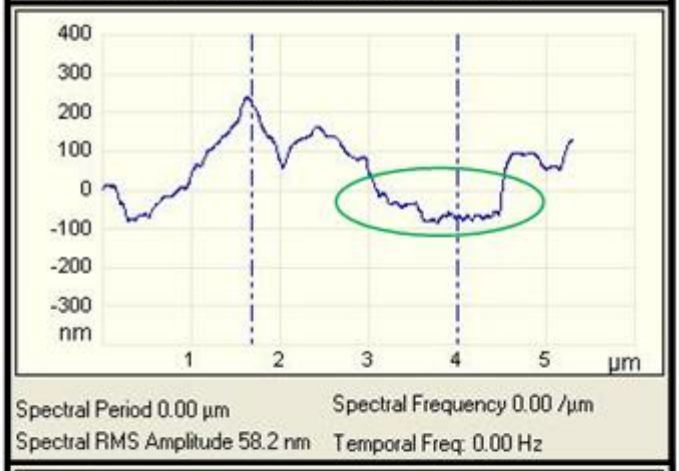

C - 2-hours Passivated

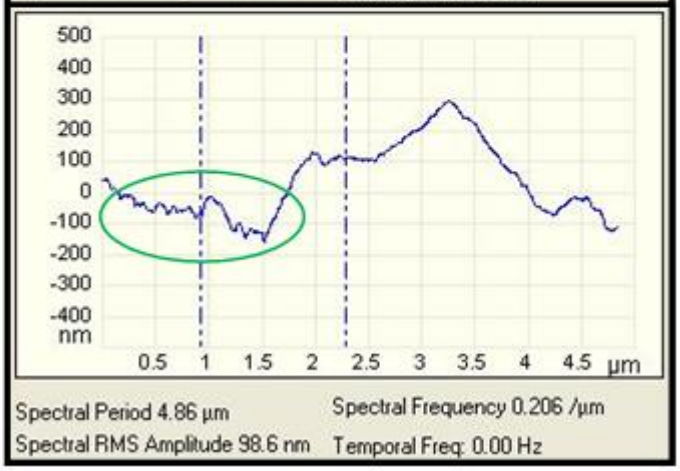

Figure 31 - AFM Spectral Graphs of Titanium Samples Passivated with HNO_3/H_2O_2 (1:1) for A) 30-minutes B)1-hour and C) 2-hours Passivation Times

The previous two images (Figure 30 and Figure 31) are spectral graphs produced from AFM section images. This type of graph shows the undulations of the surface (peaks and troughs) as the AFM tip scans over the sample at a measured length. On samples passivated with the stronger nitric acid strength, the spectral graphs show a smooth line with micron sized peaks and troughs (Figure 30, smooth line circled in green). However, for the samples passivated with the novel H_2O_2/HNO_3 mixture, the line on the spectral graph shows nano sized peaks in a tight jagged pattern, indicating small peaks and troughs tightly packed together (Figure 31, rough line circled in green). This could indicate a surface roughness at the nano level, possibly making up the nano bumpy texture previously seen on the SEM and AFM 3D images.

The following AFM spectral image also indicates no nanoscale bumpy texture (smooth profile line) on the titanium alloy surface passivated with the weaker nitric acid solution, HNO_3/H_2O (3:7) (Figure 32, area circled in green).

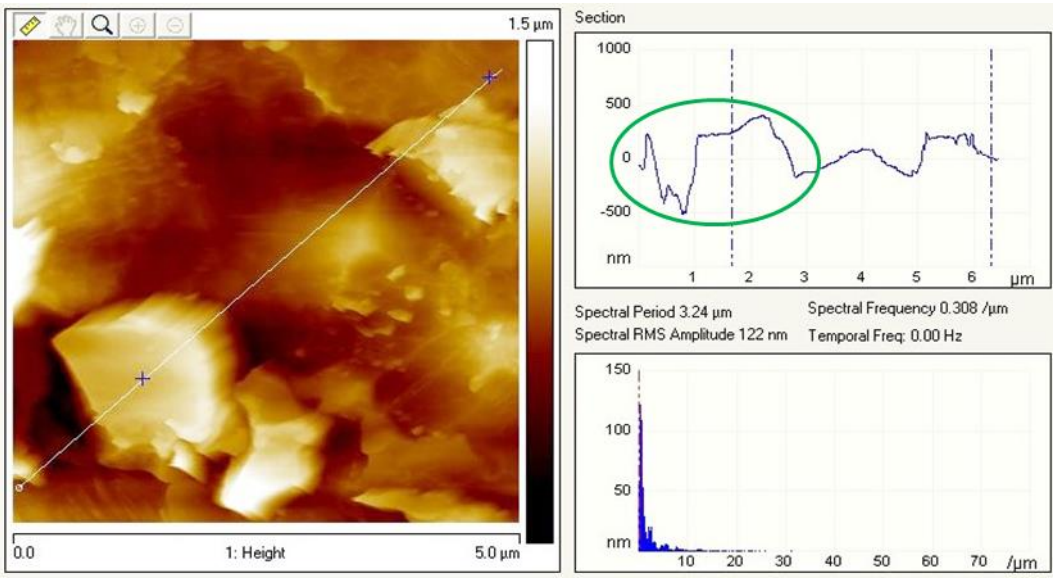

Figure 32 - Spectral Image and Graph from AFM of Titanium Alloy Surface Passivated with HNO_3/H_2O (3:7) Following 30-minute Passivation. Area Circled in Green Shows Intimate Surface Profile (Peaks and Troughs), Revealing no Nanoscale Bumpy Texture.

3.3.5 Surface Roughness

The most important parameters that are considered to characterise the topography of a surface are amplitude parameters. These are used to measure vertical distances (peaks and valleys) of the surface deviations. Ra is defined as the arithmetic mean of the profile height deviations from the mean line across one sampling length, and is one of the most popularised roughness parameters describing average roughness irregularities, being easy to measure and providing a good generalisation of the height deviations of a sample surface. Though it does not give information regarding wavelength and is not sensitive to occasional profile changes. Therefore, the roughness parameter Rq or RMS (Root Mean Squared) is often used in conjunction as it gives the standard deviation of the distribution heights, making it more sensitive to occasional highs and lows, whereas the Ra parameter averages all the peaks. The final roughness parameter that was measured here is Rmax. This parameter gives the vertical distance between the lowest valley and highest peak along a sampling length, and is thus very sensitive to high peaks or deep scratches (Gadelmawla *et al.*, 2002).

The aforementioned parameters are the most widely used, and functionally important, height parameters to assess the roughness profile of a material surface in two dimensions along a single sampling length; a lower value for each of these parameters indicates a smooth surface, while a higher value indicates a rough surface topography.

Table 4 - Surface Roughness Parameters of all Passivated Surfaces, including Raw Titanium Disc (as Measured by AFM). Roughness Parameters Measured Include Ra, Rmax and RMS. All Roughness Values Measured in nm.

	Roughness Parameters		
Passivation Solution	Ra (nm)	Rmax (nm)	RMS or Rq (nm)
Raw Titanium Alloy (No Passivation)	28.0	401	38.5
H_2O_2 30%wt, 24 hours	105	1026	147
HNO_3/H_2O (3:7), 30 minutes	155	1374	198
HNO_3/H_2O (1:1), 30 minutes	194	1330	236
HNO_3/H_2O (1:1), 1 hour	93.8	1128	129
HNO_3/H_2O (1:1), 2 hours	78.1	680	99.3
H_2O_2/HNO_3 (1:1), 30 minutes	75.3	763	90.3
H_2O_2/HNO_3 (1:1), 1 hour	64	629	83.3
H_2O_2/HNO_3 (1:1), 2 hours	81.5	979	104

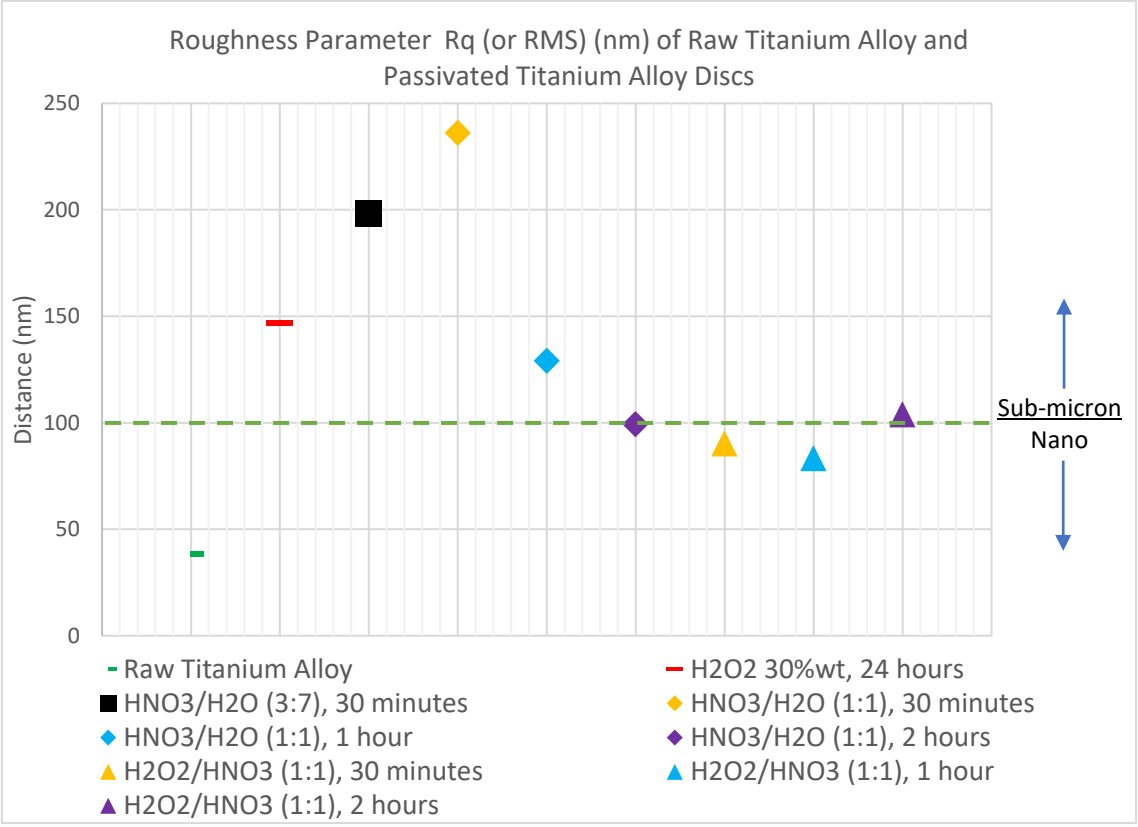

Figure 33 - Surface roughness results for Raw and Passivated sample surfaces. Graph shows that titanium surfaces passivated with the novel hydrogen peroxide/nitric acid solution, to yield surface roughness at the nano scale.

The surface roughness results (Table 4) show the H_2O_2/HNO_3 solution following 1-hour passivation yielded the second lowest Ra value of 64 nm, after the raw titanium surface. This passivation solution also gave the second lowest value for Rmax (629 nm). Unlike the nitric acid passivation; which yields a smoother surface as the passivation time increases, the H_2O_2/HNO_3 solution increased the roughness of the surface with increasing passivation time from 1-hour to 2-hours, indicating that it may further etch the titanium surface if given more time. Passivating with H_2O_2 alone for 24-hours revealed that the average roughness of the surface lies at the nano scale boundary, with a Ra value of 105 nm and RMS of 147 nm (Table 4 and Figure 33), though passivating with the novel hydrogen peroxide/nitric acid solution provides a truly nano rough surface with Ra values less than 100 nm (for all three passivation times).

The higher concentration of HNO_3 (1:1) yielded the roughest surface with a Ra value of 194 nm, which is in agreement with literature reports, such as that obtained by Mante *et al.* (2004) who reported an Ra value of 208.1 nm following HNO_3 passivation in accordance with ASTM F 86-01 protocol. The novel passivation mixture H_2O_2/HNO_3 yielded the smoothest surfaces (not including the raw sample), with Ra values of 75.3 nm, 64.0 nm and 81.5 nm following 30-minutes, 1-hour and 2-hours passivation, respectively. The H_2O_2 30%wt and HNO_3 solutions all generated an average roughness greater than 100 nm (except the higher strength HNO_3 (1:1) after 1 and 2-hour passivation). Nano is defined as a length of 100 nm and below therefore, the H_2O_2 30%wt and HNO_3 solutions yielded roughness levels that can be considered at the sub-micron level, and the novel H_2O_2/HNO_3 solution can be said to yield a nano rough surface on titanium.

Disregarding the raw titanium surface, all titanium samples show Rmax values at the micron level, whereas the novel H_2O_2/HNO_3 mixture provides a titanium surface with Rmax values at the sub-micron level. Also, the Ra and Rq values for all samples are at the sub-micron level, but passivating the titanium surface with H_2O_2/HNO_3 produces roughness values at the nano level. Thus, the novel passivating solution is the only mixture that produces both sub-micron and nano scale topographic features when passivating the titanium surface.

Although many studies suggest that nano surface topography can enhance interactions between implant surfaces and cells, through the theory of biomimesis, micro surface topography has also been shown to achieve similar results. By itself, RGD has been shown to increase cell attachment and proliferation (Ruoslahti and Pierschbacher, 1987, Ruoslahti, 1996), including the attachment and proliferation of osteoblasts to tissue culture polystyrene (Dee *et al.*, 1998, Schuler *et al.*, 2006a, Schuler *et al.*, 2006b). These studies suggested that

osteoblast differentiation was promoted by substrates that fostered reduced spreading like microstructured Ti (Boyan *et al.*, 2001) and PLL-g-PEG (Tosatti *et al.*, 2004).

3.3.4 EDS

Table 5 - EDS Elemental Analysis of Titanium Disc Surfaces Passivated with HNO3/H2O (3:7 and 1:1), and H2O2/HNO3.

	Element Weight%					
Passivation Solution and Time	Carbon	Oxygen	Aluminium	Silicon	Titanium	Vanadium
Raw Titanium Alloy (No Passivation)	0.91	1.21	4.13	0.06	89.34	4.35
HNO_3/H_2O (3:7) 30-minutes	0	0.38	4.03	-	91.33	4.25
HNO_3/H_2O (1:1) 30-minutes	0.46	0.98	3.89	0.12	90.36	4.19
HNO_3/H_2O (1:1) 1-hour	0.62	1.19	3.89	0.16	89.83	4.3
HNO_3/H_2O (1:1) 2-hours	0.13	0.50	3.95	0.1	90.91	4.41
H_2O_2/HNO_3 (1:1) 30-minutes	0.53	2.13	4.14	-	89.91	3.3
H_2O_2/HNO_3 (1:1) 1-hour	0.6	2.32	4.03	-	89.49	3.57
H_2O_2/HNO_3 (1:1) 2-hours	0.6	2.44	4.03	-	89.45	3.48

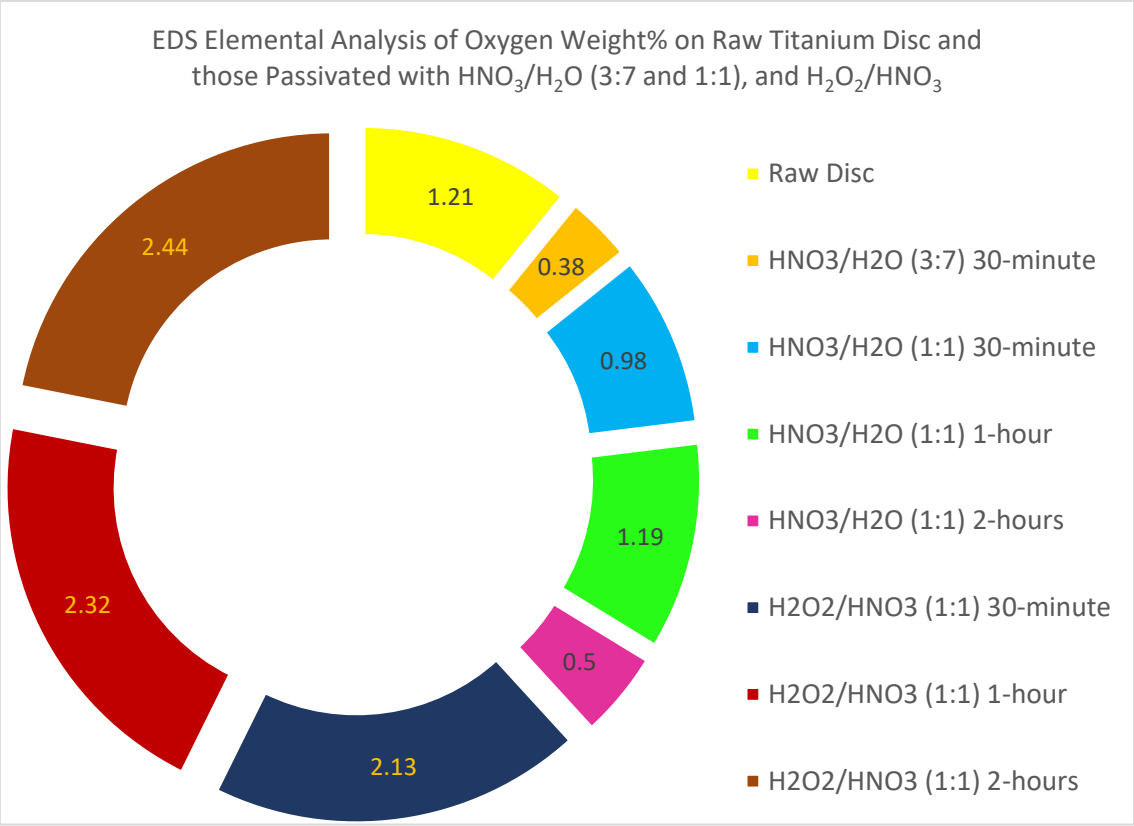

Figure 34 - Doughnut graph showing the elemental oxygen weight% on Raw titanium and Passivated surfaces.

EDX elemental analysis showed no distinct change in oxygen weight% between the two HNO_3 strengths, possibly indicating a similar extent of formation of a thin oxide coating. Also, increasing the passivation time from 30-minutes through to 2-hours yielded no significant change in oxygen %weight for the higher strength HNO_3.

The EDX elemental analysis does reveal the hydrogen peroxide/nitric acid passivating mixture to increase the weight% of oxygen over all other passivating solutions. This could indicate a highly oxidised titanium surface containing more TiO_2 and/or TiOH groups. Furthermore, passivating with hydrogen peroxide/nitric acid increased the surface oxygen weight% by an average of 171% (compared to all other sample surfaces), which correlates with the increased hydrophilicity of the titanium surface following this passivation treatment.

Rougher surfaces generally tend to show hydrophobicity due to frictional forces. The passive oxide layer coating the titanium alloy is a major factor that dictates the wettability of the surface; containing hydroxyl groups in the outer oxide layer for hydrogen bonding with water. A greater extent of oxide layer formation could render the titanium surface hydrophilic, and vice versa. The raw titanium surface therefore may have the thinnest oxide layer covering its surface, given that the vanadium portion of this titanium alloy generally yields corrosion resistance. Passivation treatment with hydrogen peroxide and/or nitric acid has the general effect of cleaning the metal surface from hydrocarbon contaminants. The untreated raw titanium alloy surface therefore may have hydrocarbon contaminants, thus increasing its hydrophobicity.

Passivation with H_2O_2 therefore produces both micro and nano surface features, both of which are conducive to differing cellular functions. Literature reports suggest that micro rough surfaces improve cell attachment, spreading, and proliferation, while nano surface features have been shown to enhance cell differentiation, bone matrix protein production, and thus improved bone matrix mineralisation (Webster and Ejiofor, 2004, Ji *et al.*, 2008, Davies, 1998, Lorenzetti *et al.*, 2015), although many studies show conflicting results.

As previously mentioned, the combination of H_2O_2 with an acid may enhance the oxidation effect of the passivating solution. This is evidenced by the EDS elemental analysis (Table 5) which shows a greater amount of oxygen content on the titanium surface passivated with this novel mixture. This indicates a greater level of oxidation of the titanium surface compared to that of the raw surface and even HNO_3 passivation. This passivation mixture may therefore increase the thickness of the oxide layer on the titanium surface. The oxide layer is important for both compatibility of the surface, and the surfaces propensity to permit bone matrix mineralisation. Literature reports suggest that the oxide layer on titanium directly reacts with calcium phosphate in simulated biological fluid (Pan *et al.*, 1996, Moore *et al.*, 2014). On

exposure of the oxide layer to biological fluids, hydroxyl groups in the oxide layer can induce the spontaneous nucleation of apatite crystals (Hydroxyapatite) (Oates *et al.*, 2011). Furthermore, the native oxide layer found on the surface of titanium (and its alloys) formed via atmospheric oxidation or chemical passivation, is absolutely essential to its biocompatibility, as well as enhanced osseointegration of titanium implants and achieving a dynamic bone-implant interface (Mandracci *et al.*, 2016).

Numerous studies in the literature have shown that titanium surface properties, such as roughness and topography, can influence cellular morphology and cell surface guidance (Manjaiah and Laubscher, 2017). Knowledge from the literature tells us that a smoother surface is better for cell support in terms of cell attachment and spreading. Conversely, a rougher surface induces cell differentiation. Some reports suggest that a substrate surface that better resembles the natural ECM environment of the cells will lead to a better cell response (otherwise known as a biomimetic surface), thus speculating at the advantageous effects of topographical surfaces at the nano level.

4 Hyperbranched Polyglycerol Polymerisation (HBPG)

The aim of this portion of the research was to covalently attach polyglycerol (PG) to the titanium alloy surface. Research in the literature has revealed surface initiated polymerisation via atom transfer radical polymerisation of other polymers to silica and aluminium surfaces, but this research utilised a simpler polymerisation scheme, whereby Hyperbranched Polyglycerol (HBPG) was polymerised from a titanium alloy surface via Ring Opening Multi Branching Polymerisation (ROMBP).

HBPG was chosen in this research due to its extremely low *in vivo* toxicity and biocompatibility. The literature has shown HBPG to accumulate in vital organs very minimally, even less so than other polymers that are currently in use for various biomedical applications, and has been found to be non-immunogenic (Abbina *et al.*, 2017). Thus, it has been researched actively by the scientific community in areas such as pharmaceutical carries and controlled drug delivery, cell supportive tissue engineering scaffolds, dialysis, organ preservation, and cell surface engineering, as imaging agents and theranostics, as well as antibacterial/antifouling agents (Abbina *et al.*, 2017).

The polymerisation protocol here uses a base catalysed ROMBP of glycidol, and was adapted from the protocol presented by Sunder and colleagues (1999) and also Kainthan *et al*. (2006). Although PG is polymerised from a multifunctional core molecule in this work the titanium surface, which bares many hydroxyl groups, acted as the functional core from which polymerisation proceeds, effectively producing HBPG covalently attached to the titanium surface. The following scheme provides an overview of the polymerisation reaction between the titanium surface and the glycidol monomer (Scheme 5), although a more in-depth reaction scheme was shown in sub chapter 2.4.2 (Scheme 1 and Scheme 2).

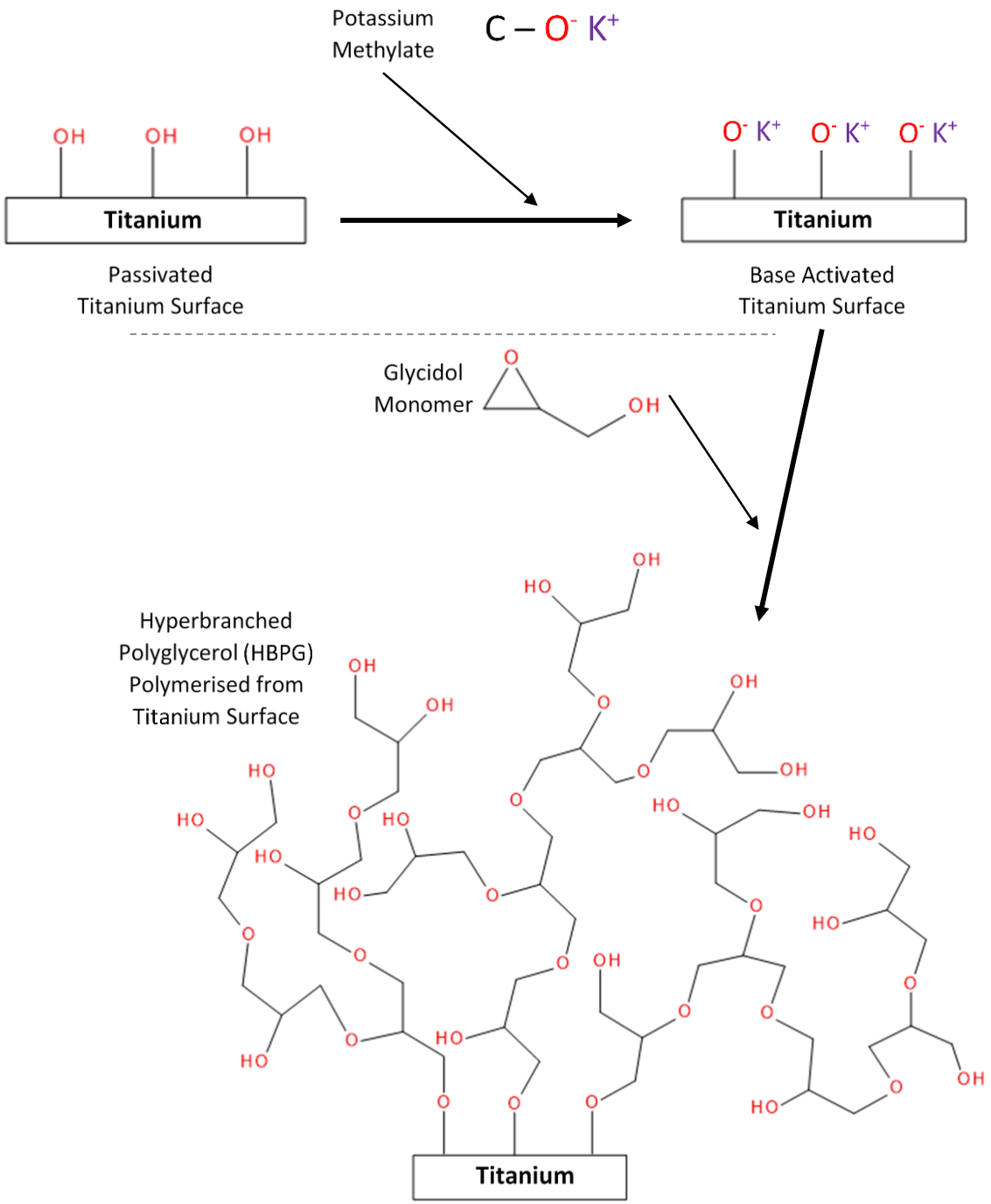

Scheme 5 - Reaction scheme for polymerisation of Hyperbranched Polyglycerol (HBPG) from the titanium surface. Reaction proceeds via base catalysis using potassium methylate to activate hydroxyl groups on titanium, followed by addition of glycidol monomer to initiate and propagate chain growth (adapted from Sunder et al. (1999).

Passivation testing revealed the novel H_2O_2/HNO_3 (2-hour passivation) solution to produce a highly oxidised surface (high wettability) with nano surface features, therefore this passivation procedure was utilised for the Passivated and Passivated/Polymerised sample titanium discs for further experiments. Surfaces were analysed for contact angle using the sessile drop technique, imaged and profiled via ESEM, AFM, and a surface elemental analysis carried out using EDX. Before samples were analysed with ESEM, they were gold sputtered, and then imaged using the following parameters: Accelerating Voltage 2kV, Working Distance 57mm, Probe Diameter Spot Magnification. Analysis using AFM was conducted in contact mode with a silicon nitride probe. Due to time constraints and no access to suitable equipment, the strength of polymer adhesion could not be measured. This is an important aspect for orthopaedic implants, as the polymeric coating would need to withstand storage, delivery, handling and implantation into the host bone.

4.1 Materials and Methods

Titanium Alloy (Ti6Al4V) circular discs (provided by SinteaPlustek and William Gregor Ltd), with dimensions of 14mm diameter by 1mm thick, machine cut; Potassium Methoxide ~25% in methanol (60402 Sigma Aldrich); Glycidol 96% (G5809 Sigma Aldrich); 1,4-Dioxane, ReagentPlus ≥99% (D201863 Sigma); single syringe infusion pump, Cole Palmer (Cranfield Health); hot plate magnetic stirrer, IKA C-MAG HS7 (Cranfield Health); CamLab Choice OS20-S LED digital overhead stirrer (DL/840102318888 CamLab Limited); Acetone ACS Reagent ≥99.5% (Sigma); triple filtered ultra-pure deionised water, Millipore (Cranfield Health); Environmental Scanning Electron Microscope (ESEM), FEI XL30 (Cranfield School of Applied Science (SAS)); Energy Dispersive X-ray Fluorescence (EDXF), Bruker S2 Ranger (Cranfield SAS); Atomic Force Microscope (AFM), Digital Instruments (Veeco) Nanoman VS (Cranfield SAS).

Ring Opening Multi-Branching Polymerisation (ROMBP) of HBPG

10 titanium discs were placed in the glass vessel, which was purged with argon gas, and placed in a silicon oil bath at 85 degrees Celsius (reflux with gas bubbler attached). Approximately 300µl of potassium methylate 30%wt (in ethanol) was dropped onto each disc over a period of 5 minutes, and left to react for 2 hours to deprotonate the hydroxyl groups on the titanium surface. After the 2 hours had elapsed, a pump was connected to the vessel to create a vacuum for 30 minutes, the aim of which was to ensure complete removal of the methanol in the base solution. This was followed by injection of a mixture of 30ml glycidol monomer (3ml per titanium disc) and 10ml of dioxane over 12 hours, and mixing of the monomer solution in the vessel using a mechanical stirrer at 200rpm.

HBPG is usually synthesised without any solvent addition, however when attempting to synthesise higher molecular weight PG, the subsequent increase in viscosity requires an inert solvent to aid mixing. Although diglyme solvent can be added, dioxane was shown to yield higher molecular weight HBPG (KAINTHAN *et al.*, 2006). Also, an undesired side-reaction can lead to the production of cyclised by-products known as macrocyclics. Addition of the glycidol monomer slowly over a period of 12 hours suppresses this side reaction (Slow Monomer Addition – SMA), which leads to a faster polymer chain propagation reaction, and also narrow polydispersity (KAINTHAN *et al.*, 2006, Sunder *et al.*, 1999).

Upon completion of the polymerisation, the titanium discs were removed from the vessel and rinsed 3 times in deionised water to remove any low molecular weight entangled polymer chains. Any polymer covering the underside of the discs was carefully scraped away to ensure only the top surface of the disc was covered with polymer. The polymerised discs were very briefly rinsed in acetone and then dried in a stream of nitrogen gas, then stored dry in a desiccator.

4.2 HBPG Polymerisation Results and Discussion

Figure 35 - Photo of Passivated/Polymerised Titanium Alloy Disc. Titanium Disc Passivated with H_2O_2/HNO_3 (1:1) 2-hours Passivation. Polymer Layer is approx. 0.7-0.8mm in Thickness, compared to the 1mm Thick Titanium Disc. Polymer is Highly Viscous, Clear and Transparent, Indicating Hyperbranched Structure.

The colour and form of polyglycerol (PG) is a good indicator as to whether the polymerisation has yielded a hyperbranched structure, specifically a viscous and transparent polymer is formed. If the polymer does not polymerise into a hyperbranched structure it becomes more free flowing, or if it contains undesired cyclised polymeric constituents its colour changes to yellow and its form changes to a waxy-like texture. In this research the polymer yielded was completely transparent with a highly viscous form, indicating a hyperbranched structure of PG (HBPG) (Figure 35).

4.2.1 Contact Angle

Table 6 - Contact angle results for Raw, Raw/Polymerised, Passivated, and Passivated/Polymerised sample surfaces. Passivated samples are passivated using the novel H_2O_2/HNO_3 solution for 2-hours passivation time. Confidence intervals calculated at 95% significance level.

	Titanium Disc Sample Surfaces and Contact Angles (Degrees °)			
	Raw (No Passivation/No Polymerisation)	Raw/ Polymerised	Passivated	Passivated/ Polymerised
Disc 1	80.72	49.18	30.76	34.13
Disc 2	82.56	56.51	38.43	43.45
Disc 3	64.71	46.02	36.87	44.99
Mean	**76.00**	**50.57**	**35.35**	**40.86**
95% Confidence Interval	**11.11**	**6.09**	**4.59**	**6.65**
Standard Deviation	9.82	5.38	4.05	5.88

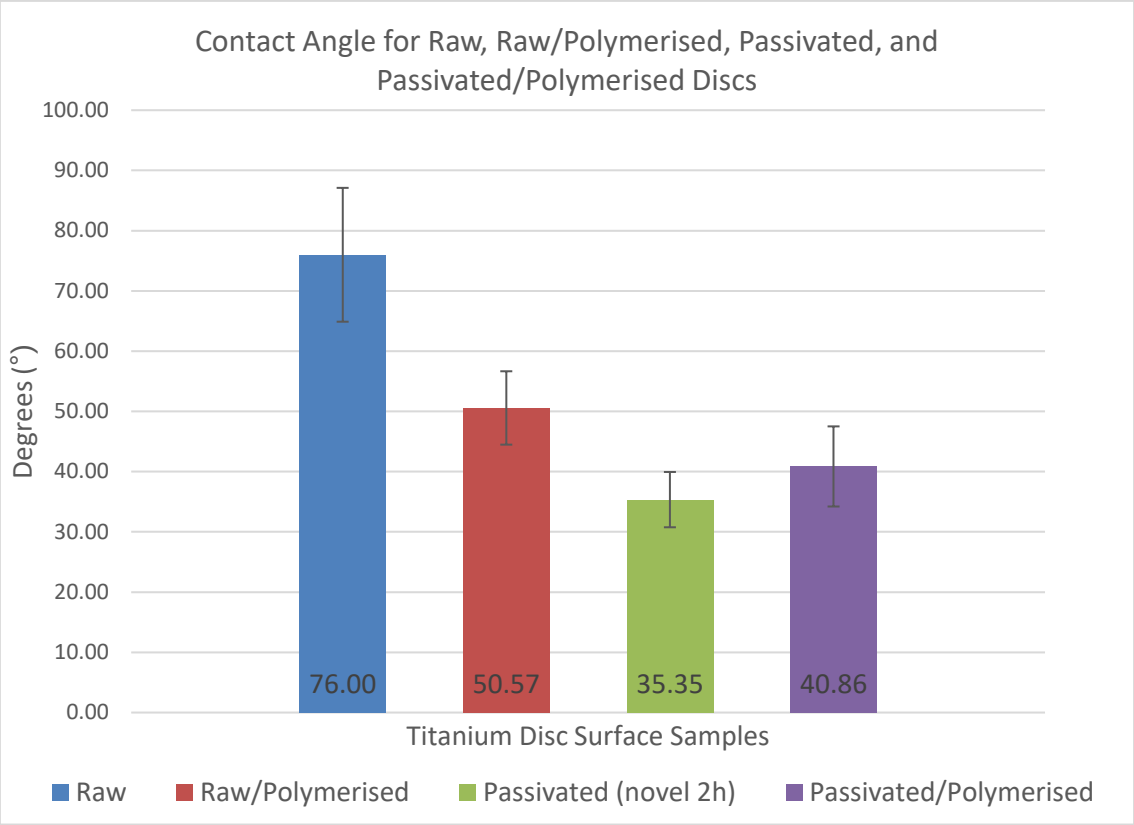

Figure 36 – Contact angle results graph for Raw, Raw/Polymerised, Passivated and Passivated/Polymerised titanium surfaces. Passivated and Passivated/Polymerised samples were passivated using H_2O_2/HNO_3 for 2-hours. Error bars calculated at 95% significance level (P=0.05).

Polymerisation of the Raw and Passivated titanium disc samples dramatically reduced the contact angle on these surfaces. The contact angle of the Raw disc was reduced by 33.5% after polymerisation however, the contact angle increased slightly when the Passivated surface was polymerised. Although ANOVA and Tukey Kramer analysis revealed no significant difference between the Passivated disc and the Passivated/Polymerised surface. The same analysis also showed no significant difference between the Raw/Polymerised, Passivated, and Passivated/Polymerised discs. ANOVA and Tukey-Kramer statistical analyses only revealed that the Raw surface was significantly different from the other three sample surfaces (Raw/Polymerised, Passivated, and Passivated/Polymerised) (see sub chapter 8.3.2 page 213).

The significantly reduced contact angle of the Raw/Polymerised surface over the Raw disc confirms the extreme hydrophilicity imparted by HBPG on the titanium surface. Such hydrophilic surfaces are known to reduce non-specific protein adsorption, with the effect of preventing undesired cell-biomaterial interactions that may produce immunogenic actions leading to implant rejection. This is known as the 'stealth effect' similar to polyethylene glycol (PEG) polymers. The hydrophilic character of the implant surface is also known to aid cell attachment and spreading, and thus may improve such desired cell-biomaterial interactions.

4.2.2 ESEM Images of Polymerised Titanium Surfaces

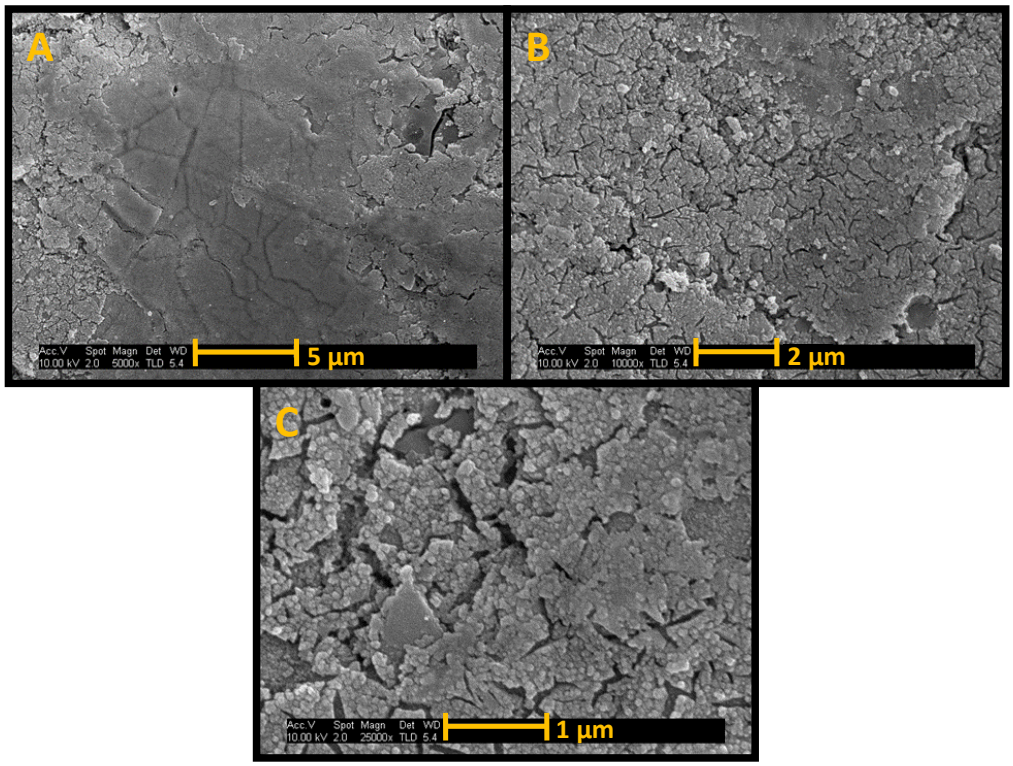

Figure 37 – Scanning Electron Microscope Images of Raw/Polymerised Titanium Alloy Surface. A) 5k, B) 10k, and C) 25k Magnifications (Scale Bars at 5, 2, and 1µm, Respectively).

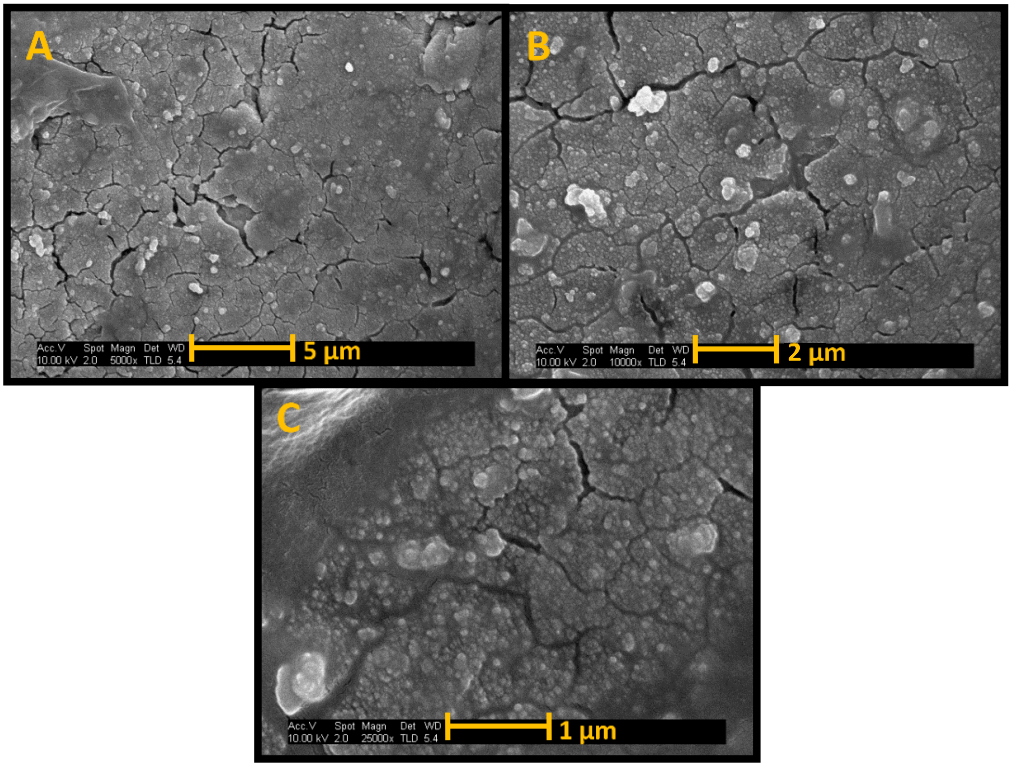

Figure 38 – Scanning Electron Microscope Images of Passivated/Polymerised Sample. Titanium Surface Passivated with H_2O_2/HNO_3 for 2-hours. A) 5k, B) 10k, and C) 25k Magnification (Scale Bars at 5, 2, and 1µm, Respectively).

SEM images (Figure 37 and Figure 38) reveal the presence of the polymer layer; the Raw/Polymerised surface showing what appears to be small globular-like polymer structures, with those globular structures being larger in size on the Passivated/Polymerised disc. The larger polymer structures seen on the Passivated/Polymerised disc surface could indicate higher molecular weight HBPG, or a greater amount of polymer synthesised on this surface, than on the Raw/Polymerised disc. This is likely due to the increased number of hydroxyl groups on the disc surface; active sites from which HBPG begins polymerising.

4.2.3 AFM 3D Images of Polymerised Titanium Surfaces

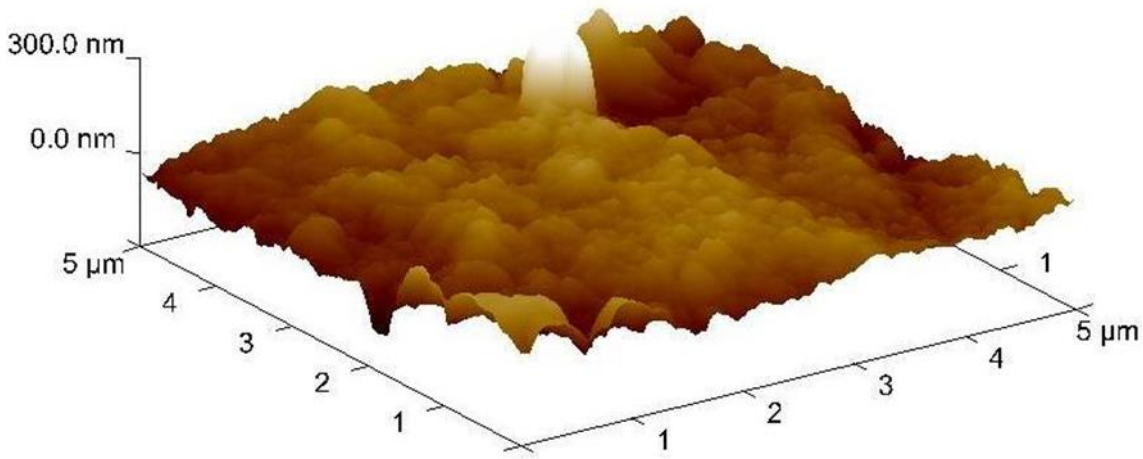

Figure 39 - 3D AFM Image of Raw/Polymerised Titanium Alloy Surface.

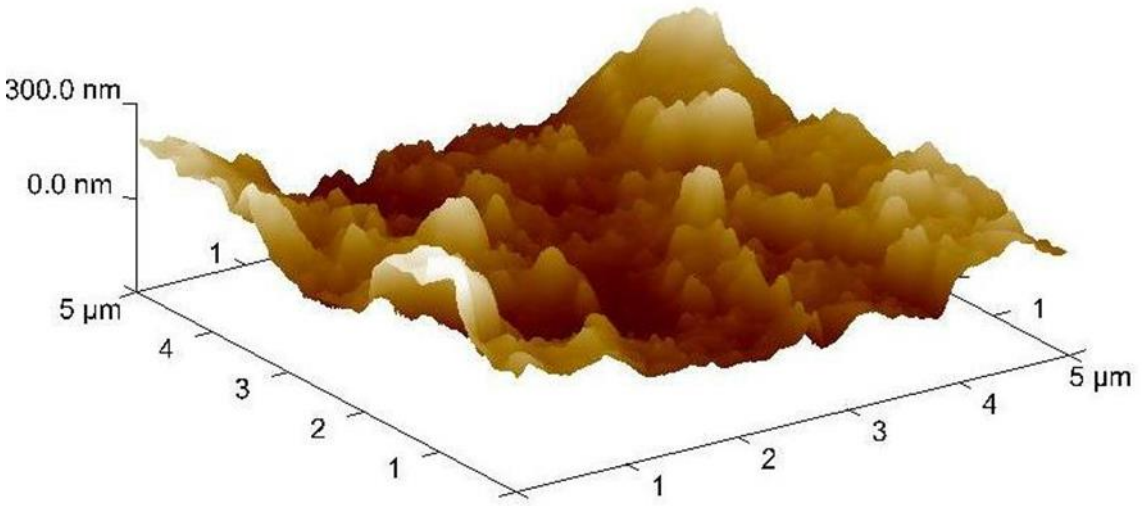

Figure 40 - 3D AFM Image of Passivated/Polymerised Titanium Alloy Surface. Titanium Disc Passivated with H_2O_2/HNO_3 (1:1) at 2-hours Passivation.

The AFM 3D images (Figure 39, Figure 40) show that polymerisation of the titanium surface yielded an increased number of topographical features, indicated by the highly irregular and bumpy surface texture. This was evident on both the Raw/Polymerised and Passivated/Polymerised surfaces. The presence of many of these peaks and troughs are important as the scientific literature informs us that focal adhesions between the cell and biomaterial surface may reside in cracks below the surface for cell anchorage. Furthermore, the AFM 3D images show the Passivated/Polymerised surface to contain much larger peaks than the Raw/Polymerised sample. Similar to the SEM images, this could also indicate more polymer at the surface which may have a higher molecular weight.

4.2.4 Surface Roughness Results and Discussion

Table 7 - Surface Roughness Parameters of Raw/Polymerised and Passivated/Polymerised Titanium Alloy Disc Surfaces (as Measured by AFM). (mean of 3 discs per group).

	Roughness Parameters		
	Ra (nm)	Rmax (nm)	Rq (RMS) (nm)
Raw (No Passivation/No Polymerisation)	28.0	401	38.5
Raw Titanium Alloy Polymerised	34.7	597	46.7
H_2O_2/HNO_3 (1:1) 2 hours Passivation	81.5	979	104
H_2O_2/HNO_3 (1:1) 2 hours Passivation and Polymerised	58.5	644	73.9

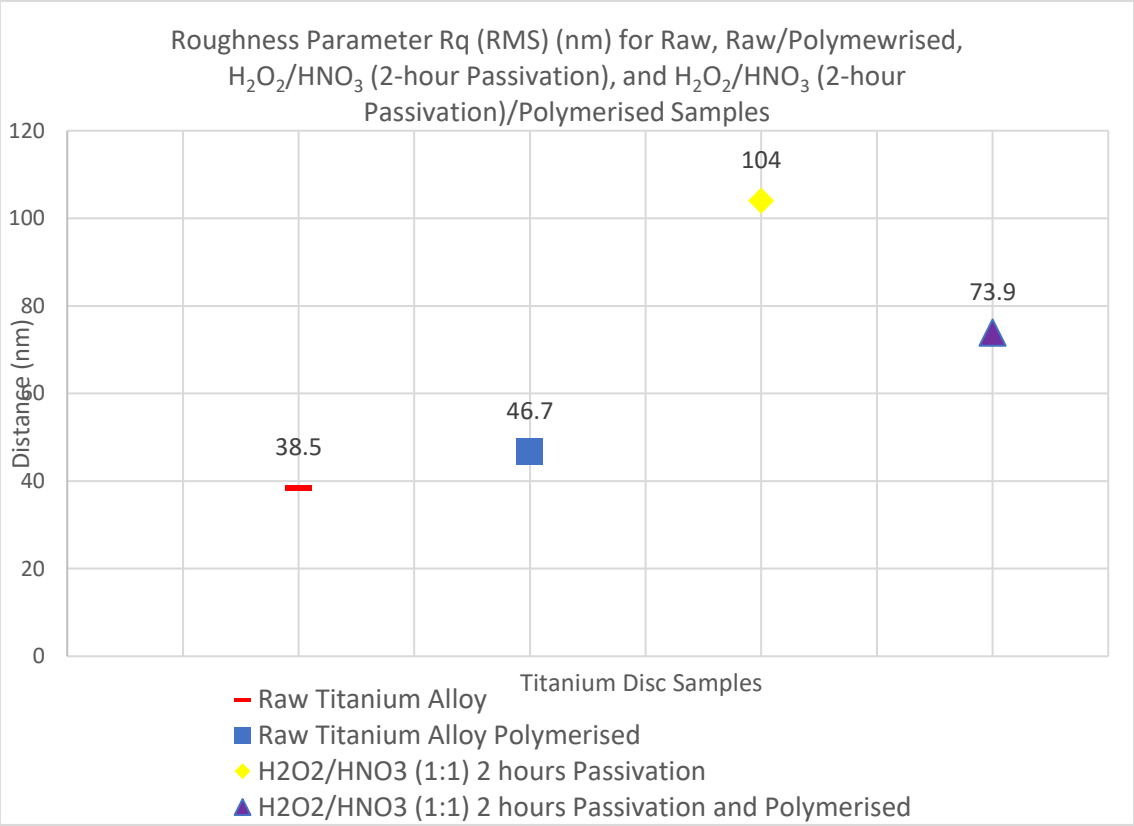

Figure 41 - Roughness Parameter Rq results graph for Raw, Raw/Polymerised, Passivated and Passivated/Polymerised samples. Passivated Titanium Disc samples passivated with H2O2/HNO3 (1:1) at 2-hours Passivation.

The AFM result shows that polymerisation of the Raw titanium surface increases the surface roughness from an Ra value of 28nm to 34.7nm, though this result may not be significant. Polymerising the Raw surface does not seem to alter the topography significantly. This change in roughness is reversed for the passivated disc, with an Ra value of 81.5 nm and 58.5 nm pre- and post-polymerisation respectively. Perhaps the cracks and pits on the surface of the passivated disc became filled with HBPG after polymerisation, leading to a smoother surface. Or perhaps as the disc was passivated, there could be an even spread of active hydroxyl groups on the surface. This may have led to polymerisation of the surface evenly, giving rise to similar amounts of polymer across the surface, hence the lower mean roughness. Although the Ra

value for the Raw/Polymerised surfaces is still less than 100nm (as well as the Passivated/Polymerised disc), indicating that both surfaces may have nano and sub-micron topographical features.

4.2.4 EDS Elemental Analysis of Polymerised Titanium Surfaces

Table 8 - Elemental Analysis of Titanium Alloy Disc Surface. Samples Analysed Include Raw, Raw/Polymerised, Passivated, and Passivated/Polymerised. (mean of 3 discs per group).

	Element Weight%				
	C	O	Al	Ti	V
Raw Disc	3.76	15.16	3.32	66.61	2.92
Raw Disc Polymerised	4.75	23.95	2.71	58.87	2.47
H_2O_2/HNO_3 (1:1) 2 hours Passivated Disc	2.89	25.17	3.11	59.67	2.46
H_2O_2/HNO_3 (1:1) 2 hours Passivated and Polymerised	5.28	30.79	2.16	54.65	2.16

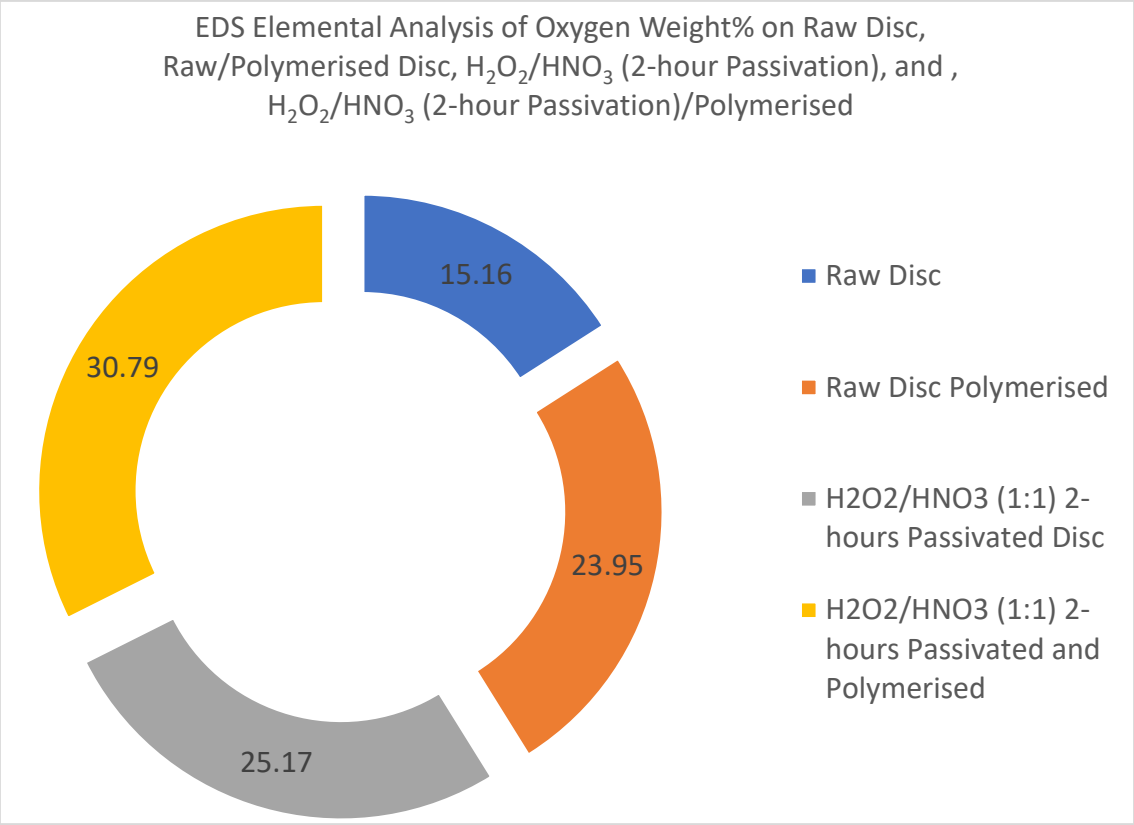

The EDS analysis also provides evidence to the presence of the polymer layer formed on the titanium surface, with an increased content of carbon and oxygen on the titanium surface after polymerisation. The EDS results agree with the SEM and AFM results in that polymerisation on the hydrogen peroxide/nitric acid passivated surface perhaps yielded more polymer at a higher molecular weight, evident here by the increased oxygen weight% which is 28.6% higher than the Raw/Polymerised sample. This could indicate a greater amount of polymer and/or greater extent of polymerisation, yielding higher molecular weight HBPG with more branching units and thus more hydroxyl groups. It is clearly evident that subsequent polymerisation, following passivation with H_2O_2/HNO_3 (2-hour passivation), yielded a greater amount of polymer on the titanium surface with nano-scale roughness. This may be due to the increased number of

active hydroxyl groups on the passivated surface, therefore more polymerisation initiation sites.

Polymerising HBPG from the titanium surface is an important aspect of this research, not only to enable functionalisation of the titanium with the RGD peptide, but also to function as a tissue engineering scaffold to support cellular infiltration and growth. Furthermore, the HBPG acts to enhance the hydrophilic nature of the titanium surface, thus limiting non-specific protein adsorption.

5 RGD Peptide Immobilisation

The RGD peptide motif has been extensively researched in the last decade or so, and has shown great promise for the use of enhancing bone formation around orthopaedic implants. The tri-peptide sequence is natively found in ECM bone proteins where it activates the integrin transmembrane receptor to induce cell-cell and cell-matrix adhesions. When found free-flowing in the serum it causes apoptosis of cells that bind it. Conversely when immobilised on a surface, osteoblasts (as well as other cell types) initiate cellular adhesion to the surface presenting the RGD signal; thus, there are no concerns regarding ectopic bone formation resulting from the immobilised peptide. Although the RGD peptide is not currently in clinical use for enhancing osseointegration of orthopaedic implants, understanding of the RGD-Integrin receptor binding has led to the development of anti-clotting drugs. Also, for the last few years RGD coated ECM mimetic tissue culture plates have been available, supporting the attachment of specific cell types, or to restrict differentiation of pluripotent stem cells. Furthermore, the RGD peptide is being trialled as a target for the delivery of anti-cancer therapeutics and diagnosis, as well as for the monitoring of treatment responses of anti-angiogenic therapies to tumours.

At present there are many studies researching the use of bone proteins such as BMPs with similar clinical outcomes (Haimov *et al.*, 2017, Hyzy *et al.*, 2017). Although these proteins and growth factors need to be released from the implant surface coating in a controlled manner, and if they creep into systemic circulation there is the possibility of these biomolecules interacting with cells away from the implant site, resulting in ectopic bone formation for example. Other issues include, but are not limited to, increased cost of sourcing the protein and immunogenic interactions, thus highlighting the importance polymerised titanium surface, the polymer of which is also covalently attached to the titanium surface, has been attempted.

The decision to use the cyclic RGDfc peptide specifically is because it has very high affinity to the αvβ3 integrin heterodimer and when activated, enhance cell adhesion and proliferation of osteoblast cells. The majority of research in the literature has focused on the covalent attachment of RGD to a biocompatible polymer, and the subsequently binding of that polymer onto a titanium surface via electrostatic adsorption. This type of ligand attachment to a surface is more characteristic of passive attachment. Although there has been an influx of new research over the last few years, in which the RGD peptide is covalently attached to a polymer that is polymerised directly from the titanium surface, covalently immobilising the ligand to the implant surface. In this work however, a polymerised titanium surface (covalently bonded HBPG) was covered with a silane layer, after which RGD was chemically grafted through fast carbodiimide coupling chemistry.

Passive coating of RGD can improve cell proliferation and decrease time to confluence, though lower mineralisation rates have been obtained in contrast to chemically grafted RGD (REZANIA and HEALY, 2000). Also techniques that use physical adsorption require much larger quantities of the biomolecule, and that may become denatured or leach into surrounding tissue causing undesired effects away from the implant site (Rezania and Healy, 1999, Nanci *et al.*, 1998). Biomolecules that are covalently attached to a surface may provide a chemically stable surface with more aligned biomolecules for optimum biological efficacy (MANTE *et al.*, 2004). Research has shown that a certain concentration of attached RGD peptide is required to elicit a biological response from surrounding cells.

5.1 Materials and Methods

Titanium Alloy (Ti6Al4V) circular discs (provided by SinteaPlustek and William Gregor Ltd), with dimensions of 14mm diameter by 1mm thick, machine cut; cyclo-RGDfc (cyclo-Arginine-Aspartic Acid-D-Phyenylalanine-Lysine-Cysteine) peptide (H-7226, Bachem UK Ltd); Acetone ACS Reagent ≥99.5% (Sigma); Dichloromethane (DCM) Anhydrous ≥99.8% (Provided by Cranfield Health); triple filtered ultra-pure deionised water, Millipore (Cranfield Health); 1,4-Butanediol diglycidyl ether (Diepoxide) (220892, Sigma); Carbonate-Bicarbonate buffer capsules, pH9.6 (C3041, Sigma); Fluoresceine 5(6)-isothiocyanate (FITC) (F3651, Sigma); Dimethyl Sulfoxide (DMSO), anhydrous (276855, Sigma); PD Miditrap G-10 by GE Healthcare; BCA protein assay (Thermo Fisher Scientific); 3-Aminopropyl Triethoxysilane (APTES); Ethanol, anhydrous ≤0.003% water (Sigma); 1-Ethyl-3-(3-dimethylaminopropyl)carbodiimide (EDC) (Cranfield Health) ; N-Hydroxysuccinimide (NHS) (Cranfield Health); Confocal Laser Scanning Microscope (CLSM), Zeiss LSM510 Meta (Cranfield SAS).

5.1.1 Fluorescent Tagging of the RGD Peptide and its Filtration

Before the RGD peptide could be immobilised onto the titanium samples it was fluorescently tagged with a dye molecule, allowing the peptide to be viewed by fluorescence microscopy. The dye molecule used to tag the RGD, Fluorescein Isothiocyanate (FITC), is a fluorescein dye conjugated with Isothiocyanate, a reactive group with the nomenclature –N=C=S, at one of the two hydrogen atoms on the ring structure. The dye molecule is highly reactive towards primary amines, as well as other nucleophiles on peptides, proteins and many other biomolecules. FITC has excitation/emission wavelengths of 494/520nm enabling it to emit green light in the visible spectrum, and therefore allowing visualisation using fluorescence

microscopy. Analysis of sample surfaces was conducted using a Confocal Laser Scanning Microscope (CLSM) for the fluorescently-tagged RGD.

Fluorescent Tagging of the RGD Peptide and Filtration Protocol

A 2mg/ml solution of RGD was prepared in a pH9 carbonate-bicarbonate buffer, and a 2mg/ml solution of FITC was prepared in anhydrous DMSO. The solutions were mixed in a 3:1 molar ratio of FITC to RGD and covered with foil. The 3:1 molar ratio of dye to peptide is the minimum standard used to fluorescently tag proteins and peptides, since roughly a third of the dye molecules conjugate, thus ensuring the highest conjugation efficiency possible. Although higher molar ratios can be used, ratios greater than 6:1 can result in unspecific over labelling and thus wastage. Similarly, a peptide concentration of 2mg/ml is also the minimum standard necessary as the reaction kinetics are heavily concentration dependent. A peptide concentration below this would require extensive time for dye-peptide conjugation. This protocol was adapted from the book Bioconjugate Techniques Third Edition (Hermanson, 2013).

The reaction mixture was incubated at room temperature in an incubator shaker with an orbital rotation speed of 40rpm for 6 hours. The fluorescently tagged RGD solution was then filtered using gravity filtration to remove unreacted dye molecules. Filtration was achieved using PD Miditrap G-10 by GE Healthcare. These disposable columns are prepacked with 5.3ml of Sephadex G-10 gel filtration medium for sample clean-up of small proteins and peptides. The filtration was carried out as per the manufacturer instructions, and using carbonate-bicarbonate buffer at pH9 as the equilibration buffer, although the filtration was completed twice. This was to ensure complete removal of the unbound FITC, as the molecular weight of

the FITC-RGD conjugate is very close to the molecular weight cut-off of the Sephadex G-10 medium. Molecular weight of the peptide-FITC conjugate is approximately 968 g/mol, while the exclusion cut-off limit for Sephadex G-10 is approximately 700 g/mol. Therefore, the fluorescently tagged peptide would be eluted first, followed closely by the untagged peptide (molecular weight 578.7 g/mol), and finally the fluorescent molecule (molecular weight 389.3 g/mol), as species with a molecular weight lower than the cut-off (the untagged peptide and the FITC molecules) would enter the pores of the sephadex medium slowing down their elution.

Briefly, the filtration medium was resuspended and the column storage solution eluted, followed by column equilibration. 1 ml of sample (fluorescently-tagged RGD peptide) was added to the column and allowed to enter the packed bed. 0.7 ml of equilibration buffer (stacker volume) was also added and again allowed to enter the packed bed completely. Up to this point any flow-through was discarded. The sample was then eluted with 4ml of buffer and the eluate collected in 0.25 µl fractions in centrifuge tubes. The collected fractions were first analysed with a UV light to fluoresce the FITC dye, thereby gauging which fractions held the highest concentration of FITC and therefore RGD peptide. This constituted the first elution profile in which each fraction was analysed for peptide content using a BCA protein assay (Thermo Fisher Scientific).

Analysis of the elution profile revealed the speed with which the peptide was released from the column, and hence the volume of equilibration buffer in which the peptide would be eluted. A second elution profile was carried out (second filtration) and again analysed for peptide content, although the eluted sample was collected in 500 µl fractions, speeding up the peptide recovery. Using the parameters by which the fluorescently-tagged peptide could be eluted, the complete FITC-RGD mixture was subsequently double-filtered. Exposing the eluted

fractions to UV light indicated that the first filtration was showing signs that unbound FITC molecules may have been eluted with the FITC-tagged peptide, as all fractions had a strong green fluorescence from FITC. A second filtration was carried out in order to completely remove any unbound dye molecules, thus a high degree of confidence that all unbound FITC and unbound RGD were removed.

5.1.2 Silanisation

Silanisation of an inorganic/organic surface provides functional groups for the attachment of biological species to that surface. Many silanisation solutions exist which differ in the number of functional groups available, and the length of the silane molecule (**Error! Reference source not found.**).

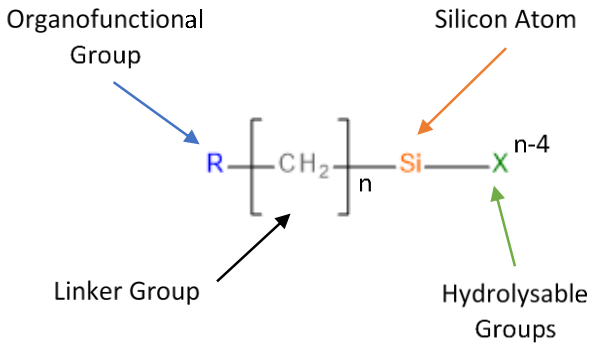

Figure 42 - General structure of an Organofunctional Silane molecule. R group represents an organic functional group such as amine, vinyl, or epoxide. The X group is usually methoxy or ethoxy (Arkles, 1977).

The silane chemical 3-Aminopropyl Triethoxysilane (APTES) was utilised. Consisting of one active functional group for biomolecule immobilisation, a highly reactable amine, and three

ethoxide groups for attachment to the substrate surface, it represents one of the more simpler and easier to use siloxanes.

The silanisation reaction is a very simple one; generally, the substrate surface is exposed to the silane solution for some time, ranging from minutes to hours (depending on the number of silane layers required, and the propensity of the substrate surface to form silane layers) (**Error! Reference source not found.**). The silane molecules self-assemble and form hydrogen bonds with chemical species on the substrate surface, thus forming a silane layer (or multiple monolayers) (**Error! Reference source not found.**, A). The silane layer is then cured, either at room temperature overnight or at elevated temperatures of around 80 to 100°C for some minutes. This dehydrates the bonding between the silane and substrate, forming covalent bonds (**Error! Reference source not found.**, B). The now silanised surface contains highly reactable functional groups for biomolecule conjugation, in this case primary amine groups.

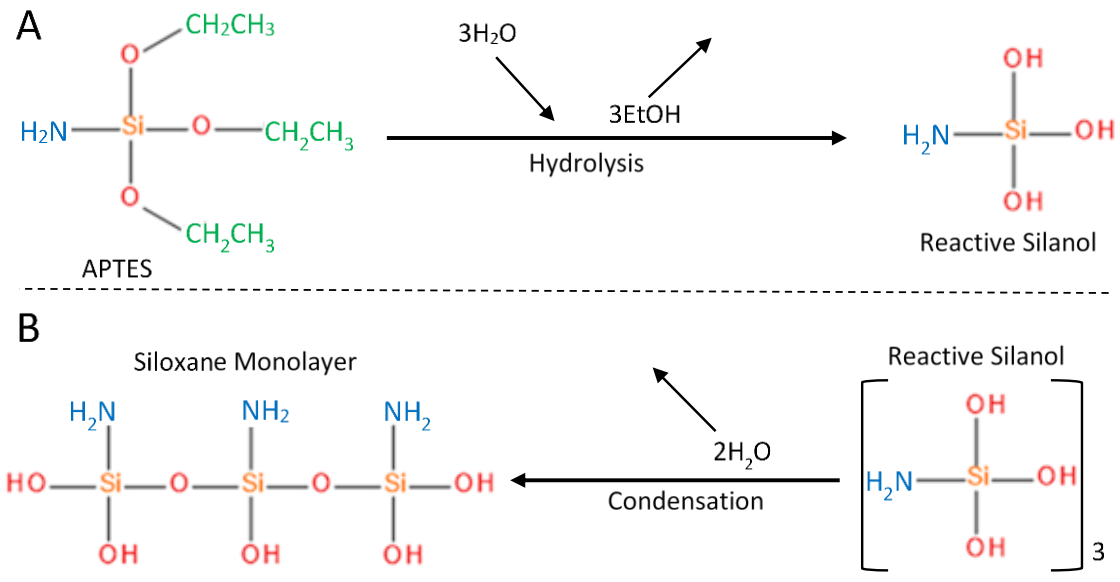

Scheme 6 - Reaction Scheme for A) Hydrolysis of Silane to the Reactive Silanol and B) Subsequent Condensation Silanol to the Siloxane Monolayer (Arkles, 1977).

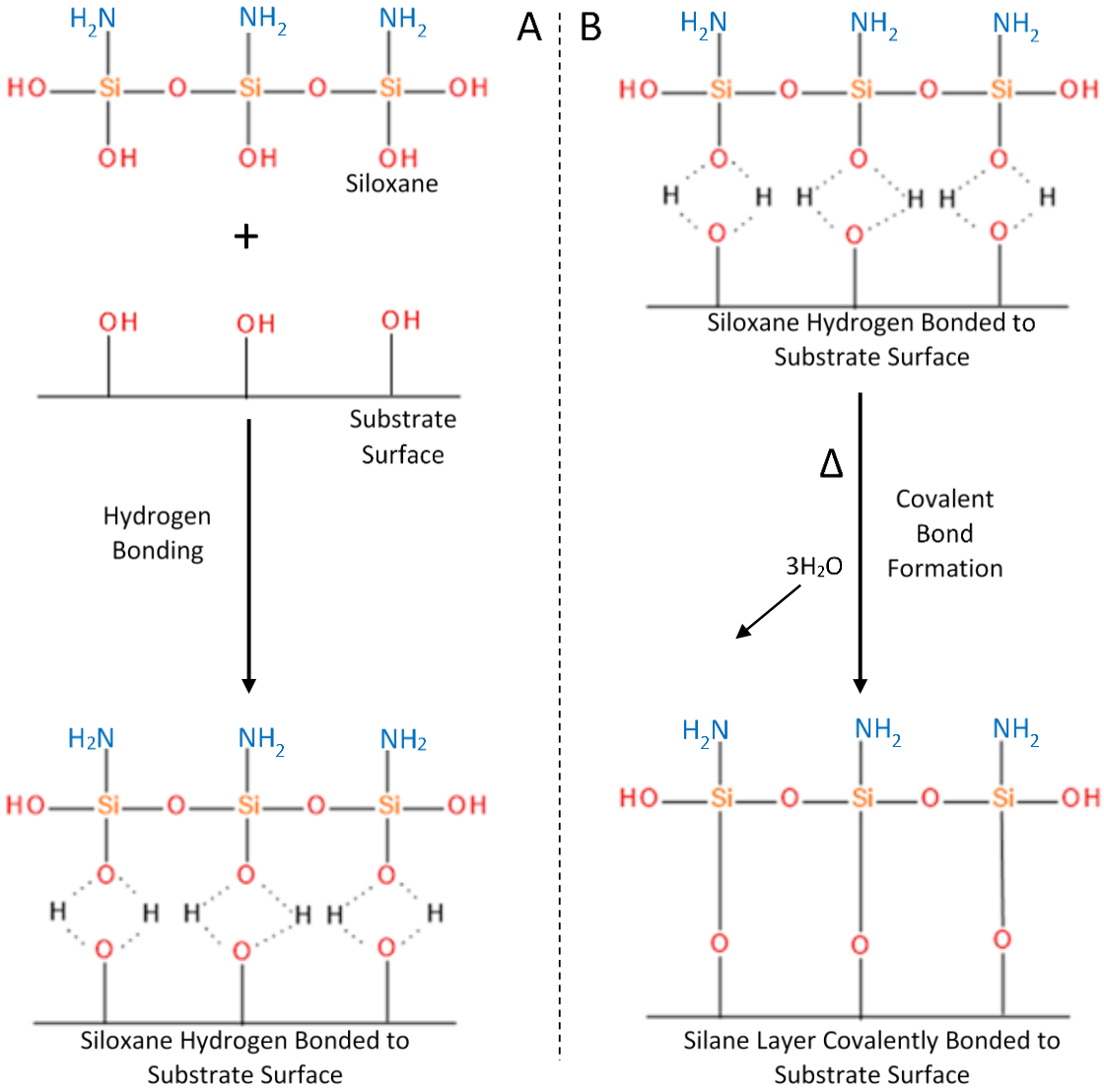

Scheme 7 - Reaction Scheme for A) Hydrogen Bonding of Siloxane Monolayer to Hydroxyl Groups on Substrate Surface and B) Covalent Bond Formation between Siloxane Monolayer and Substrate Surface After Temperature Curing (Arkles, 1977).

In this research silanisation of the polymerised titanium surface was attempted. It was theorised that the abundant hydroxyl groups on the polymer could provide hydrogen bonding

sites for the silane molecules to attach. The silanised layer would then provide amine groups for further biomolecule conjugation, namely the RGD peptide.

Silanisation Protocol

Pre-frozen polymerised discs (-80°C) were submerged in a 20% silane solution (APTES in 95% ethanol/5% water) in an ice bath and left to react for 15 minutes. Only enough silane solution was prepared so that the surface of the polymerised discs was completely submerged (approximately 5ml of silane solution per disc). After formation of the silane layer, the discs were rinsed in ethanol (in an ice bath) for 5 minutes, and then cured at room temperature for 24 hours before being stored dry in a desiccator (Protocol adapted from (Arkles, 2014)). By conducting the silanisation in an ice bath, it ensured that the polymer form remained a glassy solid (lower temperature than the glass transition temperature of the polymer), allowing the silane layer to be formed with minimal polymer dissolution/degradation. Also, curing the silane layer at room temperature prevented melting of the polymer to a free-flowing liquid.

5.1.3 RGD Coupling via Carbodiimide Chemistry

Carbodiimides are cross-linking molecules containing the functional group RN=C=NR. For the purposes of synthetic organic chemistry, carbodiimides are most notably used to activate carboxylic acids to produce amide bond formations when coupled with a primary amine (Mattson *et al.*, 1993). They are sometimes referred to as 'zero-length' cross-linking agents as they do not introduce any additional chemical structures amidst the conjugating molecules.

The chemical reaction of carbodiimides generally begins as a proton transfer from a carboxylic acid to the carbodiimides basic nitrogen, and subsequent addition of the carboxylate yields an O-acylisourea (Khorana, 1953, Bellucci and Volonterio, 2012), a highly reactive acylating ester intermediate species that is unstable. This intermediate can then react with a nucleophile, such as a primary amine, and form an amide bond and a urea by-product (Porte-Durrieu *et al.*, 2004) (Scheme 8). The O-acylisourea intermediate may react with other nucleophiles, such as sulfhydryl groups and form a thioester bond, although these are less stable and therefore uncommon.

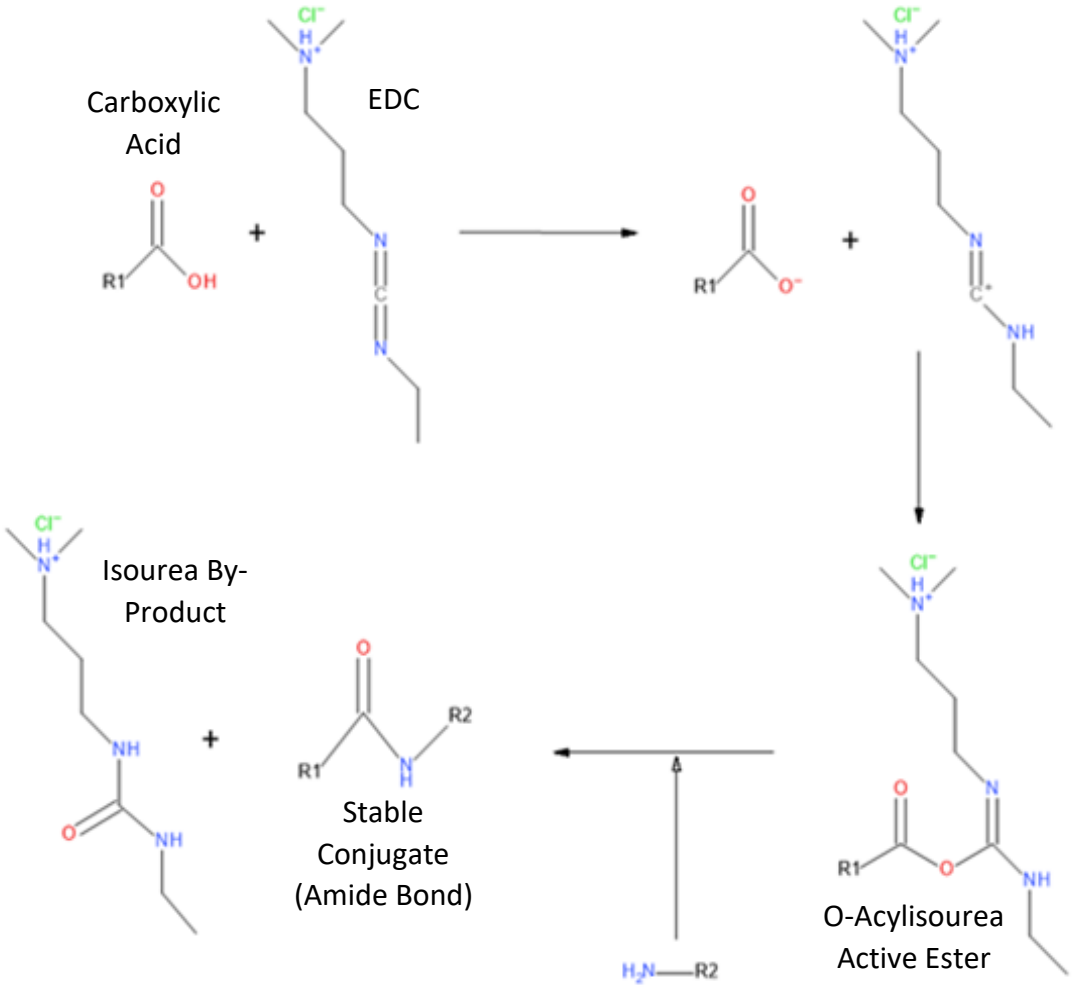

Scheme 8 - Reaction Mechanism Scheme for the Conjugation of a Carboxylic Acid with a Primary Amine to Yield an Amide Bond, Using EDC as a Fast Coupling Carbodiimide (Bellucci and Volonterio, 2012).

The formation of an amide bond using a carbodiimide cross-linker is straightforward, however certain side-reactions can occur which produce either the required product or an undesired one. One of the side reactions that can occur is hydrolysis of the active ester intermediate. In the presence of water, the oxygen atoms may act as the attacking nucleophile, thus hydrolysis by water is a strong competing reaction leading to inactivation of the carbodiimide, cleaving off the ester intermediate and producing an isourea and reforming the carboxylic acid. Another side-reaction, although less detrimental, is the reaction of the O-acylisourea

intermediate with another carboxylate to form an acid anhydride (Scheme 9, B) (Hermanson, 2013). This side reaction is less worrisome as the acid anhydride can further react to yield the desired amide bond, albeit with less efficiency. If the carboxylic acid is in excess, the acid anhydride pathway will predominate, but if it is equimolar with the carbodiimide, then the reaction will proceed via the O-acylisourea pathway (WILLIAMS and IBRAHIM, 1981).

The main undesired side reaction is the intramolecular acyl transfer, or rearrangement, of the O-acylisourea intermediate to the stable N-acylurea, sometimes referred to as the O-N shift (Scheme 9, A) (Bellucci and Volonterio, 2012). The stable N-acylurea prevents any further reaction, although this undesired pathway predominates in long reaction times such as in solid phase peptide synthesis (Hermanson, 2013).

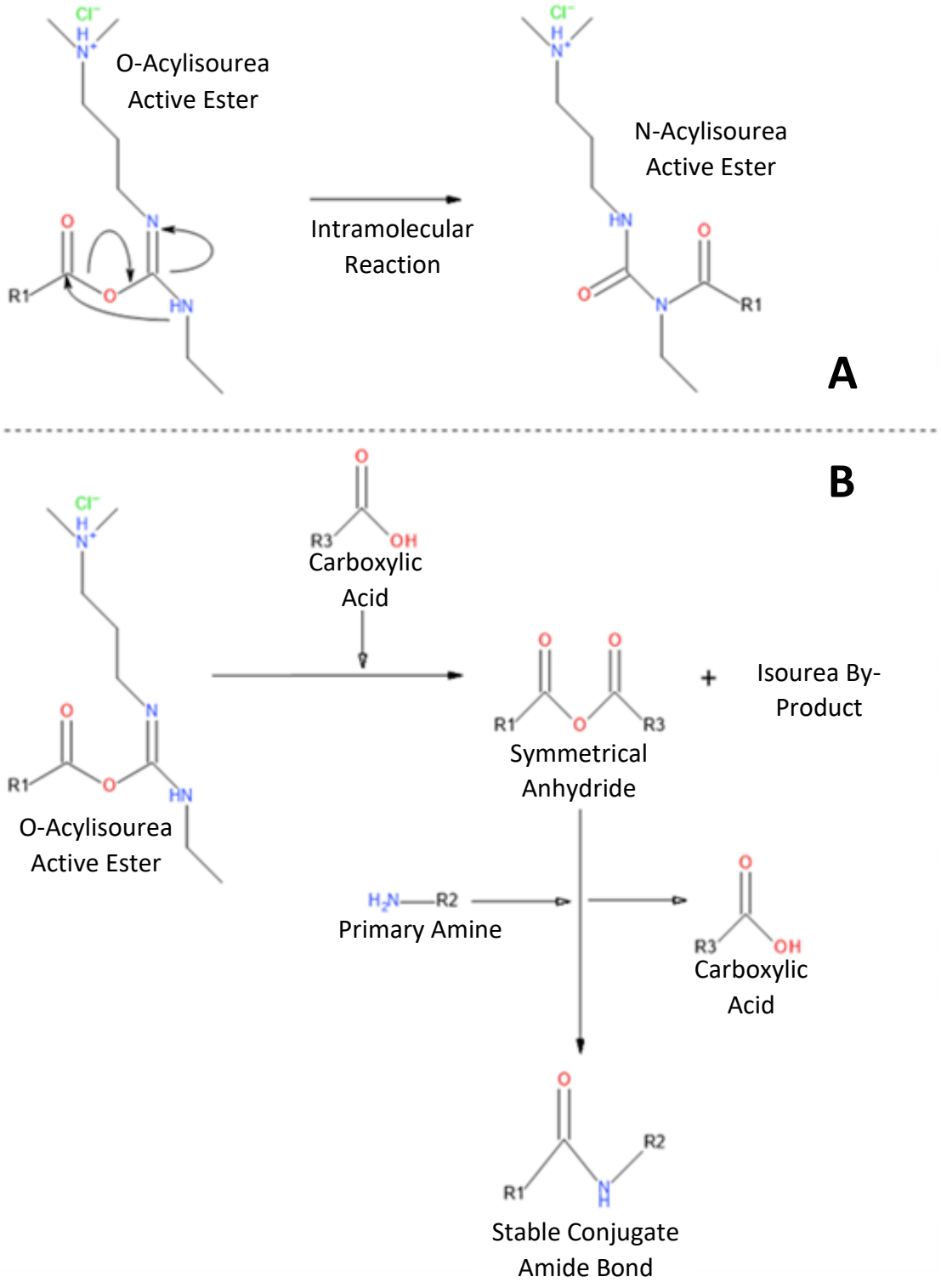

Scheme 9 - Reaction Mechanism Schemes Showing Major Side Reactions of the EDC Carbodiimide Coupling. A) Rearrangement of the O-acylisourea Intermediate to the Stable N-acylisourea (O-N shift) and B) Formation of Stable Amide Bond from Reaction of the Active Ester Intermediate with Carboxylic Acid (via Acid Anhydride) (Montalbetti and Falque, 2005)

Certain measures can be taken to keep side reactions to a minimum and increase conjugation efficiency, such as the possibility to stabilise the active ester intermediate with the addition of a hydroxylated amine such as N-Hydroxysuccinimide (NHS) or N-Hydroxybenzotriazole (HOBt), and as such is frequently included in such carbodiimide coupling reactions (Scheme 10). When combined with NHS, carbodiimide couples NHS to the carboxylic acid, forming an NHS ester, the NHS therefore acting as a transfer agent. The amine-reactive NHS ester is far more stable than the O-acylisourea in aqueous conditions, and affords more efficient coupling to amine groups under physiological pH (Mattson *et al.*, 1993). Furthermore, to prevent rearrangement and subsequent inactivation of the O-acylisourea (O-N shift), solvents with low dielectric constants are used in concert with NHS or HOBt that can minimise this side reaction, the most popular choices being chloroform or dichloromethane (DCM).

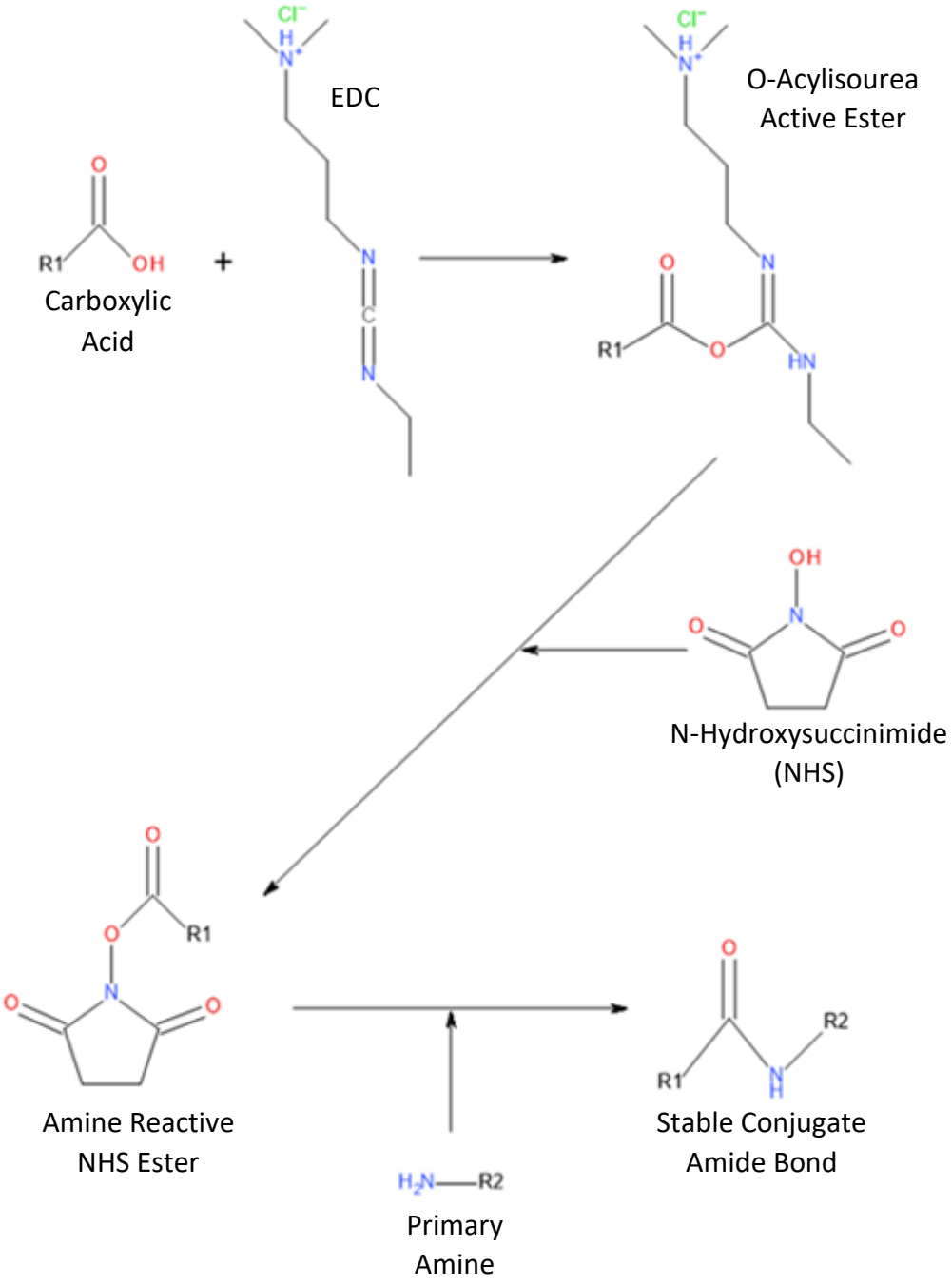

Scheme 10 - Reaction Mechanism Scheme for the EDC Carbodiimide Coupling, with Addition of NHS to form stable Amine-Reactive NHS Ester, and Subsequent Amide Bond Formation (Montalbetti and Falque, 2005)

Carbodiimide Coupling Protocol

Coupling carbodiimide to carbonyl groups is predominantly favoured in reduced pH conditions at around pH 4-5. An MES buffer is best used for this stage of the reaction however, the use of a buffering system in this work was avoided completely due to the high dissolution rate of the polymer in aqueous solutions. Unlike other carbodiimides, such as dicyclohexylcarbodiimide (DCC), EDC can be used under mild conditions in solvents such as water, DMF, THF or DCM. Low coupling efficiencies arising from the omission of a buffer system can be compensated by increasing the EDC amount in the reaction.

The solvent DCM was chosen for this experiment in order to prevent the O-N shift side reaction and subsequent inactivation of the O-acylisourea active intermediate. Also, PG showed the highest stability in this solvent in terms of dissolution and polymer loss/degradation. In efforts to further stabilise the polymer in DCM for longer periods, the experiment was conducted in an ice bath (similar to the silanisation reaction). The decreased temperature ensured the polymer form was a glassy solid (as previously explained), thus reducing dissolution/degradation.

30ml of DCM was poured into a large beaker and put on ice. This volume of solvent was enough to ensure complete submersion of the titanium disc surfaces, but not so much as to dilute the reactants. The titanium disc samples were then immersed in the DCM (titanium discs were pre-frozen at -80°C prior to use, ensuring glassy solid phase).

Initial testing of the RGD coupling to the titanium discs revealed an extremely small amount of immobilised RGD (when viewed with Confocal Microscopy of the fluorescently tagged RGD). Therefore, the amount of RGD used was just 1mg per every 4 titanium discs to prevent

wastage of the costly peptide. The amount of EDC used was a 10-molar excess over the amount of RGD, and the same number of moles of NHS was also used.

EDC, NHS and RGD were dissolved separately in small beakers containing 5ml of DCM each. Dissolution testing revealed this volume of solvent was sufficient to dissolve the three substituents within 20 minutes. Upon dissolution of the three components, the EDC solution was added to the RGD solution and left at room temperature to react for 5 minutes (with occasional swirling and protected from light). After which the NHS solution was added and left to react for a further 10 minutes (again with occasional swirling). The solution complex now containing all three substituents was pipetted into the large beaker containing the titanium discs immersed in DCM. The reaction was run for up to 2.5 hours in an ice bath protected from light. All beakers were covered with aluminium foil to protect the fluorescently tagged RGD from photo-bleaching.

The reaction was stopped by removing the titanium discs from the beaker and rinsing thoroughly in deionised water (in ice bath) for 5 minutes, allowing any excess chemicals and the water-soluble by-product to be removed. The titanium discs were flash dried with nitrogen gas and left in a desiccator at 4°C (refrigerated) until analysis. Control samples were prepared in the same way, although no EDC or NHS was included in the reaction mixture. The following reaction scheme outlines the interactions of the RGD peptide with EDC, NHS and the silane layer (Scheme 11).

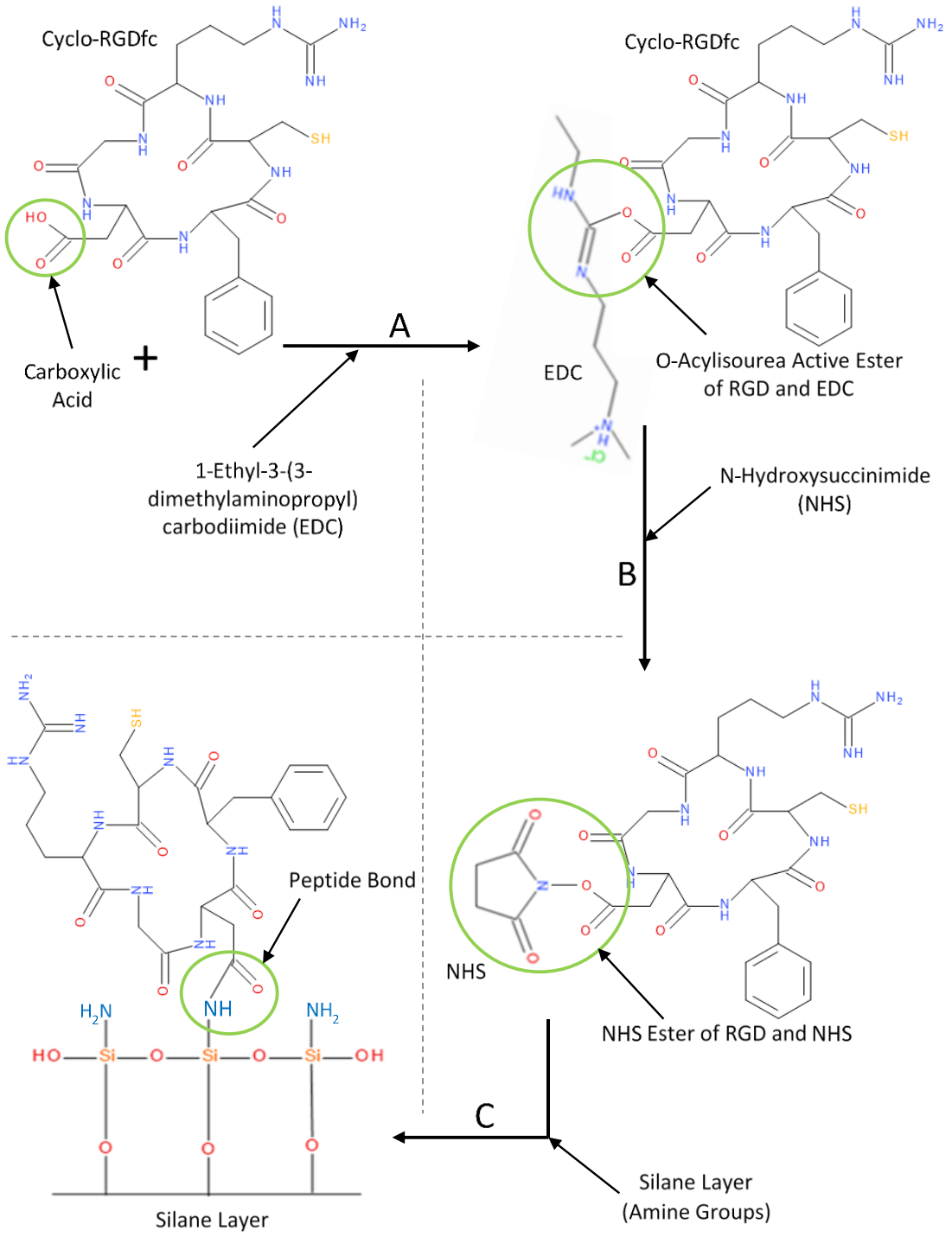

Scheme 11 - RGD peptide and silane layer reaction scheme. Green circled areas indicate reacting groups. A) Reaction between carboxylic acid group on cyclo-RGDfc and EDC carbodiimide to yield O-Acylisourea active ester B) Reaction between O-Acylisourea active ester (of EDC and cyclo-RGDfc) and NHS to yield the NHS ester of cyclo-RGDfc C) Reaction of NHS ester of cyclo-RGDfc with silane layer (on Passivated/Polymerised titanium disc) to yield peptide bond formation. Chemical structures were drawn using Acelrys Draw software. Reaction scheme adapted from Montalbetti and Falque (2005).

5.2 RGD Immobilisation Results

5.2.1 Fluorescent Tagging of the RGD Peptide and Filtration

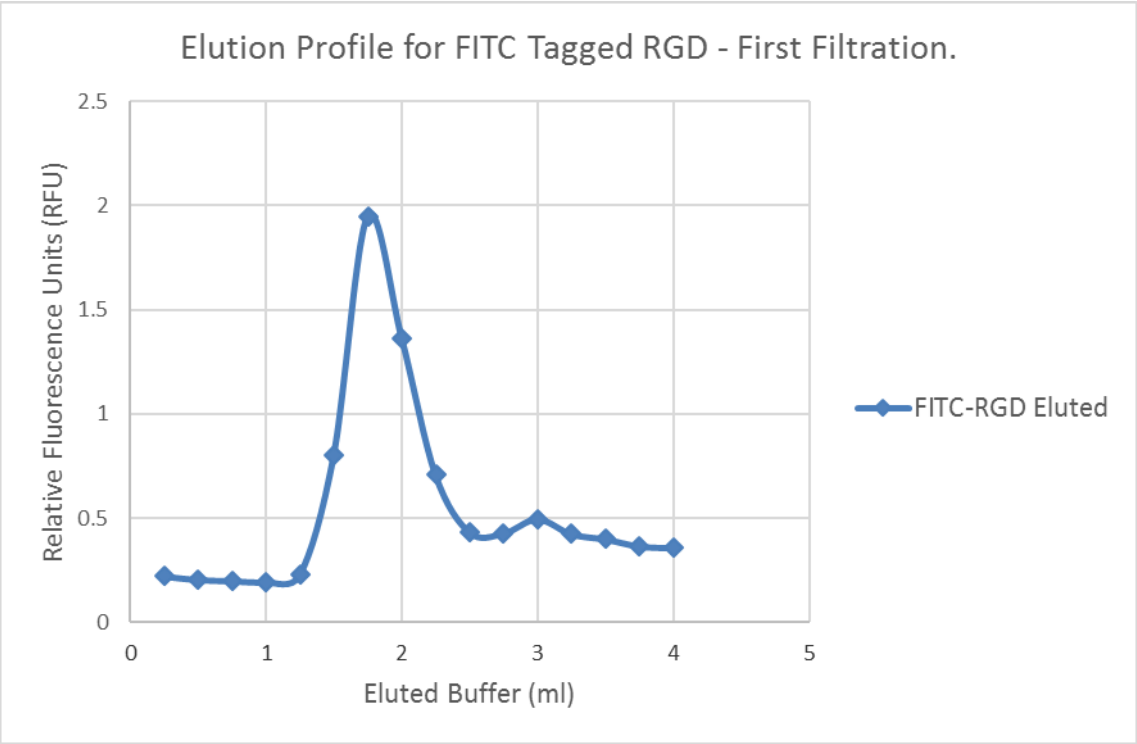

Figure 43 - Graph Showing the Elution Profile of FITC-Tagged RGD Peptide. Represents the 1st Filtration. Peptide is Eluted within the First 2.5ml of elution buffer.

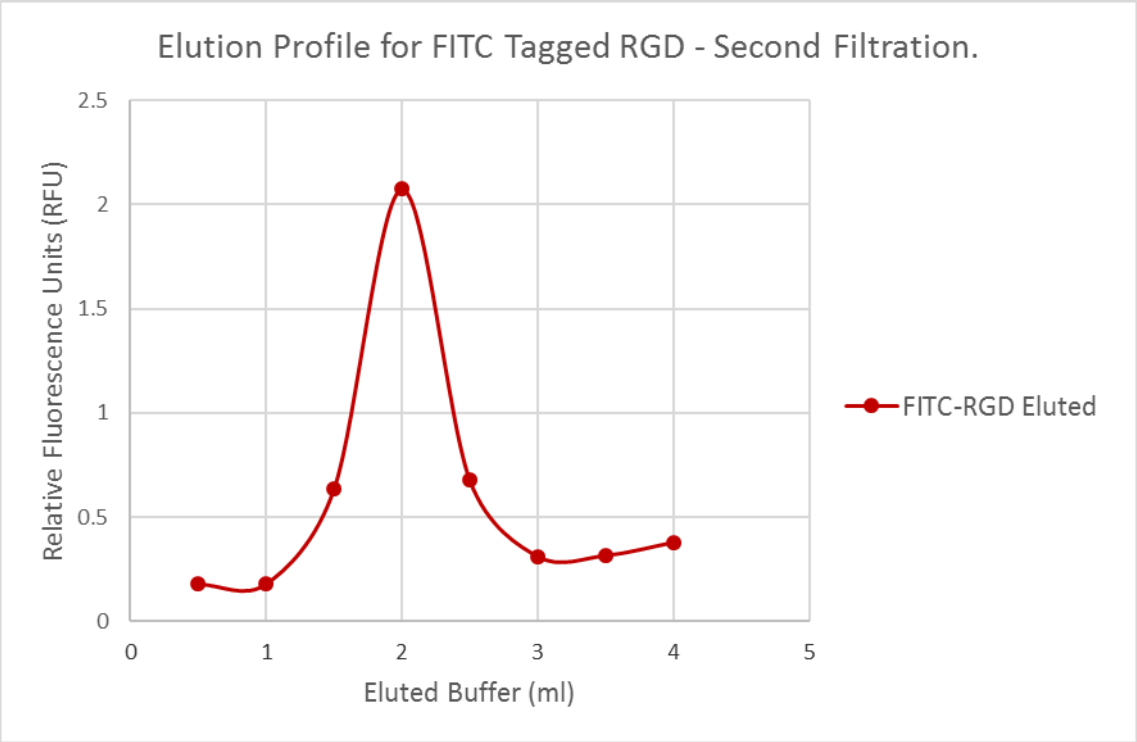

Figure 44 - Graph Showing the Elution Profile of FITC-Tagged RGD Peptide. Represents the 2nd Filtration. Peptide is again Eluted within the First 2.5ml of elution buffer.

The previous two figures (Figure 44 and Figure 44) show that the fluorescently tagged peptide was successfully filtered twice via gravity filtration, and recovered. Through both filtration cycles, the fluorescently tagged peptide was recovered between 1.5 and 2.5 ml of elution buffer. All other elution buffer volumes outside of this range were discarded. UV light exposure to the collected peptide filtration fractions showed a faint green fluorescence, also indicating successful fluorescence tagging of RGD, although discarded fractions showed high fluorescence indicating low fluorescence tagging efficiency.

5.2.2 Confocal Microscope Images of RGD Immobilisation

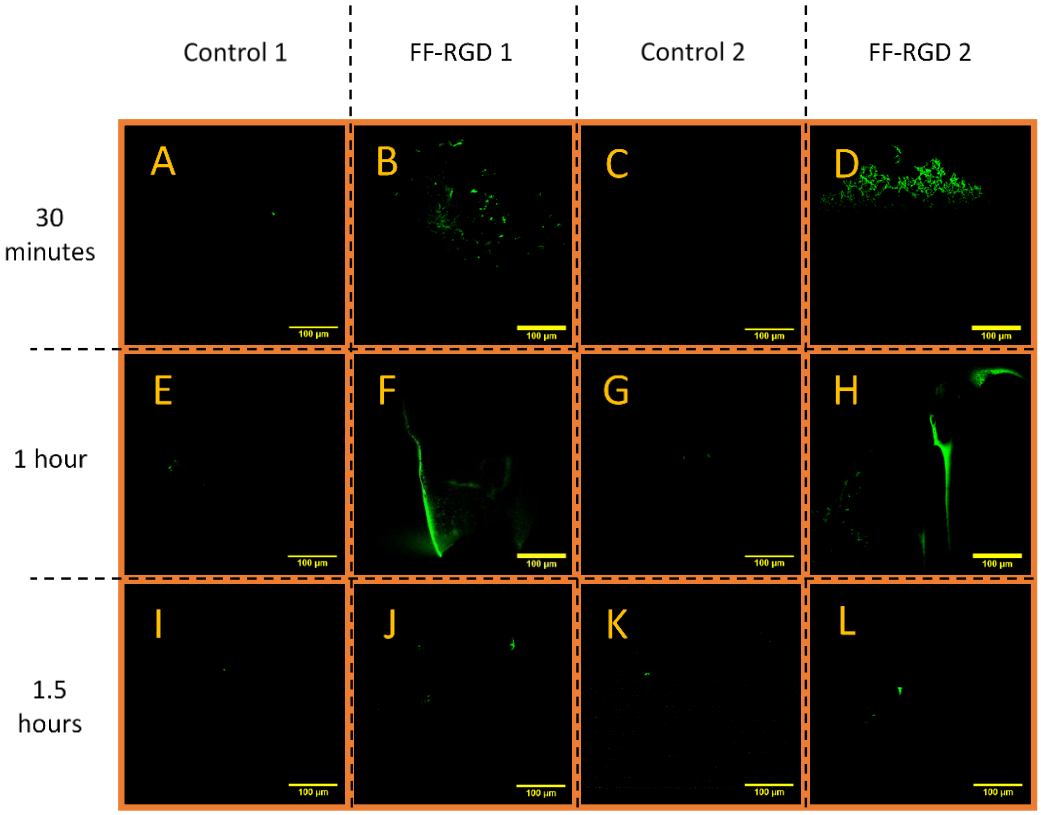

Figure 45 - Confocal Microscope Images of RGD Peptide Immobilisation on Control Discs A, C, E, G, I and K, and Fully-Functionalised RGD (FF-RGD) Discs B, D, F, H, J, and L. Peptide Immobilised Using Carbodiimide Coupling. FF-RGD Discs are Passivated/Polymerised/Silanised/RGD Titanium Discs. Peptide immobilised after 30-minutes (A-D), 1-hour (E-H) and 1.5-hours (I-L) of Immobilisation Reaction Time. Peptide is Visible due to Green Fluorescence Emitted from FITC Tagging of Peptide (Scale Bars Represent 100 µm).

The Confocal Microscope images give clear indication that the FITC-tagged RGD peptide was immobilised on the polymer surface of the titanium discs (**Error! Reference source not found.** B, D, F, H, J, and L). After each immobilisation time the control discs show virtually no RGD immobilised on the titanium disc surfaces (**Error! Reference source not found.**, A, C, E, G, I, and K). After 30-minutes there is some fluorescence from the peptide on the FF-RGD discs, although it is a very small amount of peptide (**Error! Reference source not found.**, B and D).

Following 1-hour of immobilisation, the amount of RGD immobilised had increased (**Error! Reference source not found.**, F and H), indicated by a larger area and intensity of the fluorescence signal which is directly proportional to the amount of peptide immobilised. As the immobilisation reaction time increased to 1.5-hours, a sharp decline in the fluorescence signal could be seen, indicating very little RGD peptide immobilised (**Error! Reference source not found.**, K and L). After 2 and 2.5-hours of reaction time, the fluorescence signal from the sample discs was comparable to the controls (Figure 58 in the Appendix sub-chapter 8.2.1).

It is entirely possible that the polymer layer had begun to dissolve/degrade after 1-hour. Dissolution of the polymer may have led to loss of the silane, and hence no immobilisation of the peptide. Furthermore, as the peptide immobilisation reaction was conducted in a non-aqueous environment, the hydrolytic instability of the silane layer would not have posed a problem here. 1-hour of peptide immobilisation using carbodiimide chemistry yielded the strongest fluorescence signal, indicating the most RGD bound to the polymerised titanium surface.

5.2.3 RGD Surface Area Analysis

Table 9 - Immobilised RGD surface area. Surface area of green fluorescence on Confocal Microscope Images of RGD immobilisation. Surface area analysed on Fully Functionalised-RGD samples (FF-RGD) and Control samples. Surface area calculated using ImageJ microscopy analysis software. Surface area expressed as µm^2. Confidence intervals calculated at 95% significance level (P=0.05).

		RGD Surface Area (µm^2)		
		30-minutes RGD Immobilisation	1-hour RGD Immobilisation	1.5-hours RGD Immobilisation
Control Disc	Control Disc 1	1.62	30.03	142.03
	Control Disc 2	19.48	40.58	163.27
	Mean	**10.55**	**35.31**	**152.65**
	Standard Deviation	12.63	7.46	15.02
	95% Confidence Interval	**17.50**	**10.34**	**20.81**
FF-RGD Disc	FF-RGD Disc 1	3605.23	7638.99	3057.38
	FF-RGD Disc 2	3188.87	6798.96	2109.41
	Mean	**3397.05**	**7218.98**	**2583.39**
	Standard Deviation	294.41	593.99	670.32
	95% Confidence Interval	**408.03**	**823.21**	**929.00**

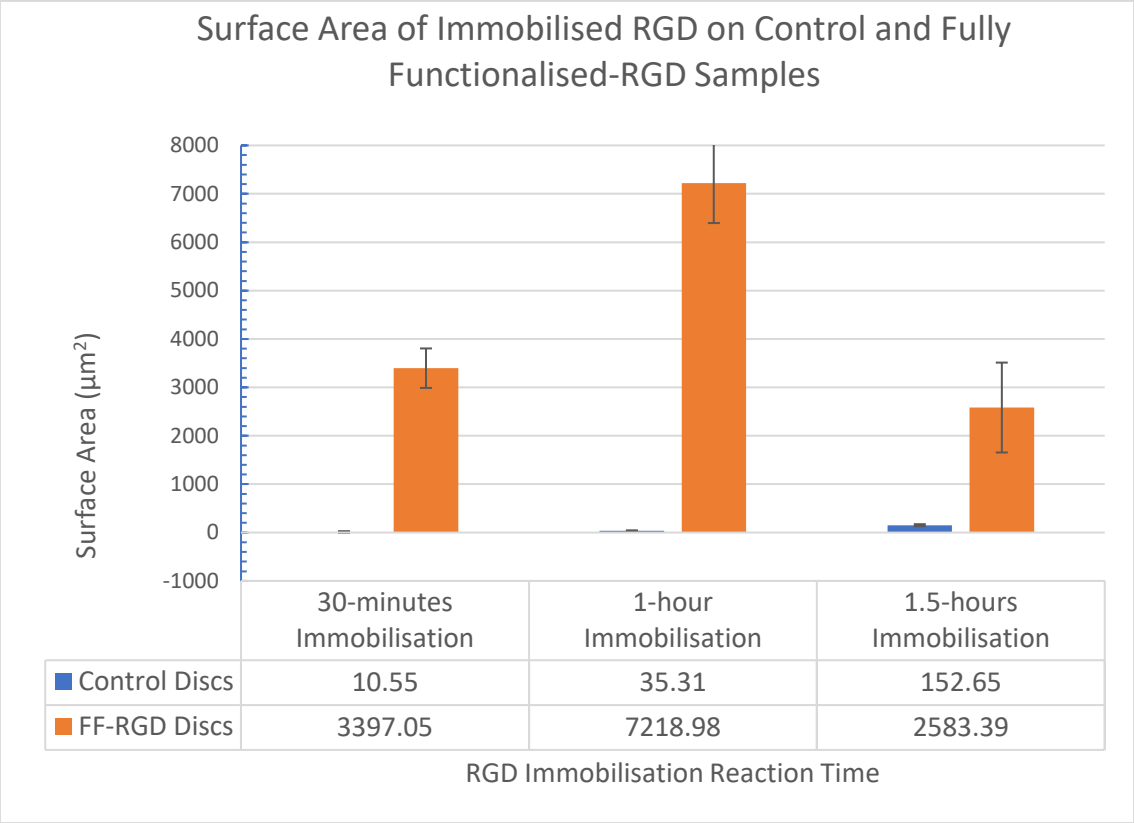

Figure 46 - Surface area of immobilised RGD. Surface area of green fluorescence from confocal microscope images of RGD immobilisation. Surface area calculated using ImageJ microscopy analysis software. Error bars indicate confidence intervals calculated at 95% significance level (P=0.05).

Analysis of the confocal microscope images using image analysis software ImageJ, allowed the surface area of the green fluorescence signal to be calculated, making comparison between controls and samples easier (Table 9 and Figure 46). Surface area analysis clearly shows that 1-hour peptide immobilisation via carbodiimide coupling to yield the highest amount of attached RGD, with a 112.5% and 179.4% increase in immobilised peptide surface area compared to the 30-minutes and 1.5-hours reaction times, respectively.

As previously mentioned, the carbodiimide coupling reaction is optimally performed at a reduced pH of around 4-5. This easily affords the carboxylate anion allowing the reaction to proceed much faster, usually in just a matter of minutes. However, omission of a buffering

system undoubtedly reduces coupling efficiency. It was thought that an aqueous buffer may dissolve/degrade the polymer layer on the titanium surface, hindering peptide conjugation altogether. Although addition of NHS and DCM solvent may have reduced the dreaded O-N shift, and allowed even a very small amount of peptide to attach. Also, utilising an excess of EDC and NHS may have bolstered the conjugation efficiency without the use of a buffering system, thus increasing the conjugation time from minutes to 1-hour.

6 Biological Investigation

Bioassays were conducted to assess the biological efficacy of the immobilised RGD and passivated surface towards murine pre-osteoblast cells. Raw, Passivated and Fully-Functionalised RGD (FF-RGD) surface were analyses for cell detachment, cell attachment, cell proliferation, differentiation and mineralised bone matrix. While Raw, Raw/Polymerised, Passivated and Passivated/Polymerised samples were analysed for their anti-infective properties against Staphylococcus aureus and Escherichia coli. Prior to any cell assay the titanium discs were sterilised with 70% isopropyl alcohol for 5 minutes, following by passive drying at room temperature.

6.1 Culture of MC3T3-E1 Murine Osteoblast Cells

6.1.1 Materials and Methods

MC3T3-E1 mouse pre-osteoblast cell (Calvaria) (CRL-2593 LGC Standards, ATCC); T75 tissue culture treated flasks, Nunc (Cranfield Health); 24-well non-treated, round flat bottom, cell culture plates, Corning Costar (CLS3738 Sigma); α-Minimum Essential Media (MEM), nucleosides, no ascorbic acid, Gibco (A10490-01 Invitrogen, Thermo Scientific); Fetal Bovine Serum, qualified, US origin, Gibco (26140-079 Invitrogen, Thermo Scientific); Dulbecco's Phosphate-Buffered Saline (DPBS) no calcium, no magnesium, Gibco (14190 Invitrogen, Thermo Scientific); Antibiotic/Antimycotic 100X, Gibco (15240-062 Invitrogen, Thermo Scientific); 0.25% Trypsin-EDTA (1X) phenol red, Gibco (25200 Invitrogen, Thermo Scientific); Dimethyl Sulfoxide (DMSO) sterile filtered (D2650 Sigma); Invitrogen Countess Automated Cell

Counter (Cranfield Health); Scanning Probe Microscope (SPM), Digital Instruments (Veeco) Nanoman VS (Cranfield SAS);

Cell Culture Protocol

The MC3T3-E1 Murine (Calvaria) pre-osteoblast cell line was used for the biological investigations. The cell suspension was cultured according to protocols suggested by the supplier; cells were grown in α-Minimum Essential Media (MEM) cell culture medium, supplemented with 10% fetal bovine serum and 1% Antibiotic-Antimycotic solution to produce the complete growth medium. Cells were incubated at 37°C in a 95% air/5% carbon dioxide atmosphere, and cultured in T75 tissue culture flasks through to passage 3 using a sub-cultivation ratio of 1:6 (medium was renewed every 2 days).

Cultured cells were then frozen at a cell concentration of 1 x 10^6 cells/ml in freezing medium (95% complete growth medium + 5% Dimethyl Sulfoxide (DMSO)) at -80°C for 24 hours, after which they were stored in liquid nitrogen vapour phase at -150°C. The cells were frozen slowly down to -150°C to prevent ice crystal formation. Prior to any cell assay, cells were thawed and re-cultured through to passage 5 before cell harvesting and seeding onto sample discs. Titanium discs were placed in 24 well plates for each cell assay before cell seeding. The diameter of the wells for these 24 well plates was only just larger than that of the titanium discs, thus leaving no room for cells to attach to the underlying plastic surface of the cell plates.

For the cell detachment, attachment and proliferation assays, cell concentrations were analysed using PrestoBlue cell viability reagent. Containing a cell permeable resazurin-based solution, the reducing power of living cells converts resazurin into a highly fluorescent product,

changing the colour of the medium from deep purple/blue to pink/red. The fluorescence of the samples was then assessed by way of a fluorescence plate reader set to the excitation/emission wavelengths of the fluorescent product (560nm/590nm respectively).

6.2 Cell Detachment

Cell detachment tests were conducted to assess the strength of cell adhesion to the sample surfaces following 24-hours of cell seeding. Cell detachment tests are commonly performed by detaching the cells from the substrate, usually with 0.25% (w/v) Trypsin-EDTA enzyme solution. Typically, 4-6 detachment cycles are performed in order to eventually remove all of the cells. The strength of cell adhesion is inversely proportional to the number of cells detached, thus giving insight into which surface provides greater strength of cell adhesion.

6.2.1 Materials and Methods

Titanium Alloy (Ti6Al4V) circular discs (provided by SinteaPlustek and William Gregor Ltd), with dimensions of 14mm diameter by 1mm thick, machine cut; MC3T3-E1 mouse pre-osteoblast cell (Calvaria) (CRL-2593 LGC Standards, ATCC); 24-well non-treated, round flat bottom, cell culture plates, Corning Costar (CLS3738 Sigma); 96-well imaging plates, tissue culture treated, black, clear flat bottom, BD Falcon (353219 BD Biosciences); α-Minimum Essential Media (MEM), nucleosides, no ascorbic acid, Gibco (A10490-01 Invitrogen, Thermo Scientific); Fetal Bovine Serum, qualified, US origin, Gibco (26140-079 Invitrogen, Thermo Scientific); Dulbecco's Phosphate-Buffered Saline (DPBS) no calcium, no magnesium, Gibco (14190 Invitrogen, Thermo Scientific); Antibiotic/Antimycotic 100X, Gibco (15240-062 Invitrogen, Thermo Scientific); 0.25% Trypsin-EDTA (1X) phenol red, Gibco (25200 Invitrogen, Thermo Scientific);

PrestoBlue cell proliferation reagent, (A-13261 Invitrogen, Thermo Scientific); Varioskan Flash Multimode Fluorescence Plate Reader (5250040 Thermo Scientific, provided by Cranfield Health); Invitrogen Countess Automated Cell Counter (Cranfield Health); Scanning Probe Microscope (SPM), Digital Instruments (Veeco) Nanoman VS (Cranfield SAS);

Cell Detachment Protocol

300,000 cells were first seeded onto each titanium disc placed in a 24 well plate, incubated for 2 hours (to alloy cell adherence), after which 1ml of growth medium was added to each well and subsequently re-incubated for 24 hours. Cells were detached using 0.25% Trypsin/EDTA enzyme solution. Cell culture medium was removed from the wells to be analysed. 0.5ml of the enzyme solution was added to each well for investigation, and the cells incubated for 4 minutes. After incubation 1ml of complete growth medium was added to inhibit the enzyme solution and prevent further cell detachments, after which the cell suspension was removed and transferred to a second plate for analysis. Complete growth medium was reintroduced into the sample wells and incubated for 15 minutes (allowing the remaining cells to re-attach).

This constitutes the first detachment cycle. Three further cell detachment cycles were conducted for 4, 7 and 10 minutes, giving a total detachment time of 25 minutes. After gathering all cell detachment samples, 50µl of PrestoBlue cell viability reagent was added to each sample of detached cells, and subsequently analysed in a fluorescence microplate reader to estimate the concentration of detached cells using the PrestoBlue standard curve.

6.2.2 Results and Discussion

Table 10 - Cell Detachment Assay Result Table for Raw, Passivated and FF-RGD Sample Surfaces (Assay Performed in Triplicate). Cell Detachment Measured as Concentration of Cells Removed Following the Detachment Cycles (cells/ml). Confidence Intervals Calculated at 95% Significance Level (P=0.05).

		Concentration of Cells Detached (cells/ml)						
		Cell Detach Cycle 1	Cell Detach Cycle 2	Cell Detach Cycle 3	Cell Detach Cycle 4	Total Cells Detached	Overall Mean Cells Detached	95% Confidence Interval
Raw Discs	1	44,620	35,421	11,544	12,168	103,754	**125,041**	**11,790**
	2	68,835	21,460	17,113	18,560	125,968		
	3	82,473	26,241	19,611	17,075	145,400		
Passivated Discs	1	147,161	47,456	35,545	29,994	260,156	**287,622**	**14,183**
	2	159,438	59,734	47,823	42,272	309,267		
	3	99,377	130,716	42,751	20,597	293,442		
FF-RGD Discs	1	12,813	13,702	14,255	14,102	54,872	**42,132**	**12,581**
	2	7,666	6,306	2,406	77	16,456		
	3	29,561	15,798	4,638	5,073	55,069		

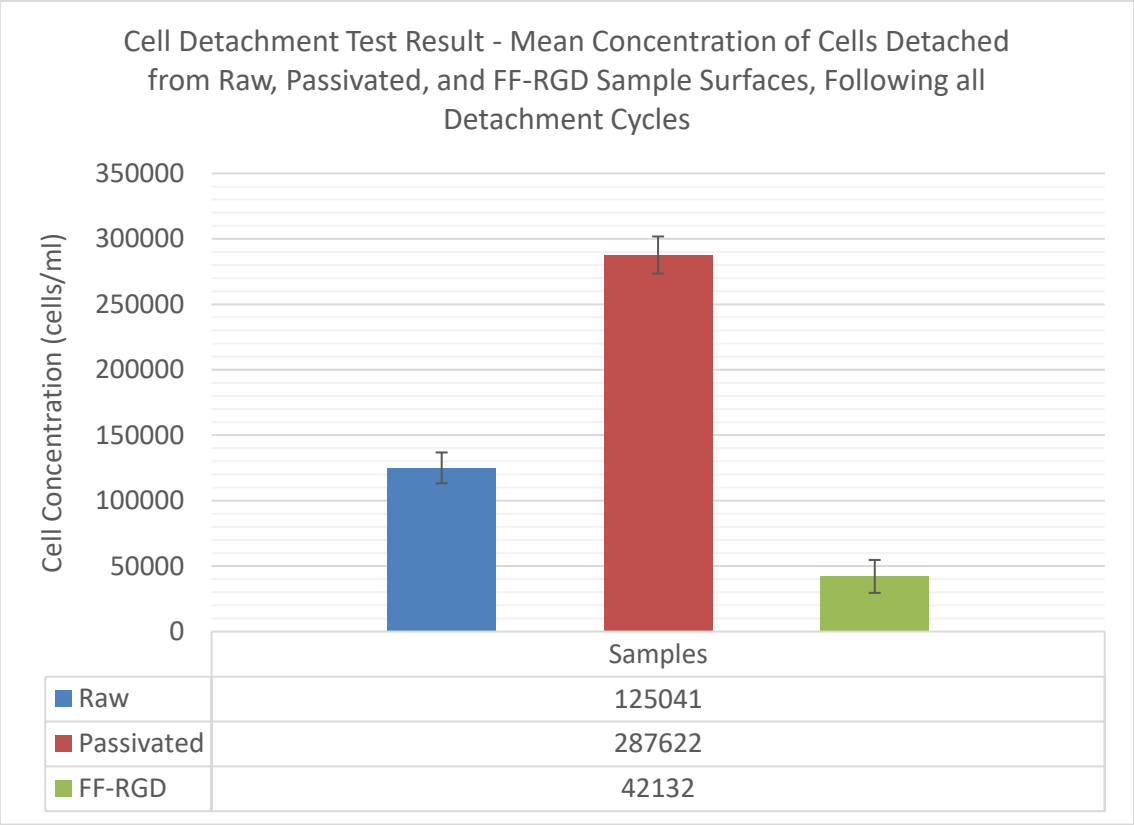

Figure 47 - Cell Detachment Test Result. Samples Analysed: Raw, Passivated, and Fully-Functionalised RGD (FF-RGD). Cell Detachment Measured as Cell Concentration of the Cells Removed following all 4 Detachment Cycles. Error Bars Represent Confidence Intervals at 95% Significance Level (P=0.05).

The cell detachment test result is both expected and surprising (Table 10 and Figure 47). The FF-RGD sample shows the fewest cells removed following all detachment cycles, indicating the highest strength of cell adhesion to the substrate surface. However, here it is thought that the 'sticky' nature of the underlying polymer could lead the cells to be trapped on the polymer matrix, imitating a stronger cell adherence. Though this may seem unlikely as the siloxane layer on the polymer could hinder cell attachment, being a hydrophobic layer. Although it is plausible that cells that have attached to the FF-RGD substrate may have died soon after attaching (Costa e Silva Filho and Conde Menezes, 2004), it is not entirely clear from this result whether the reduced number of cells detached from the FF-RGD substrate surface (indicating a

strong level of cell adhesion) is directly linked to a biological response elicited by the RGD peptide itself.

The passivated sample shows the poorest cell adhesion strength, with the most cells removed following the detachment cycles. The passivated surface is expected to perform better than the raw titanium, containing an abundance of hydroxyl groups from the extensively oxidised surface and enhanced hydrophilicity. The native oxide layer on titanium has a Point of Zero Charge (PZC) below pH7. The PZC is a physicochemical phenomenon that describes the charge density of a substrate in relation to an electrolyte's pH. Therefore, at physiological pH (approximately 7.4) the native oxide layer will be slightly negatively charged (negative OH- groups) (Born *et al.*, 1998, Tanaka *et al.*, 2008). Many of the ECM proteins related to osteoblast function, such as fibronectin and vitronectin, are negatively charged and therefore may experience electrostatic interactions, preventing their attachment to negatively charged surfaces and limiting cell adhesion (LEE *et al.*, 1994). Passivating the titanium surface with hydrogen peroxide/nitric acid is likely to increase the thickness of the outer oxide layer and present more surface hydroxyl groups than the raw surface (Pan *et al.*, 1996). This could explain the greater number of detached cells from the passivated surface than the raw titanium.

Research in the literature shows that smoother surfaces are often better for cell attachment and spreading, although some report the opposite. The raw titanium surface, which is also the smoothest, here showed better cell adhesion than the rougher passivated surface, supporting most of the literature, although the passivated titanium surface is rougher at the nano scale. The FF-RGD surface is also passivated and rougher (again at the nano level) than the raw titanium surface, but it exhibited the strongest cell adhesion. The RGD peptide may have elicited a biological response from osteoblast cells, perhaps enhancing focal adhesions to the

substrate surface, and/or stimulating increased ECM protein secretion, thereby making the rougher surface more viable to cell attachment. Cells will eventually attach to any surface, although if the surface is not optimal for cell adhesion, the cells will secrete more ECM proteins to acclimatise to the surface for their attachment, as previously explained in sub-chapter 2.2.

6.3 Cell Attachment

A cell attachment assay was conducted to gauge the initial speed of osteoblast cell attachment to the sample surfaces. Following cell seeding the cells were allowed to attach for a specified period of time (1 and 2-hours) before removing the unbound cells and analysing the cell concentrations. Degree of cell attachment is inversely proportional to the number of cells removed (or unbound cells).

6.3.1 Materials and Methods

Titanium Alloy (Ti6Al4V) circular discs (provided by SinteaPlustek and William Gregor Ltd), with dimensions of 14mm diameter by 1mm thick, machine cut; MC3T3-E1 mouse pre-osteoblast cell (Calvaria) (CRL-2593 LGC Standards, ATCC); 24-well non-treated, round flat bottom, cell culture plates, Corning Costar (CLS3738 Sigma); α-Minimum Essential Media (MEM), nucleosides, no ascorbic acid, Gibco (A10490-01 Invitrogen, Thermo Scientific); Fetal Bovine Serum, qualified, US origin, Gibco (26140-079 Invitrogen, Thermo Scientific); Dulbecco's Phosphate-Buffered Saline (DPBS) no calcium, no magnesium, Gibco (14190 Invitrogen, Thermo Scientific); Antibiotic/Antimycotic 100X, Gibco (15240-062 Invitrogen, Thermo Scientific); 0.25% Trypsin-EDTA (1X) phenol red, Gibco (25200 Invitrogen, Thermo Scientific); PrestoBlue cell proliferation reagent, (A-13261 Invitrogen, Thermo Scientific); Varioskan Flash

Multimode Fluorescence Plate Reader (5250040 Thermo Scientific, provided by Cranfield Health); Invitrogen Countess Automated Cell Counter (Cranfield Health); Scanning Probe Microscope (SPM), Digital Instruments (Veeco) Nanoman VS (Cranfield SAS);

Cell Attachment Protocol

100,000 cells were seeded onto each titanium disc in a 24 well plate and incubated for 1 or 2 hours, after which 1ml of complete growth medium was added to each well and the 24 well plate re-incubated. After 1 or 2 hours the medium was aspirated from each well and transferred to a new plate to which Prestoblue was added (50µl). The plate was analysed in a fluorescence plate reader to estimate the cell concentration of the cells that were removed (the cells that did not attach) using the PrestoBlue standard curve.

6.3.2 Results and Discussion

Table 11 - Cell Attachment Assay Result Table for Raw, Passivated and Fully-Functionalised RGD (FF-RGD) Sample Surfaces (Assay Performed in Triplicate). Cell Attachment Measured as Concentration of Cells Removed Following 1-hour of cell attachment time. Confidence Intervals Calculated at 95% Significance Level (P=0.05).

Cell Attachment 1-hour	**Concentration of Cells Removed from Sample Surface (cells/ml)**		
	Raw Sample	Passivated Sample	FF-RGD Sample
Sample Disc 1	40,673	28,475	5,892
Sample Disc 2	39,124	35,955	7,427
Sample Disc 3	51,106	33,744	7,117
Mean Cells Detached	**43,634**	**32,725**	**6,812**
Standard Deviation	6,516	3,843	812
95% Confidence Interval	**7,374**	**4,348**	**919**

Table 12 - Cell Attachment Assay Result Table for Raw, Passivated and Fully-Functionalised RGD (FF-RGD) Sample Surfaces (Assay Performed in Triplicate). Cell Attachment Measured as Concentration of Cells Removed Following 2-hours of cell attachment time. Confidence Intervals Calculated at 95% Significance Level (P=0.05).

Cell Attachment 2-hours	**Concentration of Cells Removed from Sample Surface (cells/ml)**		
	Raw Sample	Passivated Sample	FF-RGD Sample
Disc 1	23499	21380	5655
Disc 2	23261	15014	6041
Disc 3	31948	20374	5847
Mean Cells Detached	**26236**	**18923**	**5847**
Standard Deviation	4948	3422	193
95% Confidence Interval	**5599**	**3872**	**218**

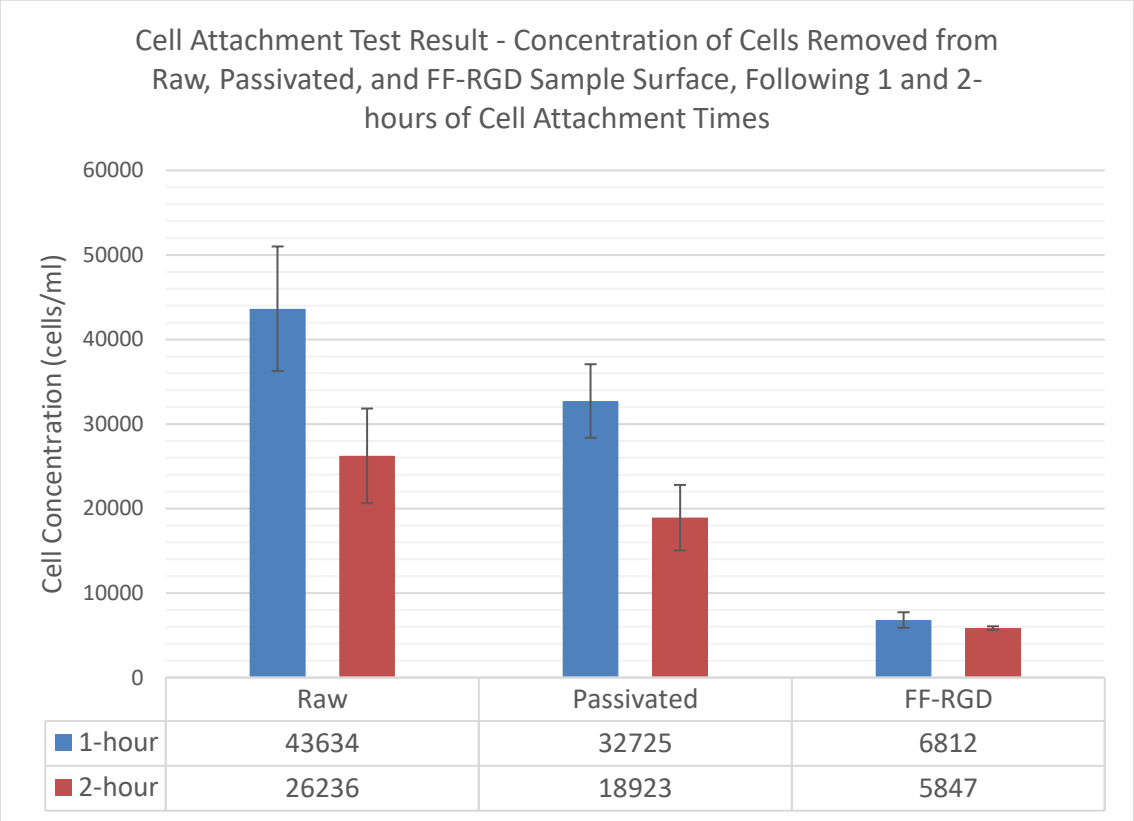

Figure 48 - Cell Attachment Test Result. Samples Analysed: Raw, Passivated, and Fully Functionalised-RGD (FF-RGD). Cell Attachment Measured as Cell Concentration of Cells Removed Following 1-hour (Blue Bars) and 2- hours (Red Bars) of Cell Attachment Time (cells/ml). Error Bars Represent Confidence Intervals at 95% Significance Level (P=0.05).

Table 11 and Table 12 show the concentration of cells removed following 1 and 2-hours of cell attachment time, respectively. From the results graph (**Error! Reference source not found.**) it is observed that all three sample substrates exhibited better initial cell attachment after 2-hours of attachment time than 1-hour (as expected), with the Raw, Passivated and FF-RGD surfaces showing a 40.2, 42.6 and 14.9% reduction in unattached cells, respectively. The FF-RGD result is substantially lower showing the fewest unattached cells being removed, therefore more cells attached to the surface. Although the result for FF-RGD after 1-hour and 2-hours attachment time is not significantly different, they are both significantly lower than Raw and Passivated samples after both attachment times. This result indicates that the FF-RGD substrate may increase the speed of initial cell attachment, although the results could again be linked to the highly 'sticky' nature of the polymer, with cells perhaps being trapped on the polymer matrix, thus leading to fewer unattached cells.

The passivated surface revealed fewer unattached cells compared to the raw titanium surface, indicating better initial cell attachment to nano rough surfaces than the smoother raw titanium surface, which is in agreement with literature reports. While the passivated surface showed better cell attachment, the cell detachment results indicated poor cell adhesion to this surface.

Clearly the highly oxidised and nano rough passivated surface is producing an effect on the cells, allowing them to attach faster than on the raw surface, although with less adhesive strength. Research in the literature suggests that hydrophilic surfaces aid initial cell attachment, which is in agreement with these results. Reduced cell adhesion strength on the passivated surface may be explained by the surface charge of the oxide layer which is negatively charged, as previously explained. Literature reports that neutral and positive charges on a surface can lead to enhanced cell adhesion, compared to negatively charged

surfaces (LEE *et al.*, 1994). Also, it is speculated that surface charge density could influence focal adhesions and cell contact guidance, affecting the strength of cell adhesion to such surfaces (MONSEES *et al.*, 2005).

6.4 Cell Proliferation

A cell proliferation assay was conducted to gauge how well the cells grew on the various sample surfaces. Cell growth is crucial to bone formation and bone healing, as it dictates cellular activity and cell differentiation. The cell proliferation was analysed using PrestoBlue cell viability reagent. When added to a cell suspension, living cells actively reduce the reagent, changing its fluorescence from blue to red.

6.4.1 Materials and Methods

Titanium Alloy (Ti6Al4V) circular discs (provided by SinteaPlustek and William Gregor Ltd), with dimensions of 14mm diameter by 1mm thick, machine cut; MC3T3-E1 mouse pre-osteoblast cell (Calvaria) (CRL-2593 LGC Standards, ATCC); 24-well non-treated, round flat bottom, cell culture plates, Corning Costar (CLS3738 Sigma); 96-well imaging plates, tissue culture treated, black, clear flat bottom, BD Falcon (353219 BD Biosciences); α-Minimum Essential Media (MEM), nucleosides, no ascorbic acid, Gibco (A10490-01 Invitrogen, Thermo Scientific); Fetal Bovine Serum, qualified, US origin, Gibco (26140-079 Invitrogen, Thermo Scientific); Dulbecco's Phosphate-Buffered Saline (DPBS) no calcium, no magnesium, Gibco (14190 Invitrogen, Thermo Scientific); Antibiotic/Antimycotic 100X, Gibco (15240-062 Invitrogen, Thermo

Scientific); 0.25% Trypsin-EDTA (1X) phenol red, Gibco (25200 Invitrogen, Thermo Scientific); PrestoBlue cell proliferation reagent, (A-13261 Invitrogen, Thermo Scientific); Varioskan Flash Multimode Fluorescence Plate Reader (5250040 Thermo Scientific, provided by Cranfield Health); Invitrogen Countess Automated Cell Counter (Cranfield Health); Scanning Probe Microscope (SPM), Digital Instruments (Veeco) Nanoman VS (Cranfield SAS);

Cell Proliferation Protocol

100 cells were seeded onto each titanium disc in a 24 well plate. The cells were incubated for 2 hours, allowing initial cell attachment to occur. Each well was then supplemented with 1ml of complete growth medium and relocated to the incubator. On the specified days for taking measurements (day 7, 9, 11, 13, 17, and 21), 50µl of PrestoBlue was added to each test well. The plate was again incubated to allow the cells to actively reduce the cell viability reagent. After the incubation period 50µl of cell culture medium was taken from each well and placed into a 96 well plate for analysis with a fluorescence plate reader. The Relative Fluorescence Units (RFU) of the samples is directly proportional to the cell concentration of the samples; higher RFU indicates higher cell concentration, and vice versa.

6.4.2 Results and Discussion

Table 13 - Cell Proliferation Results for Raw, Passivated and FF-RGD Samples (Performed in Triplicate). Cell Proliferation Measured on Days 7, 9, 11, 13, 17 and 21. Cell Proliferation Measured as Relative Fluorescence Units (RFU) which is Directly Proportional to the Cell Concentration. Confidence Intervals Calculated at 95% Significance Level (P=0.05).

		Cell Proliferation Measured as Relative Fluorescence Units (RFU)					
		Day 7	Day 9	Day 11	Day 13	Day 17	Day 21
Raw Discs	1	4.00	4.14	5.99	4.96	3.98	4.37
	2	3.62	4.17	7.29	4.57	3.94	5.23
	3	3.17	4.68	5.39	4.60	3.92	5.02
	Mean	**3.60**	**4.33**	**6.22**	**4.71**	**3.95**	**4.87**
	Standard Deviation	0.42	0.31	0.97	0.22	0.03	0.45
	95% Confidence interval	**0.47**	**0.35**	**1.10**	**0.24**	**0.04**	**0.51**
Passivated Disc	1	3.41	28.07	6.68	10.69	28.11	17.39
	2	5.04	28.77	14.11	18.40	30.87	13.29
	3	4.98	28.61	6.27	11.71	28.48	18.21
	Mean	**4.47**	**28.48**	**9.02**	**13.60**	**29.15**	**16.30**
	Standard Deviation	0.93	0.37	4.41	4.19	1.50	2.64
	95% Confidence interval	**1.05**	**0.41**	**4.99**	**4.74**	**1.69**	**2.98**
FF-RGD Discs	1	23.23	5.57	11.45	5.56	3.98	14.19
	2	17.81	4.89	35.67	5.33	3.92	16.00
	3	22.48	18.00	11.70	5.16	3.94	15.40
	Mean	**21.17**	**9.49**	**19.61**	**5.35**	**3.95**	**15.20**
	Standard Deviation	2.94	7.38	13.91	0.20	0.03	0.93
	95% Confidence interval	**3.32**	**8.35**	**15.74**	**0.23**	**0.04**	**1.05**

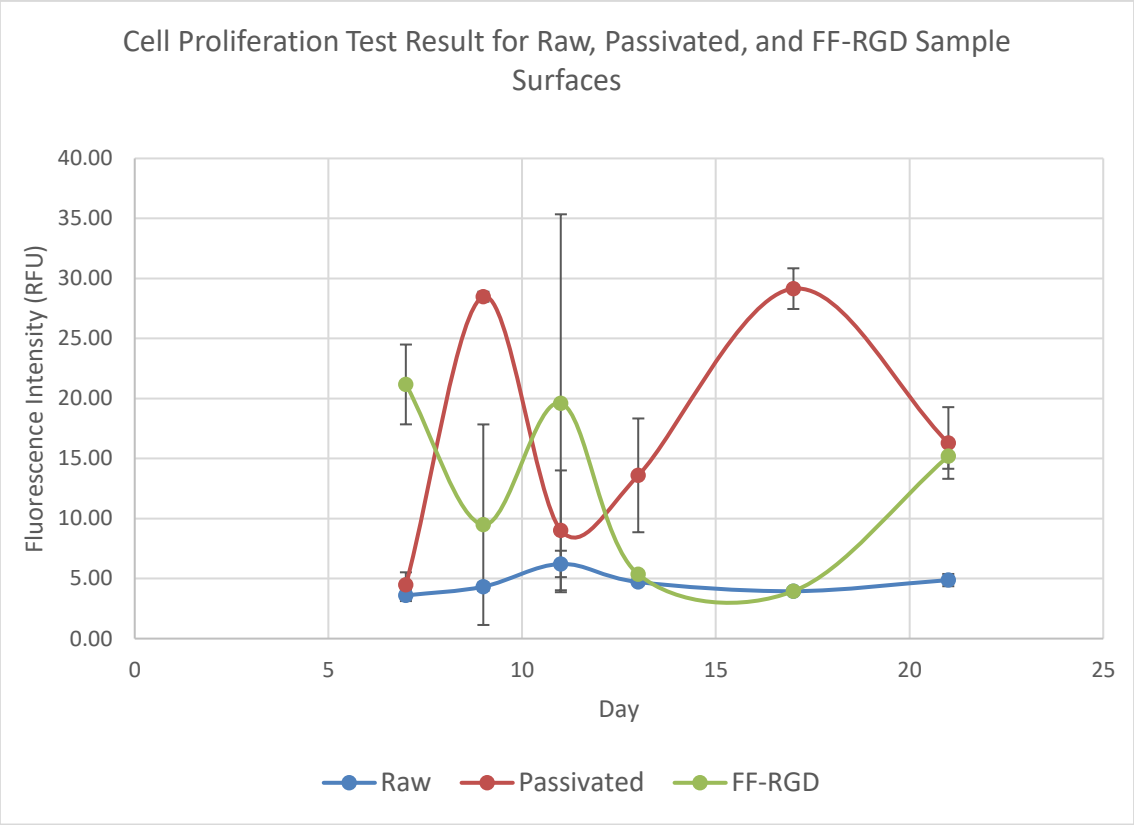

Figure 49 - Cell Proliferation Level at 7, 9, 11, 13, 17 and 21 Days Following Incubation. Samples Tested: Raw, Passivated, and Fully Functionalised-RGD. Cell Proliferation Level Measured as RFU (Relative Fluorescence Units). Error Bars Represent Confidence Intervals at 95% Significance Level (P=0.05).

The cell proliferation result is extremely poor. The error bars of all three sample groups overlap at almost every measurement, indicating no differences between the groups. Literature reports have indicated increased cell proliferation with RGD coated titanium surfaces. There are many reasons why this research failed to show different cell proliferation rates between the three groups studied, such as the isopropyl alcohol sterilisation step. If enough time had not elapsed for the discs to dry following sterilisation, a small amount of alcohol may have resided on all the discs, equally disrupting cell growth. Also, inadequate maintenance of the incubators may have led to drying out of the cell medium, leading to cell death and reduced proliferation in all three sample groups.

Another reason why the RGD peptide failed to elicit a biological response leading to enhanced cell proliferation, could be due to cell spreading. Biologists describe cell adhesion to a substrate surface using four main stages: serum protein adsorption, cell contact, cell attachment, cell spreading, and finally cell growth (VOGLER, 1989). Before exponential cell growth, or cell proliferation, cells must spread out on the substrate surface. The cell detachment and attachment results were produced in this work clearly show that the FF-RGD surface has an enhanced ability for cell attachment and increased strength of cell adhesion, fulfilling the initial stages of cell adhesion. However, the poor cell proliferation shown in the work could be due to poor cell spreading on the polymerised titanium surface. If the osteoblast cells failed to fully spread on the polymerised titanium surface, then cell proliferation would be stunted.

Although the results here failed to show any substantial increase in osteoblast proliferation, this aspect has been studied extensively in the literature. Such works in the literature have shown improved cell proliferation on surfaces functionalised with RGD peptides (Bell *et al.*, 2011, Huang *et al.*, 2003, Kantlehner *et al.*, 2000), as well as increased osseointegration in vivo ((ELMENGAARD *et al.*, 2005), although some studies show conflicting evidence (Barber *et al.*, 2007, Petrie *et al.*, 2008). The bioactivity of the RGD peptide has been shown to be less potent than the ECM protein fibronectin, or even the fibronectin peptide fragment FNIII7-10 (Garcia and Reyes, 2005, Petrie *et al.*, 2006). This suggests that the RGD peptide alone may be insufficient to elicit an optimal response from cell interactions. Some have suggested that a combination of binding domains need to be presented in the proper spatial configuration to maximize the biological efficacy of RGD (Healy *et al.*, 1999, Dettin *et al.*, 2002, Reyes and Garcia, 2004, Garcia, 2005, Cavalcanti-Adam *et al.*, 2006, Cavalcanti-Adam *et al.*, 2007).

6.5 Alkaline Phosphate Enzyme Activity

The Alkaline Phosphatase (ALP) enzyme is a marker for the differentiation of osteoblast cells. When osteoblasts begin to differentiate their ALP enzyme level rises and is the highest at the point of differentiation (as well as other protein markers such as osteocalcin). This assay was performed in parallel with the mineralisation assay as it does not require adding of a reagent to the seeded cells. Also, the cells subjected to the mineralisation assay were cultured in osteogenic medium that helps initiate cell differentiation and mineralisation. The ALP enzyme produced by osteoblast cells is released into the cell culture medium, and a small sample of the medium can be removed for analysis, leaving the remaining cells, medium and sample titanium discs undisturbed for subsequent analysis of mineralised bone matrix.

6.5.1 Materials and Methods

Titanium Alloy (Ti6Al4V) circular discs (provided by SinteaPlustek and William Gregor Ltd), with dimensions of 14mm diameter by 1mm thick, machine cut; MC3T3-E1 mouse pre-osteoblast cell (Calvaria) (CRL-2593 LGC Standards, ATCC); 24-well non-treated, round flat bottom, cell culture plates, Corning Costar (CLS3738 Sigma); 96-well imaging plates, tissue culture treated, black, clear flat bottom, BD Falcon (353219 BD Biosciences); α-Minimum Essential Media (MEM), nucleosides, no ascorbic acid, Gibco (A10490-01 Invitrogen, Thermo Scientific); Fetal Bovine Serum, qualified, US origin, Gibco (26140-079 Invitrogen, Thermo Scientific); Dulbecco's Phosphate-Buffered Saline (DPBS) no calcium, no magnesium, Gibco (14190 Invitrogen, Thermo Scientific); Antibiotic/Antimycotic 100X, Gibco (15240-062 Invitrogen, Thermo Scientific); 0.25% Trypsin-EDTA (1X) phenol red, Gibco (25200 Invitrogen, Thermo Scientific);

Alkaline Phosphatase (ALP) assay kit (fluorometric) (ab83371, Abcam); Varioskan Flash Multimode Fluorescence Plate Reader (5250040 Thermo Scientific, provided by Cranfield Health); Invitrogen Countess Automated Cell Counter (Cranfield Health); Scanning Probe Microscope (SPM), Digital Instruments (Veeco) Nanoman VS (Cranfield SAS);

ALP Enzyme Protocol

Similar to the cell proliferation assay, the ALP measurement was taken on day 7, 9, 11, 13, 17, and 21.

80µl of cell culture medium was removed from each of the sample wells of the 24 well plate and transferred to a 96 well plate (black BD Falcon round flat-bottom wells). The volume of the sample medium in each well of the 96 well plate was brought up to 110µl using assay buffer (contained in the ALP assay kit). A sample of complete growth medium was also placed in the 96 well plate as a background, to which 20µl of the stop solution was added (contained in the ALP assay kit). To each well of the 96 well plate (including background well), 20µl of 0.5mM 4-Methylumbelliferyl phosphate disodium salt (MUP) substrate was added (from the ALP assay kit). The MUP is a substrate for the ALP enzyme which cleaves the phosphate group from this non-fluorescent substrate, yielding a fluorescent signal from the dephosphorylated MUP substrate. The 96 well plate was incubated at room temperature for 30 minutes protected from light.

After 30 minutes 20µl of the stop solution was added to all wells of the 96 well plate (except the background well which already contained the stop solution). The fluorescence of the samples was measured in a fluorescent plate reader at an excitation/emission wavelength for the dephosphorylated MUP substrate (360nm/440nm respectively). The Relative Fluorescence

Units (RFU) of the samples is directly proportional to the amount of ALP enzyme present in the samples; higher RFU indicates higher amount of ALP enzyme, and vice versa.

6.5.2 Results and Discussion

Table 14 - ALP Assay Result for Raw, Passivated and FF-RGD Sample Surfaces (Assay Performed in Triplicate). ALP Activity Measured at Days 7, 9, 11, 13, 17 and 21. ALP Activity Measured as Relative Fluorescence Units (RFU) which is Directly Proportional to Cell Concentration. Confidence Intervals Calculated at 95% Significance Level (P=0.05).

		ALP Activity Measured as Relative Fluorescence Units (RFU)					
		Day 7	Day 9	Day 11	Day 13	Day 17	Day 21
Raw Discs	1	23.21	20.06	14.29	16.03	18.70	21.08
	2	21.71	20.33	12.95	18.65	20.47	21.93
	3	21.10	16.68	13.05	18.67	21.75	21.90
	Mean	**22.01**	**19.02**	**13.43**	**17.78**	**20.31**	**21.64**
	95% Confidence interval	**1.23**	**2.30**	**0.84**	**1.72**	**1.73**	**0.54**
Passivated Discs	1	22.58	19.78	23.12	17.91	27.29	22.16
	2	17.73	18.00	20.87	11.24	24.29	22.41
	3	19.14	22.91	19.31	18.93	25.66	23.19
	Mean	**19.82**	**20.23**	**21.10**	**16.03**	**25.75**	**22.59**
	95% Confidence interval	**2.82**	**2.81**	**2.16**	**4.73**	**1.70**	**0.60**
FF-RGD Discs	1	25.45	20.88	24.78	18.12	24.96	25.86
	2	21.82	18.16	21.59	17.90	27.43	26.55
	3	26.69	18.44	22.13	23.99	27.37	25.63
	Mean	**24.65**	**19.16**	**22.83**	**20.00**	**26.58**	**26.02**
	95% Confidence interval	**2.87**	**1.69**	**1.93**	**3.91**	**1.59**	**0.54**

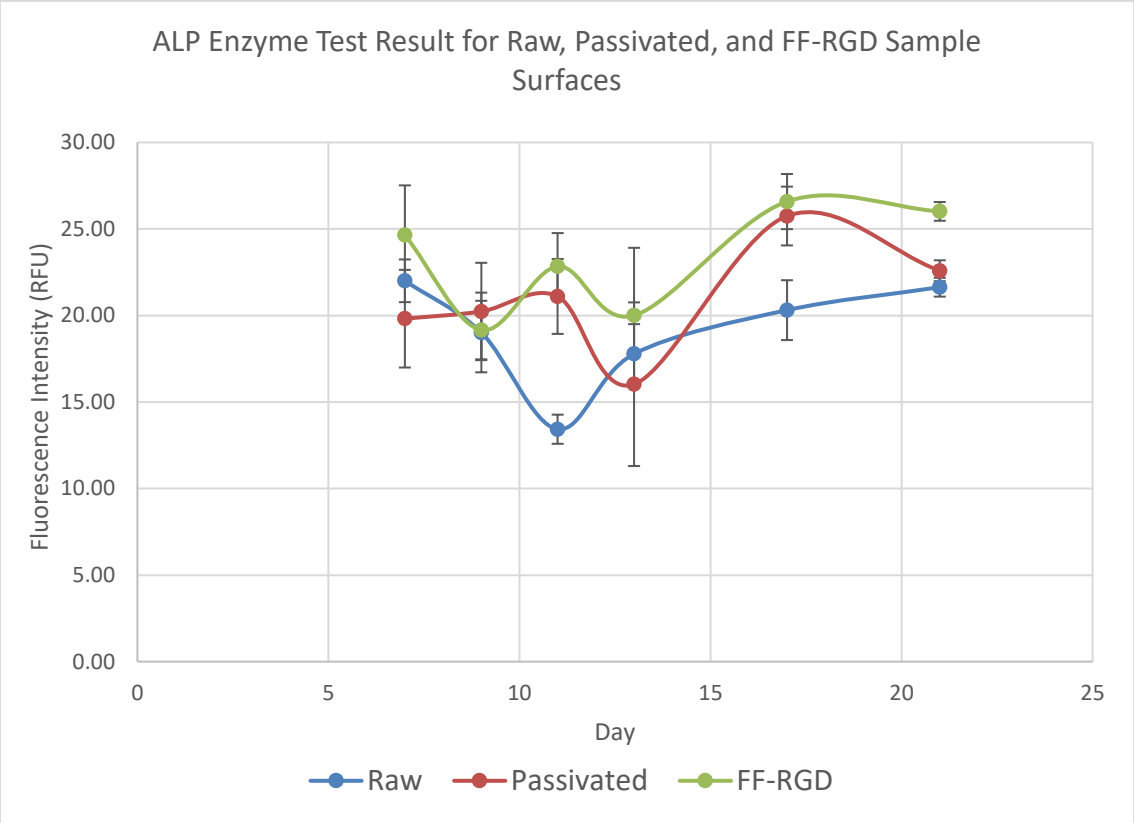

Figure 50 - Alkaline Phosphatase (ALP) Enzyme Level at 7, 9, 11, 13, 17 and 21 days Following Incubation. ALP Enzyme Level Measured as RFU (Relative Fluorescence Units). Error Bars Represent Confidence Intervals at 95% Significance Level (P=0.05).

The ALP enzyme level on the Passivated and FF-RGD samples is greater than on the Raw sample, although the error bars at all time points are merged except at days 11 and 17, and the graph shows that the Passivated and FF-RGD samples are quite similar. This could indicate that these two surfaces are showing similar levels of reactivity with the osteoblast cells, and thus may give rise to a higher level of differentiation over that of the Raw surface, which shows the least amount of reactivity. The difference in ALP level between the three groups could be attributed simply to operator error.

Evidence in the literature suggests that the RGD peptide in fact could reduce the differentiation of osteoblast cells (Bell *et al.*, 2011), opposing the hypothesis for this work but

corroborating the results. Work done by Tosatti *et al*. on poly(L-lysine)-graft-poly(ethylene glycol) coated titanium surfaces (PLL-PEG) with attached RGD peptides, revealed that the PLL-PEG coated surface alone enhanced cell differentiation, possibly by stimulating growth factor release and osteocalcin. However, attachment of RGD blocked the stimulatory effect of the PLL-PEG layer on the differentiation of osteoblast-like cells (Tosatti *et al.*, 2004). Also, it has been suggested that while the RGD peptide is recognised by the αvβ3 and α5β1 integrin heterodimers (of which α5β1 is greatly expressed in osteoblast cells), high affinity of RGD to α5β1 requires the PHSRN peptide site to fully activate the osteoblastic signalling pathway (Bell *et al.*, 2011). The PHSRN peptide, also known as the synergy site, is a peptide cell adhesion site within the fibronectin protein, and is believed to activate integrin receptors on osteoblast cells to stimulate cell attachment and adhesion, which can be regarded as prerequisites for eventual cell differentiation.

6.6 Bone Matrix Mineralisation

The mineralisation assay was performed using a mineralisation assay kit by OsteoImage (Lonza). This assay kit uses a fluorescent molecule which binds to and stains hydroxyapatite specific portions of mineralised bone, as well as bone-like nodules, deposited by osteoblasts. This assay kit is far superior to the von Kossa and Alizarin Red assays as they stain any calcium phosphate deposits. Also, the OsteoImage mineralisation assay requires fewer and simpler steps to perform and is much faster.

6.6.1 Materials and Methods

Titanium Alloy (Ti6Al4V) circular discs (provided by SinteaPlustek and William Gregor Ltd), with dimensions of 14mm diameter by 1mm thick, machine cut; MC3T3-E1 mouse pre-osteoblast cell (Calvaria) (CRL-2593 LGC Standards, ATCC); 24-well non-treated, round flat bottom, cell culture plates, Corning Costar (CLS3738 Sigma); α-Minimum Essential Media (MEM), nucleosides, no ascorbic acid, Gibco (A10490-01 Invitrogen, Thermo Scientific); Fetal Bovine Serum, qualified, US origin, Gibco (26140-079 Invitrogen, Thermo Scientific); Dulbecco's Phosphate-Buffered Saline (DPBS) no calcium, no magnesium, Gibco (14190 Invitrogen, Thermo Scientific); Antibiotic/Antimycotic 100X, Gibco (15240-062 Invitrogen, Thermo Scientific); 0.25% Trypsin-EDTA (1X) phenol red, Gibco (25200 Invitrogen, Thermo Scientific); Osteolmage bone mineralisation assay kit, Lonza (PA-1503 Stratech Scientific); L-ascorbic acid (A4403 Sigma); β-Glycerophosphate disodium salt hydrate (G9422 Sigma); Varioskan Flash Multimode Fluorescence Plate Reader (5250040 Thermo Scientific, provided by Cranfield Health); Invitrogen Countess Automated Cell Counter (Cranfield Health); Scanning Probe Microscope (SPM), Digital Instruments (Veeco) Nanoman VS (Cranfield SAS);

Bone Mineralisation Protocol

Titanium discs for evaluation were placed in a 24 well plate and 200 cells seeded onto each disc. The plate was placed in an incubator for 1-2 hours to allow the cells to initially attach to the substrate surface. 1ml of complete growth medium was then added to each well and the plate relocated to the incubator (37°C, 95% air + 5% carbon dioxide atmosphere). The 24 well plate was kept in the incubator for a full 21 days before analysing. Medium was replaced every 2 days.

After 7 days of incubation the culture medium was replaced with osteogenic medium. For the mineralisation assay ascorbic acid and β-glycerophosphate were added to the culture medium in order to help induce mineralised bone nodule formation, as well as provide inorganic phosphate. Supplementing the cell culture medium with ascorbic acid and β-glycerophosphate induces differentiation of the pre-osteoblast cells, giving these cells the ability to form mineralised bone nodules. The mineralised bone nodules that form display morphological and biochemical characteristics similar to that of woven bone formed in vivo, thus mimicking in vivo bone growth. Therefore it creates an osteogenic model of mineralised bone growth (Beresford *et al.*, 1993). Complete growth medium was supplemented with 200μM ascorbic acid and 10mM β-glycerophosphate. From day 7 to day 21 of the assay this osteogenic medium was supplied to the cells, and again replenished every 2 days.

On day 21 the medium was removed, and the cells washed once with D-PBS. The cells were fixed using 70% ethanol for 20 minutes and then rinsed twice with wash buffer (diluted from a 10x stock buffer contained in the assay kit). 0.5ml of staining reagent (diluted from the 100x stock reagent in the assay kit) was added to each well of the 24 well plate and incubated at room temperature for 30 minutes protected from light.

After the 30 minutes had elapsed, the staining reagent was discarded, and the wells washed with diluted wash buffer 3 times (leaving the wash buffer in the wells for 5 minutes each time before removing). The titanium discs were removed from the 24 well plate and fixed onto glass slides and covered with glass cover slips. The surfaces of the discs were analysed using CLSM with a fluorescein filter set to match the excitation/emission of the staining reagent (492nm/520nmm respectively). Stained mineralised bone matrix was seen in green colour which is also directly proportional to the amount mineralised bone present. Finally, image analysis software ImageJ was used to calculate the surface area of immobilised RGD

fluorescence on the confocal microscope images. ImageJ is an open-source software package developed by scientists in the field, and it was utilised to assess the area of mineralisation on the confocal microscope images. Converting the image to binary and subsequently adjusting the threshold to select all the fluorescence signal, the software can calculate the area encompassed by the fluorescence.

6.6.2 Results and Discussion

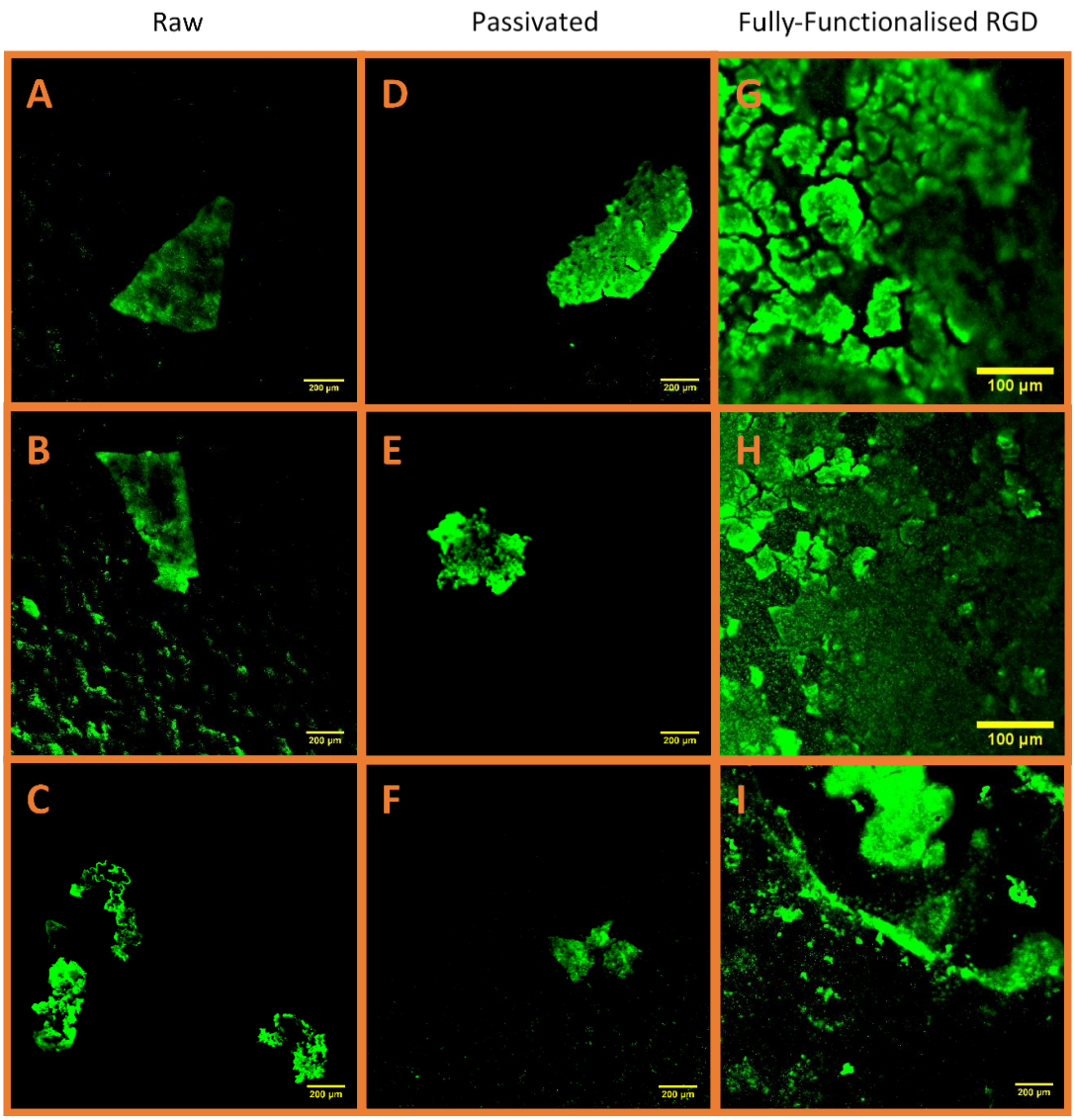

Figure 51 - Fluorescence Images from Confocal Laser Scanning Microscope (CLSM) of Mineralised Bone Matrix on Raw (A, B and C), Passivated (D, E and F), and Fully-Functionalised RGD (G, H and I) Titanium Discs, Following 21 days of Cell Culture. Images of 3 Discs Recorded from Each Sample. Error Bars Indicate 100µm Length.

Table 15 - Mineralised Bone Matrix Surface Area on Raw, Passivated and Fully-Functionalised RGD (FF-RGD) Surfaces. Mineralised Bone Matrix Area is Calculated by ImageJ Software for Confocal Microscope Image Analysis, and units of Area are μm². Confidence Intervals are Calculated at 95% Significance Level (P=0.05).

	Mineralised Bone Matrix Surface Area (μm²)		
	Raw Discs	Passivated Discs	FF-RGD Discs
Titanium Disc 1	68,194	44,405	149,822
Titanium Disc 2	51,231	66,041	133,225
Titanium Disc 3	58,229	57,301	181,622
Mean Area	**59,218**	**55,916**	**154,890**
95% Confidence Interval	**9,646**	**12,317**	**27,829**

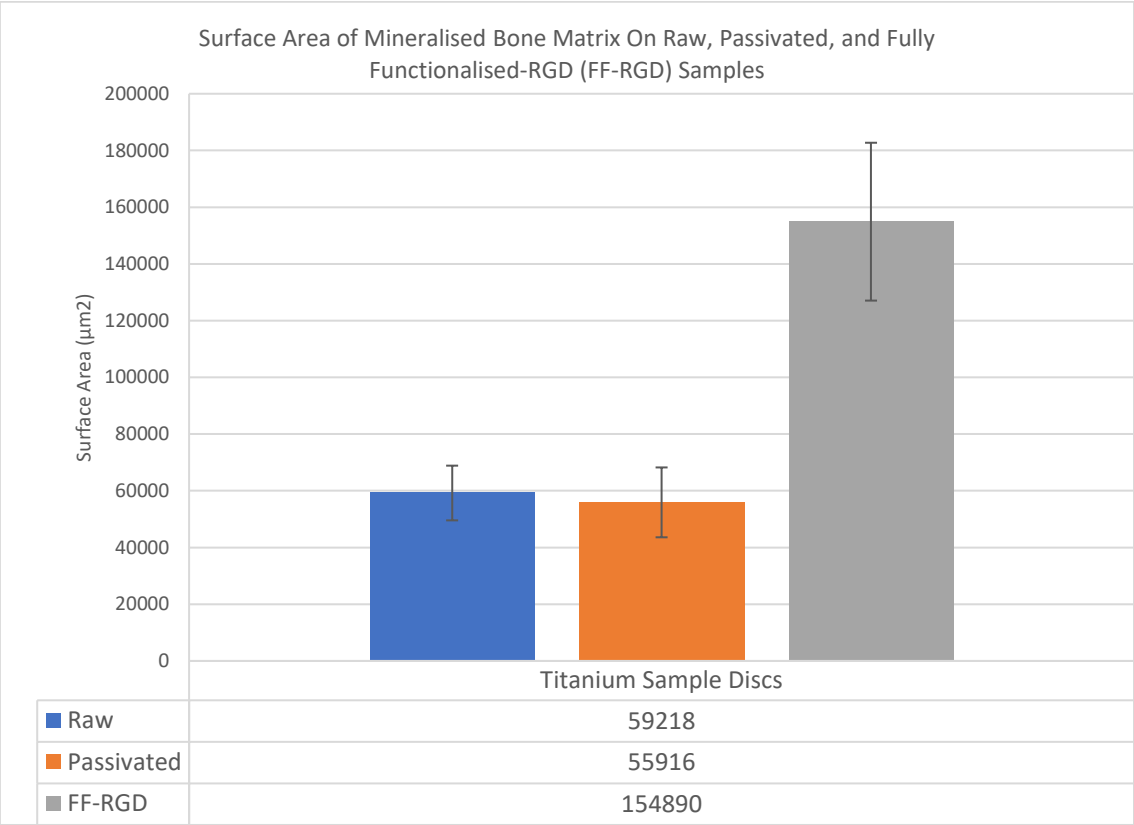

Figure 52 - Mineralised Bone Matrix Area on Raw, Passivated and Fully-Functionalised RGD (FF-RGD) Surfaces. Mineralised Bone Matrix Area Measured in μm2. Error Bars Represent Confidence Intervals at 95% Significance Level (p=0.05).

The CLSM images (**Error! Reference source not found.**) clearly show that the fluorescence chemical from the OsteoImage mineralisation assay kit, which stains HA specific calcium phosphate or mineralised bone, exhibits a higher signal on the FF-RGD discs. Large interlocking clumps of mineralised bone matrix of roughly 40 to 80µm, and even 100µm, in size can be seen (**Error! Reference source not found.**). The Raw and Passivated surfaces do show some mineralisation occurring, although it is very limited. This is one of the most definitive results that show the clinical potential of the RGD peptide to enhance bone healing around titanium alloy implants.

The FF-RGD sample showed a 161.6% increase in area of mineralised bone matrix than the Raw surface, and a 177% increase over that of the Passivated surface. Furthermore, ANOVA and Tukey Kramer statistical analyses revealed that the FF-RGD sample had significantly increased mineralised bone matrix compared to both the Raw and Passivated surfaces, and that there was no difference in mineralisation between Raw and Passivated samples (see Appendix sub-chapter 8.3.4).

Research in the literature has shown that surface topography can affect levels of mineralised bone matrix. Furthermore, they have shown that chemical-based surface treatments, such as peroxidation and acid etching that produce various random nano structured surface features, can enhance the level of mineralisation (Depprich *et al.*, 2008). As well as the biological effects of the RGD peptide on the FF-RGD disc, the surface nano features and enhanced oxidation of the oxide layer, imparted by passivation, may have worked in concert to enhance apatite nucleation on the titanium surface, leading to increased levels of mineralised bone matrix. As previously mentioned, the native oxide coating on titanium plays an important role in mineralisation. It has the ability to adsorb calcium ions from the ECM as well as initiate hydroxyapatite nucleation. Also, enhanced oxide layer growth from hydrogen peroxide

passivation further improves phosphate ion adsorption as well, thereby boosting apatite nucleation and calcium phosphate mineralisation.

Research by Schneider *et al.* (2001) showed that perturbation of certain integrin receptors such as α1β2 and αVβ3 (which also recognise the RGD peptide sequence) led to decreased mineralisation. Also, targeting of just a subunit rather than the integrin heterodimer resulted in only partial reduction in mineralisation, suggesting that a combination of the αβ integrin heterodimer may be important to control mineralisation initiation (Schneider *et al.*, 2001). From their findings it can be suggested that the RGD peptide may contribute to the ability of the MC3T3-E1 cell line to mediate the initiation of the mineralisation phenotype, through integrin-mediated signal transduction pathways. Furthermore, the cyclic RGD peptide used in this research may activate both integrin heterodimers, vastly increasing the mineralisation.

6.7 Antibacterial Testing

Antibacterial testing was conducted to evaluate theories in the literature that hydrophilic polymers, such as HBPG and PEG, could prevent bacterial cell adhesion to a biomaterial surface via non-specific protein adsorption. ECM proteins and certain bacterial adhesive proteins, such as fibronectin and MSCRAMM, are necessary for cell adhesion to biomaterial surfaces. Hydrophilic polymers make it difficult for such proteins to adhere to the surface via formation of a hydration layer, thereby preventing or delaying the onset of bacterial cell adhesion.

A selection of titanium alloy samples (Raw, Raw/Polymerised, Passivated, and Passivated/Polymerised) were seeded with the bacterial cells (gram-negative Escherichia coli

(ATCC11229) and gram-positive Staphylococcus aureus (ATCC6538) provided by Cranfield Health, Cranfield University), incubated and then the surface of the discs analysed for colony forming bacteria.

6.7.1 Materials and Methods

Titanium Alloy (Ti6Al4V) circular discs (provided by SinteaPlustek and William Gregor Ltd), with dimensions of 14mm diameter by 1mm thick, machine cut; Escherichia coli (ATCC11229, provided by Cranfield Health); Staphylococcus aureus (ATCC6538, provided by Cranfield Health) T75 tissue culture treated flasks, Nunc (Cranfield Health); 24-well non-treated, round flat bottom, cell culture plates, Corning Costar (CLS3738 Sigma); Petri Dishes, Sterilin (Thermo Scientific); Lysogeny broth medium, Fluka (Sigma); nutrient agar, Fluka (Sigma); Dimethyl Sulfoxide (DMSO) sterile filtered (D2650 Sigma); Invitrogen Countess Automated Cell Counter (Cranfield Health); Scanning Probe Microscope (SPM), Digital Instruments (Veeco) Nanoman VS (Cranfield SAS);

Antibacterial Testing Protocol

Bacterial cells were incubated towards the middle of their exponential phase using Lysogeny broth medium to yield a suspension of around 5*106cells/ml. Titanium alloy disc samples were sterilised with IPA for 5 minutes, then transferred to a pre-sterilised 24-well plate (Costar 3526, Corning). 0.5ml of the bacterial cell suspension was added to each well containing a sample disc, followed by 1.5ml of complete growth medium (DMEM and FBS from Invitrogen, Life Science Technology) to mimic the in vivo environment, and subsequently incubated at 37°C for 24 hours allowing enough time for the formation of a biofilm. The disks were

removed and rinsed thoroughly with PBS, and the bacterial cells collected from the disc surfaces. 0.1ml of the collected bacterial suspension was spread onto a nutrient agar (Fluka, Sigma Aldrich) plate (Sterilin, Thermo Fisher Scientific); three samples were taken from each disc. The agar plates were incubated overnight at 25°C after which the colony numbers were counted.

6.7.2 Results and Discussion

Table 16 - Colony Count of Escherichia coli on Raw, Passivated, and Passivated/Polymerised Titanium Surfaces. Passivated titanium samples are passivated using the novel hydrogen peroxide/nitric acid solution for 2-hours passivation. Confidence Intervals Calculated at 95% Significance Level (P=0.05).

E. coli	**E. coli Colony Count**		
	Raw Sample	Passivated Sample	FF-RGD Sample
Titanium Disc 1	1720	2078	360
Titanium Disc 2	1944	1790	477
Titanium Disc 3	2000	1784	489
Titanium Disc 4	2744	1084	592
Titanium Disc 5	3664	904	160
Titanium Disc 6	3920	1474	174
Mean	**2665**	**1519**	**375**
Standard Deviation	942	453	177
95% Confidence Interval	**754**	**362**	**142**

Table 17 - Colony Count of Staphylococcus Aureus on Raw, Passivated, and Passivated/Polymerised Titanium Surfaces. Passivated titanium samples are passivated using the novel hydrogen peroxide/nitric acid solution for 2-hours passivation. Confidence Intervals Calculated at 95% Significance Level (P=0.05).

S. aureus	**S. aureus Colony Count**		
	Raw Sample	Passivated Sample	FF-RGD Sample
Disc 1	3604	1860	500
Disc 2	3200	1260	692
Disc 3	3560	1764	594
Disc 4	2600	2964	622
Disc 5	2270	1844	660
Disc 6	3150	3570	440
Mean	**3064**	**2210**	**585**
Standard Deviation	531	869	97

95% Confidence Interval	**425**	**695**	**77**

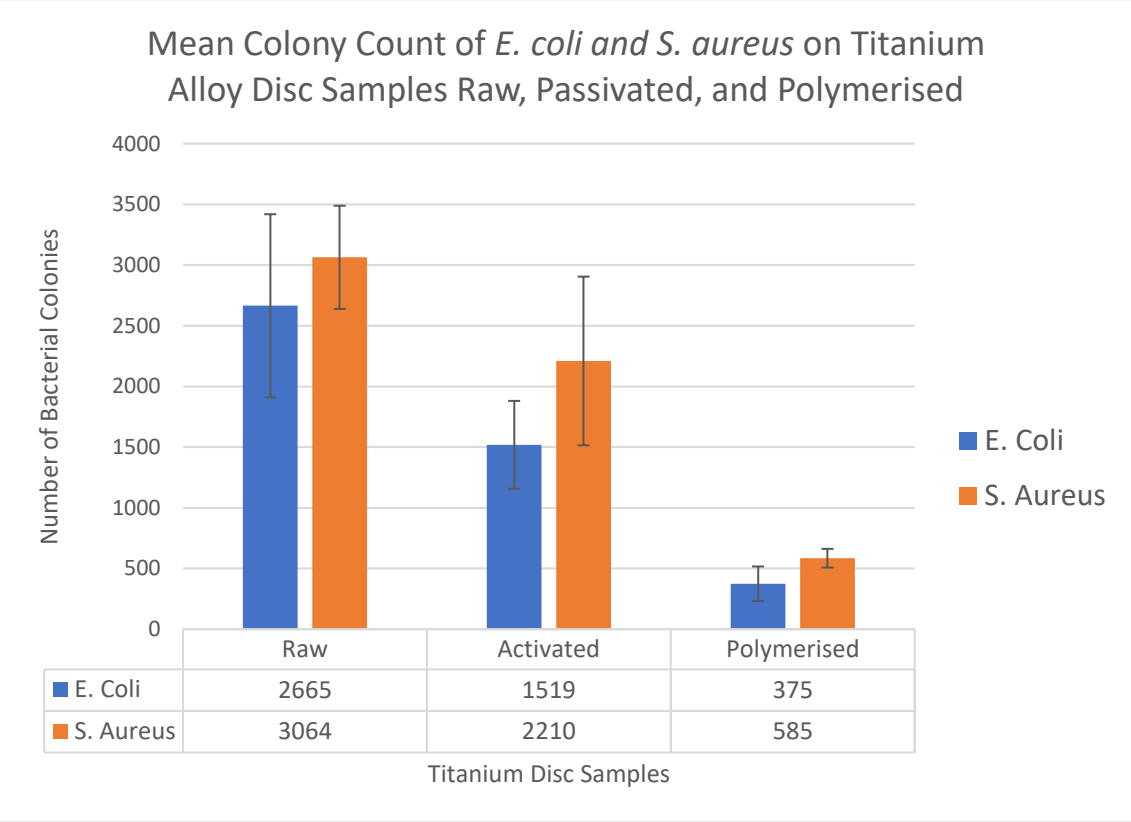

Figure 53 - Mean Colony Count of Escherichia Coli and Staphylococcus Aureus on Raw, Passivated and Passivated/Polymerised Titanium Surfaces. Passivated titanium samples are passivated using the novel hydrogen peroxide/nitric acid solution for 2-hours passivation. Assay Performed on Six Discs per group. Error Bars Indicate Confidence Intervals Calculated at 95% Significance level (P=0.05).

Results of the antibacterial test show decreased cell colonies of both E. *coli* and S. *aureus* on the Passivated/Polymerised discs. Theories in the literature discussing the anti-adhesive actions of hydrophilic polymers is clearly evidenced here. The hydrophilic character of the HBPG may reduce non-specific protein adsorption, including limiting the adsorption of bacterial cell adhesins, proteins that are necessary for bacterial cell attachment to the surface.

Another view is that of steric hindrance from the highly branched polymer matrix of HBPG, making it difficult for bacterial cells to reach the underlying titanium disc surface, and hence preventing attachment. As well as the formation of a hydration layer that is able to repel hydrophobic bacterial cells, such as E. *coli* and S. *aureus*.

The polymerised disc surface yielded an 85.9% reduction in the mean colony number of E. coli compared to the Raw disc, and a 75.3% reduction compared to the Passivated disc. ANOVA analysis and Tukey Kramer comparison revealed that the mean colony number for E. coli was significantly different across the three groups tested (Raw, Passivated, and Polymerised) (see Appendix chapter 8.3.5)

Regarding S. aureus, the Polymerised disc yielded an 80.9% reduction in mean colony number compared to the Raw disc, and a 73.5% reduction compared to the Passivated disc. ANOVA and Tukey Kramer analysis revealed no difference in S. aureus colonies between the Raw and Passivated samples, although the Polymerised disc showed significantly reduced colonies (see Appendix chapter 8.3.5)

ANOVA analysis between E. coli and S. aureus colonies on the Raw samples showed no significant differences (see Appendix chapter 8.3.5), and the same was found of the Passivated samples (see Appendix chapter 8.3.5). However, the mean colony number of E. coli was significantly lower than that of S. aureus on the Polymerised discs (see Appendix chapter 8.3.5). These analyses indicate that the Passivated and Polymerised surfaces showed a greater level of activity against E. coli than S. aureus.

The significantly reduced mean colony count of E. coli and S. aureus on Polymerised discs compared to Raw and Passivated discs could be explained by a difference in cell surface properties between E. coli and S. aureus. Using electrophoretic mobility measurements,

Sonohara *et al*. (1995) were able to detect a more negatively charged surface on E. coli cells compared to S. aureus cells. It is likely that the greater negative charge on E. coli is due to carboxylic acid derivatives on the bacterial cell surface (Hamadi *et al.*, 2008). Due to the negatively charged oxide layer, which on the passivated surface is extensively enhanced through peroxidation, electrostatic repulsive forces may have been greater on the Passivated disc, thereby preventing the adhesion of E. coli cells more so than S. aureus. Furthermore, both E. coli and S. aureus cells are hydrophobic due to extensive hydrocarbons on their cell surfaces. These hydrophobic cells would be repelled by the hydrophilic oxide coating on the Passivated disc, as well as the Passivated/Polymerised disc. The Raw and Passivated surfaces failed to show a difference in response to E. coli and S. aureus however, the Passivated/Polymerised surface showed a greater level of activity against E. coli than S. aureus, a result that is significant as analysed by ANOVA and Tukey-Kramer analysis (p=?). The greater level of antibacterial activity against E. coli than S. aureus is likely due to greater electrostatic interaction between the more negative E. coli and the Passivated and Polymerised discs, whereas S. aureus is less negative but more hydrophobic (Gogra *et al.*, 2010). Perhaps the electrostatic repulsive force is greater than that of the hydrophobic repulsive force. Also, as the Polymerised disc was passivated prior to polymerisation, it showed the least mean colony number for E. coli and S. aureus as the bacterial cells may have exhibited both electrostatic forces of repulsion as well as hydrophobic repulsion.

7. Discussion

The novel hydrogen peroxide/nitric acid (H_2O_2/HNO_3) (2-hours) passivation solution developed in this research, produced one of the most hydrophilic titanium alloy surfaces tested (contact-angle 35.35°), coming second only to hydrogen peroxide (24-hours) peroxidation (contact-angle 18.87°). The H_2O_2/HNO_3 (2-hours) passivation solution gave a similar contact-angle to that of Piranha solution (sulphuric acid/hydrogen peroxide, 50:50) (Ketonis *et al.*, 2009), one of the most highly oxidising solutions popularised with biomaterial surface preparation. In vitro cell adhesion to metals is well known to be linked to the hydrophilicity of the surface, and therefore surface energy. Studies have demonstrated that hydrophilic surfaces generally reduce cell proliferation but increase cell differentiation, and thus increase the release of local growth factors in vitro (Tosatti et al., 2004). Meanwhile, in vivo studies have shown that increased hydrophilicity of implant surfaces yields greater bone-implant contact and better initial bone apposition (Petrie et al., 2008). Surfaces showing increased wettability are able to adsorb matrix proteins with a more dynamic conformation in vitro, allowing adhering cells to reorganise the proteins as they see fit (Huang et al., 2003), thus improving cellular adhesion and spreading (Lee et al., 2004 - nanoscale).

The same H_2O_2/HNO_3 (2-hours) passivation solution produced surface roughness at the nano level, with a circular bumpy nanotexture, alongside sub-micron surface features such as pits and crevasses. Surface modifications at the nano scale have been shown to affect protein adsorption, cell morphology and the function of varying cell types including fibroblasts and osteoblasts. In addition, the increased accumulation of bone matrix proteins, most notably osteopontin and bone sialoprotein, on a titanium nanotopography indicates an increased level of cell differentiation, while the efficiency of protein adsorption and/or retention is greatly

improved on such nano-featured surfaces (Bueno 2011). The results obtained from the titanium surface passivation experiment fulfilled the first objectives of both aims, which were shared. These were; the passivation of titanium surface to enhance wettability, and to etch the titanium surface with nanoscale roughness. Also, the first hypothesis was proved right, that passivation of the titanium surface will enhance the wettability, and develop nano surface roughness.

Polymerisation of Hyperbranched Polyglycerol (HBPG) was successfully conducted, synthesising a transparent, viscous polymer from the titanium surface. Elemental analysis and contact-angle measurements confirmed the presence of the polymer layer, with increased oxygen and carbon content at the surface (attributed by the hydroxyl groups and hydrocarbon backbone of the polymer structure), and high wettability of the polymerised surface, and thus fulfilling the second objectives of both aims, the polymerisation of HBPG from the titanium surface. Although the passivated/polymerised surface showed a very low contact-angle, the polymer did not significantly lower the contact-angle over that of the passivated disc. Furthermore, the passivated/polymerised sample surface revealed a highly bumpy texture at the sub-micron level with an average roughness in the nano scale. Therefore, the results of the polymerisation experiment proved the second hypothesis, polymerisation of HBPG from the titanium surface will enhance wettability and further develop surface nano features.

The RGD peptide was successfully tagged with a fluorophore, FITC, and filtered. The CLSM images clearly show that the fluorescently labelled RGD was immobilised onto the polymerised titanium surface, via silanisation and subsequent carbodiimide coupling. Surface area analysis of the CLSM images indicated that the immobilised RGD was significantly higher than the controls, which showed virtually no fluorescent peptide. This result fulfilled the final objective of the first aim, immobilisation of the RGD peptide onto the Passivated/Polymerised titanium surface. Although the fluorescently labelled RGD was successfully immobilised, the confocal

microscope images show it to possibly be a small amount. Research has shown that the concentration of RGD ligand on a surface can affect its ability to manipulate host cell responses. RGD density greater than 0.6 pmol/cm^2 were shown to enhance osteogenic cell spreading and attachment compared with peptide densities below 0.01 pmol/cm^2 (Rezania and Healy, 2000, Rezania et al., 1999, Liu et al., 1992). Consequently, RGD density greater than 0.62 pmol/cm^2 revealed greater cell maturation and mineralisation of ECM (Rezania and Healy, 2000). Rezania and Healy hypothesised that an optimum surface concentration of adsorbed fibronectin is required for cell adhesion and movement (Rezania and Healy 2000). As this research did not focus on RGD density, it may have a causal relationship to the poor cell proliferation and differentiation results.

Four out of six biological investigations yielded positive results. The cell detachment on the Fully-Functionalised RGD (FF-RGD) surface indicated stronger cell adhesion compared to the Raw and Passivated surfaces. The cell attachment test also revealed that the FF-RGD surface showed improved initial cell attachment as well.

The FF-RGD sample failed to show improved cell proliferation and differentiation of the osteoblasts. This could have been due to operator errors, although it is more likely that the RGD peptide does not improve such cellular functions, as is discussed in the literature where the research is conflicted. It is entirely plausible that the amount of RGD attached to the FF-RGD titanium surface, was too little to elicit an efficacious biological response from osteoblast cells, regarding cell proliferation and ALP enzyme activity. Although some evidence in the literature does suggest use of the RGD peptide can reduce cell differentiation. Furthermore, studies have shown that for high affinity of RGD to integrin receptor sites, additional peptide sites may be required to fully activate the integrin signalling pathways, as previously explained in section 6.5.2.

The bone matrix mineralisation result is the most compelling evidence that the RGD peptide elicits a sufficient biological response from osteoblast cells, that leads to enhanced bone matrix production and mineralisation. The FF-RGD surface showed higher levels and areas of fluorescence on the CLSM images, with surface area analysis showing the FF-RGD sample to have 161.6% and 177.0% increase in mineralised bone matrix over that of the Raw and Passivated surface, respectively. The production of bone matrix and its subsequent mineralisation is crucial for implant success. It means a greater rate and amount of bony on growth onto the implant surface, improving BIC, and leading to full osseointegration of the implant. The bone matrix mineralisation results from this work also indicate faster growth of mineralised bone matrix, thereby reducing time to osseointegration and therefore reduced patient healing time.

Antibacterial testing showed that the Polymerised surface led to a substantial reduction in bacterial colonies for both E. *coli* and S. *aureus*, compared to the Raw and Passivated surfaces. The enhanced antibacterial activity of HBPG against these bacterial species could be explained by hydrophobic repulsion. Hydrophobic repulsion of the hydrophobic bacterial cells with the hydrophilic polymer could have hindered the bacterial cells from contacting the titanium surface. Also, the Passivated sample surface showed a significant reduction in E. *coli* colony numbers compared to the Raw surface, perhaps due to electrostatic repulsion of the negatively charged bacterial cells with the negatively charged titanium oxide layer. As the Polymerised sample was also passivated, it showed a drastic reduction in colony numbers most likely due to the combined effects of the oxide layer and the polymer.

The results of the antibacterial testing proved the third hypothesis, that the HBPG can reduce infection from pathogenic microorganisms. However, not all facets of the fourth hypothesis were proved, namely cell proliferation and differentiation. Although cell attachment, adhesion strength, and mineralised bone matrix were all improved.

8. Conclusion

The novel hydrogen peroxide/nitric acid passivation mixture used in this work has been shown to be more advantageous than nitric acid alone, producing a more oxidised surface with anisotropic nano features, and when compared to hydrogen peroxide passivation alone (peroxidation), it yields a similar hydrophilic character but in a much shorter amount of time (just 2-hours passivation compared to 12-hours). The hydrogen peroxide/nitric acid passivation mixture has also been shown in this research to yield a nano-rough surface topography, as well as surface features in the sub-micron range, such as pits and crevasses.

Cell proliferation and ALP enzyme assays in this research failed to show the biological efficacy of the RGD peptide, which has been numerously documented in the literature to be conflicted. However, the cell detachment assay conducted here showed that chemically grafted RGD on a polymerised titanium surface may enhance the strength of osteoblast cell adhesion. Also, the cell attachment assay showed a significant increase in cell attachment on the Fully-Functionalised RGD surface after 1 and 2-hours of attachment time, compared to the Raw and Passivated samples.

This research has fundamentally shown that by covalently attaching a cyclic RGD peptide to Hyperbranched Polyglycerol (HBPG), on a titanium alloy surface, it could greatly enhance bone matrix secretions which are subsequently mineralised, producing hydroxyapatite specific bone matrix.

Work done in this research has also revealed an antibacterial nature of HBPG, most likely an antiadhesive action. Due to its extreme hydrophilicity, it has been shown capable of repelling both Staphylococcus aureus and Escherichia coli bacterial cells from the titanium alloy surface,

thereby reducing implant infection and could prevent implant loosening and failure from such infections. Furthermore, the protective titanium oxide layer, which is negatively charged at physiological pH, may electrostatically repel negatively charged bacterial cells, such as E. *coli* and S. *aureus*.

Although the product of this work has shown its viability, and the main aims that were set out have been accomplished, more research needs to be carried out in order to increase the biological efficacy of the cyclic-RGD peptide. Further research is warranted in areas such as optimal ligand distance/spacing from the biomaterial surface, and efficient strategies to optimally increase RGD density on the surface. Although work in this research has shown the benefits of the hydrogen peroxide/nitric acid passivating solution to improve surface hydrophilicity and gain nano surface features on titanium, optimisation of this passivation technique is required to produce titanium surfaces with a more isotropic nano patterning, which may enhance cell surface contact guidance and cell spreading, and thus improve cell proliferation. Lastly, optimisation of the polymerisation of HBPG is needed. This research found that HBPG was a viscous liquid with high dissolution/degradation. Cross-linking of HBPG may provide a route to a more stable polymer structure, able to resist harsher chemical conditions, thereby allowing the use buffering systems in the carbodiimide conjugation reaction, and increasing RGD immobilisation efficiency.

This work has successfully shown the potential biological effects of cyclic-RGD and HBPG as they pertain to orthopaedic implants, as well as improved titanium surfaces by passivation with the novel hydrogen peroxide/nitric acid solution, in hopes that further research with their concomitant use may be carried out.

8. Appendix

8.1 Titanium Surface Passivation Results

8.1.1 AFM

3D AFM of Titanium Surface Passivated with HNO_3/H_2O (1:1) Following 1-hour Passivation

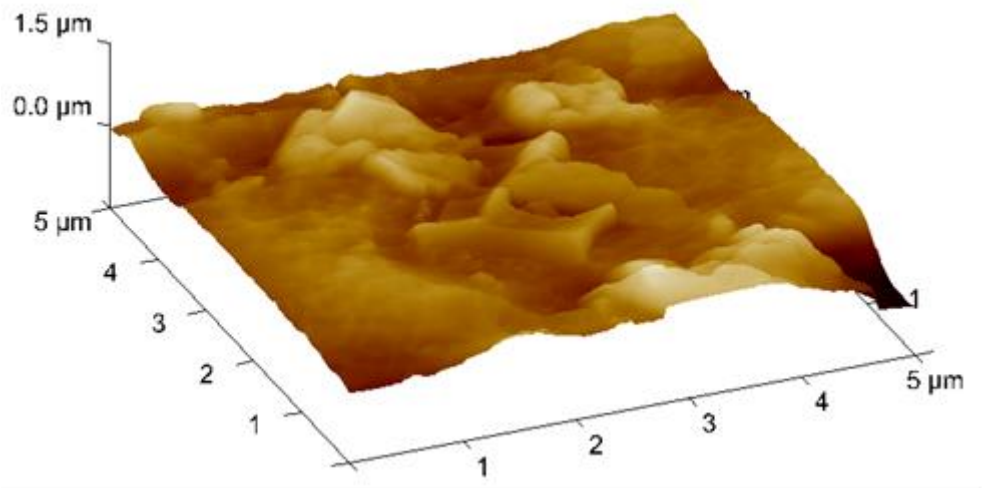

Figure 54 - 3D AFM Image of Titanium Alloy Surface Passivated with HNO_3/H_2O (1:1) Following 1-hour Passivation.

3D AFM of Titanium Surface Passivated with HNO_3/H_2O (1:1) Following 2-hour Passivation

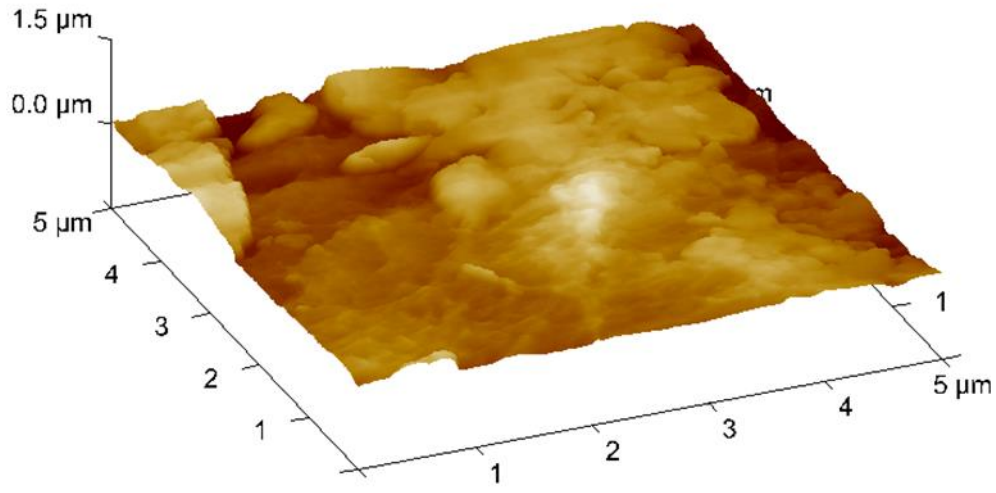

Figure 55 - 3D AFM Image of Titanium Alloy Surface Passivated with HNO_3/H_2O (1:1) Following 2-hour Passivation.

After passivating the titanium surface with the stronger nitric acid solution (HNO_3/H_2O, 1:1) following 1-hour and 2-hours passivation times, the topography of the surfaces, as shown in the AFM 3D images (Figure 54 and Figure 55), are similar to the 30-minutes passivation with the same solution (maximum height deviation of approximately 0.4 µm). This indicates that the ability of nitric acid to etch the titanium surface is limited beyond 30-minutes of passivation.

3D AFM of Titanium Surface Passivated with H_2O_2/HNO_3 (1:1) Following 1-hour Passivation

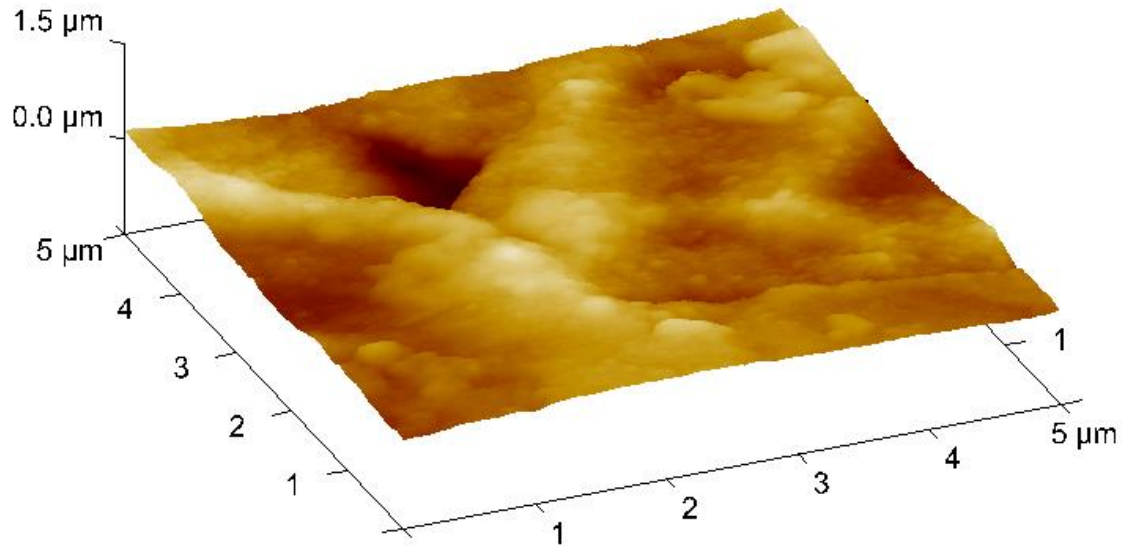

Figure 56 - 3D AFM Image of Titanium Alloy Surface Passivated with H_2O_2/HNO_3 (1:1) Following 1-hour Passivation

3D AFM of Titanium Surface Passivated with H_2O_2/HNO_3 (1:1) Following 30-minutes Passivation

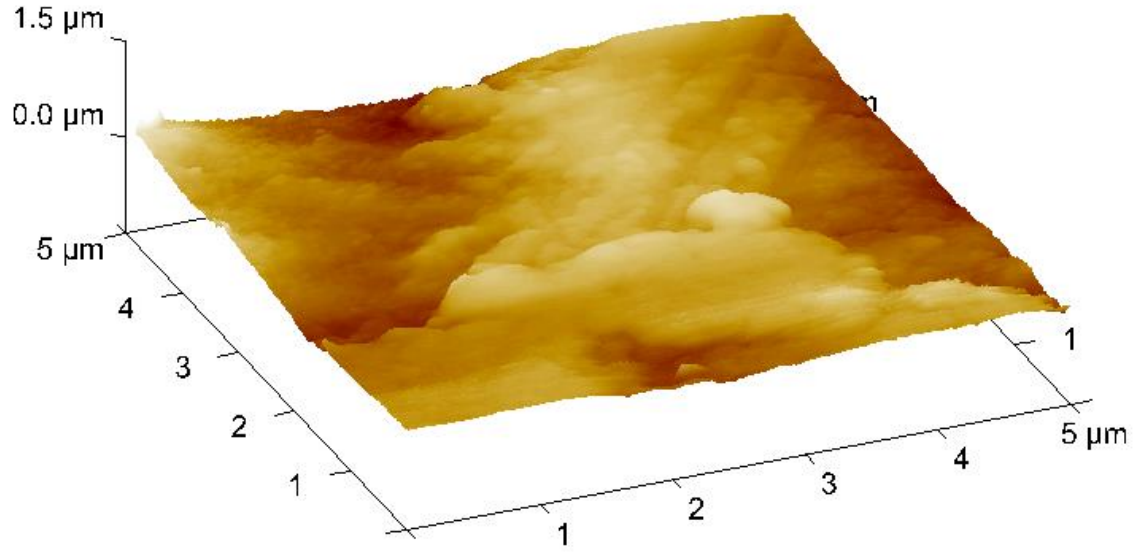

Figure 57 - 3D AFM Image of Titanium Alloy Surface Passivated with H_2O_2/HNO_3 (1:1) Following 30-minutes Passivation

The former two figures (Figure 56 and Figure 57) show the topography of the titanium surfaces passivated with the novel H_2O_2/HNO_3 solution at passivation times of 1-hour, and 30-minutes respectively. These AFM 3D images were omitted from the main results section as they show no substantial difference in topography compared to the 2-hours passivation time with the same solution. Also, they fail to show the circular bumpy nanotexture seen on the AFM, and SEM image, for the 2-hours passivation time.

8.2 RGD Peptide Immobilisation Results

8.2.1 CLSM

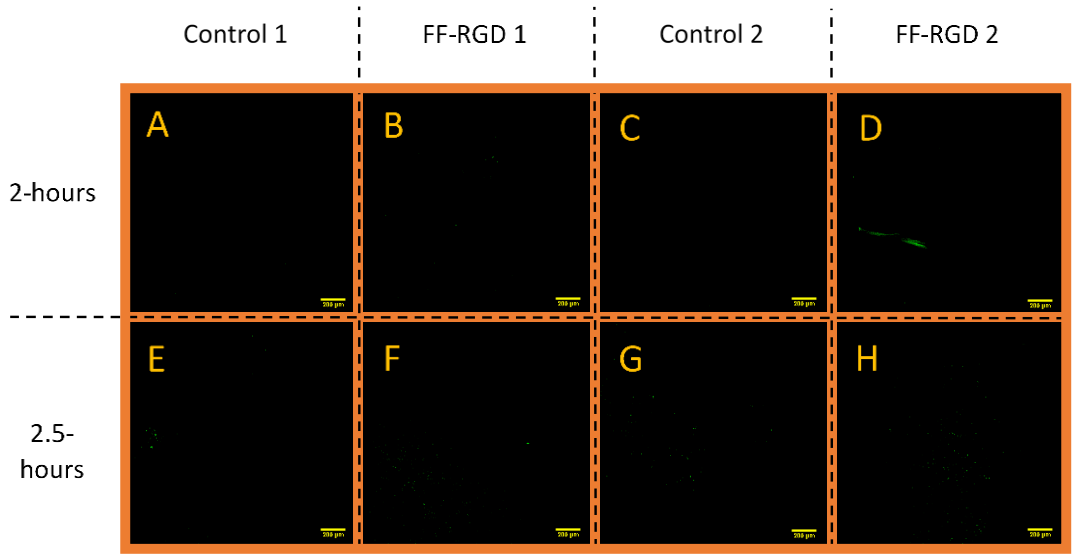

Figure 58 - Confocal Microscope Images of RGD Peptide Immobilisation on Control Discs A, B, E, F and FF-RGD Sample Discs C, D, G, and H. Peptide Immobilised Using Carbodiimide Coupling onto Passivated/Polymerised/Silanised Titanium Discs with 2-Hours Immobilisation Reaction Time (A-D) and 2.5-Hours Immobilisation Time (E-H). Green Fluorescence Emitted From FITC-Tagged RGD Peptide (Scale Bars Represent 100 µm).

The previous image (Figure 58) of the peptide immobilisation result shows that the FF-RGD discs are comparable to the controls. This indicates that the peptide immobilisation is near zero efficiency when the immobilisation time is 2-hours and beyond using the carbodiimide coupling strategy. This could be attributed to an instability of the silane layer and/or excessive dissolution/degradation of the polymer layer in the DCM solvent, thus completely inhibiting the RGD peptide conjugation.

8.3 Statistical Analyses

8.3.1 Passivation Results Statistical Analysis

ANOVA Statistical Analysis for Contact Angle Between Raw, H_2O_2 (12h), H_2O_2 (24h), and HNO_3/H_2O (3:7, 30m) Passivation Solutions

Anova: Single Factor

SUMMARY

Groups	*Count*	*Sum*	*Average*	*Variance*
1) Raw	3	227.99	76.00	96.39
2) H_2O_2 12h	3	102.87	34.29	29.11
3) H_2O_2 24h	3	56.60	18.87	5.97
4) HNO_3/H_2O (3:7) 30m	3	213.44	71.15	104.80

ANOVA

Source of Variation	*SS*	*df*	*MS*	*F*	*P-value*	*F crit*
Between Groups	7017.22	3	2339.07	39.60	3.79939E-05	4.066
Within Groups	472.54	8	59.07			
Total	7489.76	11				

F value of 39.60 is larger than the F critical of 4.066, indicating that the population means are different.

Tukey-Kramer Comparison Tables for Contact angle analysis between Raw, H_2O_2 (12h), H_2O_2 (24h), and HNO_3/H_2O (3:7, 30m) Passivation Solutions

Tukey-Kramer Comparison Table

Total no. of samples	15
Pooled Variance = MS from ANOVA	59.07
Number of Groups	4
Number of samples per group	3
Num *df (number of groups)*	4
Den *df* (total no. samples - *df*)	11
Critical value of Studentized Range, Q	4.26

Sample Comparisons	Absolute Difference	Critical Range	Result
1 vs 2	41.71	20.63	Different
1 vs 3	57.13	20.63	Different
1 vs 4	4.85	20.63	not different
2 vs 3	15.42	20.63	not different
2 vs 4	36.86	20.63	Different
3 vs 4	52.28	20.63	Different

Tukey-Kramer comparison analysis reveals that the Raw sample has a contact angle that is significantly greater than both hydrogen peroxide passivations (12-hour and 24-hour), but the same as HNO_3/H_2O (3:7) 30-minute passivation. Also, both hydrogen peroxide passivations (12-hour and 24-hour) are the same but both produce a significantly lower contact angle than the HNO_3/H_2O (3:7) 30-minute passivation solution. In this test group, the hydrogen peroxide passivation (12-hours and 24-hours) yields a significantly lower contact angle, and therefore a more hydrophilic surface.

ANOVA Statistical Analysis for Contact Angle Between HNO_3/H_2O (1:1) and H_2O_2/HNO_3 (1:1) Passivation Solutions Following 30-minutes, 1-hour and 2-hours Passivation Times

Anova: Single Factor

SUMMARY

Groups	*Count*	*Sum*	*Average*	*Variance*
1) HNO_3/Water (1:1) 30m	3	225.23	75.08	0.01
2) H_2O_2/HNO_3 (1:1) 30m	3	143.83	47.94	8.83
3) HNO_3/Water (1:1) 1h	3	209.33	69.78	65.77
4) H_2O_2/HNO_3 (1:1) 1h	3	129.60	43.20	67.57
5) HNO_3/Water (1:1) 2h	3	218.94	72.98	18.58
6) H_2O_2/HNO_3 (1:1) 2h	3	106.06	35.35	16.43

ANOVA

Source of Variation	*SS*	*df*	*MS*	*F*	*P-value*	*F crit*
Between Groups	4456.52	5	891.30	30.18	2.12343E-06	3.11
Within Groups	354.35	12	29.53			
Total	4810.87	17				

The F value of 30.18 is substantially greater than the F critical value of 3.11, indicating a difference between the sample populations.

Tukey-Kramer Comparison Tables for Contact angle analysis between HNO_3/H_2O (1:1) and H_2O_2/HNO_3 (1:1) Passivation Solutions Following 30-minutes, 1-hour and 2-hours Passivation Times

Tukey-Kramer Comparison Table

Total no. of samples	18
Pooled Variance = MS from ANOVA	29.53
Number of Groups	6
Number of samples per group	3
Num *df (number of groups)*	6
Den *df* (total no. samples - *df*)	12
Critical value of Studentized Range, Q	4.75

Sample Comparisons	Absolute Difference	Critical Range	Result
1) vs 2)	27.13	14.90	different
1) vs 3)	5.30	14.90	not different
1) vs 4)	31.88	14.90	different
1) vs 5)	2.10	14.90	not different
1) vs 6)	39.72	14.90	different
2) vs 3)	21.83	14.90	different
2) vs 4)	4.74	14.90	not different
2) vs 5)	25.04	14.90	different
2) vs 6)	12.59	14.90	not different
3) vs 4)	26.58	14.90	different
3) vs 5)	3.20	14.90	not different
3) vs 6)	34.42	14.90	different
4) vs 5)	29.78	14.90	different
4) vs 6)	7.85	14.90	not different
5) vs 6)	37.63	14.90	different

Following each passivation time (30-minutes, 1-hour and 2-hours), the novel hydrogen peroxide/nitric acid solution yields a consistently lower contact angle than nitric acid passivation. Also, the contact angles between all three passivation times for nitric acid is the same. The same is also true for hydrogen peroxide/nitric acid passivation, with no difference

between the three passivation times however, the comparison between hydrogen peroxide/nitric acid 30-minutes and 2-hours yields an absolute difference (12.59) which is very close to the critical range of 14.90. This indicates that the 2-hours passivation with hydrogen peroxide/nitric acid may give a lower contact angle than passivating for 30-minutes.

ANOVA Statistical Analysis for Contact Angle Between H_2O_2 (12h), H_2O_2 (24h), and H_2O_2/HNO_3 (1:1, 2h) Passivation Solutions

Anova: Single Factor

SUMMARY

Groups	*Count*	*Sum*	*Average*	*Variance*
1) H_2O_2 12h	3	102.87	34.29	29.11
2) H_2O_2 24h	3	56.60	18.87	5.97
3) HNO_3/H_2O_2 (1:1) 2h	3	106.06	35.35	16.43

ANOVA

Source of Variation	*SS*	*df*	*MS*	*F*	*P-value*	*F crit*
Between Groups	510.82	2	255.41	14.87	0.0047	5.14
Within Groups	103.03	6	17.17			
Total	613.85	8				

A larger F value (14.87) than the F critical of 5.14 indicates a difference between the sample means.

Tukey-Kramer Comparison Tables for Contact angle analysis between H_2O_2 (12h), H_2O_2 (24h), and H_2O_2/HNO_3 (1:1, 2h) Passivation Solutions

Tukey-Kramer Comparison Table

Total no. of samples	9
Pooled Variance = MS from ANOVA	17.17
Number of Groups	3
Number of samples per group	3
Num *df (number of groups)*	3
Den *df* (total no. samples - *df*)	6
Critical value of Studentized Range, Q	4.34

Sample Comparisons	Absolute Difference	Critical Range	Result
1) vs 2)	15.42	10.38	different
1) vs 3)	1.06	10.38	not different
2) vs 3)	16.49	10.38	different

The Tukey-Kramer comparison reveals that that the novel hydrogen peroxide/nitric acid solution (at 2-hours passivation) yields a contact angle which is similar to that of hydrogen peroxide alone for 12-hours, but achieved 10-hours faster. This shows the industry scale-up advantages of this novel passivating solution to yield a very hydrophilic titanium surface quickly, easily and cheaply.

ANOVA Analysis of Reproducibility for HNO_3/H_2O (1:1) at 30-minute, 1-hour, and 2-hours Passivation Times (3 batches of discs analysed for each passivation time)

Anova: Single Factor

SUMMARY

Groups	*Count*	*Sum*	*Average*	*Variance*
1) 30m Batch 1	4	303.91	75.98	16.33
2) 30m Batch 2	4	296.39	74.10	7.37
3) 30m Batch 3	4	300.53	75.13	17.07
4) 1h Batch 1	4	281.91	70.48	7.71
5) 1h Batch 2	4	267.12	66.78	379.83
6) 1h Batch 3	4	288.21	72.05	46.55
7) 2h batch 1	4	283.67	70.92	8.93
8) 2h batch 2	4	280.98	70.25	26.93
9) 2h batch 3	4	311.02	77.76	86.61

ANOVA

Source of Variation	*SS*	*df*	*MS*	*F*	*P-value*	*F crit*
Between Groups	374.77	8	46.85	0.71	0.683876974	2.31
Within Groups	1791.95	27	66.37			
Total	2166.71	35				

The F value of 0.71 obtained from ANOVA is less than the F critical, indicating that the population means are the same. Passivating the titanium surface with nitric acid yields reproducible contact angles, although there are no differences in contact angles between the three passivation times.

ANOVA Analysis of Reproducibility for the novel H_2O_2/HNO_3 (1:1) at 30-minute, 1-hour, and 2-hours passivation times (3 batches of discs analysed for each passivation time)

Anova: Single Factor

SUMMARY

Groups	*Count*	*Sum*	*Average*	*Variance*
1) 30m Batch 1	4	181.89	45.47	15.32
2) 30m Batch 2	4	188.66	47.17	51.51
3) 30m Batch 3	4	204.70	51.18	6.00
4) 1h Batch 1	4	164.56	41.14	185.08
5) 1h Batch 2	4	164.79	41.20	47.40
6) 1h Batch 3	4	189.01	47.25	67.05
7) 2h batch 1	4	143.38	35.85	90.11
8) 2h batch 2	4	126.74	31.69	23.50
9) 2h batch 3	4	153.71	38.43	32.79

ANOVA

Source of Variation	*SS*	*Df*	*MS*	*F*	*P-value*	*F crit*
Between Groups	1234.92	8	154.36	2.68	0.026281862	2.31
Within Groups	1556.28	27	57.64			
Total	2791.20	35				

The F value of 2.68 is greater than the F critical, indicating a difference between the population means.

Tukey-Kramer Comparison Table for Analysis of Reproducibility for the novel H_2O_2/HNO_3 (1:1) at 30-minute, 1-hour, and 2-hours passivation times

Tukey-Kramer Comparison Table

Total no. of samples	36
Pooled Variance = MS from ANOVA	57.64
Number of Groups	9
Number of samples per group	4
Num *df (number of groups)*	9
Den *df* (total no. samples - *df*)	27
Critical value of Studentized Range, Q	4.76

Sample Comparisons	Absolute Difference	Critical Range	Result
1) vs 2)	1.69	18.07	not different
1) vs 3)	5.70	18.07	not different
1) vs 4)	4.33	18.07	not different
1) vs 5)	4.28	18.07	not different
1) vs 6)	1.78	18.07	not different
1) vs 7)	9.63	18.07	not different
1) vs 8)	13.79	18.07	not different
1) vs 9)	7.05	18.07	not different
2) vs 3)	4.01	18.07	not different
2) vs 4)	6.02	18.07	not different
2) vs 5)	5.97	18.07	not different
2) vs 6)	0.09	18.07	not different
2) vs 7)	11.32	18.07	not different
2) vs 8)	15.48	18.07	not different
2) vs 9)	8.74	18.07	not different
3) vs 4)	10.04	18.07	not different
3) vs 5)	9.98	18.07	not different
3) vs 6)	3.92	18.07	not different
3) vs 7)	15.33	18.07	not different
3) vs 8)	19.49	18.07	different
3) vs 9)	12.75	18.07	not different
4) vs 5)	0.06	18.07	not different
4) vs 6)	6.11	18.07	not different
4) vs 7)	5.30	18.07	not different
4) vs 8)	9.46	18.07	not different
4) vs 9)	2.71	18.07	not different

5) vs 6)	6.05	18.07	not different
5) vs 7)	5.35	18.07	not different
5) vs 8)	9.51	18.07	not different
5) vs 9)	2.77	18.07	not different
6) vs 7)	11.41	18.07	not different
6) vs 8)	15.57	18.07	not different
6) vs 9)	8.83	18.07	not different
7) vs 8)	4.16	18.07	not different
7) vs 9)	2.58	18.07	not different
8) vs 9)	6.74	18.07	not different

Tukey-Kramer comparison reveals that the contact angles between the batches of all three passivation times are the same, indicating that the contact angle results from passivation using the novel hydrogen peroxide/nitric acid solution is reproducible.

8.3.2 Polymerisation Results Statistical Analysis

ANOVA Statistical Analysis of Contact Angle between Raw, Raw/Polymerised, Passivated, and Passivated/Polymerised titanium samples (Passivated and Passivated/Polymerised samples are both passivated using novel H_2O_2/HNO_3 (1:1) 2-hours solution)

Anova: Single Factor

SUMMARY

Groups	*Count*	*Sum*	*Average*	*Variance*
1) Raw	3	227.99	76.00	96.35
2) Raw/Polymerised	3	151.71	50.57	28.96
3) Passivated	3	106.06	35.35	16.43
4) Passivated/ Polymerised	3	122.57	40.86	34.53

ANOVA

Source of Variation	*SS*	*df*	*MS*	*F*	*P-value*	*F crit*
Between Groups	2917.22	3	972.41	22.07	0.00032	4.07
Within Groups	352.54	8	44.07			
Total	3269.76	11				

F value is greater than the F-crit value = Population means are different

Tukey-Kramer Comparison Tables for Analysis of Contact Angle between Raw, Raw/Polymerised, Passivated, and Passivated/Polymerised titanium samples (Passivated and Passivated/Polymerised samples are both passivated using novel H_2O_2/HNO_3 (1:1) 2-hours solution)

Tukey-Kramer Comparison Table

Total no. of samples	12
Pooled Variance = MS from ANOVA	44.07
Number of Groups	4
Number of samples per group	3
Num *df (number of groups)*	4
Den *df* (total no. samples - *df*)	8
Critical value of Studentized Range, Q	4.53

Sample Comparisons	Absolute Difference	Critical Range	Result
1 vs 2	25.43	17.36	different
1 vs 3	40.64	17.36	different
1 vs 4	35.14	17.36	different
2 vs 3	15.22	17.36	not different
2 vs 4	9.71	17.36	not different
3 vs 4	5.50	17.36	not different

Contact angle of the Raw sample surface is significantly higher than the Raw/Polymerised, Passivated and Passivated/Polymerised samples. Tukey-Kramer comparison shows no significant difference in contact angles between the Raw/Polymerised, Passivated and Passivated/Polymerised samples. Polymerisation of the Raw titanium yields a surface with hydrophilicity that is comparable to the Passivated surface. Also, polymerisation of the Passivated surface does not further lower the contact angle, as the passivated surface is already very hydrophilic.

8.3.3 RGD Immobilisation Statistical Analysis

ANOVA Analysis of Immobilised RGD Surface Area between Control and Fully-Functionalised RGD surfaces, Following RGD Immobilisation Times of 30-minutes, 60-minutes, and 90-minutes

Anova: Single Factor

SUMMARY

Groups	*Count*	*Sum*	*Average*	*Variance*
1) Control 30m	2	21.10	10.55	159.42
2) Control 60m	2	70.61	35.31	55.66
3) Control 90m	2	305.31	152.65	225.55
4) FF-RGD 30m	2	6794.09	3397.05	86678.66
5) FF-RGD 60m	2	14437.95	7218.98	352824.36
6) FF-RGD 90m	2	5166.79	2583.39	449328.30

ANOVA

Source of Variation	*SS*	*Df*	*MS*	*F*	*P-value*	*F crit*
Between Groups	80869426.63	5	16173885.33	109.13	8.34 E-06	4.39
Within Groups	889271.95	6	148211.99			
Total	81758698.57	11				

F value is greater than the F-crit value = Population means are different

Tukey-Kramer Comparison Tables for Immobilised RGD Surface Area between Control and Fully-Functionalised RGD surfaces, Following RGD Immobilisation Times of 30-minutes, 60-minutes, and 90-minutes

Tukey-Kramer Comparison Table

Total no. of samples	12
Pooled Variance = MS from ANOVA	148211.99
Number of Groups	6
Number of samples per group	2
Num *df (number of groups)*	6
Den *df* (total no. samples - *df*)	6
Critical value of Studentized Range, Q	5.63

Sample Comparisons	Absolute Difference	Critical Range	Result
Control 30m vs Control 60m	24.755	1532.622044	not different
Control 30m vs Control 90m	142.103	1532.622044	not different
Control 30m vs RGD 30m	3386.495	1532.622044	different
Control 30m vs RGD 60m	7208.425	1532.622044	different
Control 30m vs RGD 90m	2572.844	1532.622044	different
Control 60m vs Control 90m	117.348	1532.622044	not different
Control 60m vs RGD 30m	3361.741	1532.622044	different
Control 60m vs RGD 60m	7183.670	1532.622044	different
Control 60m vs RGD 90m	2548.089	1532.622044	different
Control 90m vs RGD 30m	3244.393	1532.622044	different
Control 90m vs RGD 60m	7066.322	1532.622044	different
Control 90m vs RGD 90m	2430.741	1532.622044	different
RGD 30m vs RGD 60m	3821.9295	1532.622044	different

RGD 30m vs RGD 90m	813.6515	1532.622044	not different
RGD 60m vs RGD 90m	4635.581	1532.622044	different

All three Control groups (30-minute, 60-minute and 90-minute RGD immobilisation time) show no difference in the surface area of immobilised RGD, corresponding to the fluorescence signal on the confocal microscope images.

All Control groups are significantly different from all RGD immobilised groups. Also, RGD immobilisation time of 60-minute shows significantly higher surface area of immobilised RGD than 30-minutes or 90-minutes of RGD immobilisation time.

8.3.4 Bone Matrix Mineralisation Statistical Analysis

ANOVA Analysis of Immobilised RGD Surface Area on Raw, Passivated, and FF-RGD sample surfaces

Anova: Single Factor

SUMMARY

Groups	*Count*	*Sum*	*Average*	*Variance*
1) Raw	3	177654	59218	72669433
2) Passivated	3	167747	55915.67	1.18 E+08
3) FF-RGD	3	464669	154889.67	6.05 E+08

ANOVA

Source of Variation	*SS*	*df*	*MS*	*F*		*P-value*	*F crit*
Between Groups	18.96 E+09	2	94.80 E+08	35.73		0.0005	5.14
Within Groups	15.92 E+08	6	26.53 E+07				
Total	20.55 E+09	8					

F value is greater than the F-crit value = Population means are different

Tukey-Kramer Comparison tables of Immobilised RGD Surface Area on Raw, Passivated, and FF-RGD sample surfaces

Tukey-Kramer Comparison Table

Total no. of samples	9
Pooled Variance = MS from ANOVA	265322084.9
Number of Groups	3
Number of samples per group	3
Num *df (number of groups)*	3
Den *df* (total no. samples - *df*)	6
Critical value of Studentized Range, Q	4.34

Sample Comparisons	Absolute Difference	Critical Range	Result
Raw vs Passivated	3302.33	40814.62	not different
Raw vs FF-RGD	95671.67	40814.62	different
Passivated vs FF-RGD	98974.00	40814.62	different

Surface area of immobilised RGD on confocal microscope images, is the same on both Raw and Passivated surfaces. The FF-RGD surface shows significantly higher surface area of RGD immobilised, compared to the Raw and Passivated surfaces.

8.3.5 Antibacterial Testing Statistical Analysis

Antibacterial analysis of Escherichia coli between Raw, Passivated, and Polymerised titanium disc samples (Passivated sample is passivated using H_2O_2/HNO_3 (1:1) 2-hours)

Anova: Single Factor

SUMMARY

Groups	*Count*	*Sum*	*Average*	*Variance*
1) Raw	6	15992.00	2665.33	8.87E05
2) Passivated	6	9114.00	1519.00	2.05E05
3) Polymerised	6	2252.00	375.33	31467.87

ANOVA

Source of Variation	*SS*	*df*	*MS*	*F*	*P-value*	*F crit*
Between Groups	157.32E05	2	78.66E05	21.01	4.48E-05	3.68
Within Groups	56.17E05	15	3.74E05			
Total	213.5E05	17				

F value is greater than the F-crit value = Population means are different

Tukey-Kramer Comparison Tables analysing Escherichia coli colonies between Raw, Passivated, and Polymerised titanium disc samples (Passivated sample is passivated using H_2O_2/HNO_3 (1:1) 2-hours)

Tukey-Kramer Comparison Table

Total no. of samples	18
Pooled Variance = MS from ANOVA	3.74E05
Number of Groups	3
Number of samples per group	6
Num *df (number of groups)*	3
Den *df* (total no. samples - *df*)	15
Critical value of Studentized Range, Q	3.67

Sample Comparisons	Absolute Difference	Critical Range	Result
1) vs 2)	1146.33	916.87	different
1) vs 3)	2290.00	916.87	different
2) vs 3)	1143.67	916.87	different

Tukey-Kramer analysis reveals that the Polymerised surface resists E. coli colonisation more so than the Passivated surface, following by the Raw titanium.

Antibacterial analysis of Staphylococcus aureus between Raw, Passivated, and Polymerised titanium disc samples (Passivated sample is passivated using H_2O_2/HNO_3 (1:1) 2-hours)

Anova: Single Factor

SUMMARY

Groups	*Count*	*Sum*	*Average*	*Variance*
1) Raw	6	18.38E03	3064.00	2.82E05
2) Passivated	6	13.26E05	2210.33	7.55E05
3) Polymerised	6	3508.00	584.67	9354.67

ANOVA

Source of Variation	*SS*	*df*	*MS*	*F*	*P-value*	*F crit*
Between Groups	19.4E06	2	95.19E05	27.29	1.005E-05	3.68
Within Groups	52.32E05	15	3.49E05			
Total	24.27E06	17				

F value is greater than the F-crit value = Population means are different

Tukey-Kramer Comparison Tables for analysis of Staphylococcus aureus colonies between Raw, Passivated, and Polymerised titanium disc samples (Passivated sample is passivated using H_2O_2/HNO_3 (1:1) 2-hours)

Tukey-Kramer Comparison Table

Total no. of samples	18
Pooled Variance = MS from ANOVA	3.49E05
Number of Groups	3
Number of samples per group	6
Num *df (number of groups)*	3
Den *df* (total no. samples - *df*)	15
Critical value of Studentized Range, Q	3.67

Sample Comparisons	Absolute Difference	Critical Range	Result
1) vs 2)	853.67	884.87	not different
1) vs 3)	2479.33	884.87	different
2) vs 3)	1625.67	884.87	different

Tukey-Kramer comparison reveals no significant difference in S. aureus colonisation between the Raw and Passivated surfaces, only that the Polymerised surface performs significantly better than both the Raw and Passivated samples.

ANOVA analysis between E. coli and S. aureus colonies on Raw titanium sample

Anova: Single Factor

SUMMARY

Groups	*Count*	*Sum*	*Average*	*Variance*
1) E. coli	6	1.60E04	2665.33	8.87E05
2) S. aureus	6	1.84E04	3064.00	2.82E05

ANOVA

Source of Variation	*SS*	*Df*	*MS*	*F*	*P-value*	*F crit*
Between Groups	47.68E04	1	47.68E04	0.82	0.39	4.96
Within Groups	58.44E05	10	58.44E04			
Total	63.20E05	11				

F value is lower than the F-crit value = Population means are the same

ANOVA analysis shows that the Raw surface performs equally against E. coli and S. aureus.

ANOVA analysis between E. coli and S. aureus colonies on Passivated titanium sample

(Passivated sample is passivated with H_2O_2/HNO_3 (1:1) 2-hours)

Anova: Single Factor

SUMMARY

Groups	*Count*	*Sum*	*Average*	*Variance*
1) E. coli	6	9114.00	1519.00	20.51E04
2) S. aureus	6	1.33E04	2210.33	75.52E04

ANOVA

Source of Variation	*SS*	*Df*	*MS*	*F*	*P-value*	*F crit*
Between Groups	14.34E05	1	14.34E05	2.99	0.11	4.96
Within Groups	48.02E05	10	48.02E04			
Total	62.35E05	11				

F value is lower than the F-crit value = Population means are the same

ANOVA analysis reveals that the Passivated surface performs equally against E. coli and S. aureus, like the Raw sample surface.

ANOVA analysis between E. coli and S. aureus colonies on Polymerised titanium sample

Anova: Single Factor

SUMMARY

Groups	*Count*	*Sum*	*Average*	*Variance*
1) E. coli	6	2252.00	375.33	31467.87
2) S. aureus	6	3508.00	584.67	9354.67

ANOVA

Source of Variation	*SS*	*df*	*MS*	*F*	*P-value*	*F crit*
Between Groups	13.15E04	1	13.15E04	6.44	0.03	4.96
Within Groups	20.41E04	10	20411.27			
Total	33.56E04	11				

F value is greater than the F-crit value = Population means are different

Tukey-Kramer Comparison Table

Total no. of samples	12
Pooled Variance = MS from ANOVA	20411.27
Number of Groups	2
Number of samples per group	6
Num *df (number of groups)*	2
Den *df* (total no. samples - *df*)	10
Critical value of Studentized Range, Q	3.15

Sample Comparisons	Absolute Difference	Critical Range	Result
1) vs 2)	209.333	183.7257	different

ANOVA and Tukey-Kramer analyses reveal that the Polymerised sample performs significantly better on E. coli than S. aureus.

8.4 PrestoBlue Standard Curve

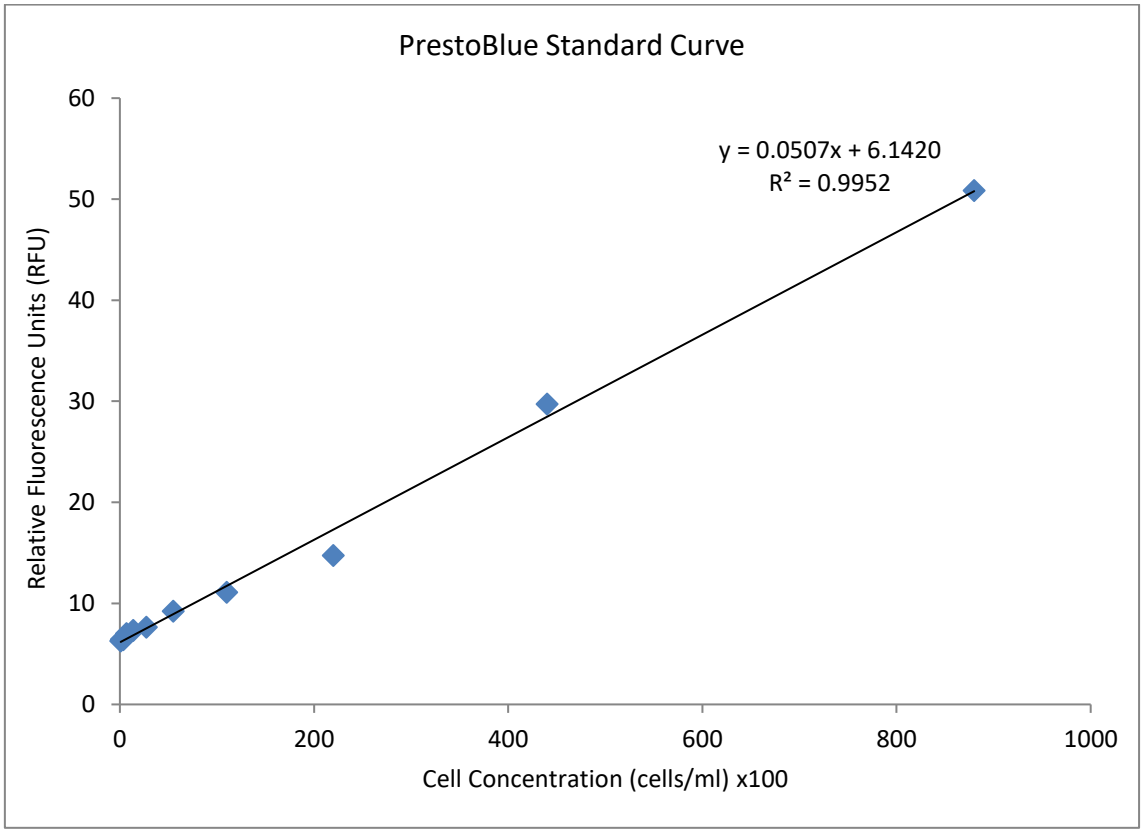

Figure 59 - Standard Curve for PrestoBlue Cell Viability Reagent. Standard Curve Generated for Cell Concentrations 86, 172, 344, 688, 1,375, 2,750, 5,500, 11,000, 22,000, 44,000, and 88,000 cells/ml.

9 References

ABBINA, S., VAPPALA, S., KUMAR, P., SIREN, E. M. J., C. LA, C., ABBASI, U., BROOKSA, D. E. & KIZHAKKEDATHU, J. N. 2017. Hyperbranched polyglycerols: recent advances in synthesis, biocompatibility and biomedical applications. *Journal of Materials Chemistry B,* 5**,** 9249-9277.

ACKART, W. B., CAMP, R. L., WHEELWRIGHT, W. L. & BYCK, J. S. 1975. Antimicrobial polymers. *Journal of Biomedical Materials Research,* 9**,** 55-68.

ALBREKTSSON, T. & JOHANSSON, C. 2001. Osteoinduction, osteoconduction and osseointegration. *European Spine Journal,* 10**,** S96-S101.

ALEXANDER, L. L. 2010. CME Accreditation Resource #9448:Healthcare-Associated Infections. Sacramento, California: CME Resource.

ALFARSI, M. A., HAMLET, S. M. & IVANOVSKI, S. 2014. Titanium surface hydrophilicity modulates the human macrophage inflammatory cytokine response. *Journal of biomedical materials research. Part A,* 102**,** 60-7.

ALTANKOV, G. & GROTH, T. H. 1994. Reorganization of substratum-bound fibronectin on hydrophilic and hydrophobic materials is related to biocompatibility. *Journal of Materials Science - Materials in Medicine,* 5**,** 732-737.

AMBARD, D. & SWIDER, P. 2006. A predictive mechano-biological model of the bone-implant healing. *European Journal of Mechanics - A/Solids,* 25**,** 927-937.

ANSELME, K. 2000. Osteoblast adhesion on biomaterials. *Biomaterials,* 21**,** 667-681.

ANSELME, K. & BIGERELLE, M. 2005. Topography effects of pure titanium substrates on human osteoblast long-term adhesion. *Acta biomaterialia,* 1**,** 211-22.

ARIMA, Y. & IWATA, H. 2007. Effect of wettability and surface functional groups on protein adsorption and cell adhesion using well-defined mixed self-assembled monolayers. *Biomaterials,* 28**,** 3074-3082.

ARKLES, B. 1977. Tailoring Surfaces with Silanes. *CHEMTECH,* 7**,** 766-778.

ARKLES, B. 2014. *Silane Coupling Agents: Connecting Across Boundaries* [Online]. Morrisville, Pennsylvania: Gelest, Inc. Available: https://www.gelest.com/wp-content/uploads/Goods-PDF-brochures-couplingagents.pdf [Accessed November 2014].

ASKARI, J. A., BUCKLEY, P. A., MOULD, A. P. & HUMPHRIES, M. J. 2009. Linking integrin conformation to function. *Journal of Cell Science,* 122**,** 165-170.

ASTM. 2013. *Standard Practice for Surface Preparation and Marking of Metallic Surgical Implants: ASTM F86-01* [Online]. West Conshohocken, Pennsylvania: ASTM International. Available: www.astm.org [Accessed January 26th 2013].

BACHEM. *Cyclo(-Arg-Gly-Asp-D-Phe-Cys) acetate salt* [Online]. Bachem. Available: http://shop.bachem.com/h-7226.html [Accessed 14th March 2012].

BARBER, T. A., HO, J. E., DE RANIERI, A., VIRDI, A. S., SUMNER, D. R. & HEALY, K. E. 2007. Peri-implant bone formation and implant integration strength of peptide-modified p(AAM-co-EG/AAC) interpenetrating polymer network-coated titanium implants. *Journal of biomedical materials research. Part A,* 80**,** 306-20.

BELL, B. F., SCHULER, M., TOSATTI, S., TEXTOR, M., SCHWARTZ, Z. & BOYAN, B. D. 2011. Osteoblast response to titanium surfaces functionalized with extracellular matrix peptide biomimetics. *Clinical oral implants research,* 22**,** 865-72.

BELLIS, S. L. 2011. Advantages of RGD peptides for directing cell association with biomaterials. *Biomaterials,* 32**,** 4205-10.

BELLUCCI, M. C. & VOLONTERIO, A. 2012. Carbodiimides-Mediated Multi Component Synthesis of Biologically Relevant Structures. *Organic Chemistry Insights,* 4**,** 1-24.

BENOIT, D. S. & ANSETH, K. S. 2005. The effect on osteoblast function of colocalized RGD and PHSRN epitopes on PEG surfaces. *Biomaterials,* 26**,** 5209-20.
BERESFORD, J. N., GRAVES, S. E. & SMOOTHY, C. A. 1993. Formation of mineralized nodules by bone derived cells in vitro: a model of bone formation? *American Journal of Medical Genetics,* 45**,** 163-178.
BESSHO, K., CARNES, D. L., CAVIN, R., CHEN, H.-Y. & ONG, J. L. 1999. BMP Stimulation of Bone Response Adjacent to Titanium Implants *in vivo*. *Clinical oral implants research,* 10**,** 212-218.
BET, M. R., GOISSIS, G., VARGAS, S. & SELISTRE-DE-ARAUJO, H. S. 2003. Cell adhesion and cytotoxicity studies over polyanionic collagen surfaces with variable negative charge and wettability. *Biomaterials,* 24**,** 131-137.
BOGDANOWICH-KNIPP, S. J., CHAKRABARTI, S., WILLIAMS, T. D., DILLMAN, R. K. & SIAHAAN, T. J. 1999a. Solution stability of linear vs. cyclic RGD peptides. *Journal of Peptide Research : official journal of The American Peptide Society,* 53**,** 530-541.
BOGDANOWICH-KNIPP, S. J., JOIS, D. S. S. & SIAHAAN, T. J. 1999b. The effect of conformation on the solution stability of linear vs cyclic RGD peptides. *Journal of Peptide Research,* 53**,** 523-529.
BORN, R., SCHARNWEBER, D., RÖßLER, S., STÖLZEL, M., THIEME, M., WOLF, C. & WORCH, H. 1998. Surface analysis of Ti based biomaterials. *Fresenius Journal of Analytical Chemistry,* 361**,** 697-700.
BOWERS, K. T., KELLER, J. C., RANDOLPH, B. A., WICK, D. G. & MICHAELS, C. M. 1992. Optimization of Surface Micromorphology for Enhanced Osteoblast Responses in vitro. *International Journal of Oral Maxillofacial Implants,* 7**,** 302-310.
BOYAN, B. D., LOHMANN, C. H., DEAN, D. D., SYLVIA, V. L., COCHRAN, D. L. & SCHWARTZ, Z. 2001. Mechanisms involved in osteoblast response to implant surface morphology. *Annual Review of Materials Research,* 31**,** 357-371.
BOYAN, B. D., LOSSDORFER, S., WANG, L., ZHAO, G., LOHMANN, C. H. & COCHRAN, D. L. 2003. Osteoblasts generate an osteogenic microenvironment when grown on surfaces with rough microtopographies. *European Cells and Materials,* 6**,** 22-27.
BOYNE, P. & JONES, S. D. 2004. Demonstration of the Osseoinductive Effect of Bone Morphogenetic Protein within Endosseous Dental Implants. *Implant Dentistry,* 13**,** 180-184.
BURAKOWSKA, E., QUINN, J. R., ZIMMERMAN, S. C. & HAAG, R. 2009. Cross-linked hyperbranched polyglycerols as hosts for selective binding of guest molecules. *Journal of the American Chemical Society,* 131**,** 10574-80.
BUSER, D., SCHENK, R. K., STEINEMANN, S., FIORELLINI, J. P. & FOX, C. H. 1991. Influence of surface characteristics on bone integration of titanium implants: a histomorphometric study in miniature pigs. *Journal of Biomedical Materials Research,* 25**,** 889-902.
CAVALCANTI-ADAM, E. A., MICOULET, A., BLUMMEL, J., AUERNHEIMER, J., KESSLER, H. & SPATZ, J. P. 2006. Lateral spacing of integrin ligands influences cell spreading and focal adhesion assembly. *Journal of Cell Biology,* 85**,** 219-224.
CAVALCANTI-ADAM, E. A., VOLBERG, T., MICOULET, A., KESSLER, H., GEIGER, B. & SPATZ, J. P. 2007. Cell spreading and focal adhesion dynamics are regulated by spacing of integrin ligands. *Biophysical Journal,* 92**,** 2964-2974.
CHANG, H.-I. & WANG, Y. 2011. Cell Responses to Surface and Architecture of Tissue Engineering Scaffolds. *In:* PROF. EBERLI, D. (ed.) *Regenerative Medicine and Tissue Engineering - Cells and Biomaterials.* InTech.
CHANG, P.-I. 1981. Polymer implant materials with improved x ray opacity and biocompatibility. *Biomaterials,* 2**,** 151-155.
CHARNLEY, M., TEXTOR, M. & ACIKGOZ, C. 2011. Designed polymer structures with antifouling–antimicrobial properties. *Reactive and Functional Polymers,* 71**,** 329-334.

CHRISTENSEN, G., BADDOUR, L., MADISON, B., PARISI, J., ABRAHAM, S., HASTY, D., LOWRANCE, J., JOSEPHS, J. & SIMPSON, W. 1990. Colony morphology of staphylococci on Memphis agar: phase variation of slime production, resistance to beta-lactam antibiotics, and virulence. *The Journal of Infectious Diseases,* 161**,** 1153-1169.
CHUA, P. H., NEOH, K. G., KANG, E. T. & WANG, W. 2008. Surface functionalization of titanium with hyaluronic acid/chitosan polyelectrolyte multilayers and RGD for promoting osteoblast functions and inhibiting bacterial adhesion. *Biomaterials,* 29**,** 1412-1421.
CIVANTOS, A., MARTÍNEZ-CAMPOS, E., RAMOS, V., ELVIRA, C., GALLARDO, A. & ABARRATEGI, A. 2017. Titanium Coatings and Surface Modifications: Toward Clinically Useful Bioactive Implants. *ACS - Biomaterials Science and Engineering,* 3**,** 1245-1261.
COOK, A. D., HRKACH, J. S., GAO, N. N., JOHNSON, I. M., PAJVANI, U. B., CANNIZZARO, S. M. & LANGER, R. 1997. Characterization and development of RGD-peptide-modified poly(lactic acid-co-lysine) as an interactive, resorbable biomaterial. *Journal of Biomedical Materials Research,* 35**,** 513-523.
COOK, A. D., SAGERS, R. D. & PITT, W. G. 1993. Bacterial adhesion to Poly(HEMA)-Based Hydrogels. *Journal of Biomedical Materials Research,* 27**,** 119-126.
COOPER, L. F. 2000. A role for surface topography in creating and maintaining bone at titanium endosseous implants. *The Journal of Prosthetic Dentistry,* 84**,** 522-534.
COSTA E SILVA FILHO, F. & CONDE MENEZES, G. 2004. Osteoblasts attachment and adhesion: how bone cells fit fibronectin-coated surfaces. *Materials Science and Engineering: C,* 24**,** 637-641.
CURTIS, A. S. G., FORRESTER, J. V., MCINNES, C. & LAWRIE, F. 1983. Adhesion of cells to polystyrene surfaces. *Journal of Cell Biology,* 97**,** 1500-1506.
DACULSIA, G., FELLAHA, B. H., MIRAMONDA, T. & DURAND, M. 2013. Osteoconduction, Osteogenicity, Osteoinduction, what are the fundamental properties for a smart bone substitutes. *Innovation and Research in Biomedical Engineering,* 34**,** 346-348.
DANG, J. M. & LEONG, K. W. 2006. Natural polymers for gene delivery and tissue engineering. *Advanced drug delivery reviews,* 58**,** 487-99.
DAVIES, J. E. 1998. Mechanisms of endosseous integration. *International Journal of Prosthodontics,* 11**,** 391-401.
DE BOER, J., EL GHALBZOURI, A., D'AMORE, P., HIRSCHI, K., ROUWKEMA, J., VAN BEZOOIJEN, R. & KARPERIEN, M. 2008. Cellular Signaling. *In:* VAN BLITTERSWIJK, C., PETER THOMSEN, ANDERS LINDAHL, JEFFREY HUBBELL, DAVID F. WILLIAMS, RANIERI CANCEDDA, BRUIJN, J. D. D. & SOHIER, J. (eds.) *Tissue Engineering.* Elsevier Inc.
DEE, K. C., ANDERSEN, T. T. & BIZIOS, R. 1998. Design and function of novel osteoblast-adhesive peptides for chemical modification of biomaterials. *Journal of Biomedical Materials Research,* 40**,** 371-377.
DEPPRICH, R., OMMERBORN, M., ZIPPRICH, H., NAUJOKS, C., HANDSCHEL, J., WIESMANN, H. P., KUBLER, N. R. & MEYER, U. 2008. Behavior of osteoblastic cells cultured on titanium and structured zirconia surfaces. *Head & face medicine,* 4**,** 29.
DESAI, N. P., HOSSAINY, S. F. A. & HUBBELL, J. A. 1992. Surface-immobilized polyethylene oxide for bacterial repellence. *Biomaterials,* 13**,** 417-420.
DETTIN, M., CONCONI, M. T., GAMBARETTO, R., PASQUATO, A., FOLIN, M., DI BELLO, C. & PARNIGOTTO, P. P. 2002. Novel osteoblast-adhesive peptides for dental/orthopedic biomaterials. *Journal of Biomedical Materials Research,* 60**,** 466-471.
DRELICH, J., CHIBOWSKI, E., MENG, D. D. & TERPILOWSKI, K. 2011. Hydrophilic and superhydrophilic surfaces and materials. *Soft Matter,* 7**,** 9804.
DUNCAN, R. & IZZO, L. 2005. Dendrimer biocompatibility and toxicity. *Advanced drug delivery reviews,* 57**,** 2215-37.

ELLINGSEN, J. E. 1991. A study on the mechanism of protein adsorption to TiO2. *Biomaterials,* 12**,** 593-596.
ELMENGAARD, B., BECHTOLD, J. E. & SOBALLE, K. 2005. In vivo effects of RGD-coated titanium implants inserted in two bone-gap models. *Journal of Biomedical Materials Research A,* 75**,** 249-255.
ESPOSITO, S. & LEONE, S. 2008. Prosthetic joint infections: microbiology, diagnosis, management and prevention. *International journal of antimicrobial agents,* 32**,** 287-93.
ESPOSTITO, M., LAUSMAA, J., HIRSCH, J. M. & THOMSEN, P. 1999. Surface analysis of failed oral titanium implants. *Journal of Biomedical Materials Research,* 48**,** 559=568.
GADELMAWLA, E. S., KOURA, M. M., MAKSOUD, T. M. A., ELEWA, I. M. & SOLIMAN, H. H. 2002. Roughness Parameters. *Journal of Materials Processing Technology,* 123**,** 133-145.
GALANAKOS, S. P., PAPADAKIS, S. A., KATEROS, K., PAPAKOSTAS, I. & MACHERAS, G. 2009. Biofilm and orthopaedic practice: the world of microbes in a world of implants. *Orthopaedics and Trauma,* 23**,** 175-179.
GARCIA, A. J. 2005. Get a grip: integrins in cell-biomaterial interactions. *Biomaterials,* 26**,** 7525-7529.
GARCIA, A. J. & REYES, C. D. 2005. Bio-adhesive Surfaces to Promote Osteoblast Differentiation and Bone Formation. *Journal of Dental Research,* 84**,** 407-413.
GARCIA, A. J., VEGA, M. D. & BOETTIGER, D. 1999. Modulation of cell proliferation and differentiation through substrate-dependent changes in fibronectin conformation. *Molecular Biology of the Cell,* 10**,** 785-798.
GERMANIER, Y., TOSATTI, S., BROGGINI, N., TEXTOR, M. & BUSER, D. 2006. Enhanced Bone Apposition Around Biofunctionalized Sandblasted and Acid-Etched Titanium Implant Surfaces. A Histomorphometric Study in Miniature Pigs. *Clinical oral implants research,* 17**,** 251-257.
GODDARD, J. M. & HOTCHKISS, J. H. 2007. Polymer surface modification for the attachment of bioactive compounds. *Progress in Polymer Science,* 32**,** 698-725.
GOGRA, A. B., YAO, J., SANDY, E. H., ZHENG, S., ZARAY, G., KOROMA, B. M. & HUI, Z. 2010. Cell surface hydrophobicity (CSH) of Escherichia coli, Staphylococcus aureus and Aspergillus niger and the biodegradation of Diethyl Phthalate (DEP) via Microcalorimetry. *Journal of American Science,* 6**,** 78-88.
GOMES, M., AZEVEDO, H., MALAFAYA, P., SILVA, S., OLIVEIRA, J., SILVA, G., SOUSA, R., MANO, J. & REIS, R. 2008. Natural Polymers in Tissue Engineering Applications. *In:* VAN BLITTERSWIJK, C., PETER THOMSEN, ANDERS LINDAHL, JEFFREY HUBBELL, DAVID F. WILLIAMS, RANIERI CANCEDDA, BRUIJN, J. D. D. & SOHIER, J. (eds.) *Tissue Engineering.* Elsevier Inc.
GOODMAN, S. B., YAO, Z., KEENEY, M. & YANG, F. 2013. The future of biologic coatings for orthopaedic implants. *Biomaterials,* 34**,** 3174-3183.
GRINNELL, F. & FELD, M. K. 1982. Fibronectin adsorption on hydrophilic and hydrophobic surfaces detected by antibody binding and analyzed during cell adhesion in serum-containing medium. *Journal of Biological Chemistry,* 257**,** 4888-4893.
GRONTHOS, S., SIMMONS, P. J., GRAVES, S. E. & ROBEY, P. G. 2001. Integrin-Mediated Interactions Between Human Bone Marrow Stromal Precursor Cells and the Extracellular Matrix. *Bone,* 28**,** 174-181.
GROTH, T., ALTANKOV, G., KOSTADINOVA, A., KRASTEVA, N., ALBRECHT, W. & PAUL, D. 1999. Altered vitronectin receptor (αv integrin) function in fibroblasts adhering on hydrophobic glass. *Journal of Biomedical Materials Research,* 44**,** 341-351.
HAHN, E. M., ESTRADA-ORTIZ, N., HAN, J., FERREIRA, V. F. C., KAPP, T. G., CORREIA, J. D. G., CASINI, A. & KÜHN, F. E. 2017. Functionalization of Ruthenium(II) Terpyridine Complexes with Cyclic RGD Peptides To Target Integrin Receptors in Cancer Cells. *European Journal of Inorganic Chemistry,* 2017**,** 1667-1672.

HAIMOV, H., YOSUPOV, N., PINCHASOV, G. & JUODZBALYS, G. 2017. Bone Morphogenetic Protein Coating on Titanium Implant Surface: a Systematic Review. *Journal of Oral and Maxillofacial Research,* 8**,** e1.
HALL-STOODLEY, L., COSTERTON, J. W. & STOODLEY, P. 2004. Bacterial biofilms: from the Natural environment to infectious diseases. *Nature Reviews Microbiology,* 2**,** 95-108.
HAMADI, F., LATRACHE, H., ZAHIR, H., ELGHMARI, A., TIMINOUNI, M. & ELLOUALI, M. 2008. THE RELATION BETWEEN ESCHERICHIA COLI SURFACE FUNCTIONAL GROUPS' COMPOSITION AND THEIR PHYSICOCHEMICAL PROPERTIES. *Brazilian Journal of Microbiology,* 39**,** 10-15.
HAMLET, S., ALFARSI, M., GEORGE, R. & IVANOVSKI, S. 2012. The effect of hydrophilic titanium surface modification on macrophage inflammatory cytokine gene expression. *Clinical oral implants research,* 23**,** 584-90.
HAN, D. K., PARK, K. D. & KIM, Y. H. 1998. Blood compatible polymers. *Journal of Biomaterials Science, Polymer Edition,* 9**,** 163-174.
HANAWA, T. 2011. A comprehensive review of techniques for biofunctionalization of titanium. *Journal of periodontal & implant science,* 41**,** 263-72.
HANAWA, T. & OTA, M. 1991. Calcium phosphate naturally formed on titanium in electrolyte solution. *Biomaterials,* 12**,** 767-774.
HANAWA, T. & OTA, M. 1992. Characterization of surface film formed on titanium in electrolyte using XPS. *Applied Surface Science,* 55**,** 269-276.
HARRIS, L. G., TOSATTI, S., WIELAND, M., TEXTOR, M. & RICHARDS, R. G. 2004. Staphylococcus aureus adhesion to titanium oxide surfaces coated with non-functionalized and peptide-functionalized poly(L-lysine)-grafted-poly(ethylene glycol) copolymers. *Biomaterials,* 25**,** 4135-4148.
HARWOOD, P. J. & GIANNOUDIS, P. V. 2005. Application of Bone Morphogenetic Proteins in Orthopaedic Practice: Their Efficacy and Side Effects. *Expert Opinion on Drug Safety,* 4**,** 75-89.
HAUBNER, R., GRATIAS, R., DIEFENBACH, B., GOODMAN, S. L., JONCZYK, A. & KESSLER, H. 1996a. Structural and functional aspect of RGD-containing cyclic pentapeptides as highly potent and selective integrin avb3 antagonist. *Journal of the American Chemical Society,* 118**,** 7461-7472.
HAUBNER, R., SCHMITT, W., HOLZEMANN, G., GOODMAN, S. L., JONCZYK, A. & KESSLER, H. 1996b. Cyclic RGD peptides containing b-turn mimetics. *Journal of the American Chemical Society,* 118**,** 7881-7891.
HEALY, K. E. & DUCHEYNE, P. 1992. The mechanisms of passive dissolution of titanium in a model physiological environment. *Journal of Biomedical Materials Research,* 26**,** 319-338.
HEALY, K. E., REZANIA, A. & STILE, R. A. 1999. Designing biomaterials to direct biological responses. *Annals of the New York Academy of Science,* 875**,** 24-35.
HELLER, M., KUMAR, V. V., PABST, A., BRIEGER, J., AL-NAWAS, B. & KÄMMERER, P. W. 2018. Osseous response on linear and cyclic RGD-peptides immobilized on titanium surfaces in vitro and in vivo. *Journal of Biomedical Materials Research Part A,* 106**,** 419-427.
HERMANSON, G. T. 2013. Fluorescent Probes. *In:* HERMANSON, G. T. (ed.) *Bioconjugate Techniques.* 3rd ed.: Elsevier - Academic Press.
HERSEL, U., DAHMEN, C. & KESSLER, H. 2003. RGD modified polymers: biomaterials for stimulated cell adhesion and beyond. *Biomaterials,* 24**,** 4385-4415.
HORBETT, T. A. & SCHWAY, M. B. 1988. Correlations between mouse 3T3 cell spreading and serum fibronectin adsorption on glass and hydroxyethylmethacrylate- ethylmethacrylate copolymers. *Journal of Biomedical Materials Research,* 22**,** 763-793.
HOSSAIN, M. M. & GAO, W. 2008. How is the Surface Treatments Influence on the Roughness of Biocompatibility? *Trends in Biomaterials & Artificial Organs,* 22**,** 144-157.
HUANG, H., ZHAO, Y., LIU, Z., ZHANG, Y., ZHANG, H., FU, T. & MA, X. 2003. Enhanced osteoblast functions on RGD immobilized surface. *Journal of Oral Implantology,* 29**,** 73-79.

HUANG, W. F., RAGHUNATH, P. & LIN, M. C. 2011. Computational study on the reactions of H2O2 on TiO2 anatase (101) and rutile (110) surfaces. *Journal of computational chemistry,* 32**,** 1065-81.
HULSHOFF, J. E., VAN DIJK, K., VAN DER WAERDEN, J. P., WOLKE, J. G., GINSEL, L. A. & JANSEN, J. A. 1995. Biological Evaluation of the Effect of Magnetron Sputtered Ca/P Coatings on Osteoblast-Like Cells in vitro. *Journal of Biomedical Materials Research,* 29**,** 967-975.
HYZY, S. L., OLIVARES-NAVARRETE, R., ORTMAN, S., BOYAN, B. D. & SCHWARTZ, Z. 2017. Bone Morphogenetic Protein 2 Alters Osteogenesis and Anti-Inflammatory Profiles of Mesenchymal Stem Cells Induced by Microtextured Titanium In Vitro. *Tissue Engineering Part A,* 23**,** 1132-1141.
INCHINGOLO, F., BALLINI, A., CAGIANO, R., INCHINGOLO, A., SERAFINI, M., DE BENEDITTIS, M., CORTELAZZI, R., TATULLO, M., MARRELLI, M. & INCHINGOLO, A. 2015. Immediately loaded dental implants bioactivated with platelet-rich plasma (PRP) placed in maxillary and mandibular region. *Clinical Therapeutics,* 166**,** e146-152.
JI, W., HAN, P., ZHAO, C., JIANG, Y. & ZHANG, X. 2008. Increased osteoblast adhesion on nanophase Ti6Al4V. *Science Bulletin,* 53**,** 1757-1762.
JUNG, H., KWAK, B., YANG, H. S., TAE, G., KIM, J.-S. & SHIN, K. 2008. Attachment of cells to poly(styrene-co-acrylic acid) thin films with various charge densities. *Colloids and Surfaces A: Physicochemical and Engineering Aspects,* 313-314**,** 562-566.
KAINTHAN, R. K., HESTER, S. R., LEVIN, E., DEVINE, D. V. & BROOKS, D. E. 2007. In vitro biological evaluation of high molecular weight hyperbranched polyglycerols. *Biomaterials,* 28**,** 4581-90.
KAINTHAN, R. K., MULIAWAN, E. B., HATZIKIRIAKOS, S. G. & BROOKS, D. E. 2006. Synthesis, Characterization, and Viscoelastic Properties of High Molecular Weight Hyperbranched Polyglycerols. *Macromolecules,* 39**,** 7708-7717.
KANTLEHNER, M., SCHAFFNER, P., FINSINGER, D., MEYER, J., JONCZYK, A., DIEFENBACH, B., NIES, B., GÜNTER HÖLZEMANN, GOODMAN, S. L. & KESSLER, H. 2000. Surface Coating with Cyclic RGD Peptides Stimulates Osteoblast Adhesion and Proliferation as well as Bone Formation. *Chembiochem : a European journal of chemical biology,* 1**,** 107-114.
KESELOWSKY, B. G., COLLARD, D. M. & GARCIA, A. J. 2005. Integrin binding specificity regulates biomaterial surface chemistry effects on cell differentiation. *Proceedings of the National Academy of Sciences of the United States of America,* 102**,** 5953-7.
KESELOWSKY, B. G., COLLARD, D. M. & GARCıA, A. J. 2003. Surface chemistry modulates fibronectin conformation and directs integrin binding and specificity to control cell adhesion. *Journal of Biomedical Materials Research Part A,* 66A**,** 247-259.
KETONIS, C., PARVIZI, J., ADAMS, C. S., SHAPIRO, I. M. & HICKOK, N. J. 2009. Topographic Features Retained after Antibiotic Modification of Ti Alloy Surfaces: Retention of Topography with Attachment of Antibiotics. *Clinical orthopaedics and related research,* 467**,** 1678-1687.
KHORANA, H. G. 1953. The Chemistry of Carbodiimides. *Chemical Reviews,* 53**,** 145-166.
KIESWETTER, K., SCHWARTZ, Z., DEAN, D. D. & BOYAN, B. D. 1996a. THE ROLE OF IMPLANT SURFACE CHARACTERISTICS IN THE HEALING OF BONE. *Critical Reviews in Oral Biology and Medicine,* 7**,** 329-345.
KIESWETTER, K., SCHWARTZ, Z., HUMMERT, T. W., COCHRAN, D. L., SIMPSON, J. & DEAN, D. D. 1996b. Surface roughness modulates the local production of growth factors and cytokines by osteoblast-like MG-63 cells. *Journal of Biomedical Materials Research,* 32**,** 55-63.
KLOKKEVOLD, P. R., NISHIMURA, R. D., ADACHI, M. & CAPUTO, A. 1997. Osseointegration enhanced by chemical etching of the titanium surface: a torque removal study in the rabbit. *Clinical oral implants research,* 8**,** 442-447.
KOHNEN, W. & JANSEN, B. 1995. Polymer Materials for the Prevention of Catheter-related Infections. *Zentralbl Bakteriol,* 283**,** 175-186.

KULKARNI, M., SCHMUKI, P., MAZARE, A. & IGLIC, A. 2014. Biomaterial Surface Modification Of Titanium and Titanium Alloys for Medical Applications. *In:* SEIFALIAN, A., MEL, A. D. & KALASKAR, D. M. (eds.) *Nanomedicine.* UK: One Central Press (OCP).
KUTSEVLYAK, V. I., STARIKOVA, S. L., STARIKOV, V. V., MAMALIS, A. G., LAVRYNENKO, S. N. & RAMSDEN, J. J. 2008. Influence of Implant Surface Modification on Integration with Bone Tissue. *Journal of Biological Physics and Chemistry,* 8**,** 147-150.
KUUSELA, P., VARTIO, T., VUENTO, M. & MYHRE, E. B. 1985. Attachment of staphylococci and streptococci on fibronectin, fibronectin fragments, and fibrinogen bound to a solid phase. *Infection and Immunity,* 50**,** 77-81.
KUZYK, P. R. T. & SCHEMITSCH, E. H. 2011. The basic science of peri-implant bone healing. *Indian Journal of Orthopaedics,* 45**,** 108-115.
LARSSON, C., THOMSEN, P., LAUSMAA, J., RODAHL, M., KASEMO, B. & ERICSON, L. E. 1994. Bone response to surface modified titanium implants: Studies on electropolished implants with different oxide thicknesses and morphology. *Biomaterials,* 15**,** 1062-1074.
LAUSMAA, J., KASEMO, B., ROLANDER, U., BJURSTEN, L. M., ERICSON, L. E., ROSANDER, L. & THOMSEN, P. 1988. Preparation, surface spectroscopic and electron microscopic characterization of titanium implant materials. *In:* RATNER, B. D. (ed.) *Surface Characterization of Biomaterials.* Amsterdam: Elsevier Science.
LEE, J. H., JUNG, H. W., KANG, I. K. & LEE, H. B. 1994. Cell behaviour on polymer surfaces with different functional groups. *Biomaterials,* 15**,** 705-711.
LEE, J. H., PARK, J. W. & LEE, H. B. 1991. Cell adhesion and growth on polymer surfaces with hydroxyl groups prepared by water vapour plasma treatment. *Biomaterials,* 12**,** 443-448.
LEE, Y. J., CUI, D. Z., JEON, H. R., CHUNG, H. J., PARK, Y. J., KIM, O. S. & KIM, Y. J. 2012. Surface characteristics of thermally treated titanium surfaces. *Journal of periodontal & implant science,* 42**,** 81-87.
LIAN, J. B. & STEIN, G. S. 1992. Concepts of osteoblast growth and differentiation: Basis for modulation of bone cell development and tissue formation. *Critical Reviews in Oral Biology and Medicine,* 3**,** 269-305.
LIEB, E., HACKER, M., TESSMAR, J., KUNZ-SCHUGHART, L. A., FIEDLER, J., DAHMEN, C., HERSEL, U., KESSLER, H., SCHULZ, M. B. & GOPFERICH, A. 2005. Mediating specific cell adhesion to low-adhesive diblock copolymers by instant modification with cyclic RGD peptides. *Biomaterials,* 26**,** 2333-41.
LISKAMP, R. M. J., RIJKERS, D. T. S. & BAKKER, S. E. 2008. Bioactive Macrocyclic Peptides and Peptide Mimics. *In:* DIEDERICH F., S. P. J., TYKWINSKI R.R. (ed.) *Modern Supramolecular Chemistry: Strategies for Macrocycle Synthesis.* Weinheim, Germany: WILEY-VCH Verlag GmbH & Co. KGaA.
LIU, C., XIA, Z. & CZERNUSZKA, J. T. 2007a. Design and Development of Three-Dimensional Scaffolds for Tissue Engineering. *Chemical Engineering Research and Design,* 85**,** 1051-1064.
LIU, X., CHU, P. & DING, C. 2004. Surface modification of titanium, titanium alloys, and related materials for biomedical applications. *Materials Science and Engineering: R: Reports,* 47**,** 49-121.
LIU, X., LIM, J. Y., DONAHUE, H. J., DHURJATI, R., MASTRO, A. M. & VOGLER, E. A. 2007b. Influence of substratum surface chemistry/energy and topography on the human fetal osteoblastic cell line hFOB 1.19: Phenotypic and genotypic responses observed in vitro. *Biomaterials,* 28**,** 4535-4550.
LIU, Y., DE GROOT, K. & HUNZIKER, E. B. 2005. BMP-2 liberated from biomimetic implant coatings induces and sustains direct ossification in an ectopic rat model. *Bone,* 36**,** 745-57.
LOHMANN, C. H., BONEWALD, L. F., SISK, M. A., SYLVIA, V. L., COCHRAN, D. L. & DEAN, D. D. 2000. Maturation state determines the response of osteogenic cells to surface roughness and 1,25-dihydroxyvitamin D3. *Journal of Bone and Mineral Research,* 15**,** 1169-1180.

LORENZETTI, M., DOGSA, I., STOSICKI, T., STOPAR, D., KALIN, M., KOBE, S. & NOVAK, S. 2015. The influence of surface modification on bacterial adhesion to titanium-based substrates. *ACS applied materials & interfaces,* 7**,** 1644-51.
MABILLEAU, G., BOURDON, S., JOLY-GUILLOU, M. L., FILMON, R., BASLE, M. F. & CHAPPARD, D. 2006. Influence of fluoride, hydrogen peroxide and lactic acid on the corrosion resistance of commercially pure titanium. *Acta biomaterialia,* 2**,** 121-9.
MADDIKERI, R. R., TOSATTI, S., SCHULER, M., CHESSARI, S., TEXTOR, M., RICHARDS, R. G. & HARRIS, L. G. 2008. Reduced medical infection related bacterial strains adhesion on bioactive RGD modified titanium surfaces: a first step toward cell selective surfaces. *Journal of Biomedical Materials Research,* 84A**,** 425-435.
MALAFAYA, P. B., SILVA, G. A. & REIS, R. L. 2007. Natural-origin polymers as carriers and scaffolds for biomolecules and cell delivery in tissue engineering applications. *Advanced drug delivery reviews,* 59**,** 207-33.
MANDRACCI, P., MUSSANO, F., RIVOLO, P. & CAROSSA, S. 2016. Surface Treatments and Functional Coatings for Biocompatibility Improvement and Bacterial Adhesion Reduction in Dental Implantology. *Coatings,* 6**,** 7.
MANGRAM, A. J. M., HORAN, T. C., PEARSON, M. L. M., SILVER, L. C. & JARVIS, W. R. M. 1999. Guideline for Prevention of Surgical Site Infection. *American Journal of Infection Control,* 27**,** 97-134.
MANJAIAH, M. & LAUBSCHER, R. F. 2017. A review of the surface modifications of titanium alloys for biomedical applications. *Materiali in tehnologije,* 51**,** 181-193.
MANTE, F. K., LITTLE, K., MANTE, M. O., RAWLE, C. & BARAN, G. R. 2004. Oxidation of Titanium, RGD Peptide Attachment, and Matrix Mineralization of Rat Bone Marrow Stromal Cells. *Journal of Oral Implantology,* 30**,** 343-349.
MARCO, F., MILENA, F., GIANLUCA, G. & VITTORIA, O. 2005. Peri-implant osteogenesis in health and osteoporosis. *Micron,* 36**,** 630-44.
MARTIN, J. Y., SCHWARTZ, Z., HUMMERT, T. W., SCHRAUB, D. M., SIMPSON, J. & LANKFORD JR, J. 1995. Effect of Titanium Surface Roughness on Proliferation, Differentiation, and Protein Synthesis of Human Osteoblast-Like Cells (MG63). *Journal of Biomedical Materials Research,* 29**,** 389-401.
MASUDA, T., YLIHEIKKILA, P. K., FELTON, D. A. & COOPER, L. F. 1998. Generalizations Regarding the Process and Phenomenon of Osseointegration. Part I. In vivo Studies. *The International Journal of Oral Maxillofacial Implants,* 13**,** 17-29.
MATTSON, G., CONKLIN, E., DESAI, S., NIELANDER, G., SAVAGE, M. D. & MORGENSEN, S. 1993. A practical approach to crosslinking. *Molecular Biology Reports,* 17**,** 167-183.
MCCARTHY, A. D., UEMURA, T., ETCHEVERRY, S. B. & CORTIZO, A. M. 2004. Advanced glycation endproducts interefere with integrin-mediated osteoblastic attachment to a type-I collagen matrix. *The international journal of biochemistry & cell biology,* 36**,** 840-8.
MENDONCA, G., MENDONCA, D. B., ARAGAO, F. J. & COOPER, L. F. 2008. Advancing dental implant surface technology--from micron- to nanotopography. *Biomaterials,* 29**,** 3822-35.
MLYNARCZYK, D. T., KOCKI, T. & GOSLINSKI, T. 2017. Dendrimer Structure Diversity and Tailorability as a Way to Fight Infectious Diseases. *In:* PROF SEEHRA, M. S. (ed.) *Nanostructured Materials - Fabrication to Applications.* InTechOpen.
MONSEES, T. K., BARTH, K., TIPPELT, S., HEIDEL, K., GORBUNOV, A., POMPE, W. & FUNK, R. H. 2005. Effects of different titanium alloys and nanosize surface patterning on adhesion, differentiation, and orientation of osteoblast-like cells. *Cells Tissues Organs,* 180**,** 81-95.
MONTALBETTI, C. A. G. N. & FALQUE, V. 2005. Amide bond formation and peptide coupling. *Tetrahedron,* 61**,** 10827-10852.
MONTANARO, L., CAMPOCCIA, D. & ARCIOLA, C. R. 2007. Advancements in molecular epidemiology of implant infections and future perspectives. *Biomaterials,* 28**,** 5155-68.

MOORE, D. 2011. *Fracture Healing* [Online]. Available: http://www.orthobullets.com/basic-science/9009/fracture-healing [Accessed 07/02/12 2012].
MOORE, E., DELALAT, B., VASANI, R., THISSEN, H. & VOELCKER, N. H. 2014. Patterning and biofunctionalization of antifouling hyperbranched polyglycerol coatings. *Biomacromolecules,* 15**,** 2735-43.
MOORE, E., THISSEN, H. & VOELCKER, N. H. 2013. Hyperbranched polyglycerols at the biointerface. *Progress in Surface Science,* 88**,** 213-236.
MORAIS, J. M., PAPADIMITRAKOPOULOS, F. & BURGESS, D. J. 2010. Biomaterials/tissue interactions: possible solutions to overcome foreign body response. *The AAPS journal,* 12**,** 188-96.
MOSSER, A. 1992. Biomaterials: Hard Tissue Repair and Replacement. *In:* MUSTER, D. (ed.) *Surface Physics Methods for Biomaterials Characterisation.* Elsevier Science and Technology Books.
MUÑOZ-BONILLA, A. & FERNÁNDEZ-GARCÍA, M. 2012. Polymeric materials with antimicrobial activity. *Progress in Polymer Science,* 37**,** 281-339.
MUSTAFA, K., WENNERBERG, A., WROBLEWSKI, J., LOPEZ, S. B., HANSSON, S. & ARVIDSON, K. 2000. Attachment, Proliferation, Differentiation and Production of TGF-beta1 by Human Osteoblast-Like Cells on Different Titanium Surfaces. *Journal of Dental Research,* 79**,** 101-105.
NANCI, A., WUEST, J. D., PERU, L., BRUNET, P., SHARMA, V., ZALZAL, S. & MCKEE, M. D. 1998. Chemical modification of titanium surfaces for covalent attachment of biological molecules. *Journal of Biomedical Materials Research,* 40**,** 324-335.
NEOH, K. G., HU, X., ZHENG, D. & KANG, E. T. 2012. Balancing osteoblast functions and bacterial adhesion on functionalized titanium surfaces. *Biomaterials,* 33**,** 2813-22.
OAKES, A. & WOOD, A. 1986. Infections in Surgery. *The New England* 315**,** 1129-1138.
OATES, C. J., WEN, W. & HAMILTON, D. W. 2011. Role of Titanium Surface Topography and Surface Wettability on Focal Adhesion Kinase Mediated Signaling in Fibroblasts. *Materials,* 4**,** 893-907.
OLIVEIRA, J. M., SALGADO, A. J., SOUSA, N., MANO, J. F. & REIS, R. L. 2010. Dendrimers and derivatives as a potential therapeutic tool in regenerative medicine strategies—A review. *Progress in Polymer Science,* 35**,** 1163-1194.
ORTIZ, M., ESCOBAR-GARCIA, D. M., ÁLVAREZ-PÉREZ, M. A., POZOS-GUILLÉN, A., GRANDFILS, C. & FLORES, H. 2017. Evaluation of the Osteoblast Behavior to PGA Textile Functionalized with RGD as a Scaffold for Bone Regeneration. *Journal of Nanomaterials,* 2017**,** 1-8.
PAN, J., THIERRY, D. & LEYGRAF, C. 1994. Electrochemical and XPS studies of titanium for biomaterial applications with respect to the effect of hydrogen peroxide. *Journal of Biomedical Materials Research Part A,* 28**,** 113-122.
PAN, J., THIERRY, D. & LEYGRAF, C. 1996. Hydrogen peroxide toward enhanced oxide growth on titanium in PBS solution: Blue coloration and clinical relevance. *Journal of Biomedical Materials Research,* 30**,** 393-402.
PARK, K. D., KIM, Y. S., HAN, D. K., KIM, Y. H., LEE, E. H. B., SUH, H. & CHOI, K. S. 1998. Bacterial adhesion on PEG modified polyurethane surfaces. *Biomaterials,* 19**,** 851-859.
PETRIE, T. A., CAPADONA, J. R., REYES, C. D. & GARCIA, A. J. 2006. Integrin specificity and enhanced cellular activities associated with surfaces presenting a recombinant fibronectin fragment compared to RGD supports. *Biomaterials,* 27**,** 5459-70.
PETRIE, T. A., RAYNOR, J. E., REYES, C. D., BURNS, K. L., COLLARD, D. M. & GARCIA, A. J. 2008. The effect of integrin-specific bioactive coatings on tissue healing and implant osseointegration. *Biomaterials,* 29**,** 2849-57.
PORTE-DURRIEU, M. C., GUILLEMOT, F., PALLU, S., LABRUGERE, C., BROUILLAUD, B., BAREILLE, R., AMEDEE, J., BARTHE, N., DARD, M. & BAQUEY, C. 2004. Cyclo-(DfKRG) peptide grafting onto

Ti-6Al-4V: physical characterization and interest towards human osteoprogenitor cells adhesion. *Biomaterials,* 25**,** 4837-4846.
QIN, H., MARUYAMA, K., AMANO, T., MURAKAMI, T. & KOMATSU, N. 2016. Hyperbranched polyglycerol-grafted titanium oxide nanoparticles: synthesis, derivatization, characterization, size separation, and toxicology. *Materials Research Express,* 3**,** 105049.
RAMAKRISHNA, S., MAYERB, J., WINTERMANTELC, E. & LEONG, K. W. 2001. Biomedical applications of polymer-composite materials: a review. *Composite Science and Technology,* 61**,** 1189-1224.
RAMAZANOGLU, M. & OSHIDA, Y. 2011. Osseointegration and bioscience of implant surfaces - Current concepts at bone-implant interface. *In:* TURKYILMAZ, I. (ed.) *Implant dentistry - A rapidly evolving practice.* InTech.
RATNER, B. D. 2001. A Perspective on Titanium Biocompatibility. *In:* BRUNETTE, D. M., TENGVALL, P., M., T. & THOMSEN, P. (eds.) *Titanium in Medicine.* Berlin & Heidelberg: Springer-Verlag.
RATNER, B. D. & BRYANT, S. J. 2004. Biomaterials: Where We Have Been and Where We are Going. *Annual Review of Biomedical Engineering,* 6**,** 41-75.
RAUT, V. P., AGASHE, M. A., STUART, S. J. & LATOUR, R. A. 2005. Molecular dynamics simulations of peptide-surface interactions. *Langmuir,* 21**,** 1629-1639.
REYES, C. D. & GARCIA, A. J. 2004. Alpha2beta1 integrin-specific collagen-mimetic surfaces supporting osteoblastic differentiation. *Journal of Biomedical Materials Research A,* 69**,** 591-600.
REZANIA, A. & HEALY, K. 2000. The effect of peptide surface density on mineralization of matrix deposited by osteogenic cells. *Journal of Biomedical Materials Research,* 52**,** 595-600.
REZANIA, A. & HEALY, K. E. 1999. Biomimetic Peptide Surfaces That Regulate Adhesion, Spreading, Cytoskeletal Organization, and Mineralization of the Matrix Deposited by Osteoblast-like Cells. *Biotechnology Progress,* 15**,** 19-32.
REZANIA, A., JOHNSON, R., LEFKOW, A. R. & HEALY, K. E. 1999. Bioactivation of Metal Oxide Surfaces. 1. Surface characterisation and cell response. *Langmuir,* 15**,** 6931-6939.
RIPAMONTI, U., RAMOSHEBI, L. N., MATSABA, T., TASKER, J., CROOKS, J. & TEARE, J. 2001. Bone Induction by BMPs/OPs and Related Family Members in Primates. *The Journal of Bone and Joint Surgery,* 83-A Suppl 1**,** S116-S127.
ROSALES-LEAL, J. I., RODRÍGUEZ-VALVERDE, M. A., MAZZAGLIA, G., RAMÓN-TORREGROSA, P. J., DÍAZ-RODRÍGUEZ, L., GARCÍA-MARTÍNEZ, O., VALLECILLO-CAPILLA, M., RUIZ, C. & CABRERIZO-VÍLCHEZ, M. A. 2010. Effect of roughness, wettability and morphology of engineered titanium surfaces on osteoblast-like cell adhesion. *Colloids and Surfaces A: Physicochemical and Engineering Aspects,* 365**,** 222-229.
RUOSLAHTI, E. 1996. Rgd and other recognition sequences for integrins. *Annual Review of Cell and Developmental Biology,* 12**,** 697-715.
RUOSLAHTI, E. & PIERSCHBACHER, M. D. 1987. New perspectives in cell adhesion: rgd and integrins. *Science,* 238**,** 491-497.
SAH, R. N. & MILLER, R. O. 1992. Spontaneous reaction for acid dissolution of biological tissues in closed vessels. *Analytical Chemistry,* 64**,** 230-233.
SANO, K.-I. & SHIBA, K. 2003. A Hexapeptide Motif that Electrostatically Binds to the Surface of Titanium. *Journal of the American Chemical Society,* 125**,** 14234-14235.
SARTORI, M., GIAVARESI, G., PARRILLI, A., FERRARI, A., ALDINI, N. N., MORRA, M., CASSINELLI, C., BOLLATI, D. & FINI, M. 2015. Collagen type I coating stimulates bone regeneration and osteointegration of titanium implants in the osteopenic rat. *International orthopaedics,* 39**,** 2041-2052.
SCHIERHOLZ, J. M. & BEUTH, J. 2001. Implant infections: a haven for opportunistic bacteria. *The Journal of hospital infection,* 49**,** 87-93.

SCHLIEPHAKE, H., SCHARNWEBER, D., DARD, M., SEWING, A., AREF, A. & ROESSLER, S. 2005. Functionalization of dental implant surfaces using adhesion molecules. *Journal of Biomedical Materials Research B: Applied Biomaterials,* 73**,** 88-96.
SCHMIDT, D. R., WALDECK, H. & KAO, W. J. 2000. Protein Adsorption to Biomaterials. *In:* PULEO, D. A. & BIZIOS, R. (eds.) *Biological Interactions on Materials Surfaces.* Springer.
SCHNEIDER, G. B., ENGLISH, A., ABRAHAM, M., ZAHARIAS, R., STANFORD, C. & KELLER, J. 2004. The effect of hydrogel charge density on cell attachment. *Biomaterials,* 25**,** 3023-3028.
SCHNEIDER, G. B., ZAHARIAS, R. & STANFORD, C. 2001. Osteoblast Integrin Adhesion and Signaling Regulate Mineralization. *Journal of Dental Research,* 80**,** 1540-1544.
SCHNEIKER, T. & FORSBERG, K. 2014. Process Chemistry and Acid Management for Titanium Pickling Processes. *International Titanium Association (ITA) - Titanium Europe 2014.* Sorrento, Italy: SCANACON AB.
SCHULER, M., OWEN, G. R., HAMILTON, D. W., DE WILD, M., TEXTOR, M., BRUNETTE, D. M. & TOSATTI, S. G. 2006a. Biomimetic modification of titanium dental implant model surfaces using the RGDSP-peptide sequence: a cell morphology study. *Biomaterials,* 27**,** 4003-15.
SCHULER, M., TRENTIN, D., TEXTOR, M. & TOSATTI, S. G. 2006b. Biomedical interfaces: titanium surface technology for implants and cell carriers. *Nanomedicine,* 1**,** 449-463.
SCHWARTZ FO, H. O., NOVAES, A. B., DE CASTRO, L. M., ROSA, A. L. & DE OLIVEIRA, P. T. 2007. In vitro osteogenesis on a microstructured titanium surface with additional submicron-scale topography. *Clinical oral implants research,* 18**,** 333-344.
SERRO, A. P., FERNANDES, A. C., SARAMAGO, B., LIMA, J. & BARBOSA, M. A. 1997. Apatite desorption on titanium surfaces - the role of albumin adsorption. *Biomaterials,* 18**,** 963-968.
SHARD, A. G. & TOMLINS, P. E. 2006. Biocompatibility and the Efficacy of Medical Implants. *Journal of Regenerative Medicine,* 1**,** 789-800.
SIEDENBIEDEL, F. & TILLER, J. C. 2012. Antimicrobial Polymers in Solution and on Surfaces: Overview and Functional Principles. *Polymers,* 4**,** 46-71.
SINGHATANADGIT, W. 2009. Biological Responses to New Advanced Surface Modifications of Endosseous Medical Implants. *Bone and Tissue Regeneration Insights,* 2**,** 1-11.
SMITH, D. C., PILLIAR, R. M., METSON, J. B. & MCINTYRE, N. S. 1991. Dental implant materials. II. Preparative procedures and surface spectroscopic studies. *Journal of Biomedical Materials Research,* 25**,** 1069-1084.
SOBIESZCZYK, S. 2010. Surface modifications of ti and its alloys. *Advances in Materials Sciences,* 10.
SONOHARA, R., MURAMATSU, N., OHSHIMA, H. & KONDO, T. 1995. Difference in surface properties between Escherichia coli and Staphylococcus aureus as revealed by electrophoretic mobility measurements. *Biophysical Chemistry,* 55**,** 273-277.
STEELE, J. G., JOHNSON, G. & UNDERWOOD, P. A. 1992. Role of serum vitronectin and fibronectin in adhesion of fibroblasts following seeding onto tissue culture polystyrene. *Journal of Biomedical Materials Research,* 26**,** 861-864.
STEIN, G. S., LIAN, I. B. & OWEN, T. A. 1990. Relationship of Cell Growth to the Regulation of Tissue-Specific Gene Expression During Osteoblast Differentiation. *Journal of the Federation of American Societies for Experimental Biology (FASEB),* 4**,** 3111-3123.
STEINHILBER, D., SEIFFERT, S., HEYMAN, J. A., PAULUS, F., WEITZ, D. A. & HAAG, R. 2011. Hyperbranched polyglycerols on the nanometer and micrometer scale. *Biomaterials,* 32**,** 1311-6.
SUNDER, A., HANSELMANN, R., FREY, H. & MULHAUPT, R. 1999. Controlled Synthesis of Hyperbranched Polyglycerols by Ring-Opening Multibranching Polymerization. *Macromolecules,* 32**,** 4240-4246.

SUNDGREN, J. E., BODO, P. & LUNDSTROM, I. 1986. Auger electron spectroscopic studies of the interface between human tissue and implants of titanium and stainless steel. *Journal of colloid and interface science,* 110**,** 9-20.
TANAKA, Y., SAITO, H., TSUTSUMI, Y., DOI, H., IMAI, H. & HANAWA, T. 2008. Active Hydroxyl Groups on Surface Oxide Film of Titanium, 316L Stainless Steel, and Cobalt-Chromium-Molybdenum Alloy and Its Effect on the Immobilization of Poly(Ethylene Glycol). *Materials Transactions,* 49**,** 805-811.
TANG, L., WU, Y. & TIMMONS, R. B. 1998. Fibrinogen adsorption and host tissue responses to plasma functionalized surfaces. *Journal of Biomedical Materials Research,* 42**,** 156-163.
TEJERO, R., ANITUA, E. & ORIVE, G. 2014. Toward the biomimetic implant surface: Biopolymers on titanium-based implants for bone regeneration. *Progress in Polymer Science,* 39**,** 1406-1447.
TENGVALI, P., LUNDSTROM, I., SJOQVIST, L., ELWING, H. & BJURSTEN, L. M. 1989. Titanium-hydrogen peroxide interaction: model studies of the influence of the inflammatory response on titanium implants. *Biomaterials,* 10**,** 166-175.
TILLER, J. C. 2008. Coatings for Prevention or Deactivation of Biological Contamination. *In:* KOHLI, R. & MITTAL, K. L. (eds.) *Developments in Surface Contamination and Cleaning - Fundamentals and Applied Aspects.* William Andrew Publishing.
TOSATTI, S., SCHWARTZ, Z., CAMPBELL, C., COCHRAN, D. L., VANDEVONDELE, S., HUBBELL, J. A., DENZER, A., SIMPSON, J., WIELAND, M., LOHMANN, C. H., TEXTOR, M. & BOYAN, B. D. 2004. RGD-containing peptide GCRGYGRGDSPG reduces enhancement of osteoblast differentiation by poly(L-lysine)-graft-poly(ethylene glycol)-coated titanium surfaces. *Journal of Biomedical Materials Research A,* 68**,** 458-472.
VAN GAALEN, S., KRUYT, M., MEIJER, G., MISTRY, A., MIKOS, A., VAN DEN BEUCKEN, J., JANSEN, J., DE GROOT, K., CANCEDDA, R., OLIVO, C., YASZEMSKI, M. & DHERT, W. 2008. Tissue Engineering of Bone. *In:* VAN BLITTERSWIJK, C., PETER THOMSEN, ANDERS LINDAHL, JEFFREY HUBBELL, DAVID F. WILLIAMS, RANIERI CANCEDDA, BRUIJN, J. D. D. & SOHIER, J. (eds.) *Tissue Engineering.* Elsevier Inc.
VANDEVONDELE, S., VOROS, J. & HUBBELL, J. A. 2003. RGD-grafted poly-L-lysine-graft-(polyethylene glycol) copolymers block non-specific protein adsorption while promoting cell adhesion. *Biotechnology and Bioengineering,* 82**,** 784-790.
VERRIER, S., PALLU, S., BAREILLE, R., JONCZYK, A., MEYER, J., DARD, M. & AMÉDÉE, J. 2002. Function of linear and cyclic RGD-containing peptides in osteoprogenitor cells adhesion process. *Biomaterials,* 23**,** 585-596.
VETRONE, F., VARIOLA, F., TAMBASCO DE OLIVEIRA, P., ZALZAL, S. F., YI, J. H., SAM, J., BOMBONATO-PRADO, K. F., SARKISSIAN, A., PEREPICHKA, D. F., WUEST, J. D., ROSEI, F. & NANCI, A. 2009. Nanoscale oxidative patterning of metallic surfaces to modulate cell activity and fate. *Nano Letters,* 9**,** 659-665.
VOGLER, E. A. 1988. Thermodynamics of short-term cell adhesion in vitro. *Biophysical Journal,* 53**,** 759-769.
VOGLER, E. A. 1989. A thermodynamic model of short-term cell adhesion

in vitro. *Colloids and Surfaces,* 42**,** 233-254.
VOGLER, E. A. 1993. Interfacial chemistry in biomaterials science. *In:* BERG, J. C. (ed.) *Wettability.* New York: Taylor & Francis.
WAGNER, V. E., KOBERSTEIN, J. T. & BRYERS, J. D. 2004. Protein and bacterial fouling characteristics of peptide and antibody decorated surfaces of PEG-poly(acrylic acid) co-polymers. *Biomaterials,* 25**,** 2247-2263.

WANG, D. A., JI, J., SUN, Y. H., SHEN, J. C., FENG, L. X. & ELISSEEFF, J. H. 2002. In situ immobilization of proteins and RGD peptide on polyurethane surfaces via poly(ethylene oxide) coupling polymers for human endothelial cell growth. *Biomacromolecules,* 3**,** 1286-1295.
WANG, R. L. C., KREUZER, H. J. & GRUNZE, M. 1997. Molecular Conformation and Solvation of Oligo(ethylene glycol)-Terminated Self-Assembled Monolayers and Their Resistance to Protein Adsorption. *Journal of Physical Chemistry B,* 101**,** 9767-9773.
WEBER, T., GIES, Y. & TERFORT, A. 2012. Bacteria-repulsive polyglycerol surfaces by grafting polymerization onto aminopropylated surfaces. *Langmuir : the ACS journal of surfaces and colloids,* 28**,** 15916-21.
WEBSTER, T. J. & EJIOFOR, J. U. 2004. Increased osteoblast adhesion on nanophase metals: Ti, Ti6Al4V, and CoCrMo. *Biomaterials,* 25**,** 4731-4739.
WEI, J., IGARASHI, T., OKUMORI, N., MAETANI, T., LIU, B. & YOSHINARI, M. 2009. Influence of surface wettability on competitive protein adsorption and initial attachment of osteoblasts. *Biomedical materials,* 4**,** 145002.
WEI, Q., KRYSIAK, S., ACHAZI, K., BECHERER, T., NOESKE, P. M., PAULUS, F., LIEBE, H., GRUNWALD, I., DERNEDDE, J., HARTWIG, A., HUGEL, T. & HAAG, R. 2014. Multivalent anchored and crosslinked hyperbranched polyglycerol monolayers as antifouling coating for titanium oxide surfaces. *Colloids and surfaces. B, Biointerfaces,* 122**,** 684-692.
WEI, Y. & LATOUR, R. A. 2008. Determination of the adsorption free energy for peptide-surface interactions by SPR spectroscopy. *Langmuir,* 24**,** 6721-6729.
WENNERBERG, A., EKTESSABI, A., ALBREKTSSON, T., JOHANSSON, C. & ANDERSSON, B. 1997. A 1-year follow-up of implants of differing surface roughness placed in rabbit bone. *International Journal of Oral Maxillofacial Implants,* 12**,** 486-494.
WESTERMAN, R. W. & SCAMMELL, B. E. 2012. Principles of bone and joint injuries and their healing. *Surgery (Oxford),* 30**,** 54-60.
WIELAND, M., TEXTOR, M., CHEHROUDI, B. & BRUNETTE, D. M. 2005. Synergistic interaction of topographic features in the production of bone-like nodules on Ti surfaces by rat osteoblasts. *Biomaterials,* 26**,** 1119-1130.
WIKESJO, U. M., SORENSEN, R. G., KINOSHITA, A. & WOZNEY, J. M. 2002. RhBMP-2/alpha BSM induces significant vertical alveolar ridge augmentation and dental implant osseointegration. *Clinical Implant Dentistry and Related Research,* 4**,** 174-182.
WILLIAMS, A. & IBRAHIM, I. T. 1981. Carbodiimide Chemistry: Recent Advances. *ACS Chemical Reviews,* 81**,** 589-636.
WILSON, C. J., CLEGG, R. E., LEAVESLEY, D. I. & PEARCY, M. J. 2005. Mediation of Biomaterial-Cell Interactions by Adsorbed Proteins: A Review. *Tissue Engineering,* 21**,** 1629-1639.
WRAIGHTE, P. J. & SCAMMELL, B. E. 2006. Principles of fracture healing. *Surgery (Oxford),* 24**,** 198-207.
XU, L. C. & SIEDLECKI, C. A. 2007. Effects of surface wettability and contact time on protein adhesion to biomaterial surfaces. *Biomaterials,* 28**,** 3273-3283.
YANG, C., CHENG, K. & WENG, W. 2009a. Immobilization of RGD peptide on HA coating through a chemical bonding approach. *Journal of materials science. Materials in medicine,* 20**,** 2349-52.
YANG, G. L., HE, F. M., YANG, X. F., WANG, X. X. & ZHAO, S. F. 2009b. In vivo evaluation of bone-bonding ability of RGD-coated porous implant using layer-by-layer electrostatic self-assembly. *Journal of biomedical materials research. Part A,* 90**,** 175-85.
YILDIRIM, E. D., BESUNDER, R., PAPPAS, D., ALLEN, F., GUCERI, S. & SUN, W. 2010. Accelerated differentiation of osteoblast cells on polycaprolactone scaffolds driven by a combined effect of protein coating and plasma modification. *Biofabrication,* 2**,** 014109.

YOSHIMOTO, K., NISHIO, M., SUGASAWA, H. & NAGASAKI, Y. 2010. Direct observation of adsorption-induced inactivation of antibody fragments surrounded by mixed-PEG layer on a gold surface. *Journal of the American Chemical Society,* 132**,** 7982-7989.
ZARRABI, A., SHOKRGOZAR, M. A., VOSSOUGHI, M. & FAROKHI, M. 2014. In vitro biocompatibility evaluations of hyperbranched polyglycerol hybrid nanostructure as a candidate for nanomedicine applications. *Journal of materials science. Materials in medicine,* 25**,** 499-506.
ZHAO, G., RAINES, A. L., WIELAND, M., SCHWARTZ, Z. & BOYAN, B. D. 2007. Requirement for both micron- and submicron scale structure for synergistic responses of osteoblasts to substrate surface energy and topography. *Biomaterials,* 28**,** 2821-2829.
ZHAO, L., CHU, P. K., ZHANG, Y. & WU, Z. 2009. Review: Antibacterial Coatings on Titanium Implants. *Journal of Biomedical Materials Research Part B,* 91B**,** 470-480.
ZHU, J. 2010. Bioactive modification of poly(ethylene glycol) hydrogels for tissue engineering. *Biomaterials,* 31**,** 4639-4656.
ZHU, X., CHEN, J., SCHEIDELER, L., REICHL, R. & GEIS-GERSTORFER, J. 2004. Effects of topography and composition of titanium surface oxides on osteoblast responses. *Biomaterials,* 25**,** 4087-103.
ZIMMERLI, W. 2006. Infection and musculoskeletal conditions: Prosthetic-joint-associated infections. *Best practice & research. Clinical rheumatology,* 20**,** 1045-63.
ZINGER, O., ANSELME, K., DENZER, A., HABERSETZER, P., WIELAND, M., JEANFILS, J., HARDOUIN, P. & LANDOLT, D. 2004. Time-dependent morphology and adhesion of osteoblastic cells on titanium model surfaces featuring scale-resolved topography. *Biomaterials,* 25**,** 2695-2711.